DURBAN UNIVERSITY OF TECHNOLOGY
INYUVESI YASETHEKWINI YEZOBUCHWEPHESHE

NON-OXIDATIVE CONVERSION OF METHANE INTO CARBON AND PETROCHEMICALS OVER Fe, W, & Mo CATALYST SYSTEMS SUPPORTED ON ACTIVATED CARBON AND HZSM-5.

A thesis submitted in fulfilment of the academic requirements for the award of the degree of.

DOCTOR OF ENGINEERING

Durban University of Technology

Faculty of Engineering and the Built Environment,

Department of Chemical Engineering

Ronald Wafula Musamali

April 2021

Supervisor: Prof. Yusuf Makarfi Isa

Declaration

I, Ronald Wafula Musamali, do hereby declare that this research project entitled "*Non-oxidative conversion of methane into carbon and petrochemicals over Fe, W, & Mo catalyst systems supported on activated carbon and HZSM-5",* is my own work and that, to the best of my knowledge and belief, it contains no material previously published or written by another person nor material to which substantial extent has been accepted for the award of any degree of any university or institution of higher learning except where due acknowledgement has been made in this text.

Ronald Wafula Musamali		20th April 2021
……	……	……
Student	**Signature**	**Date**

Prof. Yusuf Makarfi Isa

……	……	……..
Supervisor	**Signature**	**Date**

Abstract

Non-oxidative conversion of methane (NOCM) is an environmentally benign route for producing carbon and valuable petrochemicals from methane. Unlike other methane conversion processes like Fischer-Tropsch and methanol synthesis which have been scaled up to commercial level, NOCM process development remains at laboratory scale due to various challenges such as catalyst deactivation due to coking, process thermodynamics, low conversion, and limited selectivity towards useful products.

In this present work, a study of non-oxidative conversion of methane into carbon and petrochemicals was done over Fe, W, & Mo catalyst systems supported on activated carbon (AC) and HZSM-5. The catalyst systems were prepared by various techniques at different metal loadings. The prepared catalysts were characterized for phase identification, structural properties, surface area, presence of functional groups, and tested for non-oxidative methane conversion at different operating conditions in a packed bed reactor. Products from non-oxidative conversion of methane were analysed using gas chromatography.

To accomplish the research objectives, synthesized binary catalyst systems were developed step by step. Phase one of the study involved synthesis of 24 single metal catalyst systems supported on activated carbon and HZSM-5 between 1.8-7.2% metal loading and tested for non-oxidative methane conversion. Prepared catalysts were screened based on methane conversion. Phase two of the study involved synthesis of 5.4% bimetallic catalyst systems supported on AC/ HZSM-5 and applied for non-oxidative methane conversion. Catalytic activity of Fe-Mo, W-Mo and Fe-W on AC and HZSM-5 supports were evaluated based on methane conversion and product distribution. In the final phase of the study, trimetallic binary catalyst systems (Fe-W-Mo) on AC and HZSM-5 supports were synthesized, characterized, and their catalytic activity evaluated at different metal loading, different metal composition, and different process conditions. The effect of support and catalyst preparation method on catalyst activity was also evaluated. Based on the results obtained, catalyst Fe-Mo/HZSM-5 showed little activity in terms of methane conversion with low C_2 and high coke formation whereas catalyst W-Mo/HZSM-5 was very active in methane conversion but less selective towards C_2 and aromatic hydrocarbons. On the other hand, catalyst Fe-W showed low methane conversion and low coke formation but exhibited high selectivity toward aromatics.

A 5.4% binary catalyst system (Fe-W-Mo/HZSM-5) with equal metal loading did not show much improvement on methane conversion, selectivity towards C_2 hydrocarbons, aromatics, and coke. However, when Fe and W metal loading were higher than Mo in this 5.4% binary catalyst system, there was notable increase in methane conversion and coke but C_2 formation decreased. On the contrary, when Mo loading was increased and Fe and W metal loading reduced, there was a subsequent decrease in methane conversion and coke formation but C_2 and aromatics formation increased by a big margin. From X-ray diffraction (XRD) results, M_2C on HZSM-5 produced by transformation of highly dispersed MoO_3, was the most active site for the activation of the C-H bond in methane molecules, but these sites were less active for further decomposition of CH_3^* radicals. Based on methane conversion, catalytic activity of Fe-W-Mo catalyst systems showed the same trend both on AC and HZSM-5 although methane conversion values were higher on AC than on HZSM-5 support. A wider range of product distribution was realized on catalysts supported on HZSM-5 than on AC support. This was attributed to the HZSM-5 zeolite channel structure and its inherent acidity which promoted shape selectivity towards benzene and its derivatives. Further, methane reacted with Mo^{6+} on HZSM-5 zeolite to produce CH_3^+ (a methoxy species on the Bronsted acid sites of the zeolite) and $[Mo\text{-}H]^{5+}$ which were further transformed into a molybdenum-carbene species ($Mo{=}CH_2$). These species further reacted with CH_4 to produce C_2 intermediates. The Bronsted acid sites located inside the zeolite channels and shape selectivity of HZSM-5 zeolite were responsible for activation of C-H bond and conversion of the C_2 intermediates into benzene and other higher carbon hydrocarbons.

Despite intensive research in this area, and to the best of the author's knowledge, no work on the development of a catalyst system for quantitative control of methane conversion and product distribution using Fe, W, and Mo catalyst systems loaded on AC/HZSM-5 has been reported. Therefore, the novelty in this work lies in the development of a tuneable binary catalyst system for quantitative control of product distribution in methane conversion to carbon and petrochemicals.

Dedication.

This study is dedicated to my son Ryan and my daughters; Tikide and Chichi, whom I dearly love.

Acknowledgements

I am most grateful to my supervisor, Dr. Yusuf Makarfi Isa for his guidance, encouragement, positive criticism, and moral support throughout this research work.

My thanks are also due to.

- My employer, The Technical University of Kenya, who granted me study leave to carry out my research project at Durban University of Technology.
- Durban University of Technology for giving me an opportunity to do my doctoral studies, use of their facilities, and financial support towards this research work.
- Swagelok South Africa for the supply of materials required for fabrication of the packed-bed reactor.
- The lab technicians at Durban University of Technology, Chemistry department, Mrs. Tebego Gwamanda and Mpumelelo for their services and guidance in the analysis of liquid hydrocarbons.

Finally, my heartfelt thanks goes to my fellow chemical engineering postgraduate students (class of 2018) who gave me emotional support and encouragement to pursue my doctorate studies.

Conference presentations and publications

Conference presentations

- Effect of metal synergy and loading on binary W-Mo/HZSM-5 catalyst for non-oxidative conversion of methane into carbon and petrochemicals. *International conference on chemical engineering, 28th-30th Oct 2020, Iasi Romania.*

  Ronald. W. Musamali[a*] and Yusuf. M. Isa[a]

  [a] *Chemical Engineering department, Durban University of Technology, P.o box 1334 Durban 4000, South Africa.*

- Hydrogen production from Biomethane over NiO-LiOH catalyst systems supported on CaO: Effect of LiOH content and reaction parameters on catalyst performance. *The 7th international conference on biorefinery, 18th-21st Aug 2019, Johannesburg South Africa.*

  Ronald. W. Musamali[a*] and Yusuf. M. Isa[a]

  [a] *Chemical Engineering department, Durban University of Technology, P.o box 1334 Durban 4000, South Africa.*

Journal papers Published/Accepted/Under review

- Effect of metal synergy and loading on binary W-Mo/HZSM-5 catalyst for non-oxidative conversion of methane into carbon and petrochemicals. *The Bulletin of the polytechnic institute of Jasi, Chemistry and Chemical Engineering Section*, 1ssue 1-2021, page 17-34, http://www.bipcic.icpm.tuiasi.ro/latestissue.html. ***Published***

  Ronald. W. Musamali[a*] and Yusuf. M. Isa[a]

  [a] *Chemical Engineering department, Durban University of Technology, P.o box 1334 Durban 4000, South Africa.*

- Production of clean hydrogen from methane decomposition over molten NiO-LiOH catalyst systems supported on CaO: Synergistic effect of molten LiOH on catalyst activity. *Asia-Pacific Journal of Chemical Engineering*. ***Accepted***

  Ronald. W. Musamali[a*] and Yusuf. M. Isa[a]

  [a] *Chemical Engineering department, Durban University of Technology, P.o box 1334*

  Durban 4000, South Africa.

- A tuneable binary Fe-W-Mo/HZSM-5 catalyst system for quantitative control of product distribution in non-oxidative conversion of methane into carbon and petrochemicals. ***Under review***

  Ronald. W. Musamali[a] and Yusuf. M. Isa[a*]

  [a] *Chemical Engineering department, Durban University of Technology, P.o box 1334*

  Durban 4000, South Africa.

- Synergetic effect of noble metals in a binary Fe-W-Mo/HZSM-5 catalyst system for non-oxidative conversion of methane into carbon and petrochemicals. ***Under review***
  Ronald. W. Musamali[a] and Yusuf. M. Isa[a*]

  [a] *Chemical Engineering department, Durban University of Technology, P.o box 1334*

  Durban 4000, South Africa.

Table of contents

Declaration....ii

Abstract....iii

Dedication....v

Acknowledgements....vi

Table of contents....ix

List of Figures....xvi

List of Tables....xx

List of Abbreviations....xxiii

List of chemical formulae....xxv

List of symbols....xxvii

CHAPTER 1. INTRODUCTION....1

1.1Background and problem statement....1

1.1.1 Introduction....1

1.1.2 Current global energy challenges....2

1.1.3 Process intensification....3

1.1.4 Gap....4

1.1.5 Problem statement....4

1.1.6 Novelty....4

1.2 Research Aims and objectives....4

1.2.1 Research Aim....4

1.2.2 Research objectives....5

1.3 Research Questions....5

1.4 Hypothesis....5

1.5 Thesis outline....6

CHAPTER 2. LITERATURE REVIEW 8
2.1 Background on methane gas 8
2.1.1 Methane sources and occurrence. 8
2.1.2 Properties of methane and the Methyl group. 9
2.1.3 Methane conversion and products 10
2.1.4 Applications of methane conversion products. 11
2.2 Methane conversion technologies 13
2.2.1 Direct methane conversion 14
2.2.2 Indirect methane conversion 15
2.2.3 Other methane conversion processes 19
2.2.3.1 Low temperature total oxidation 19
2.2.3.2 Halogenation and oxyhalogenation of methane 19
2.2.3.3 Electrochemical oxidation 21
2.2.3.4 Photochemical conversion 22
2.2.3.5 Dry (carbon dioxide) photocatalytic reforming of methane 23
2.3 Fundamentals of non-oxidative conversion of methane 23
2.3.1 Formation and nature of active sites 24
2.3.2 Effect of Zeolite pore structure on catalyst activity 27
2.3.3 Effect of Zeolite Si/Al ratio on the structure of Mo species on HZSM-5 28
2.3.4 The role of Bronsted acid sites 29
2.3.5 Coke formation and catalyst deactivation 29
2.3.6 Catalyst regeneration 31
2.3.6.1 Catalyst regeneration by gasification 31
2.3.6.2 Catalyst regeneration by combustion 32
2.3.6.3 Catalyst regeneration by partial regeneration 32

2.3.7 NOCM reaction mechanism 33
2.3.7.1 Methyl radical (CH_3*) formation 36
2.3.7.2 Formation of carbene-like species for hydro aromatization. 36
2.3.7.3 Formation of methyl carbenium ions (CH_3^+) 37
2.3.7.4 Properties of calcined Mo species at 500℃ on HZSM-5 38
2.3.8 Effect of operating conditions on NOCM reactions 38
2.3.8.1 Effect of reaction temperature 38
2.3.8.2 Effect of pressure. 39
2.3.8.3 Effect of gas hourly space velocity 40
2.3.8.4 Effect of reactor surface area 41
2.3.8.5 Effect of methane residence time 41
2.4 NOCM reaction kinetics and reactor designs 42
2.4.1 NOCM reaction kinetics 42
2.4.1.1 Establishment of intrinsic kinetic model 43
2.4.1.2 Estimation of parameter 44
2.4.2 Reactor designs commonly used in conversion of methane. 46
2.4.2.1 Coupled reactor 46
2.4.2.2 Two -zone reactor fluidized bed reactor 47
2.4.2.3 Membrane reactors 47
2.4.2.4 Fluidized bed reactors 48
2.4.3 Thermodynamics of non-oxidative conversion of methane 49
2.4.4 Thermodynamic challenges facing non-oxidative methane conversion. 50
2.5 Various attempts to improve methane conversion to hydrocarbons over Mo/HZSM-5 .. 52
2.5.1 Suppression of Bronsted acid sites on the zeolite surface 52
2.5.2 Co-feeding methane with small amounts of CO and CO_2 52

2.5.3 Co-feeding methane with small amounts of O_2, H_2 and H_2O 53
2.6 Catalyst development for NOCM reaction 54
2.6.1 The active phase 54
2.6.2 The promoter 54
2.6.3 The support 55
2.6.4 Metal and support interaction 56
2.6.5 Catalytic activity of different transition metals 56
2.6.6 Promotion of Mo/HZSM-5 with the second transition metal 57
2.6.7 Catalytic activity of molybdenum on different supports in NOCM reaction. 58
2.6.8 Carbonaceous catalysts 60
2.6.8.1 Application of activated carbon as catalyst supports in petrochemical industry. 61
2.7 Common catalyst preparation methods. 65
2.7.1 Impregnation 65
2.7.2 Precipitation and co-precipitation. 66
2.7.3 Sol-gel method 68
2.7.4 Mechanical mixing 68
2.8 Market value of non-oxidative conversion of methane products 68
2.9 Summary 70
CHAPTER 3. EXPERIMENTAL 74
3.1 Introduction 74
3.2 Materials and methods 74
3.2.1 Materials 74
3.2.2 Equipments used 74
3.3 Catalyst preparation methods 75

3.3.1 Incipient wetness impregnation 75
3.3.2 Sequential impregnation 75
3.3.3 Co-impregnation by mechanical mixing 76
3.4 Characterization of synthesized catalysts 76
3.4.1 XRD-analysis 76
3.4.2 SEM analysis 77
3.4.3 BET analysis 77
3.4.4 FT-IR Analysis 77
3.5 Catalyst evaluation 77
3.6 NOCM reaction operating conditions 80
3.7 Analytical equipment operating conditions 80
3.7.1 TCD analysis 80
3.7.2 FID analysis 80
3.7.3 Degree of uncertainty 80
3.8 Characterization of spent catalyst 81
3.8.1 TGA Analysis 81
3.8.2 TEM analysis 81
CHAPTER 4. RESULTS AND DISCUSSIONS 82
4.1 Objective I: To investigate the effect of catalyst metal loading on methane conversion and product distribution. 82
4.1.1 Catalyst screening 82
4.1.2.1 First catalyst screening. 83
4.1.2.2 Selected binary catalyst systems 84
4.1.2.3 Second catalyst screening based on methane conversion 85
4.1.3 Catalyst characterization 87

4.1.3.1 XRD-analysis 87
4.1.3.2 SEM Analysis 89
4.1.3.3 BET analysis 91
4.1.3.4 FT-IR analysis 93
4.1.4 Catalyst evaluation 96
4.1.5 Characterization of the spent catalyst 101
4.1.5.1 TGA analysis of catalyst systems supported on HZSM-5 101
4.1.5.2 TEM analysis of deposited carbon 103
4.1.6 Summary of the findings 106
4.2 Objective II: To investigate the effect of metal synergy on methane conversion and product distribution. 108
4.2.1 Materials and methods 108
4.2.2 Catalyst characterization 108
4.2.2.1 XRD-analysis 108
4.2.2.2. SEM Analysis 111
4.2.2.3 BET analysis 114
4.2.2.4 FT-IR analysis 116
4.2.3 Catalyst evaluation 119
4.2.4 Characterization of the spent catalyst 122
4.2.4.1 TGA analysis of deposited carbon 122
4.2.4.2 TEM analysis of deposited carbon 123
4.2.5 Summary of the findings 126
4.3. Objective III: To investigate the effect of process conditions on methane conversion and product distribution. 128
4.3.1 Catalyst synthesis 128
4.3.2 Catalyst characterization 128

4.3.3 Catalyst evaluation 128
4.3.3.1 Effect of temperature on methane conversion and product distribution. 128
4.3.3.2 Effect of gas hourly space velocity on methane conversion and product distribution. 129
4.3.3.3 Effect of reaction time on catalyst activity. 132
4.4 Objective IV: To investigate the effect support on methane conversion and product distribution. 134
4.4.1 Catalyst synthesis and designation 134
4.4.2 Catalyst characterization 134
4.4.3 Catalyst evaluation 134
4.4.4 Summary of the findings 137
4.5 Objective V: To investigate the effect of catalyst preparation method in the catalyst system on methane conversion and product distribution. 138
4.5.1 Catalyst synthesis 138
4.5.2 Catalyst characterization 138
4.5.3 Catalyst evaluation 138
4.5.4 Summary of the findings 142
CHAPTER 5: GENERAL CONCLUSIONS 143
CHAPTER 6: RECOMMENDATIONS FOR FURTHER STUDY 145
REFERENCES 146
APPENDIX A: CATALYST PRECURSORS 182
APPENDIX B: PARTICLE SIZE DISTRIBUTION USING IMAGE-J SOFTWARE 183

List of Figures

Chapter 1

Figure		Page no.
Figure 1-1	Natural gas reserves to production ratio in 2019	2

Chapter 2

Figure		Page no.
Figure 2-1	Different routes of methane conversion	11
Figure 2-2	High temperature and low temperature methane conversion technologies.	14
Figure 2-3	Effect of reaction temperature on conversion and selectivity using 2%Mo/HZSM-5 at 1 atm and 1400 mL/(g.h)	39
Figure 2-4	Effect of pressure on benzene formation rate over 6%Mo/HZSM-5 at 700℃ and 1350 mL/(g.h)	40

Chapter 3

Figure		Page no.
Figure 3-1	Process flow diagram for methane conversion	79

Chapter 4

Figure		Page no.
Figure 4-1	XRD patterns for catalyst; HZSM-5, 1.8F1.8W1.8M/HZSM-5, 2.25F2.25W0.9M/HZSM-5, and 1.35F1.35W2.7M/HZSM-5.	88
Figure 4-2	XRD patterns for catalyst; AC, 1.8F1.8W1.8M/AC, 2.25F2.25W0.9M/AC, and 1.35F1.35W2.7M/AC.	89

Figure 4-3	SEM Images of various catalyst loaded on HZSM-5; E(1.8F1.8W1.8M/HZSM-5), F(2.25F2.25W0.9M/HZSM-5), G(1.35F1.35W2.7M/HZSM-5).	90
Figure 4-4	SEM Images of various catalysts loaded on AC; I(1.8F1.8W1.8M/AC), J(2.25F2.25W0.9M/HZSM-5), K(1.35F1.35W2.7M/AC).	91
Figure 4-5	FT-IR spectra of various catalysts; HZSM-5, 1.8F1.8W1.8M/HZSM-5, 2.25F2.25W0.9M/HZSM-5, and 1.35F1.35W2.7M/HZSM-5.	95
Figure 4-6	FT-IR spectra of various catalysts; AC, 1.8F1.8W1.8M/AC, 2.25F2.25W0.9M/AC, and 1.35F1.35W2.7/AC.	96
Figure 4-7	Methane conversion, C_2 hydrocarbon and coke selectivity of various catalyst systems. at different temperatures, 0.96$Lg^{-1}cat.h^{-1}$ and 1 atm.	99
Figure 4-8	Benzene, toluene, xylene, and hydrogen selectivity at different temperatures at 0.96$Lg^{-1}cat.h^{-1}$ and 1atm.	101
Figure 4-9	TGA pattern of catalyst 1.8F1.8W1.8M/HZSM-5, 2.25F2.25W0.9M/HZSM-5, and 1.35F1.35W2.7M/HZSM-5	102
Figure 4-10	TGA pattern of catalyst 1.8F1.8W1.8M/AC, 2.25F2.25W0.9M/AC, and 1.35F1.35W2.7M/AC	103
Figure 4-11	TEM Image of various catalysts; K(1.8F1.8W1.8M/HZSM-5), L(2.25F2.25W0.9M/HZSM-5), M(1.35F1.35W2.7M/HZSM-5)	105
Figure 4-12	TEM Image of various catalysts; N(1.8F1.8W1.8M/AC), O(2.25F2.25W0.9M/AC), P(1.35F1.35W2.7M/AC)	106
Figure 4-13	XRD patterns for catalyst HZSM-5, 2.7F2.7M/HZSM-5, 2.7W2.7M/HZSM-5, 2.7F2.7W/HZSM-5, and 1.8F1.8W1.8M/HZSM-5	110
Figure 4-14	XRD patterns for catalyst AC, 2.7F2.7M/AC, 2.7W2.7M/AC, 2.7F2.7W/AC, and 1.8F1.8W1.8M/AC	111

Figure 4-15	SEM Images of various catalysts; P (2.7F2.7M/HZSM-5), Q (2.7W2.7M/HZSM-5), R (2.7F2.7W/HZSM-5), and S (1.8F1.8W1.8M/HZSM-5).	112
Figure 4-16	SEM Image of various catalysts; L(2.7F2.7M/AC), M(2.7W2.7M/AC), N (2.7F2.7W/AC), and O(1.8F1.8W1.8M/AC).	114
Figure 4-17	FT-IR spectra of catalysts; HZSM-5, 2.7F2.7M/HZSM-5, 2.7W2.7M/HZSM-5, 2.7F2.7W/HZSM-5, and 1.8F1.8W1.8M/HZSM-5.	118
Figure 4-18	FT-IR spectra of catalysts; AC, 2.7F2.7M/AC, 2.7W2.7M/AC, 2.7F2.7W/AC, and 1.8F1.8W1.8M/AC	119
Figure 4-19	TGA pattern of catalysts; HZSM-5, 2.7F2.7M/HZSM-5, 2.7W2.7M/HZSM-5, 2.7F2.7W/HZSM-5, and 1.8F1.8W1.8M/HZSM-5	122
Figure 4-20	TGA pattern of catalysts AC, 2.7F2.7M/AC, 2.7W2.7M/AC, 2.7F2.7W/AC, and 1.8F1.8W1.8M/AC.	123
Figure 4-21	TEM Image of various catalyst; P(2.7F2.7M/HZSM-5), Q(2.7W2.7M/HZSM-5), R(2.7F2.7W/HZSM-5), and S(1.8F1.8W1.8M/HZSM-5)	125
Figure 4-22	TEM Image of various catalysts; T(2.7F2.7M/AC), U(2.7W2.7M/HZSM-5), V(2.7F2.7W/AC), and W (1.8F1.8W1.8M/AC)	126
Figure 4-23	Effect of GHV on methane conversion and product selectivity over various catalysts at 750℃, 1atm.	130
Figure 4-24	Effect of GHSV on xylene, hydrogen, and coke selectivity over different catalysts at 750℃, and 1atm.	131
Figure 4-25	Effect of reaction time on methane conversion, C_2 hydrocarbon selectivity, and coke selectivity over various catalysts at 750℃, 0.96 $Lg^{-1}cat.h^{-1}$ and 1 atm.	133

Figure 4-26	Effect of catalyst preparation method on methane conversion, C_2 hydrocarbon selectivity, and coke selectivity over various catalysts at 750℃, 0.96 $Lg^{-1}cat.h^{-1}$ and 1 atm.	139
Figure 4-27	Effect of catalyst preparation method on benzene, toluene, xylene, and hydrogen selectivity over various catalysts at 750℃, 0.96 $Lg^{-1}cat.h^{-1}$, and 1 atm.	141

List of Tables

Chapter 2

Table		Page no.
Table 2-1	CH_4 conversions and product selectivity of 0.5%Metal/HZSM-5 catalysts.	57
Table 2-2	Methane conversion and product selectivity over Mo-doped catalysts loaded on HZSM-5.	58
Table 2-3	Catalytic activity of Mo catalysts loaded on different supports in non-oxidative methane conversion.	60
Table 2-4	Assignment of FT-IR bands to specific oxygen containing surface functional groups of activated carbon material	64
Table 2-5	Global market price of hydrogen gas of different purities (2017)	69
Table 2-6	Global market price of CH_4 conversion products (OPEC 8th July 2020)	70

Chapter 4

Table		Page no.
Table 4-1	Methane conversion over single metal catalyst systems loaded on HZSM-5 and AC.	83
Table 4-2	Composition of monometallic, bimetallic, and trimetallic catalyst systems at 5.4%wt metal loading before loading onto HZSM-5/AC.	84
Table 4-3	Nomenclature of the binary catalyst systems loaded on HZSM-5 and AC**.**	85
Table 4-4	Methane conversion over various catalysts loaded on HZSM-5 and AC at 750℃, 0.96Lg^{-1}cat.h^{-1} and 1 atm.	86
Table 4-5	Selected binary catalyst systems for use in non-oxidative methane conversion.	87

Table 4-6	Catalyst surface area, pore volume and pore size.	93
Table 4-7	Nomenclature of various binary catalyst systems.	108
Table 4-8	Catalyst surface area, pore volume and pore size.	116
Table 4-9	Methane conversion and product selectivity over different catalysts loaded on HZSM-5 at 750℃, and GHSV 0.96 $Lg^{-1}cat.h^{-1}$, and 1 atm.	121
Table 4-10	Methane conversion and product selectivity over various catalysts loaded on activated carbon at 750℃, 0.96 $Lg^{-1}cat.h^{-1}$ and 1 atm.	122
Table 4-11	Binary catalyst systems for methane composition**.**	128
Table 4-12	Methane conversion and C_2 selectivity over various catalysts at different temperatures, 0.96 $Lg^{-1}cat.h^{-1}$ and 1 atm.	135
Table 4-13	Benzene and toluene selectivity at different temperatures over different catalysts at 0.96 $Lg^{-1}cat.h^{-1}$ and 1 atm.	136
Table 4-14	Xylene and coke selectivity at different temperatures over different catalysts at 0.96 $Lg^{-1}cat.h^{-1}$ and 1 atm.	136
Table 4-15	Hydrogen selectivity over catalyst, at different temperatures, 0.96 $Lg^{-1}cat.h^{-1}$ and 1 atm.	137

Appendix

Table		**Page no.**
Table A-1	Elemental composition of catalyst precursors	182
Table B-1	Particle size distribution in HZSM-5 obtained using Image-J software.	183
Table B-2	Particle size distribution in catalyst 2.7F2.7M/HZS-5 obtained using Image-J software.	185
Table B-3	Particle size distribution in catalyst 2.7W2.7M/HZS-5 obtained using Image-J software.	187
Table B-4	Particle size distribution in catalyst 2.7F2.7W/HZS-5 obtained using Image-J software.	189

Table B-5	Particle size distribution in catalyst 1.8F1.8W1.8M/HZS-5 obtained using Image-J software.	191
Table B-6	Particle size distribution in catalyst 2.25F2.25W0.9M/HZS-5 obtained using Image-J software.	193
Table B-7	Particle size distribution in catalyst 1.35F1.35W2.7M/HZS-5 obtained using Image-J software.	195
Table B-8	Particle size distribution in catalyst AC obtained using Image-J software.	197
Table B-9	Particle size distribution in catalyst 2.7F2.7M/AC obtained using Image-J software.	199
Table B-10	Particle size distribution in catalyst 2.7W2.7M/AC obtained using Image-J software.	201
Table B-11	Particle size distribution in catalyst 2.7F2.7W/AC obtained using Image-J software.	203
Table B-12	Particle size distribution in catalyst 1.8F1.8W1.8/AC obtained using Image-J software.	205
Table B-13	Particle size distribution in catalyst 2.25F2.25W/0.9M/AC obtained using Image-J software.	207
Table B-14	Particle size distribution in catalyst 1.35F1.35W2.7M/HZS-5 obtained using Image-J software.	209

List of Abbreviations

Abbreviation	Full English Name
a.u	Arbitrary units
AC	Activated carbon
AHM	Ammonium heptamolybdate
Al	Aluminium
APT	Ammonium Para tungstate
BDE	Bond dissociation energy
B.E.T	Brunauer-Emmett-teller
BTEX	Benzene Toluene Xylene
CB	Carbon Black
CNT	Carbon nanotube
DFT	Density function theory
EA	Electron affinity
FC	Filamentous Carbon
FID	Flame ionization detector
FT-IR	Fourier transform infrared
GC	Gas chromatograph
HUMO	Highest occupied molecular orbital
IPO	Ionization potential
LUMO	Lowest unoccupied molecular orbital
MWCNT	Multi walled carbon nanotube

NGH	Natural gas hydrate
NOCM	Non oxidative conversion of methane
PAH	Poly aromatic hydrocarbon
SEM	Scanning electron microscopy
Si	Silicon
SMR	Steam methane reforming
SWCNT	Single walled carbon nanotube
TEM	Transmission electron microscopy
TCD	Thermoconductivity detector
TGA	Thermogravimetric analysis
TOS	Time on stream
TPR	Temperature programmed reduction
XPS	X-Ray photoelectron spectroscopy
XRD	X-Ray diffraction

List of chemical formulae

Chemical formula	**English name**
CH_4	Methane
C_2H_6	Ethane
C_2H_4	Ethene/Ethylene
C_6H_6	Benzene
C_7H_8	Toluene
C_8H_{10}	Xylene
$C_{10}H_8$	Naphthalene
CO_2	Carbon dioxide
CO	Carbon monoxide
Co	Cobalt
Cr	Chromium
Fe	Iron
$Fe\ (NO_3)_3.9H_2O$	Ferric nitrate nonahydrate
H_2	Hydrogen
Ir	Iridium
K	Potassium
MgO	Magnesium oxide
Mn	Manganese
Mo	Molybdenum

Mo_2C	Molybdenum carbide
MoO_3	Molybdenum oxide
$(NH_4)_6Mo_7O_{24}.4H_2O$	Ammonium heptamolybdate
$(NH_4)_{10}W_{12}.4H_2O$	Ammonium Para tungstate
NH_4ZSM-5	Ammonium zeolite Socony molecular five
$Al_2(MoO_4)_3$	Aluminium molybdate
Pt	Platinum
Re	Rhenium
Rb	Rubidium
SiO_2/Al_2O_3	Silica/Alumina
V	Vanadium
W	Tungsten
WO_3	Tungsten oxide
Zn	Zinc

List of symbols

Symbol	Meaning
≥	greater or equal to
≤	less or equal to
W	Weight (g)
T	temperature (℃)
t	time (h)
F	flow rate
$\Delta H°r$	Standard enthalpy of reaction
$\Delta G°$ (T)	Gibb's energy
K_p	equilibrium constant
R_u	Universal gas constant (8.314J/mol.K).
p_{CH4}	partial pressure of methane
p_{H_2}	partial pressure of hydrogen
θ	theta (angle of diffraction)
nm	nanometre (10^{-9}m)
Å	angstrom (10^{-10}m)

CHAPTER 1. INTRODUCTION

1.1Background and problem statement

1.1.1 Introduction

Currently, oil, natural gas, and coal are relied on as the primary energy sources. However, these primary energy sources are of fossil origin. Generation of energy from fossil fuels is associated with emission of greenhouse gases which are harmful to the environment (Brandt *et al.* 2018). Notable greenhouse gases are water vapour, carbon dioxide, methane, nitrous oxide, ozone, chlorofluorocarbons, and hydrofluorocarbons. Therefore, non-oxidative conversion of methane into value added chemicals is touted as one of the useful technologies in reducing greenhouse gas emissions into the atmosphere. According to the British petroleum statistical world energy review report 2019 (Petroleum 2019), global energy reserves of primary energy sources in million tons of oil equivalent (mtoe) were as follows; crude oil (244100) , natural gas (169334), and coal (1054782). In 2019, global production of oil was estimated at 4474.3 mtoe for oil, 3325.8 mtoe for natural gas and 3916.8 mtoe for coal against a global consumption of 4662.1 mtoe for oil, 3309.4 mtoe for natural gas, and 3772.1 mtoe for coal in the same year.

Further, global energy consumption grew at 2.9%, almost double its 10-year average growth of 1.5% per year, and the fastest since 2010. Natural gas consumption contributed to more than 40% of the total increase in global energy consumption. In 2018, fuel consumption grew faster than their 10-year averages, apart from energy from renewable sources. Global oil consumption growth averaged at 1.5%, approximately 1.4 million barrels per day with natural gas consumption rising by 195 billion cubic meters (bcm), approximately 5.3% of the total global energy. This growth was a record high since 1984. Coal consumption in 2018 grew by 1.4%, doubling its 10year-average and renewable power consumption grew by 14.5% slightly below its 10-year average. According to the National petroleum Council in the United States of America (USA), global energy demand is projected to hit 50% growth by 2030 (Balzani and Armaroli 2010).

International world Energy Agency (Mohn 2020) reports that, the world's energy demand from natural gas in 2018 increased by 4.6%, accounting for nearly half of the increase in global energy demand. Since 2010, 80% of growth has been concentrated in three key regions: The United states where the shale gas revolution is in full swing, China where economic expansion and air

quality concerns have underpinned rapid growth, and in the middle East, where gas is regarded as the gate way to economic diversification from oil. Although natural gas is abundant, large quantities of its reserves are in remote areas hence a challenge in transportation to potential markets. From Figure 1-1, Africa had a natural gas reserves to production ratio of about of about 61 against the world leaders, Middle East whose natural gas reserves to production ratio was about 110 in 2018. Despite huge gas natural reserves, natural gas reserves to production ratio is still low in Africa.

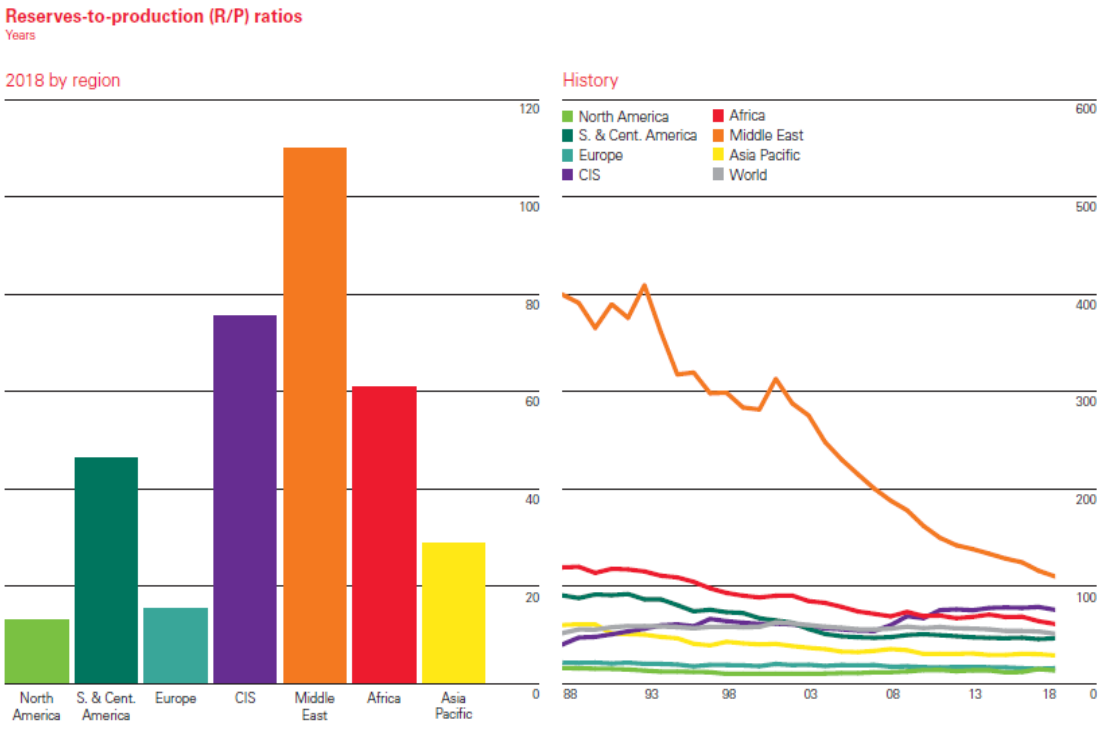

Figure 1-1. Natural gas reserves to production ratio in 2019. Adapted from (Petroleum 2019)

1.1.2 Current global energy challenges

According to the United Nations survey in 2019, global human population was estimated at 7.7 billion people. This projected population growth is expected to hit 8.5 billion in 2030, 9.7 billion in 2050, and 10.9 billion in 2100 (Nations 2019). To cater for this population growth and demand in energy, various energy sources need to be explored. One such energy source is methane gas.

Methane is the major component of natural gas. It is produced in huge quantities as associated gas in oil production, oil drilling, and oil refining as well as petrochemical processes. It is also available in huge quantities as methane hydrate in seabed. Methane gas can also be found in

coal deposits and can also be formed by bacterial decomposition of biomass. Methane gas can be converted into fuels and useful chemicals using various technologies.

The main problem associated with mature methane conversion technologies is the emission of greenhouse gases which lead to environmental degradation. Apart from environmental pollution, initial capital investment on equipment, process scale-up, and thermodynamic challenges affect full scale exploitation of these energy producing technologies (Wassie *et al.* 2018). Therefore, an alternative route to producing clean energy needs to be explored.

1.1.3 Process intensification

Non-oxidative conversion of methane (NOCM) is one of the pathways for producing carbon and valuable petrochemicals from methane. Unlike other methane conversion processes like Fischer-Tropsch (De Klerk 2011) and methanol synthesis (Olah *et al.* 2018) which have been scaled up to commercial levels, the NOCM process development still remains at laboratory scale due to various challenges such as high equipment cost, catalyst deactivation due to coking, process thermodynamics, low conversion, and limited selectivity towards useful products. Most research in this area has been built around molybdenum catalyst which was first reported in 1993 (Wang *et al.* 1993). Since then, a lot of research work has focused on catalyst development and equipment design. On catalyst development, molybdenum has been doped with various transition metal catalysts supported on different supports. To suppress formation of reactive coke which is responsible for catalyst deactivation, some researchers have reported that addition of small amounts of oxygen (Yuan *et al.* 1999), hydrogen (Ma *et al.* 2003), and water (Fouty *et al.* 2017) in methane feed have been found to have a positive influence on the NOCM reaction. Despite intensive research in this area, no catalyst has been formulated to give selectivity towards C_2 hydrocarbon yield of more than 25% and selectivity to higher hydrocarbons by more than 80% (Chen *et al.* 2018).

Another research group (Alipour-Dehkordi and Khademi 2019), investigated the effect of various side-feeding strategies on reactor performance containing CH_4 and CO_2. They found out that O_2, CO_2, and water side-feeding strategies were feasible, beneficial, and flexible in terms of membrane thickness and shell-side pressure control for syngas production when the H_2/CO molar ratio was 1 for Fischer-Tropsch process and when the H_2/CO molar ratio was 1.2 for dimethyl ether. From the results obtained, they showed that micro-porous membrane reactors

had a higher CO_2 conversion when H_2/CO molar ratio was 2 compared to the traditional reactor. Recently, (Ogihara *et al.* 2020) investigated the pyrolysis mixture of methane and ethane at temperatures between 700-800℃ and revealed that methane alone could not react in that temperature range but upon mixing methane with ethane, they reported significant yields of propane and toluene. From the results obtained, it was inferred that CH_4 was attacked by radical species generated from the pyrolysis of C_2H_6 and then converted into methyl radicals. Their study clarified the fact that methane can also be activated by radicals generated from existing molecules without the help of catalysts or extremely high temperatures.

Based on continuous research into this area, the new and innovative concepts that are being developed at laboratory and pilot scales, we expect the growth and maturation of commercial technologies for methane conversion to useful petrochemicals. Some process intensified approaches including the combination of nanostructured catalysts, microchannel reactors, permselective membranes, closely coupled reactors, and temperature control represent significant advances to commercialize the methane conversion process.

1.1.4 Gap

Despite intensive research this area, and to the best of the author's knowledge, there has not been work done in synthesizing catalyst systems to quantitatively control product distribution during methane conversion.

1.1.5 Problem statement

Non-oxidative conversion of methane process has limited selectivity to desired products. The need to exploit the potentials of methane gas as a source of petrochemicals over tuneable catalyst system is of interest to present day researchers.

1.1.6 Novelty

The novelty in this present work lies in the development of tuneable catalyst systems for quantitative control of product distribution in methane conversion to carbon and petrochemicals

1.2 Research Aims and objectives

1.2.1 Research Aim

The main aim of this study is to develop a catalyst system that is selective towards useful petrochemicals in non-oxidative methane conversion.

1.2.2 Research objectives

- ✓ To investigate the effect of Fe, W, and Mo metal loading in the catalyst system on methane conversion and product distribution.
- ✓ To investigate the synergetic effect of transition metals in the catalyst system on methane conversion and product distribution.
- ✓ To study the effect of process operating conditions on methane conversion and product distribution.
- ✓ To study the effect of support type in the catalyst system on methane conversion and product distribution.
- ✓ To synthesize catalyst systems using incipient wetness impregnation, sequential impregnation, and mechanical mixing and study the effect of catalyst preparation method on catalyst activity.

1.3 Research Questions

In this project, key research questions are.

- ✓ Can the trimetallic Fe, W, & Mo metal catalyst system perform better than bimetallic and monometallic catalysts supported on activated carbon and HZSM-5?
- ✓ What role does the transition metal loading play in methane conversion and product distribution?
- ✓ What role does the support type play in terms of catalyst activity?
- ✓ What is the effect of catalyst preparation method on catalyst performance?
- ✓ How does process conditions affect methane conversion and product distribution?

1.4 Hypothesis

Catalyst activity in methane conversion will be proportional to the quantity of metal promoters (Fe, W, and Mo) in the catalyst system. In the trimetallic Fe, W, and Mo catalyst systems supported on HZSM-5 or AC, (Fe, W, and Mo) will be the active component. Metal synergy will have an effect on methane conversion and product distribution. Best catalytic activity results will be achieved when the trimetallic binary catalyst system is supported on HZSM-5 than on activated carbon. Catalysts prepared by incipient impregnation method will show more catalytic

activity in methane conversion and product distribution than those catalyst systems prepared by sequential impregnation and mechanical mixing.

1.5 Thesis outline

This Thesis is structured as follows.

Chapter 1. Introduction

This chapter gives background information on non-oxidative conversion of methane, common methods of methane conversion, problem statement, contributions of the study, research aims and objectives, research questions, hypothesis, scope, and scientific thrust for the study.

Chapter 2. Literature review

In this chapter, extensive literature review of other people's work on different methane conversion processes and in particular non-oxidative conversion of methane into carbon and petrochemicals is given. Methane conversion processes, methane conversion products, catalyst preparation methods, fundamentals of non-oxidative methane conversion, catalyst development, and latest attempt to improve non-oxidative methane conversion reaction are given in this section.

Chapter 3. Experimental

In this chapter, materials and methods for catalyst synthesis, characterization, and evaluation are clearly spelled out. Catalyst nomenclature, product analysis, mathematical equations, and formulae used to interpret data are given. A brief description of each equipment used, and software used to interpret data are given here.

Chapter 4. Results and Discussions

In this chapter, findings/results from study in terms of catalyst synthesis, catalyst characterization, catalyst evaluation are covered under the specific objectives of the study. The findings from the study are compared with previous studies documented literature on some specific aspects of the study. Conclusions from each objective are documented under this section.

Chapter 5. General conclusions.

General conclusions from the study, covering all the study objectives are documented under this section.

Chapter 6. Recommendations for further study

To exhaust all the research aspects in non-oxidative methane conversion into carbon and petrochemicals over a binary (Fe, W, Mo) catalyst system supported on AC and HZSM-5, recommendations for further study to interested researchers in this research domain are outlined in this section.

References.

A bibliography of all referenced material in-text is listed here.

Appendix.

Detailed information on elemental composition of catalyst precursors and SEM raw data on catalyst crystallite size distribution using Image-J Software is documented under this section.

CHAPTER 2. LITERATURE REVIEW

2.1 Background on methane gas

2.1.1 Methane sources and occurrence.

Methane is an important greenhouse gas that contributes immensely to global warming (Myllykangas *et al.* 2020) and ranks second in radiative forcing by well mixed greenhouse gases with an estimated global net atmospheric emission of about 592Tg per year (Lohrberg *et al.* 2020). It plays a critical role in influencing atmospheric chemistry through a chain of complex reactions (Cicerone and Oremland 1988). A large proportion of current global methane on earth is produced by methanogenesis, which is the ultimate route of anaerobic fermentation of organic matter occurring in various environments (Knittel and Boetius 2009). From this atmospheric methane, wetlands and fresh water systems are the most significant, while agriculture, fossil fuels, waste water treatment, and other sources make up between 46-67% of global methane emissions (Kirschke *et al.* 2013). Due to human activities, methane concentration in the atmosphere has doubled since pre-industrial age (Blasing and Smith 2016).

Huge amounts of methane is found at the sea bed-water interface where aerobic and anaerobic microbial oxidation of methane efficiently dissolves it from the sediment into the water column (Knittel and Boetius 2009). Natural gas hydrates (NGHs) are non-stoichiometric and ice-like solids in which methane gas molecules occupy the lattice structure formed by water under harsh environmental conditions. These NGHs have emerged as viable clean energy sources of methane and their increased exploitation is of interest to present day researchers (Sun *et al.* 2020). Another rich source of methane is mud volcanoes produced by outflow of mud water and gas phases with traces of other hydrocarbon gases (Farhadian Babadi *et al.* 2020). Natural gas is a preferred source of raw material for producing value added petrochemicals because it is considered to be the cleanest fossil fuel and is a safe source of energy when transported and used properly (Faramawy *et al.* 2016). The major component of natural gas is methane though, it may also contain (C_2 hydrocarbons, N_2, CO_2, He, H_2S, and noble gases). Other sources of methane gas include coal mines, gas & oil industry, landfills & waste, ruminants, rice agriculture, biomass burning, wild fires, and termites among others (Van Amstel 2012).

Methane gas is used primarily as a fuel for heating in conventional heat burners and lighting, as a raw material for manufacture of industrial chemicals, manufacture of petrochemicals, and in

electricity generation. Other than using methane in raw form, it can also be converted into transportable and storable high-density energy sources or valuable petrochemicals. Petrochemical products such as ethylene, propylene, and benzene are applied in the manufacture of industrial products like polymers, cosmetics, lubricants, and detergents.

2.1.2 Properties of methane and the Methyl group.

From thermodynamic point of view, a methane molecule is highly stable and hence, its activation and conversion is difficult. The molecule of methane has a tetrahedral geometry with four equivalent C-H bond angle of 109.5^0. The absence of a dipole moment and a rather small polarizability of ($2.84 \text{ X } 10^{-40} C^2.m^2.J^{-1}$) (Schwach *et al.* 2017) means that a methane molecule requires a high local electric field to be polarized and allow nucleophilic or electrophilic attack.

In comparison with other alkanes, methane possesses the highest C-H bond strength with the first bond dissociation energy (BDE) of $439.3 kJmol^{-1}$ under standard conditions (Luo 2007). This high stability implies that methane is least reactive of all the alkanes. The ionization potential (IPO) of methane is high (12.6 eV) and its electron affinity (EA) is (-1.9eV). This implies that methane anion (CH_4-) is less stable than the neutral methane. Methane is a very weak acid with a high pKa (∼ca.48) (Paganini *et al.* 2003) and a moderate proton affinity ($543.9 kJmol^{-1}$) (Komornicki and Dixon 1992). These properties of methane make it hard for reactions involving electron transfer and proton transfer with methane, especially oxidation and reduction reactions. Activation of methane leads to the removal of a hydrogen atom from methane giving rise to a methyl species which can either be a radical, a cation, or an anion depending on the catalyst used. The methyl radical has a planar structure (Schwach *et al.* 2017) with a central carbon atom in sp^2 hybridization, a bond length of 1.09Å (Dixon *et al.* 1997), and a binding energy of $461.5 kJmol^{-1}$ (Lü and Lin 2014). The ionization potential of CH_3* (9.84eV.) (Dixon *et al.* 1997) required to form methyl cation CH_3+ is lower than the ionization potential of methane. This characteristic is important in distinguishing CH_3* from CH_4 using threshold ionization technique (Horn *et al.* 2006).

Alkyl substitution stabilizes both C- radicals and carbenium ions in both radical and electrophilic reaction. The rate of reactivity follows the C-H bond basicity order: tertiary > secondary > primary (Schwach *et al.* 2017). Unlike a methyl group which can lose a hydrogen atom if well catalysed by a super acid, methane can gain a hydrogen atom and become hyper-coordinated.

The methenium ion (CH_5+) is the smallest non classical carbonium and has been found to play a critical role in electrophilic and acid catalysed transformation of alkanes. The structure of CH_5+ carbonium consists of a pyramidalized CH_3+ units which are strongly bound on a hydrogen molecule leading to the formation of a three-center, two electron bond arrangement (Schreiner 2000). As reported by (Schwach *et al.* 2017) , the difficulty in activation of methane lies in its molecular orbitals. Since the level of the lowest unoccupied molecular orbital (LUMO) is high and that of the highest occupied molecular orbital (HOMO) is low, it becomes very difficult to donate an electron to the LUMO and to remove an electron form the HOMO. The distortion of methane symmetry alters the relative position of LUMO and HOMO eventually leading to activation of methane.

2.1.3 Methane conversion and products

Despite the thermodynamic challenges associated with methane activation, intensive research into this area has remained alive for the past three decades. One such reaction mechanism of converting methane into petrochemicals was suggested by (Chen *et al.* 1996). They considered that methane oligomerization reaction is catalysed by a molybdenum species inside the zeolite channels and the Bronsted acid sites of HZSM-5. Studies on methane aromatization over supported and unsupported molybdenum-based catalysts by (Wenlong 2000) show that Mo_2C on ZSM-5 produced by transformation of highly dispersed MoO_3 is the active site for the activation of the C-H bond in methane molecules, but these sites are less active for further decomposition of CH_3 and CH_2 species produced. Consequently, these radicals have enough lifetime to dimerize into C_2H_6 and C_2H_4 either on the catalyst or in the gas phase.

A synergistic effect between these two kinds of centres is believed to influence the catalysis of methane conversion to benzene. The reaction scheme for the above reactions is represented by the following equations.

$$CH_4 \xrightarrow[HZSM-5]{MoOx} CH_3^* + H^* \quad (1)$$

$$2CH_3^* \xrightarrow{MoOx} C_2H_4 + H_2 \quad (2)$$

$$3C_2H_4 \xrightarrow{HZSM-5} C_6H_6 + 3H_2 \quad (3)$$

From Figure 2-1, a methane molecule can be converted into different products via different routes. The uniqueness of each route is defined in terms of process conditions, type of catalyst used, and the reactor used.

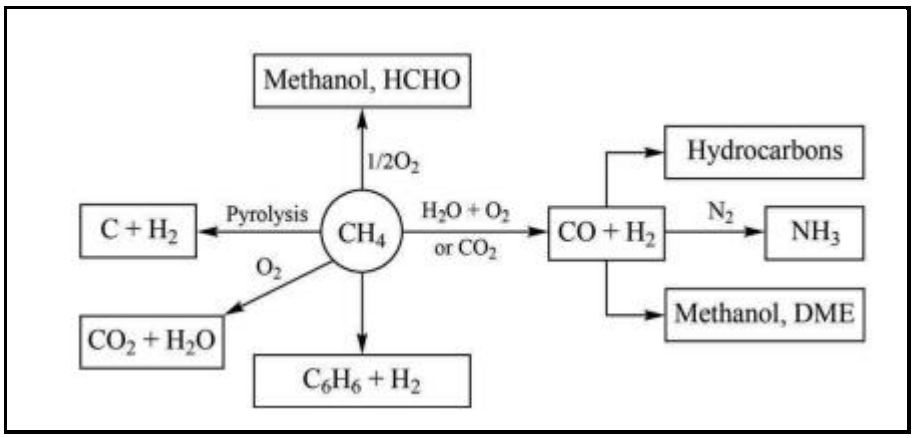

Figure 2-1. Different routes of methane conversion. Adapted from (Wenlong 2000)

2.1.4 Applications of methane conversion products.

Successful nonoxidative conversion of methane yields hydrogen and various grades of C_2 hydrocarbons and higher carbon hydrocarbons. However, major petrochemical chemical products arising from nonoxidative conversion of methane are, but not limited to the following: hydrogen, ethane, ethene, benzene, toluene, xylene, and naphthalene. These petrochemicals find numerous applications both in domestic and industrial sectors.

Hydrogen gas can be used in many industrial sectors, including chemicals, pharmaceutical, paint, textile fibre manufacturing, glass, electronics, and metallurgy. Hydrogen combined with a fuel harbours potential to produce clean energy since it makes it possible to produce electricity directly on-board electric vehicles. It is also used as a fuel for rocket launchers. It can be used in environmental preservation as a scrubber of Sulphur that is naturally contained in oil to produce cleaner fuels.

Ethane being one of the key products from NOCM reaction is used in the production of ethylene for making plastics, anti-freeze agent and detergents, a ripening agent for foods, a refrigerant, a substance in production of welding gas and a primary ingredient in mustard gas. Ethane can also be used directly as a fuel for power generation, in pure form and also when blended with CH_4. Ethene is used in the production of ethylene glycol (1,2-ethanediol) which is used in automotive

as an antifreeze agent and as a precursor to polymers. It is used in the production of polymers such as polyethylene (PE), polyvinyl chloride (PVC), polystyrene (PS), and polyester. Low-density polyethylene and linear low-density polyethylene are used in making both food and non-food packaging materials, sandwich bags, cling wraps, liners for tanks and ponds, shrink and stretch film, squeeze bottles, and as moisture barriers in construction. Ethene is also used in production of ethanol (industrial alcohol), which is used as an organic solvent. Ethene derivative, vinyl acetate monomer is used in adhesives, paper coatings, paints, and barrier resins. It is also used in the production of styrene. Polymerization of styrene leads to the formation of polystyrene which is used as synthetic rubber.

Propane is commonly used for space and water heating, for cooking, and as fuel for engine applications such as forklifts, farm irrigation engines, fleet vehicles, and buses. When used as vehicle fuel, it is called propane Auto gas. Butane, a colourless gas with almost the same odour as natural gas is used in aerosol propellant as a fuel source, and in making chemicals for solvents, rubber, and plastic industries.

Benzene is a widely used industrial chemical. It is found in crude oil and it is a major part of gasoline and it can also be produced naturally from volcanoes and forest fires. Being one of the key products of NOCM reaction, benzene is used in the manufacture of plastics, resins, synthetic fibres, rubber, lubricants, dyes, detergents, drugs, and pesticides. Toluene can be used as an octane booster in gasoline fuels used in internal combustion engines. Absolute toluene can be used as a fuel for both two-stroke and four-stroke engines. Toluene solvent is used in carbon nanotubes like fullerenes, and as a cement for fine polystyrene kits. Biological applications of toluene include breaking or disrupting red blood cell to extract haemoglobin in Biochemistry.

Xylene is the principal precursor to terephthalic acid and dimethyl terephthalate. These two monomers are used in the production of polyethylene terephthalate (PET) plastic bottles and polyester clothing. O-xylene is an important raw material for making phthalic anhydride. It is substituted for toluene where slow drying is required and thus used by conservators of art objects in solubility testing. In histology, xylene is used as a clearing agent. Xylene is used to remove paraffin from dried microscope slides prior to staining. Naphthalene is used as a mouth repellent and in commercial production of phthalic anhydride. It is used in making insecticide and tanning

agent. Other uses of naphthalene include but not limited to the manufacture of dyes, explosives, and synthetic resins.

2.2 Methane conversion technologies

To exploit full potential of natural gas, various methods have been employed with an attempt to break down methane gas into carbon nanomaterial and more useful petrochemicals. Some of the methods used include; methane decomposition (García-Sancho *et al.* 2018), pyrolysis of methane (An *et al.* 2018), aromatization of methane (Li *et al.* 2018) and oxidative coupling of methane (Karakaya *et al.* 2018). In oxidative methane coupling process kinetics (Varghese *et al.* 2018), a methane molecule first dissociates on the metal to form M-CxHy, and then proceed to form ethane and ethylene before reacting with metallic oxide to form metallic carbide. The formed carbide is either transformed into benzene or the carbonaceous deposit is reacted with M-H to form benzene.

Methane conversion into different products can further be divided into direct and indirect methods. In direct method, natural gas is converted into higher hydrocarbons without production of syngas (mixture of CO and H_2). The indirect method involves the production of syngas mainly from steam reforming, dry reforming or partial oxidation followed by a Fischer-Tropsch process that converts the syngas into higher hydrocarbons. The direct method is therefore advantageous as it eliminates the intermediate step of syngas production which is energy intensive (Majhi *et al.* 2013a). Figure 2-2 shows direct and indirect mature methane conversion technologies which are further classified based on the process operating temperature.

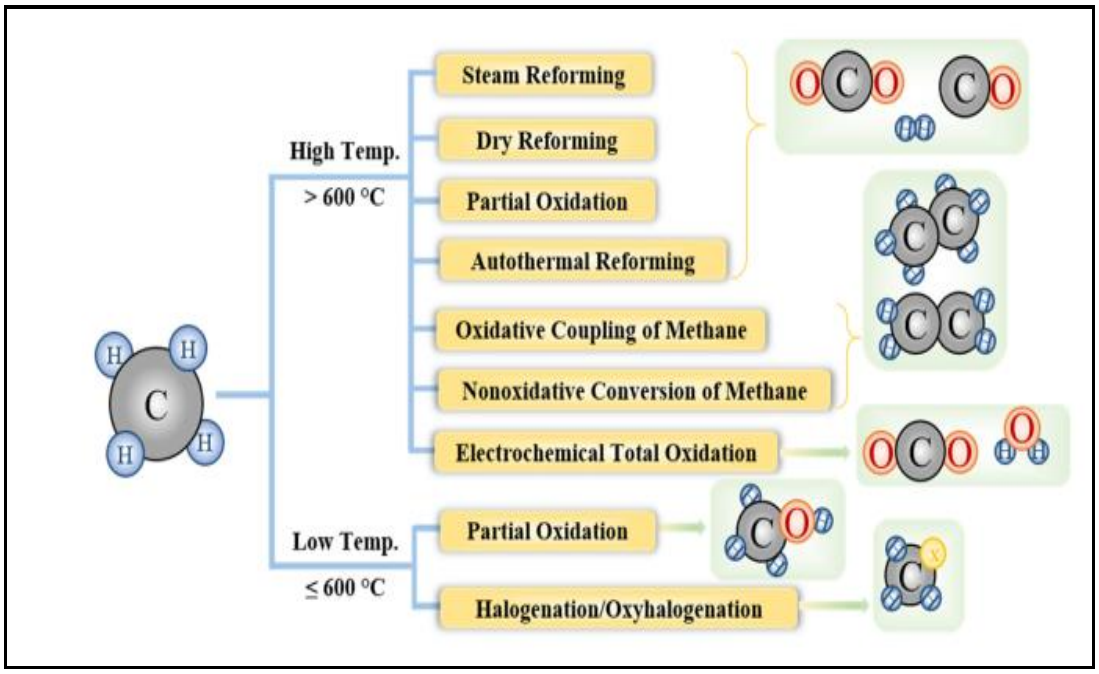

Figure 2-2. High temperature and low temperature methane conversion technologies. Adapted from (Majhi *et al.* 2013a)

2.2.1 Direct methane conversion

Converting methane directly to higher hydrocarbons has been studied over the last 5 decades using the following approaches.

- Thermal and catalytic pyrolysis of methane
- Oxidative coupling of methane
- Partial oxidation of methane
- Other processes (such as halogenation, plasma, photo catalysis, membranes, etc.)

Thermal oxidative coupling of methane or methane pyrolysis can yield acetylene as the main product. Other notable products in this reaction are ethylene, benzene and hydrogen provided coking is avoided (Holmen *et al.* 1995) . Coking by formed carbon can be avoided by using short reaction times, high methane partial pressures and by incorporation of hydrogen in the feed. Acetylene can also be produced at higher operating temperatures ($<$ 2000K) and short reaction time ($>$ 10^{-2} s).

In oxidative coupling, methane and oxygen react over a suitable catalyst to form C_2H_6 and C_2H_4 hydrocarbons. The single pass yields of C_2 products and is usually limited to a conversion of

less than 25% and C_2 selectivity of about 80%. Despite intensive research in this area, this technology has not yet been commercialized due to the following challenges: C_2 hydrocarbons are more reactive than methane itself, low methane conversion, high reaction temperatures, and unavailability of commercial high thermal stability catalysts.

Partial oxidation of methane to methanol was first demonstrated by Blair and Wheeler (Du *et al.* 2006). It is a process of converting methane directly into oxygenates, particularly methanol and formaldehyde. This reaction is usually conducted in quartz and Pyrex glass-lined reactors to avoid contact of feed gas with the metal wall due to possible reaction with the reactor wall. From reported results, a selectivity of 30-40% at a conversion of 5-10% at 723-773K and pressure of 30-60 bar were achieved (Lodeng *et al.* 1995). Catalysts based on iron such as; Fe/SiO_2 (Kobayashi *et al.* 1996), Fe/ZSM-5 (Michalkiewicz 2004), FeOx/SBA-15 (Zhang *et al.* 2009), and $FePO_4$) have displayed remarkable results in direct methane conversion.

2.2.2 Indirect methane conversion

Most commercial processes based on methane conversion to petrochemicals and fuels are done using indirect methods via the synthesis gas. The production of synthesis gas ($CO+H_2$) is achieved through the following processes.

- Steam methane reforming
- Dry carbon dioxide reforming
- Partial oxidation of methane
- Auto thermal methane reforming

Steam methane reforming is the most industrially developed process of producing hydrogen from methane. The process involves transformation of CH_4 and H_2O (steam) into syngas according to the following equation.

$$CH_4 + H_2O \rightleftarrows CO+3H_2 \qquad (\Delta H_{298} = 206\text{kJ/mol} \qquad (4)$$

Steam and carbon monoxide are converted into CO_2 and hydrogen in an exothermic water gas shift (WGS) process. The reaction takes place according to the following equation.

$$CO + H_2O \rightleftarrows 2CO_2+2H_2 \qquad (\Delta H_{298} = -41.2\text{KJ/mol} \qquad (5)$$

Production of synthesis gas was first reported by Neumann and Jacob in 1924 (Enger *et al.* 2008). In this process, nickel supported on various supports (Al_2O_3, MgO, $MgAl_2O_4$, and ZrO_2) is a preferred industrial catalyst because it is cheap, and has high catalyst activity in methane conversion (Rostrup-Nielsen 1984). Remarkable results for this reaction have been achieved at temperatures 900-1000℃ and 1.5-3 MPa pressure with volume flow rates of 1000 h^{-1} (Rostrup-Nielsen *et al.* 2002). The major challenges of this process technology are rapid catalyst deactivation due to coking, affected by impurities such as sulphur present in methane feed, sintering of the nickel crystallites due to high reaction temperatures leading to loss of catalyst active surface area. This leads to low catalyst activity over time (Rostrup-Nielsen and Christiansen 1995), high cost of overhead steam, CO_2 formation in huge quantities, and the syngas formed is not suitable for methanol and hydrocarbon synthesis by the Fischer-Tropsch method.

Dry reforming of methane entails the reaction of methane with a readily available greenhouse gas like carbon dioxide to generate syngas. The reaction is represented by the following equation.

$$CH_4 + CO_2 \rightleftarrows 2CO + 2H_2 \qquad (\Delta H_{298} = 247 kJ/mol) \qquad (6)$$

It is an exothermic process catalysed by transition metal catalysts supported on metal oxides. Methane conversion studies by (Wang *et al.* 2007) revealed that cleavage of C-H bond is the rate limiting step for the reaction and it is facilitated by noble metal catalysts. It has been suggested that if the metal is supported on basic or acidic oxides, it occurs on the oxide whereas on more neutral supports the activation of C-O takes place on the metal surface. In dry reforming reaction (Mokrani and Scurrell 2009), platinum group metals (Pompeo *et al.* 2007), and iron group metals supported on various supports are used. The draw backs of this method are catalyst deactivation, carbonisation, and the presence of ethane in the syngas which calls for further purification. The use of basic supports such as; CeO_2 and La_2O_3 has been found to minimise carbon formation by aiding dissociation of CO_2 with low energy barriers via the formation of oxy-carbonates and providing surface oxygen atoms which facilitate the removal of surface C atoms formed during the C-H bond activation in methane (Djinović *et al.* 2012).

Partial oxidation of methane involves integrating oxygen separation and catalytic reaction to yield syngas which is an important feedstock for the downstream process. However, the major drawback of this method is the requirement of high reaction temperature (> 850℃) which hampers catalyst thermal stability (Elbadawi *et al.* 2020). In this process, complete methane conversion can be achieved at much lower temperature (~750℃) using nickel and catalysts based on noble metals (Majocchi *et al.* 2000). The net cost of syngas production by partial oxidation of methane is about 1.5 times lower than that produced by steam methane reforming. Despite lower syngas production cost, this process is associated with high cost of oxygen, explosion risk, catalyst destruction due to local overheating, and formation of catalyst residues. Production of syngas is an energy-consuming process which significantly diminishes the competitiveness of the chemical products from methane compared with their production form crude oil. Capital investment on process equipment is another challenge associated with reforming of methane to syngas (Holmen 2009).

Auto thermal methane reforming (ATR) is a combination of steam reforming and partial oxidation reactions. It is an advantageous process for syngas production both technically and economically due to opposite contribution of the exothermic methane oxidation and endothermic steam reforming. A combination of these two processes improves reactor temperature control, reduces dangers of explosion due to remote heating, and limits catalyst deactivation by sintering or carbon deposition. It also allows for generation of syngas of various H_2/CO ratio through manipulation of the relative concentrations of H_2O and O_2 in the feed (Wilhelm *et al.* 2001). It has been reported that $Pt/ZrO_2/Al_2O_3$ catalyst systems are effective formulations for CO_2 reforming of methane (Souza *et al.* 2001), partial oxidation (Souza and Schmal 2003) and steam reforming (Souza and Schmal 2004).

Dehydro-aromatization of methane to produce benzene and hydrogen over a zeolite (HZSM-5) in a fixed-bed reactor was first reported in 1993 by (Wang *et al.* 1993). Subsequently, various transition metals supported on HZSM-5 were tested to develop a stable catalyst for the reaction. From the catalysts tested, Mo/HZSM-5 showed outstanding results (Ding *et al.* 2001). The outstanding results of this catalyst was attributed to its structural framework (Majhi *et al.* 2013a), active sites located in the pores or channels in the zeolite in terms of shape, and pore size. The products formed in the reaction depended on the properties of the zeolite. Given that the HZM-

5 structure is two-dimensional, porous, and with a pore diameter close to dynamic diameter of a benzene molecule, its use as catalyst support favours the formation of other products (Majhi *et al.* 2013a). In oxidative conversion of methane, O_2 is mixed with CH_4 in the feed. In this case, methane molecules are activated through haemolytic splitting on the catalyst surface to form methyl radicals as a result of interaction with O^- species (Okolie *et al.* 2018). The basicity of a catalyst plays a major role in a sense that, at first methane first splits into CH^{3+} and H^+ on the catalyst surface and then the CH^{3+} species are transformed into methyl radicals. Despite intensive research in this area, no catalyst has been formulated to give selectivity towards C_2 yield of more than 25% and selectivity to higher hydrocarbons by more than 80% (Chen *et al.* 2018).

In oxidative coupling, methane reacts with oxygen over a catalyst forming CH_3* radicals on the surface of the catalyst. These CH_3* radicals react further with methane gas to form ethane. Dehydrogenation of ethane leads to the formation of ethylene. This process has not attracted much attention due to low yields and low product selectivity. In the recent past, non-oxidative conversion of methane has been explored by researchers to study the reaction mechanism (Karakaya *et al.* 2018).

Non-oxidative conversion of methane can proceed via different pathways depending on the catalyst used and the reaction conditions. Remarkable catalyst activity takes place at temperatures (>800℃). Globally recognised reactions (Karakaya and Kee 2016), are as follows.

$$CH_4 \rightarrow C + 2H_2 \quad (7)$$

$$2CH_4 \rightarrow C_2H_6+H_2 \quad (8)$$

$$2CH_4 \rightarrow C_2H_4 + H_2 \quad (9)$$

$$6CH_4 \rightarrow C_6H_6 + 9H_2 \quad (10)$$

$$7CH_4 \rightarrow C_7H_8 + 10H_2 \quad (11)$$

$$8CH_4 \rightarrow C_8H_{10} + 11H_2 \quad (12)$$

$$10CH_4 \rightarrow C_{10}H_8 + 16H_2 \quad (13)$$

Major products of non-oxidative conversion of methane are carbon and petrochemicals. Olefins (ethene, propene, butene and butadiene) are important industrial chemicals. Ethylene and propylene are important sources of plastic products and rubber. Aromatics like benzene, toluene, and xylenes (BTX) find a lot of application in chemical industries. Benzene is a raw material for making dyes and synthetic detergents, and both benzene and toluene are suitable raw materials for making polyurethanes. Manufacturers use xylenes to produce plastics and synthetic fibres.

2.2.3 Other methane conversion processes

2.2.3.1 Low temperature total oxidation

This reaction is employed purposely to minimize methane emissions from automobile exhausts. Popular catalysts for this reaction are palladium-based supported on oxides which enable the process to take place at low temperature (<400℃). Further, it has been demonstrated that encapsulation of Pd crystallites with reducible oxides such as ceria, can greatly enhance the activity and stability of these catalysts (Cargnello *et al.* 2012). The improvement in catalytic activity and stability of these catalysts is linked to the structural and chemical properties of the Pd-O-Ce moieties (Colussi *et al.* 2009).

2.2.3.2 Halogenation and oxyhalogenation of methane

In this process, activation of the C-H bond in methane is based on halogenation and oxyhalogenation (Peringer *et al.* 2009). The reaction chemistry of halogen involves reacting methane with a halogen (mostly Cl_2 and $Br_{2)}$ under mild reaction conditions to yield methyl halides (CH_3X) which can be transformed by catalytic hydrolysis reactions to yield; oxygenates, alkanes, olefins, and aromatics. In oxyhalogenation, the C-H bond in methane is activated by a reactive halogen that is formed by oxidation of a hydrogen halide with O_2. The formed alkyl halide then reacts to produce aromatics or olefins via coupling reactions (Podkolzin *et al.* 2007). Although halogenation reactions are attractive owing to relatively low energy barrier for methane C-H bond activation via the halogen, the process is confounded by challenges such as regeneration of the halogen to close the cycle.

Various attempts have been made by researchers to address the problem of halogen regeneration. From literature (Li and Yuan 2006), halogen regeneration problem could be overcome by adopting a direct catalytic partial oxidation of methane to methanol and dimethyl ether over

$MoO_2Br_2(H_2O)_2$ supported on Zn-MCM-48. This process entails forming Br_2 by decomposition of $MoO_2Br_2(H_2O)_2$ in the presence of oxygen, followed by halogenation of methane to form CH_3Br species, which is further transformed into oxygenated products by reaction of MoO_3 simultaneously with the regeneration of the MoO_2Br_2 species. This reaction is regarded as a closed pathway for partial oxidation of methane such that the efficiency of each step in the process is optimized to enhance product selectivity. There are different halogen based CH_4 activation routes that generate MeX (M-CH_3; X-Cl or I) intermediate that can later be catalytically combined to yield value added chemicals.

In gaseous halogenation for C-H bond activation**, s**ingle halogen methanes (CH_3Cl or CH_3Br) are analogous to CH_3OH in the production of higher hydrocarbons and oxygenates. Methane halogenation using gaseous reactants is a typical example of the conventional electrophilic substitution reaction. Studies on solid superacid by (Olah 1987) showed that high selectivity to monohalogenated methane i.e. CH_3X, a desired intermediate for further heterogeneous coupling reactions could only be achieved via methane to halogen ratio of 10:1 either thermally or photochemically. The same research group used methane and halogen (Cl or Br) and passed them through a solid acid catalyst like Fe_2OCly/Al_2O_3, $ZrOF_2/Al_2O_3$, and $Pd/BaSO_4$ at 200-250℃ and atmospheric pressure. These catalysts showed over 90% selectivity towards monohalogenated methane and methane conversion of up to 58%. From this study, they concluded that the reaction mechanism consisted of an insertion of a surface halogen species or electron deficient metal site into methane's C-H bond leading to the formation of a five-coordinated carbonium ion followed by bond cleavage to give CH_3X. Results from his work was in agreement with what was reported elsewhere (Degirmenci *et al.* 2005). From the two studies, they concluded that the formed dibromoethane (CH_2Br_2) deposits coke during the coupling reaction. To address this challenge, a small amount of I_2 in the mixture with bromine resulted in a very selective monobromination with Br_2 via a secondary (repropriationation) reaction as shown in the following equation.

$$CH_2Br_2 + CH_4 = 2CH_3Br,\ \Delta Gr^0_{298K} = -0.07kJ/mol \qquad (14)$$

Catalyst deactivation due to coking of dibromomethane was also addressed via Pd_6C/SiO_2 catalyst conversion to higher hydrocarbons and using Ru/SiO_2 to convert CH_2Br_2 to CH_3Br (Ding *et al.* 2012). In CH_4 oxyhalogenation on metal oxides and phosphate catalysts, the yield

of monohalogenated species takes place according to the following globally recognized equation.

$$CH_4 + HCl(HBr) + \frac{1}{2}O_2 \rightarrow CH_3Cl(CH_3Br) + H_2O, \ \Delta Gr^0_{298K} = -145.45\ (-152.59) kJ/mol \qquad (15)$$

Metal oxides and phosphate catalysts (Liu *et al.* 2010) as well as Rh/SiO_2 (Liu *et al.* 2010), CeO_2 (He *et al.* 2012), and Ru/SiO_2 are active for generation of both CO and CH_3Br. The design of these catalysts is tailored towards functioning and facilitating both monobromination and partial oxidation of CH_4 simultaneously to yield CO and CH_3Br which would have passed on to the next step of converting them to CH_3COOH. Metal oxides lacking facile redox ability such as BaO can be employed to replace the supported Ru and Rh catalysts leading to much more economic activity (Lin *et al.* 2009). The main problem with these catalysts is rapid deactivation due to aggregation of barium particles and prevention of metathesis between BaO and $BaBr_2$ from taking place. Oxybromomination of CH_4 based on iron phosphate supported on silica (Lin *et al.* 2010) is another class of active catalysts. When this catalyst was used, 50% methane conversion with total selectivity towards CO and CH_3Br of 95% with the ratio of main products being equimolar.

2.2.3.3 Electrochemical oxidation

This is a direct route of generating electricity from methane. Popular electrochemical systems for direct electrochemical methane oxidation are solid fuel cells (SOFCs). These devices have the potential to convert the chemical energy of combustible fuels such as hydrogen, carbon monoxide, and hydrocarbons into electrical energy. The cathode in SOFCs is responsible for reducing the gas-phase oxygen into oxygen ions in the presence of electrons. Oxygen ions are then transported through an ion conducting oxide such as Yttria stabilized zirconia (YSZ) to the SOFC anode, the electrode where the fuel is fed and oxidized in the presence of the oxygen ions to CO_2 and H_2O, thereby releasing electrons to an external circuit. The main challenge of this conversion technology is rapid deactivation of the conventional anode electro catalyst (Ni) due to carbon poisoning (Takeguchi *et al.* 2002). Several attempts have been made in previous research to circumvent around this challenge. One such mitigation measure is to develop a SOFC anode electro catalyst that can resist carbon poisoning. From another research group (Gorte and Vohs 2003), it was demonstrated that replacing Ni/YSZ with Cu/CeO_2/YSZ anodes led to an improvement in carbon-tolerance during on-cell electro-oxidation of methane. Another

study on electrochemical oxidation of methane (Nikolla *et al.* 2009) revealed that tin and nickel-based SOFC anode electro catalyst demonstrated improved tolerance to carbon-induced deactivation relative to conventional monometallic nickel electro catalysts. More research into this area focused on identification of carbon-tolerant anode electro catalyst for direct electro-oxidation of methane in SOFCs have paid more attention on the use of mixed ionic-electronic conducting oxides as anode electro catalysts (Pillai *et al.* 2008). Despite substantial breakthroughs on the use of mixed ionic-electronic conducting oxides, their catalytic activity towards methane electro-oxidation was much lower than that obtained by the nickel-based anodes.

2.2.3.4 Photochemical conversion

Photochemical methane conversion entails using a combination of deep ultra-violet (UV) in the range of 180-200 nm to break a very strong C-H bond (Sastre *et al.* 2011). Using this method, C_1 oxygenates were obtained with CH_4 conversion of up to 13% on 1g of commercial beta 811 zeolite with formic acid, formaldehyde, and CH_3OH in the condensed phase after 1h irradiation. This reaction achieved 95% conversion when oxygen was present. Theoretically, this reaction has been found to yield reactive HS* and H* radicals in the presence of 200 nm light to convert CH_4 into CH_3SH which is an active intermediate that can later be transformed into methanol to olefins (MTO)-like process using well known pathways (Baltrusaitis *et al.* 2013). These two processes (direct splitting of C-H bonds and external reactant facilitated) require high energy UV lights and high electricity supply.

Studies on photochemical activation of methane in the presence of water was done by (Ogura and Kataoka 1988). Results from their study revealed that that the dominant product was CH_3OH ($\sim$70% at 90℃) followed by formic acid (11%), ethanol (5%), acetone (4%) and acetic acid (3%) at the same temperature. This was because of the hydroxyl radical formation from the photolysis of water at less than 100℃. In a halogen inspired photocatalytic process, a chlorine radical mediated photocatalytic C-H bond activation on TiO/BiOBr photo catalyst was able to proceed under visible light ($420 < \lambda < 780$) nm in the presence of oxygen at ambient temperature with selectivities ($>$85%) towards C(sp^3)-H bond activation. Chlorine radicals formed on a photo catalyst surface acted as active centres eventually leading to oxygenated organic compounds.

2.2.3.5 Dry (carbon dioxide) photocatalytic reforming of methane

Dry (carbon dioxide) photocatalytic conversion of methane occurs via the following Globally recognized equation.

$CH_4 + CO_2 \rightarrow 2CO + 2H_2$ (ΔG_{298K} = 171 kJ/mol) $\rightarrow$ hydrocarbon, oxygenates (16)

Products from the reaction consists of a variety of oxygenated compounds produced in a single step, different from those obtained from reforming syngas. To achieve this conversion, various band gap semiconductors have been used; Beta-Ga_2O_3, Cu/Cds-TiO_2/SiO_2 (Shi *et al.* 2004), ZrO_2 (Kohno *et al.* 2000), ZnO (Mahmodi *et al.* 2013), TiO_2, and copper phthalocyanine modified TiO_2 (Yazdanpour and Sharifnia 2013) on stainless steel mesh and on MgO (Teramura *et al.* 2004). Even though quite a number of oxygenates like acetic acid, ethane, acetone, and carbon monoxide were obtained, economic viability of this process is very low considering the fact that residence times required are very long. In another study on photocatalytic conversion of methane, a photochemical reforming process on non-metal oxides was reported using transition metal chalcogenide photo catalyst (Chianelli and Torres 2013). In this process, a series of metal sulphides including RuS_2 in a UV light reactor with a CH_4: CO_2 (50%:50%) stream was used to produce a wide range of unknown paraffins, olefins, and alcohols. Despite the yield of wide product range from this process, the overall efficiency is very low. A better approach to tackle these drawbacks could arise from combining both conventional heterogeneous catalysis utilizing catalysts or reactants that have a strong plasmon or photo electrochemical response with light or electron enhanced processes.

2.3 Fundamentals of non-oxidative conversion of methane

Non-oxidative methane conversion to benzene over Mo/HZSM-5 catalyst has been studied close to 3 decades from now. Work on this catalyst was first reported in 1993 (Wang *et al.* 1993). Among all the catalysts studied by several research groups, Mo/HZSM-5 has stood out as the best catalyst for non-oxidative conversion of methane (Zhang 2019) because it catalyses the reaction in a bifunctional manner. Its bifunctional mechanism occurs when the Mo sites located inside the zeolite channels work on activation of C-H bonds in CH_4 and formation of C_2 intermediates (C_2H_6, C_2H_4, and C_2H_2) (Meriaudeau and Ha 2000) and the nearby free Bronsted acid sites provide the center for cyclization and aromatization of C_2 intermediates into benzene and its derivatives (Zhang 2019). Using the same catalyst, 70% selectivity towards benzene and

20% selectivity to naphthalene have been achieved due to shape selectivity of the zeolite channels. Benzene has a kinetic diameter of 5.8Å, slightly larger than the channel diameters of HZSM-5 zeolite (5.3 X 5.6Å and 5.1 X 5.5Å). Non-oxidative conversion of methane reaction can occur as a low-temperature two-step methane coupling reaction or one-step high temperature coupling reaction (Choudhary *et al.* 2003). According to (Amariglio *et al.* 1995) , when 6%wt Pt/SiO_2 catalyst was flushed with hydrogen at 250℃, C_2 to C_7 hydrocarbons formed with benzene being the main product. This is a typical illustration of a two-step low-temperature NOCM reaction.

At high temperatures, methane conversion entails step-wise dehydrogenation (Holmen *et al.* 1995) as shown in the following equation.

$$2CH_4 \overset{H_2}{\rightarrow} C_2H_6 \overset{H_2}{\rightarrow} C_2H_4 \overset{H_2}{\rightarrow} C_2H_2 \overset{H_2}{\rightarrow} 2C \qquad (17)$$

In equation 17, hydrogen is produced as a reaction product without involving an oxygen containing species, hence selectivity towards C_2H_6 and C_2H_4 could be increased. Formation of graphitic coke is more prevalent than that of Aliphatics (C_2H_6 and C_2H_4). At 500℃, equilibrium conversion of C_2H_6 and C_2H_4 were 0.6% and 1% respectively. Due to thermodynamic limitations of the NOCM process, (C_2H_6 and C_2H_4) are formed at high temperatures. Based on Gibb's free energy change, converting methane directly to C_2H_6 and C_2H_4 is only possible at (>725℃) with remarkable formation of C_2H_4 than C_2H_6. At 900℃, methane conversion to C_2H_6 was only 5% with higher selectivity towards aromatics than ethylene.

2.3.1 Formation and nature of active sites

Non oxidative methane conversion occurs in three distinct phases: (i) initial C-H activation of methane by dehydrogenation; (ii) C-C coupling to ethylene and subsequent oligomerization; (iii) aromatization at the Bronsted acid sites of the zeolite (Sim *et al.* 2020). With respect to iron, carburized (Fe_3C) is the active species formed during the induction period. Activation of methane molecules occurs on the Fe_3C sites (Denardin and Perez-Lopez 2019).

From literature (Tan 2016), it has been established that the stability of carbene, a primary intermediate of activated methane plays an important role in conversion of methane to carbon or to C_2-hydrocarbons. Carbene is usually unstable on metallic sites and therefore its C-H bond splits further to produce hydrogen. Conversely, F_2C can stabilize carbene by formation of metal-

carbene complex (C-Fe=CH_2) so that carbene can dimerize into ethylene, which further oligomerizes into aromatics on the acid sites. This shows a relationship between the degree of carburization and catalyst performance whereby, a highly carburized catalyst material possesses higher selectivity towards the aromatics and vice versa.

Methane hydrogenates and dimerizes on Mo species when Mo/HZSM-5 catalyst is used (Solymosi *et al.* 1999). A lot of research on bifunctional catalysis of Mo/HZSM-5 (Wang *et al.* 1993) revealed that MoO_3 crystallites were the active sites for methane activation. An interaction between MoO_3 and the acid sites of the HZSM-5 constitute the active component of the catalyst (Zhang *et al.* 1998). Calcining molybdenum catalyst precursor (Ammonium heptamolybdate) and HZSM-5 at 673-773K yields MoO_3 catalyst. During calcination, the MoO_3 species diffuses into the HZSM-5 where it interacts with the Bronsted acid sites. Once inside the zeolite channel, the MoO_3 reacts with H^+ associated with Bronsted acid sites to form $[MoO_2(OH)]^+$ species, which condenses to form $[MoO_2(H_2O)]$ dimers and H_2O according to the following scheme.

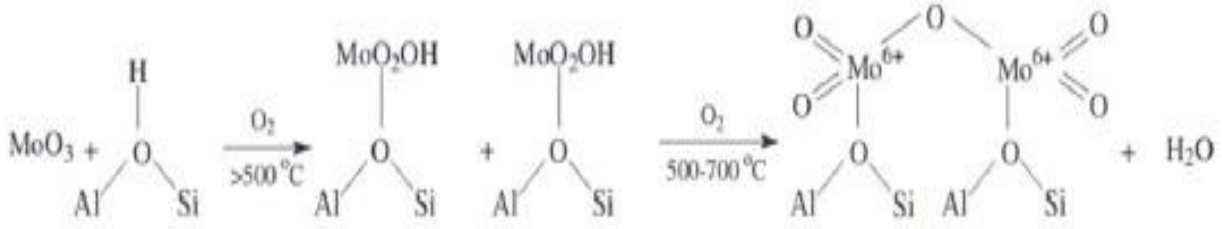

Scheme 1. Formation of a coordinated $[Mo_2O_5]^{2+}$ dimer on Bronsted acid sites

According to (Li *et al.* 2000), the molybdenum species anchored on the Bronsted acid sites both as $[Mo_2O_7]$ dimer and MoO_4 tetrahedral monomer. They also concluded that there was a possibility of $[MoO_2(OH)]^+$ species reacting with the OH groups to form $[MoO_2]^{2+}$ monomer. The resultant monomer was held on two bridging acid sites as shown in scheme 2.

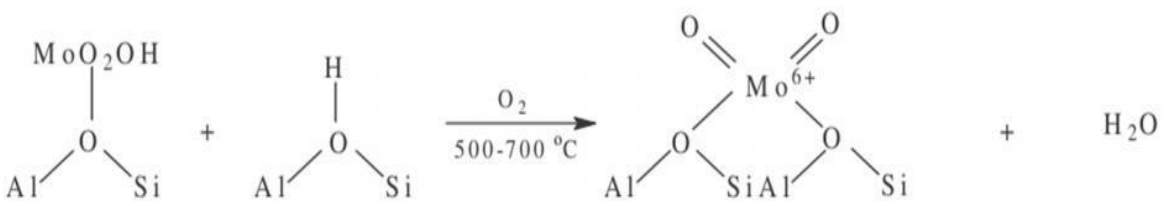

Scheme 2. Formation of $[MoO2]^{2+}$ cation bridging two Bronsted acid sites.

Calcining precursors of the Mo/HZSM-5 at temperatures in excess of 973K destroys the catalyst structure such that the extra-framework aluminium atoms reacts with Mo to form aluminium molybdate which is an irreducible species (Mestl and Knözinger 2008). Formation of this irreducible species was also confirmed by (Zaikovskii *et al.* 2006). High zeolite Si/Al ratios favour the growth of dimeric species as shown in scheme (2) while low Si/Al ratio favours the formation of monomeric structures.

Preparation of MoHZSM-5 has been done severally by incipient wetness impregnation (IWI) where an aqueous solution containing $(NH_4)_6Mo_7O_{24}$ ammonium heptamolybdate is made to fill the zeolite pores up to the point of incipient wetness, above which it becomes wet. In the impregnating solution, Mo exists as $Mo_7O_{24}^{6-}$, an ion that does not fit into the pores of the zeolite and therefore remains on the outer surface of the zeolite. Upon increase in temperature (calcination) $Mo_7O_{24}^{6-}$ is transformed into MoO_3 moieties which can migrate into the zeolite channels and anchor there (Ma *et al.* 2000b). Calcination step is done at a desired temperature ramping of 0.5-2K/min to avoid fast expansion of the liquid in the zeolite pores which can damage its ability to facilitate migration of the Mo species and cause agglomeration. From literature on preparation of Mo/HZSM-5 catalyst (Kosinov *et al.* 2017) , calcination is done between 773 and 973K. Calcining the Mo/HZSM-5 at 873K is preferred for good dispersion of the Mo species in the zeolite, retention of the zeolite structure, and limiting the extraction framework Al to form irreducible Al_2MoO_4 which is catalytically inactive.

As reported elsewhere (Lezcano-González *et al.* 2016b), MoO_3 powder can be mixed directly with the zeolite and calcined. This process is called solid ion exchange (SIE). The volatility of MoO_3 enables it to migrate into the zeolite channel pores. However, MoO_3 has a high melting point of 1068K, hence it starts to evaporate at around 973K in an inert atmosphere.

2.3.2 Effect of Zeolite pore structure on catalyst activity

ZSM-5 zeolite is a 3-dimensional pore structure that consists of both straight and zigzagging pores and their intersections. The two structures are formed by a 10-membered oxygen ring with entrance (~5.5 Å) in diameter. One pore is straight with an elliptical cross-section, while the second type has a circular cross-section. The straight pores are linked by zigzag channels. The effective pore diameter of ZSM-5 is 5.9Å which is almost equal to the kinetic diameter of benzene (5.8 Å). This is the reason why Mo/HZSM-5 exhibits higher selectivity towards benzene and its derivatives. Altering Si/Al ratio of HZSM-5 with phosphorus and rare earth (RE) oxides gives rise to ZRP-1 zeolites. These types of zeolites are prepared using the concept of blocking the active acid sites on the outside surface of ZSM-5 using rare earth oxides. This is done to enhance their catalytic activity which arises from dealumination and evolution of various P- and Al- containing compounds inside the pores hence decreasing the channel size (Shu *et al.* 2000a).

Zeolite MCM-22 has larger pores than those of ZSM-5 and is made up of a 12-membered oxygen ring with dimensions 18 x 7.1 x 7.1Å connected through a 10-membered ring window. The interconnecting building unit in MCM-22 forms two independent pore units; Two-dimensional sinusoidal 10-member interlayer channels 4.0X5.9Å and 12-mebered interlayer cages of 7.1X 8.1Å with 4.0X 5.9Å entrance apertures.

ZSM-11 has a tetragonal crystal lattice and a two-dimensional pore structure consisting of straight, perpendicularly intersecting channels, the pores have a 10- membered oxygen ring and have dimensions of 5.1 x 5.5Å. It has a pore structure which resembles that of ZSM-5. ZSM-8 structure is orthorhombic and has a two-dimensional system of channels with an average entrance aperture of ~5Å. SAPO-34 has 8-membered oxygen rings with narrow pores of ~4.3Å which limits diffusion of aromatic compounds. In β-zeolite, there exists three crystal systems (tetragonal, anorthic, and monoclinic) which are highly irregular and have many defects. This type of zeolite has a two-dimensional structure with pore entrance dimensions of 6.6 x 8.1Å, and 5.5 x 6.5Å.

Other zeolite materials like X, Y, SAPO-5, and SAPO-11 have large pores with a three-dimensional straight channels, super cages, and large pore entrance diameter of ~7.5Å which is much larger than that of benzene molecule. The zeolite pore structure plays a role in catalytic

activity of different catalysts in NOCM reactions. Modification of Mo catalyst with porous materials containing pores with diameters of 5.3-5.6 Å (ZSM-5, MCM-22, ZSM-11, and ZRP-1), which is close to kinetic diameter of benzene molecule are considered superior catalysts for NOCM reaction. Conversely, modifying Mo-based catalysts with zeolites whose pore sizes are greater than 6Å reduces their catalytic activity. Such catalysts suffer rapid deactivation due to coking (Baba and Miyaji).

2.3.3 Effect of Zeolite Si/Al ratio on the structure of Mo species on HZSM-5

After calcination of Mo/HZSM-5 catalyst, the Mo species may exist as species II ($Mo_2O_5^{2+)}$ and species III (MoO_3) while dealuminated Al species can react with MoO_3 to produce species IV and species V (molybdic complexes). It has been reported that nanostructured Mo forms on HZSM-5 (Gao *et al.* 2015). Formation of anchored species (II) and species (III) is dependent on the distance between Al atom and the next nearest Al atom in the zeolite lattice (Rice *et al.* 1999). The structure of $Mo_2O_7^{2+}$ resembled that of $MgMo_2O_7$ dimer which is considered as the standard structure of the zeolite frame work (Li *et al.* 2000). Results from density functional theory (DFT), show that MoO_2^{2+} species (III) was the dominant structure formed on HZSM-5 after calcination (Zhou *et al.* 2001).

The Si/Al ratios for ZSM-5 zeolite of the formula ($Na_n(Al_nSi_{(96-n)}O_{192}).6H_2O$) ranges from 12-1000. Since the number of Si/Al atoms in the unit cell is 96, the number of aluminium atoms per unit cell can only be more than 1 when the Si/Al ratio is smaller than 95. The sites occupied with Al or Si atoms are described as T sites. According to (Goodman *et al.* 2000), all T-sites are within 4.75Å of the axis running down the centre of the zeolite channel (Si/Al ratio <25) in HZSM-5 zeolite. From the works of (Borry *et al.* 1999), the ratio of the number of acidic protons to the number of Mo atoms in the zeolite channel (H^+/Mo) is 14.3. Results from these studies revealed that the ratio (H^+/Mo) ratio was approximately 1.24 when the Mo content in the catalyst was lower than 3.6%wt. After increasing the Mo %wt. loading to 6.3%wt, the H+/Mo ratio reduced to 0.64. This implies that, the formation of species (III) manifested more than species (II). Similar studies by (Tessonnier *et al.* 2008) on 2%Mo/HZSM-5 with the zeolite Si/Al ratio of 40 revealed that the H+/Mo was approximately 1, signifying the formation of species (II). Conversely, when 2%Mo and 4%Mo were supported on HZSM-5 with Si/Al of 15, the H^+/Mo ratio was almost 2 in each case with the formation of monomeric bidentate Mo species (III).

When the zeolite Si/Al ratio is high (low aluminium content), the distance between the Bronsted acid sites becomes too wide for this bidentate Mo complex to form (Baba and Miyaji). Therefore, the dimeric species (II) is usually formed through condensation of the two monomeric Mo species to overcome the distance between the two Bronsted acid sites.

2.3.4 The role of Bronsted acid sites

In nonoxidative conversion of methane, aromatization of alkane intermediates occurs at the Bronsted acid sites inside the zeolite channels. Most research in NOCM reactions affirm that the aromatization of C_2 intermediates is facilitated by Bronsted acid sites and not Lewis acid sites. Benzene formation on Mo/HZSM-5 is dependent on the zeolite SiO_2/Al_2O_3 ratio. According to (Liu *et al.* 1999), maximum benzene selectivity on Mo/GZSM-5 were obtained when a SiO_2/Al_2O_3 of 40 was used. In their work, they revealed that the concentration of Bronsted acid sites was maximum when the SiO_2/Al_2O_3 was 40. Increasing SiO_2/Al_2O_3 ratio beyond 40 resulted into poor catalytic activity of Mo/HZSM-5. Therefore, Bronsted acid sites greatly influence the diffusion of MoO_X species into the zeolite channel during calcination.

Higher SiO_2/Al_2O_3 ratios of the zeolite limit the migration of the MoO_X species into the zeolite channel. Depending on the catalyst preparation method, the MoO_X species could be located both on the outside and inside the zeolite channel. Those MoOx species residing on the zeolite surface are less active and less stable than those residing inside the zeolite channel (Ding *et al.* 2002). In the work of (Borry *et al.* 1999), SiO_2/Al_2O_3 ratio plays a critical role in the dispersion of Mo species in the zeolite channel. The MoO_X species replaces the zeolite proton in a 1:1 stoichiometry ratio to for $[Mo_2O_5]$ dimers. Carbonaceous deposits also anchor on the Bronsted acid sites leading to catalyst deactivation. Therefore, only small concentrations of Bronsted acid sites are required in NOCM reaction because high concentrations of Bronsted acid sites results into rapid catalyst deactivation due to coking (Tan *et al.* 2002).

2.3.5 Coke formation and catalyst deactivation

The formation of coke takes place through progressive dehydrogenation, polymerization, condensation, and cyclization of hydrocarbon species on the catalyst surface (Sahoo *et al.* 2003). Most of the formed coke from C_2 hydrocarbons and aromatics deposits on the metallic active sites and migrate into the support through condensation and polymerization reactions to form graphitic coke (Mann 1997). Linear poly-aromatics such as naphthalene, anthracene, and

tetracene are all products of graphitic coke. Operating the reactor at high temperatures and low pressures favours coke formation. In NOCM reactions, carbonaceous deposits lead to aromatization of alkane with the involvement of transition metal species and acid sites. The hydrogenating ability of metal catalysts and the condensation-polymerization capacity of the acid sites (Shu *et al.* 2000b) favour coke formation (Lee *et al.* 2012). According to (Ma *et al.* 2000a), the rate of coke formation at low %wt. metal loading in Mo/MCM-22 (0-2%wt) increases linearly with an increase in Mo loading and remains constant thereafter between (2-20%wt).

Using XPS technique, (Weckhuysen *et al.* 1998a) identified three types of carbon species deposited on the Mo/HZSM-5 catalyst when the NOCM reaction was carried out at 973K for 13hrs. The identified carbon carbide species was located inside the zeolite channels (C1 BE of 282.7 eV) while the remaining two other carbon species; (C1 BE of 283.2 eV) conforming to less-graphitic carbon and the graphitic carbon manifested at (C1 BE of 284.6 eV). Graphitic carbon was located inside the zeolite channel while the less graphitic carbon was found deposited on the catalyst surface. Even though all forms of deposited carbon can cause catalyst deactivation, hydrogen sp-type carbon is associated with catalyst poisoning because it anchors on the active sites and covers both the zeolite surface and molybdenum carbide species.

To obtain more information on the nature of deposited carbon, a lot of research in NOCM reaction using both TPO and TPR techniques has been done on Mo/HZSM-5 and Mo/MCM-22 catalysts (Liu *et al.* 2005). From the results obtained, the TPO profiles of Mo/HZSM-5 showed the existence of three oxidation peaks at different temperatures. The peaks at (459,511, and 558C) conformed to three types of carbon material i.e. (i) carbon formed on the Mo sites on the zeolite surface, (ii) carbon formed in the zeolite channels, and (iii) polymeric carbon formed on the Bronsted acid sites, respectively (Liu *et al.* 2005). From their findings, they concluded that the amount of coke associated with Mo species remained almost constant while that formed on the Bronsted acid sites became less when the catalyst was calcined at over 600℃. This is due to reduction in concentration of Bronsted acid sites at higher calcination temperatures. Therefore, in catalyst pre-treatment step, a lot of care should be taken to optimize the concentration of Bronsted acid sites in the catalyst because they are desired for aromatic selectivity, but they are also a recipe for catalyst deactivation.

Catalyst deactivation is a major concern in petrochemical industries. Since the rate of catalyst deactivation is directly proportional to the type of reaction intermediates formed, every catalyst system will deactivate differently depending on the individual process line. In steam methane reforming, only 1carbon atom out of 200 000 carbon atoms activated by the catalyst changes to coke, whereas in the cracking of heavy petroleum, 1 out of 20 carbon atoms activated by the catalyst changes to coke (Trimm 1999). In NOCM reaction, catalyst deactivation is caused by (i) covering of catalyst active sites to limit reactant and catalyst contact (Guisnet and Magnoux 2001), (ii) Blocking pore cavities of the catalyst to limit tortuosity and diffusion of methane molecules into the catalyst (Van Donk *et al.* 2001), and (iii) structural alterations thereby changing the density and strength of catalyst active sites (Tessonnier *et al.* 2008).

2.3.6 Catalyst regeneration

Coke deposition on the catalyst surface blocks its active sites hence its inability to access the reactant. Apart from coking by carbon nanomaterial, catalyst activity is affected by sintering. During methane conversion process, coke deposition on the catalyst surface is inevitable because coke is one of the products of methane decomposition; hence regeneration of encapsulated carbon at high temperatures is the only solution for an efficient NOCM process. Common methods employed for catalyst regeneration are combustion and gasification of the deposited carbon nanomaterial. In combustion, oxygen is used (Villacampa *et al.* 2003) and in gasification, steam is used (Aiello *et al.* 2000) or Carbon dioxide (Suelves *et al.* 2006). Catalyst regeneration can be accomplished using any one or combination of the following reactions.

$C + O_2 \rightarrow CO_2$ ΔH_{1073}= -394.7 kJ/mol (18)

$C + H_2O \rightarrow CO_2 + H_2$ ΔH_{1073}= 135.9 kJ/mol (19)

$C + CO_2 \rightarrow 2CO$ ΔH_{298}= 171 kJ/mol (20)

2.3.6.1 Catalyst regeneration by gasification

Both metal-based catalysts and carbon-based catalysts can be regenerated using various methods under different process conditions. Catalyst regeneration by gasification is widely used in most NOCM reactions because it prevents further oxidation, eliminates heat shocks, and increases hydrogen yields. Studies on catalyst regeneration have revealed that when 3.4 moles of hydrogen were produced from 1methane molecule, 1.4 extra moles of hydrogen were produced when

gasification method was employed for catalyst regeneration (Zhang and Amiridis 1998). The amount of carbon yield in gasification process is less compared to the amount obtained in the main methane conversion reaction. A study of the relationship between catalyst surface area and converted carbon (Liu *et al.*), revealed that higher O_2 groups were found on the lower surface area after the regeneration process followed by low carbon accumulation and higher conversion rates.

Methane conversion experiments were studied by (Choudhary *et al.* 2001) in two fixed bed reactors at 500℃ using nickel-metal oxide and nickel-zeolite catalysts followed by catalyst regeneration. From the results obtained 82:100 carbons to catalyst in grams after 6hrs were obtained and 95% of the coke formed on the catalyst was removed through gasification.

2.3.6.2 Catalyst regeneration by combustion

Combustion of formed coke on the catalyst with oxygen removes deposited carbon more efficiently compared to gasification using steam. The advantage of this method is that the process heat generated promotes continuous methane decomposition and is much faster as opposed to gasification. Regeneration of low metal %wt. loaded catalysts are easily accomplished using combustion method (Cunha *et al.* 2009) because low metal support interaction (MSI) promotes carbon accumulation at the backside of the metal catalyst.

Catalyst regeneration studies by (Saraswat and Pant 2013) on spent Ni-Cu/SiO_2 catalyst was done by passing O_2 with N_2 in a volumetric ratio of 1:3 at 550℃. Based on the results obtained, they concluded that meaningful catalyst recovery could only be achieved at high temperatures. They also observed a decrease in catalyst activity from 88% to 80% after lowering the reaction temperature from 550℃ to 500℃ . This was because carbon deposition occurred only on the catalyst face which was more exposed to gasification.

2.3.6.3 Catalyst regeneration by partial regeneration

This method of catalyst regeneration is employed to eliminate problems associated with sintering of the catalyst and eventual poisoning of the catalyst during regeneration. Since oxidation of deposited carbon nanomaterial is a difficult process, partial regeneration method is usually employed to oxidize the encapsulated carbon hence, carbon filaments continue to grow to sustain the metallic particle on the filament's edge from where carbon nanomaterial

accumulates. Therefore, the life of the catalyst is regained after several heat cycles leaving the main filament un-affected. Apart from full gasification, partial gasification of deposited carbon nanomaterial is a viable option of maintaining continuous catalyst life in non-oxidative methane conversion process.

2.3.7 NOCM reaction mechanism

During initial stages of non-oxidative methane conversion, CO, CO_2, H_2 and H_2O are formed when methane gas comes into contact with Mo/H^+- exchanged zeolite at 900K. During this phase, the following molybdenum species may be formed; molybdenum carbide $MoC_{(1-X)}$ (Budde *et al.* 2018), Mo_2C (Baba and Miyaji 2020), and /or MoCxOy (Lezcano-González *et al.* 2016a), as well as Mo (Solymosi *et al.* 1997). When Mo, MoO_2, Mo_2C and $MoC_{(1-X)}$ catalysts were used methane in methane conversion at 700℃, only trace amounts of C_2H_6 were recorded after the induction period (Solymosi *et al.* 1997). When Mo_2C and $MoC_{(1-X)}$ catalysts were used under the same conditions, small amounts of C_2H_4 and C_2H_6 were observed alongside CO and H_2. Based on these observations, it was concluded that carburized Mo species was responsible for the activation of C-C bond formation to yield ethane and ethylene from methane.

Several mechanisms for non-oxidative conversion of methane have been proposed by a number of researchers but research in this area is still inconclusive. However, the reaction mechanism considered likely is as follows.

(i) Catalysis of the formation of C_2H_6 by MoCx

A reaction mechanism suggested by (Xu and Lin 1999) shows that during the induction phase, MoCx species react with methane to form carbonaceous intermediate (Intermediate I) on the catalyst surface. This intermediate is then transformed into C_2H_6 by additional reaction of methane with CHx and / or CHz species as follows.

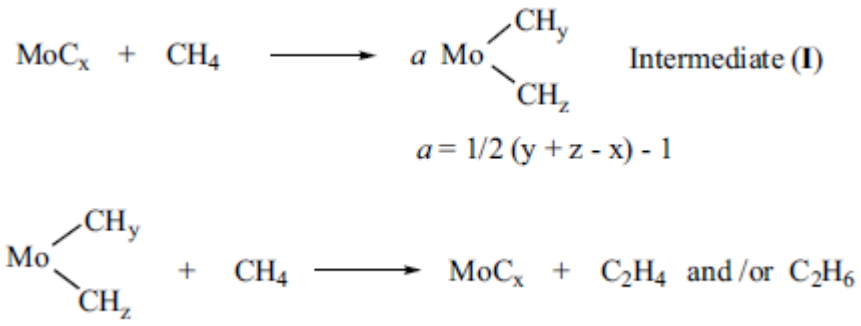

Scheme 3. Formation of C_2H_6 by reaction of methane with CH_X species.

(ii) Formation of C_2H_6 from molybdenum-carbene intermediates

Two research groups (Pierella *et al.* 1997) and (Xu *et al.* 1994) opine that in this mechanism, CH_4 reacts with Mo^{6+} on the H^+ exchanged zeolite to produce $*CH_3$ (methoxy species on the Bronsted acid sites of the zeolite), and $[Mo\text{-}H]^{5+}$. These two species are further transformed into molybdenum-carbene species ($Mo{=}CH_2$) which reacts with CH_4 to produce C_2H_6 according to following scheme.

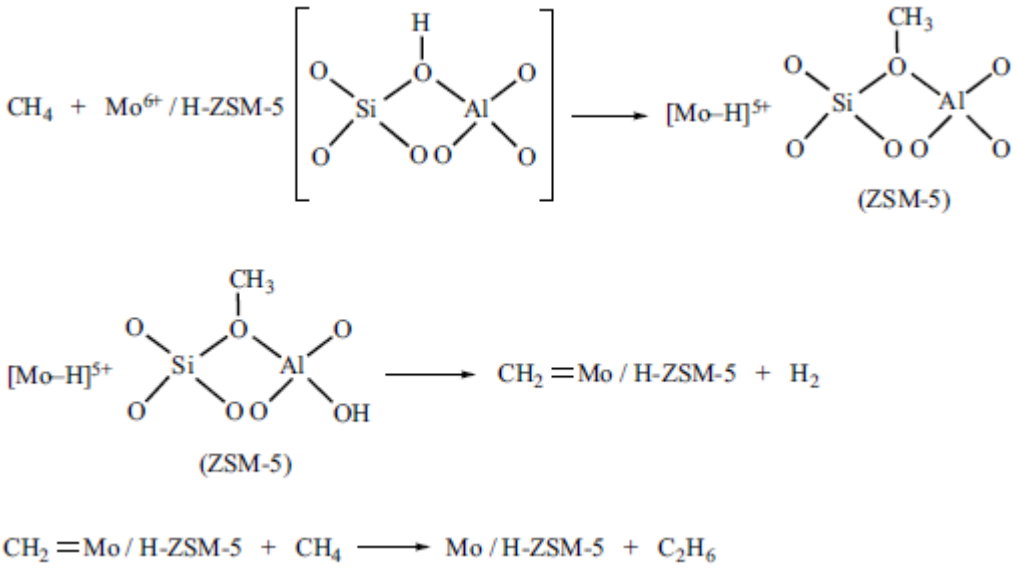

Scheme 4. Formation of molybdenum-carbene species ($Mo{=}CH_2$) which further reacts with CH_4 to produce C_2H_6.

(iii) Combining of methyl radicals (CH_3^*) to yield C_2H_6

The methyl radical (CH_3^*) species then undergoes oxidative coupling to form C_2H_6 as shown in the following equations.

$$CH_4 + MoOx \rightarrow CH_3^* + MoO_{(x-1)}OH \quad (21)$$

$$CH_3^* + CH_3^* \rightarrow C_2H_6 \quad (22)$$

This reaction takes place through a bifunctional mechanism, with Mo (in carbide form or oxide form) as the active sites in the reaction and zeolite acid sites also as catalyst active sites in the reaction (Majhi *et al.* 2013b).

According to (Wang *et al.* 1993), activation of methane occurs through the formation of carbonium ion with Mo^{6+} or with the acid sites acting as receptors of protons according to equations 23 and 24.

$$CH_4 + Mo^{6+} \rightarrow CH^{3+} + [Mo\text{-}H]^{5+} \quad (23)$$

$$CH_4 + H^+ \rightarrow CH^{3+} + H_2 \quad (24)$$

When HZSM-5 was used as a catalyst, low methane conversion was achieved (Chen *et al.* 1995). From the above proposed mechanisms, it is generally believed that the NOCM reaction proceeds through the formation of CH_3^*, which dimerizes to form ethylene. The formed ethylene is then converted into benzene with the aid of zeolite acidic sites. Characterization of the spent catalyst using x-ray photoelectron spectroscopy identified the formation of molybdenum carbide (Szöke and Solymosi 1996). This molybdenum carbide species from reduction of Mo is believed to have been formed during the induction period after formation of CO, CO_2, and H_2O species. After this phase, methane would activate on Mo_2C to form hydrogen deficient CHx species. Methane conversion studies by (Liu *et al.* 2006) revealed that in a typical reaction, 60-80% of the initial Mo^{6+} reduced to Mo^{4+} while the remaining portion of Mo^{6+} and traces of Mo^{5+} were heavily covered by carbon deposits.

From the above findings, (Wang *et al.* 1997) proposed a mechanism based on slow reduction of molybdenum oxide in addition to production of Mo_2C, CO, CO_2 and H_2O as the only products identified during the induction period as follows.

$$CH_4 \rightarrow C + H_2 \quad (25)$$

$$MoO_3 + H_2 \rightarrow MoO_2 + H_2O \quad (26)$$

$$MoO_2 + C \rightarrow MoC + CO + CO_2 \quad (27)$$

$$MoO_2 + 3C \rightarrow MoC + 2CO \quad (28)$$

Upon characterization of the spent catalyst, (Solymosi *et al.* 1999) found out that the main products of the reaction of CH_3^* adsorbed on Mo_2C were CH_4 and C_2H_4, while the coupling of CH_3^* and C_2H_6 was not observed, instead the CH* hydrogenated CH_4 to C_2H_4. The reaction of C_2H_5* species on Mo_2C results into the formation C_2H_4 and C_2H_6. This implies that the Mo_2C formed during catalyst activation process is responsible for promotion of the additional species CH_2* to C_2H_4, which is subsequently transformed into aromatics on the acidic sites of the zeolite.

2.3.7.1 Methyl radical (CH_3*) formation

Generated methyl radical (CH_3*) by haemolytic scission of a C-H bond in CH_4 conversion is an important reaction intermediate that can produce hydrocarbons using heterogeneous catalysts. The formation of CH_3* radicals on metal oxides or on methoxy groups occurs according to the following globally recognised equation.

$$M - O + CH_4 \rightarrow M\text{-}OH + CH_3^* \quad (29)$$

Methyl radicals (CH_3*) radicals can also be generated from a methane conversion reaction where monooxygenase catalyst has been used according to the following equation.

$$CH_4 + O_2 + 2H^+ + 2e^- \rightarrow CH_3OH + CH_3^* \quad (30)$$

From equation 30, an oxygen atom is incorporated into the methanol molecule while the remaining forms H_2O which supplies H^+ and e^- to the methane conversion reaction.

2.3.7.2 Formation of carbene-like species for hydro aromatization.

Carbene-like species (CHx) where ($0<X<3$) are dominant intermediates in dehydroaromatization reaction involving metal ions such as molybdenum and tungsten ions supported on various zeolites. The CHx species can be generated in the pores and on the surface of zeolites when MoO_3 reacts with methane followed by calcination. During the induction phase

of NOCM reaction, ethylene is formed and later transformed into aromatics through a series of steps.

2.3.7.3 Formation of methyl carbenium ions (CH_3^+)

Coupling of methane and H^+ to produce C_2H_6 and hydrogen can also occur in the presence of super acids such as FSO_3H-SbF_5 to generate methyl carbenium ions (CH_3+). This reaction is represented by the following reaction where CH^+ is expressed as CH_5^+.

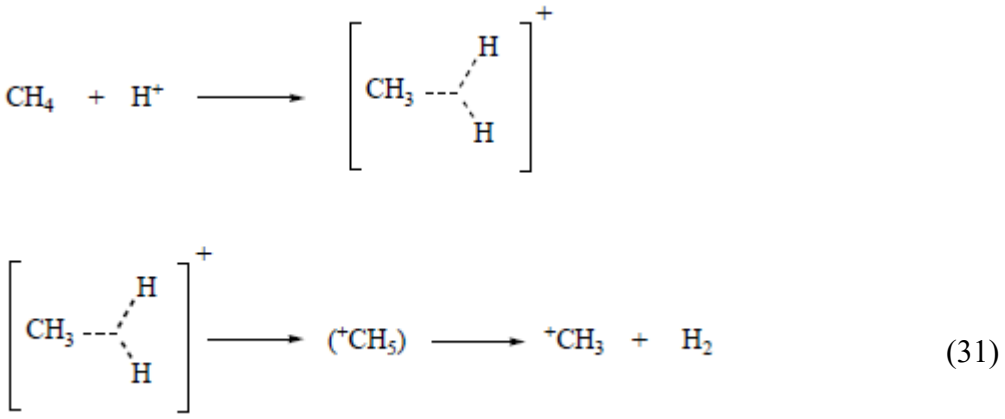

(31)

Methane is protonated to form the CH^+ ion in the super acid solutions where CH_5^+ ion then undergoes deprotonation by loss of hydrogen to form the CH_3^+, which subsequently reacts with methane to form C_2H_6 according to the equation 32.

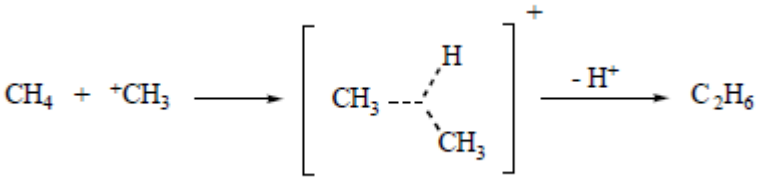

(32)

Carbenium ions produced by other catalysts such as Ag^{+}-exchanged zeolites play a very crucial role in electrophilic reactions for activation of C-C bond. This implies that apart from super acids, catalysts also have the potential to participate actively in C-C bond formation.

2.3.7.4 Properties of calcined Mo species at 500℃ on HZSM-5

The most common molybdenum catalyst precursor is ammonium heptamolybdate ($(NH_4)_6Mo_7O_{24}$) which is easily transformed into MoO_3 crystallites after calcination. These MoO_3 crystallites can react with surface functional groups (OH) such as acidic protons of Bronsted acid sites to form various Mo species. These Mo species are usually formed on the HZSM-5 zeolites after calcinating the catalyst precursor at 700-1000K. The use of ammoniacal solution to extract the molybdenum species on the Mo-HZSM-5 whose Si/Al ratio was 25 and calcined at 773K for 3hrs has been studied by (Xu *et al.* 1996). From their work, they observed two kinds of the molybdenum species on the Mo/HZSM-5 catalyst: a soluble species (Mo extracted in NH_3 solution) and an insoluble residual Mo species. The amount of the soluble species depended on the initial Mo loading in the Mo/HZSM-5 catalyst i.e., the amount of residual Mo species increased with Mo loading after 3%wt Mo loading. This non-linear relationship of the amount of residual Mo on the original Mo loading implies that some molybdenum species were anchored either on the surface or inside the HZSM-5 zeolite channels.

2.3.8 Effect of operating conditions on NOCM reactions

In most NOCM reactions, operating parameters that control overall methane conversion, product yield, and selectivity are among others, temperature, pressure, and gas hourly space velocity.

2.3.8.1 Effect of reaction temperature

Non-oxidative oxidation of methane is an endothermic reaction limited by equilibrium. As shown in equation 33, high temperatures in excess of 700℃ is required to achieve any remarkable methane conversion in a fixed bed reactor (Majhi *et al.* 2013a).

$$CH_4 = \frac{1}{6}C_6H_6 + \frac{3}{2}H_2\ , \quad \Delta H^0_{290} = 7165 kJmol^{-1} \tag{33}$$

From thermodynamics, the rate of methane conversion is a function of temperature. At higher temperatures, catalyst deactivation becomes prevalent due to coke deposition, sintering and

reduction in active phase (Zhang and Smirniotis 1999) and the overall process becomes uneconomical due to high energy demand. In view of this, a lot of research in this area has been employed to exploit alternative pathways of operating the reaction at lower temperature (Cui *et al.* 2011). According to (Chen *et al.* 1995), optimum methane conversion can be achieved between 700-800℃ above which, conversion and product selectivity begins to decrease following the loss of active component as shown in the Figure 2-3.

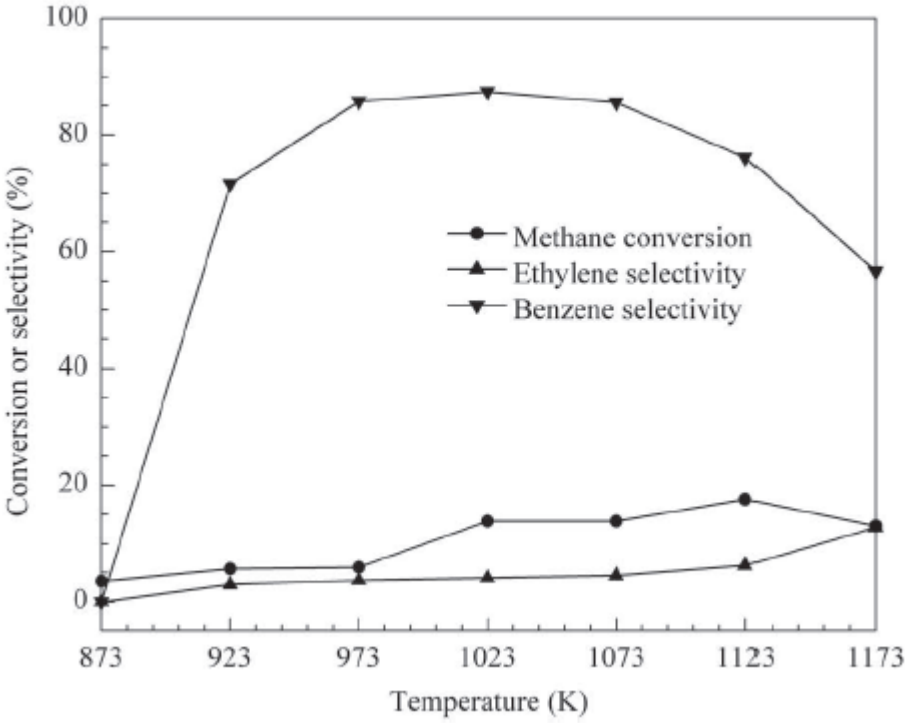

Figure 2-3. Effect of reaction temperature on methane conversion and product selectivity using 2%Mo/HZSM-5 at 1 atm and 1400 mL/ (g.h). Adapted from (Wang *et al.* 2005).

2.3.8.2 Effect of pressure.

It is envisaged that operating the NOCM reaction at low pressure favours the conversion of methane to aromatics because the variation in molar number of reactants and products is positive. The effect of methane pressure over time on the rate of benzene formation rate at 700℃ and 1350 $mLg^{-1}cat.h^{-1}$ gas hourly space velocity over 6%Mo/HZSM-5 was investigated by (Shu *et al.* 2002). Their findings are presented in Figure 2-4. Based on the results obtained, they observed a sharp decline in benzene yields with time when the pressure was low i.e., from 0-0.1

MPa. A stable NOCM operation was achieved when the operating pressure was raised to (greater than 0.5 MPa) but still the conversion rates were low. According to (Shu *et al.* 2002), most stable reactions were carried out at moderate pressures (0.1-0.3 MPa). This could be explained by the fact that a slight increase in pressure leads to a greater variation in molar number which favours side reactions leading to coke formation.

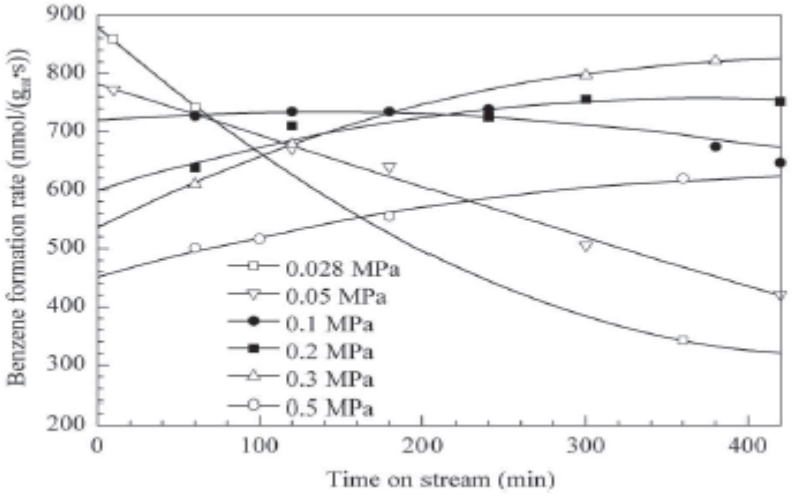

Figure 2-4. Effect of pressure on benzene formation rate over 6%Mo/HZSM-5 at 700℃ and 1350 mL/(g.h). Adapted from (Shu *et al.* 2002).

2.3.8.3 Effect of gas hourly space velocity

The effect of gas hourly space velocity on methane conversion and product selectivity was investigated by (Skutil and Taniewski 2006). Based on the results obtained, they concluded that reducing the gas hourly space velocity (GHSV) not only increases the conversion of methane to aromatics, but also increases the induction period for the reaction in the temperature range between 600-725℃ , and gas hourly space velocity between 270-500 $mLg^{-1}cat.h^{-1}$. According to (Chen *et al.* 1995) and (Solymosi *et al.* 1996), an increase in gas hourly space velocity leads to an increase in selectivity to ethylene and a decrease in selectivity to benzene. Another author (Sun *et al.* 2009) observed that an increase in gas hourly space velocity measured in the range of 270-770 $mLg^{-1}cat.h^{-1}$ resulted in higher coke selectivity and rapid catalyst deactivation. However, this characteristic behaviour of the NOCM reaction could change when CO_2 is incorporated in the feed (Shu *et al.* 2002). These authors investigated the effect of GHSV of methane on the rate of formation of benzene at 800℃ and 0.3 MPa, 3-5%CO_2 over

6%Mo/HZSM-5 and noted a linear growth rate in terms of benzene yields between 1350-900 $mLg^{-1}cat.h^{-1}$.

2.3.8.4 Effect of reactor surface area

Reactor surface area plays a critical role in the kinetics of the NOCM reaction. Most methane conversion reactions have been studied in stainless steel and copper metallic reactors, but further attempts have been made to commercialize the use of inert materials like quartz, pyrex, and various forms of alumina in reactor design. When a NOCM reaction is carried out at ~600℃ in the presence of oxygen and silica, up to 4.5% of methane is converted into formaldehyde (CH_2O) as the main product. Formation of CH_2O at high temperatures is believed to occur due to methane coupling reaction to yield products, especially ethylene due to generation of methyl radicals on their surfaces. Both heterogeneous and homogeneous catalytic oxidation of methane at 600-700℃ showed that the reaction occurs on the surface and in bulk with the heterogeneous reaction of alumina being much more intense than it is on silica.

It has been reported that increasing internal surface area of a quartz reactor using quartz or pyrex packing increases the initiation temperature hence, an increase in residence time of the reactants in the reactor (Vella *et al.* 2010). Introduction of quartz or pyrex packing in the reactor increases the initiation temperature and this phenomenon increases with a decrease in the size of the packing balls. Further, the catalytic activity of pure SiO_2 catalyst in methane conversion to formaldehyde was observed with the selectivity of formaldehyde being lower when the SiO_2 surface was coated with a metal oxide catalyst (Arena *et al.* 2009). It can therefore be inferred that, catalytic oxidation of methane proceeds with the formation of methoxide (CH_3OM) on the active site of the catalyst. Partial oxidation of methane by (Ding *et al.* 2015) over SiO_2 using semi-empirical methods revealed that activation of CH_4 by lattice oxygen in strained siloxane bonds requires high activation energy and hence, thermodynamically not favourable.

2.3.8.5 Effect of methane residence time

The efficiency of methane conversion process using kinetic parameters documented in literature were used to determine the process residence time.

The rate equation describing the process is.

$$r = \mathrm{K}P^{m}{}_{CH4} \tag{34}$$

Where P_{CH4} is the partial pressure of methane at atmospheric pressure, m is the reaction order (-1) and K is the rate constant for the reaction (Ermakova and Ermakov 2002).

From Arrhenius equation.

$$K = \text{A}.e^{-E_a/R_uT} \tag{35}$$

Where A, is the frequency factor, $T$is the temperature (K), $E_a$is the activation energy in kJ/mol) and R_u, is the universal gas constant. In this case, the determination of the reaction rate is done by considering both the forward and reverse reaction steps according to the equation 36.

$$r = \frac{dN}{dt} = K_{foward}.P^m{}_{CH_4} - K_{reverse}.\ P^n{}_{H_2} \tag{36}$$

Where N, is the quantity of feed in (mol), t is the time in (s), the rate constant (K_{foward}), is calculated from equation 36 and n, is the reaction order for the reverse reaction, which is near unity, while $K_{reverse}$ is calculated from equation 36 and taken as zero in most cases. To determine residence time of methane in a reactor, useful experimental data can be obtained from (Hornés *et al.* 2012) for unsupported nickel catalyst and from (Ermakova and Ermakov 2002) for activated carbon. The effect of residence time is studied by assuming that constant reaction rates are equal with reaction rates irrespective of catalyst deactivation.

2.4 NOCM reaction kinetics and reactor designs

2.4.1 NOCM reaction kinetics

In non-oxidative conversion of methane the relative importance of gas-phase chemistry depends on residence time, temperature, and pressure in the reactor (Karakaya and Kee 2016). Experimental studies show that the formation rate of C_2 hydrocarbons strongly depend on gas-phase methyl radical concentrations (Xu and Lunsford 1991). Increasing temperature and pressure increases the formation rate of methyl radicals irrespective of whether the process is catalytic or not. Since catalysts contribute to an increase in methyl radical formation, they too increase the rate of C_2 hydrocarbon formation. Even though there are differences in the active sites on a specific catalyst, there is a consensus that at high temperature methane needs to be activated to form CH_3* radicals. This CH_3* formation step is regarded as the rate limiting step.

2.4.1.1 Establishment of intrinsic kinetic model

There are three dominant NOCM reactions (Yao *et al.* 2008) represented by the following globally recognized equations.

$6CH_4 \rightleftarrows C_6H_6 + 9H_2$ (37)

$CH_4 \rightleftarrows C + 2H_2$ (38)

$C_6H_6 \rightleftarrows 6C + 3H_2$ (39)

Equation 38 and 39 are regarded as independent equations and the Langmuir-Hinshelwood model was chosen as the intrinsic kinetic model for the reaction. The reaction rate was calculated by considering the gas fugacity of each component.

In the Langmuir-Hinshelwood model, the reaction rate can be represented as.

$$r_1 = \frac{k_1 . f_{CH_4}^6 . (1 - \beta_1)}{(1 + K_{CH_4} . f_{CH_4} + K_{H_2} . f_{H_2} + K_{C_6H_6} . f_{C_6H_6})^6} \quad (40)$$

$$r_2 = \frac{k_2 . f_{CH_4} . (1 - \beta_2)}{1 + K_{CH_4} . f_{CH_4} + K_{H_2} . f_{H_2} + K_{C_6H_6} . f_{C_6H_6}} \quad (41)$$

$$k_i = A_i . \exp\left(-\frac{E_i}{R}\left(\frac{1}{T} - \frac{1}{\bar{T}}\right)\right) \quad (42)$$

$$k_i = \exp\left(a_i - b_i \left(\frac{1}{T} - \frac{1}{\bar{T}}\right)\right) \quad (43)$$

$$\beta_1 = \frac{f_{C_6H_6} . f_{H_2}^9}{K_{f1} . f_{CH_4}^6} \quad (44)$$

$$\beta_2 = \frac{f_{H_2}^2}{K_{f2} . f_{CH_4}} \quad (45)$$

Where f_i is the fugacity of component *i*, which can be considered as pressure at atmospheric pressure and the temperature constant of 913-973K, K_f is the equilibrium constant of the reaction in equation 44 and in equation 45 (Liu *et al.* 1999); k_1 and k_2 are the rate constants of the reaction in equation 40 and in equation 41, respectively. K_i is the adsorption equilibrium constant of component *i* and βi is the departure amount balance*;* $\bar{T}$ =943.15 K.

2.4.1.2 Estimation of parameter

From mass balance,

$$N = N_{in} + \Delta N_{rA} + \Delta N_{rB} \tag{46}$$

$$\Delta N_{rA} = 4N_{C_6H_6} \tag{47}$$

$$\Delta N_{rB} = 4N_{CH_{4in}} - 4N_{C_6H_6} - N_{CH_{4out}} \tag{48}$$

So,

$$N = N_{in}.\frac{1 + y_{CH_{4in}}}{1 + y_{CH_{4in}} + 2y_{C_6H_6}} \tag{49}$$

As

$$\frac{dN}{d\omega} = 4r_1 + r_2 \tag{50}$$

Therefore,

$$\frac{dN_{CH_4}}{d\omega} = \frac{dN(N.y_{CH_{4in}})}{d\omega} = \frac{dN}{d\omega}.y_{CH_4} + \frac{dy_{CH_4}}{d\omega}.N = -6r_1 - r_2 \tag{51}$$

Because,

$$\frac{dy_{CH_4}}{d\omega} = \frac{1}{N}\left(-6r_1 - r_2 - \frac{dN(N.y_{CH_{4in}})}{d\omega}\right) \quad (52)$$

Thus,

$$\frac{dN_{C_6H_6}}{d\omega} = \frac{d\left(N.y_{C_6H_6}\right)}{d\omega} = \frac{dN}{d\omega}.yC_6H_6 + \frac{dyC_6H_6}{d\omega}.N = r_1 \quad (53)$$

$$\frac{dyC_6H_6}{d\omega} = \frac{1}{N}\left(r_1 - \frac{dN}{d\omega}.yC_6H_6\right) \quad (54)$$

Having chosen $y\mathrm{CH_4}$, $y\mathrm{C_6H_6}$ as variables, and the total reactor considered as a plug flow reactor, a fraction of the components was chosen from the feed and product streams during the reaction. Equations 53 and 54 were calculated using the method of Runge-Kutta in the parameter estimation.

The objective function of parameter estimation was.

$$S = \sum_{i=1}^{M}\left(\omega_{CH_4}^2(yCH_{4,i,e} - yCH_{4,i,c}\right)^2 + \omega_{C_6H_6}^2\left(yC_6H_{6,i,e} - yC_6H_{6,i,c}\right)\Big)^2 \quad (55)$$

The Levenberg-Marquardt model (Huang and Ma 2019) was used to determine the parameters of the kinetic model as follows.

$$k_1 = 8.1283 \times 10^{-3}.\exp\left(-\frac{2.0909 \times 10^5}{R}\left(\frac{1}{T} - \frac{1}{943.15}\right)\right) \quad (56)$$

$$k_2 = 2.3252 \times 10^{-3}.\exp\left(-\frac{1.2096 \times 10^5}{R}\left(\frac{1}{T} - \frac{1}{943.15}\right)\right) \quad (57)$$

$$k_{CH_4} = \exp\left(-1.1963 - 1.3209 \times 10^2 \left(\frac{1}{T} - \frac{1}{943.15}\right)\right) \quad (58)$$

$$k_{H_2} = \exp\left(1.6736 + 1.5796 \times 10^3 \left(\frac{1}{T} - \frac{1}{943.15}\right)\right) \quad (59)$$

$$k_{C_6H_6} = \exp\left(-9.09 + 1.1770 \times 10^5 \left(\frac{1}{T} - \frac{1}{943.15}\right)\right) \quad (60)$$

2.4.2 Reactor designs commonly used in conversion of methane.

Different researchers have proposed different reactor designs with the aim maximizing conversion, product selectivity and suppressing the effects of coke deposition on catalyst activity. Most promising reactor designs have an in-build mechanism of regenerating the catalyst, either continuously (typical in circulating fluid bed) or periodically i.e., in multi-station beds. Heat integration is also another key point to consider when designing a reactor for methane conversion. Representative examples of reactors used in methane conversion among others include membrane reactors, fluid bed reactors, coupled reactors, and two-zone reactors.

2.4.2.1 Coupled reactor.

This type of reactor is characteristic in a way that it integrates an oxidative coupling of methane (OCM) reactor which converts methane to ethylene while the second reactor uses Ga/ZSM-5 (Qiu *et al.* 1997) or SLC-6%Mo/HMCM-49 (Li *et al.* 2005) to transform the formed ethylene to aromatics. In this reactor, evolution of H_2O and CO_2 reduces coke formation in the methane aromatization stage. After operating the coupled reaction for 5 hours on the SLC-6%Mo/HCM-49 catalyst system, they observed that methane conversion and yield of aromatics reached 15.4% and 8.9%, respectively. After 62 hours' time on stream, methane conversion dropped to 10.9% and the yields dropped to 6.0% with too much coke formation. Even though the aromatics yield was 10.7-13.8% after 5 hours' time on stream, it reduced to 0.7% at 2.7% methane conversion after operating the reaction for 38 hours. After running the reaction for 20 hours, they observed an improvement in aromatics and longer catalyst life. Coke selectivity increased much more slowly with SLC-6%Mo/HMCM-49 compared with 6%Mo/HCM-49 alone. Therefore, methane

coupling and dehydroaromatization over SLC-6%Mo/HMCM-49 catalyst system demonstrated a more effective improvement in the performance of methane dehydro-aromatization. This can be attributed to an efficient removal of deposited coke on 6%Mo/HMCM-49 catalyst via CO_2 and steam generated in the system.

2.4.2.2 Two -zone reactor fluidized bed reactor

A two-zone fluidized bed reactor (TZFBR) is a chemical process equipment in which two chemical reactions are made to occur simultaneously. In this type of reactor, methane gas is fed to the middle of the reaction zone, thereby creating two zones in the bed with different environments; an oxidizing atmosphere in the lower part and a reducing atmosphere in the upper part (Herguido and Menéndez 2017). Continuous catalyst deactivation due to coke formation causes the dense catalyst to fall into the lower part of the reactor where it is regenerated and then rises to the upper part of the reactor (reaction) zone. It has been demonstrated that using Mo/HZSM-5 in this type of reactor, 8% methane conversion and selectivities of up to 90% (benzene and other hydrocarbons) selectivity were achieved. The gas bubbles, just as in normal fluidized beds, transport solids between the two zones in such a way that each particle resides in one zone for some time.

The type of reactions taking place in a two-zone reactor are classified into two. The first reaction is the one in which the catalyst acts as an oxygen carrier like in oxidative coupling of methane. In this case the catalyst is oxidized by oxygen in the lower part of the reactor and the catalyst transports oxygen in the crystalline lattice to the upper part of the reactor where desired reaction is taking place i.e., reduction of the solid oxide. The second reaction is the one in which the catalyst is deactivated by coke during the reaction.i.e., dehydrogenation. In that case, the catalyst is regenerated by an oxidizing gas in the lower zone of the reactor and the catalyst transports coke from the reaction zone to the regeneration zone. Research work in the development of two-zone fluidized bed reactors by (Talebizadeh *et al.* 2009) have confirmed that these type of reactors offer more advantages than conventional fixed bed reactors in terms of improved selectivity and improved catalyst life due continuous catalyst regeneration mechanism.

2.4.2.3 Membrane reactors

Thermodynamic and kinetic challenges in NOCM reactions leads to low methane conversion (Ismagilov *et al.* 2008). Efforts by researchers to improve the process has been focused on

enhancing the reaction temperature or decreasing the reaction pressure. These two process parameters do not favour the process industrially. Confinement of the catalyst active sites within the shape-selective zeolite channels minimizes the formation of poly-aromatic hydrocarbons typical in homogeneous pyrolytic reactions, has failed to influence the position of chemical equilibrium. It is therefore envisaged that, selective purge of hydrogen from the reaction can shift the chemical equilibrium towards product selectivity.

Therefore, membrane reactors are designed to drive the methane aromatization reaction towards benzene formation by removing the formed hydrogen through a selective membrane. Its configuration consists of a packed tube containing a solid catalyst and a radially centred tube coated with a selective membrane through which hydrogen permeates. A study using such a reactor yielded promising results in hydrogen removal using Pd-Ag membrane (Wang *et al.* 2001). A similar study (Liu *et al.* 2002) investigated the application of $SrCe_{0.95}Yb_{0.05}O_3$-a thin film (ca.2μm) to eliminate H_2 in NOCM reaction to higher hydrocarbons over Mo/HZSM-5 and establish the influence of H_2 removal on methane conversion and product distribution. Results from their work showed that at 950K, only 7% of H_2 produced was removed and methane conversion was not any different from that achieved using ordinary reactors. However, on increasing reaction temperature to 993K, a slight increase in methane conversion and C_2 hydrocarbon yield was recorded, but catalyst deactivation was rapid. This challenge was addressed by co-feeding CO_2 with methane in the feed. Another study done by (Kinage *et al.* 2003) revealed the steady-state formation rates of hydrogen, benzene, naphthalene, and toluene in NOCM reaction over 3wt%Mo/HZSM-5 catalyst and the hydrogen removal was 2-10 times higher when a Pd membrane was used.

2.4.2.4 Fluidized bed reactors

Most experimental work in non-oxidative methane conversion has been done in fixed bed reactors. However, fluidized bed reactors (FBRs) are more advantageous than fixed bed reactors in terms of efficient heat dissipation, easier catalyst regeneration, and relative homogeneous temperature inside the reaction zone. The general configuration of a fluidized bed reactor entails a bubbling or circulating fluidized bed. Methane conversion studies using different reactors by (Ma *et al.* 2013) reported interesting results on conversion of methane into aromatics in a fluidized bed reactor. Based on their findings, they concluded that the catalyst induction period

and the rate of methane conversion were influenced by reaction temperature, methane partial pressure, and space velocity but yield, and selectivity were like those results obtained in a fixed-bed reactor. Another research group (Cook *et al.* 2009), studied methane dehydroaromatization in both fixed and fluidized bed reactors over Mo_2C/ZSM-5 catalyst and reported better yields despite rampant catalyst deactivation. Recently, (Gimeno *et al.* 2010) operated NOCM reaction in a two-zone fluidized bed reactor (TZFBR) to study catalyst deactivation. The two zones created in fluidized bed reactor enabled feeding at an intermediate point and regenerating at the bottom of the reactor. This type of reactor provided a stable operation of NOCM reaction because of in situ generation of the catalyst at the lower part of the reactor. The three commonly used regenerating agents are oxygen, steam, and carbon dioxide. When 1% CO_2 was used as a regenerating agent, about 8%methane conversion and over 90% selectivity towards aromatics was achieved on a 6%Mo/HZSM-5 at 700℃. According to (Xu *et al.* 2011), a circulating fluidized bed reactor is desired for periodic operation and catalyst regeneration. By using this type of reactor, they achieved improved continuous operation and better heat transfer.

2.4.3 Thermodynamics of non-oxidative conversion of methane

Non-oxidative conversion of methane reactions are usually carried out between 900-1100K with key products being benzene and its derivatives with traces of ethylene and ethane (Xu *et al.* 2003). Therefore, NOCM reactions are ideal for production of aromatics especially when methane is used as the only reactant. Methane conversion at equilibrium to C_6H_6, C_2H_6, C_2H_4, C, and H_2 can be achieved at 773K according to the following equations.

$$6CH_4(g) \rightleftarrows C_6H_6(g) + 9H_2(g) \quad (61)$$

Equilibrium CH_4 conversion: 3.1% at 773K

$$2CH_4(g) \rightleftarrows C_2H_6(g) + H_2(g) \quad (62)$$

Equilibrium CH_4 conversion: 0.45% at 773K

$$2CH_4(g) \rightleftarrows C_2H_4(g) + 2H_2(g) \quad (63)$$

Equilibrium CH_4 conversion: 0.62% at 773K

$$CH_4(g) \rightleftarrows C(s) + 2H_2(g) \quad (64)$$

Equilibrium CH_4 conversion: 52% at 773K

From equations 61-64, formation of coke in methane conversion is most favourable without the use of oxidants. Conversely, methane conversion into aromatics is more thermodynamically favourable than it is to ethylene or ethane. Hydrogen selectivity is more favourable at higher reaction temperatures due to characteristic dehydrogenation reaction. This is the opposite in methane conversion to benzene under oxidative conditions in which equilibrium methane conversion of 100% occurs at 773K as follows.

$$6CH_4 + \frac{9}{2}O_2 = C_6H_6 + 9H_2O \quad (65)$$

Even though selectivity towards C_2 hydrocarbons is low, methane conversion to benzene is thermodynamically complete with 100% conversion at 623K.

2.4.4 Thermodynamic challenges facing non-oxidative methane conversion.

Despite intense research in non-oxidative conversion of methane for close to three decades from now, no breakthrough process has been developed. Major challenges of methane conversion arise from both kinetics and thermodynamics. The inherent thermochemical properties of methane are responsible for the high stability of the molecule and the difficulties in its activation and conversion. The absence of a dipole moment and a rather small polarizability ($2.84X10^{-40}C^2.m^2.J^{-1}$)[6] means that a methane molecule requires a relatively high local electric field for polarization to allow nucleophilic or electrophilic attack to occur. Activation C-H bond in a methane molecule into carbon and petrochemicals takes place in several steps. These chain reactions yield intermediates which are more reactive than methane itself and therefore, separation and recycling of unconverted methane in the product stream can only be achieved at low conversion levels. High temperatures do favour high syngas production rendering the catalyst less important due to radical reactions and deactivation of catalysts increases with an increase in temperature. The strength of C-H bond in methane is stronger than the C-H bond in the products, hence the products will be more reactive than methane itself (Holmen 2009). This therefore possess a challenge of selectivity rather than reactivity. Most methane conversion processes are operated batch wise due to catalyst deactivation, hence the need to stop the process and regenerate the catalyst first before proceeding.

At high temperatures(>1000℃), clogging of the reactor by deposited carbon becomes more prevalent (Keipi *et al.* 2016) and the residence times can be very short. Hardness of deposited carbon increases with temperature which complicates carbon removal from the reactor. In the presence of the catalyst, the methane decomposition process can occur at (<1000℃), but the main challenge is catalyst becoming deactivated as a result of carbon deposition (Keipi *et al.* 2016). To mitigate these methane conversion challenges, different approaches based on catalysis and reaction engineering have been proposed and tested. Such proposals have been centred around thermal and catalytic pyrolysis of methane, oxidative coupling of methane, partial oxidation of methane to formaldehyde, and exploitation of various processes such as plasma, halogenation, photo catalysis, and membrane technology.

Membranes and membrane reactors are possible mitigators of the challenges associated with direct methane conversion. In a typical example of dehydroaromatization of methane to benzene which may be represented using globally recognized equation as,

$$6CH_4 \rightleftarrows 9H_2 + C_6H_6 \quad \Delta H_{298} = +532\text{kJ}. \tag{66}$$

Direct production of ethylene from methane is represented globally by the equation below.

$$2CH_4 \rightleftarrows 2H_2 + C_2H_4 \quad \Delta H_{298} = +202\text{kJ}. \tag{67}$$

In equations 66 and 67 above, the extent of methane conversion is thermodynamically limited by hydrogen accumulation within the reactor. This means, the reaction can equilibrate with only a fraction of methane being converted. Therefore, employing a hydrogen-permeable membrane reactor that selectively removes hydrogen can greatly promote an increase in methane conversion and product yield. Even though membranes can increase conversion, they can also affect (favourably or unfavourably) selectivity to desired products and give rise to unwanted products. Undesired side products may include catalyst fouling coke and polyaromatic hydrocarbons (PAH). Therefore membranes can play an important role in limiting or controlling the undesired products (Karakaya and Kee 2016). Another challenge of NOCM reaction is that the possible products from methane conversion are limited to a few components mainly hydrogen, C_2 hydrocarbons, and aromatics.

2.5 Various attempts to improve methane conversion to hydrocarbons over Mo/HZSM-5

2.5.1 Suppression of Bronsted acid sites on the zeolite surface

In order to address both thermodynamic and process limitations of the NOCM reaction, various attempts have been made by researchers to improve the process. One of the key products of methane conversion is coke, which apparently is responsible for catalyst deactivation. Therefore, to reduce coke formation and prolong catalyst life, salination treatments have been employed to limit the amount of Bronsted acid sites on the external surface of the HZSM-5 zeolite. This technique does not affect the acidic O-H functional groups (Bronsted acid sites) located inside the zeolite channels. In a typical silanation process, 3-aminopropyl triethoxysilane was used to silane the HZSM-5 zeolite.

The process involved adding an optimum amount (0.5wt% as SiO_2) of the silanizing agent to HZSM-5 relative to the final weight of the 6%wtMo/HZSM-5 to tune the apertures of the external micro pores of the HZSM-5 zeolite to a molecular diameter of ~5 Å, which is similar to the molecular diameter of MCM-22 zeolite. The resultant catalyst (0.5%SiO_2-6%Mo/HZSM-5 enhanced benzene selectivity up to ~90% in the NOCM reaction by suppression of both coke and naphthalene formation.

2.5.2 Co-feeding methane with small amounts of CO and CO_2

Another approach to enhance catalytic activity of MO/HZSM-5 in non-oxidative methane conversion is by co-feeding methane with CO and CO_2. As reported by (Skutil and Taniewski 2006), these carbonaceous compounds promote benzene formation and improves catalyst stability. Another research group (Ohnishi *et al.* 1999), investigated the influence of adding CO and CO_2 in methane feed on the overall catalyst activity HZSM-5 zeolite doped with various transitional metals such as Re, Mo, and Fe (Shu *et al.* 2002). Results from their work show that, when 3%MO/HZSM-5 was doped with Fe and also co-doped with carbon monoxide (CO-3%Mo/HZSM-5) and used as catalysts for the conversion of methane containing 1.8%(v/v) CO at 973K, benzene yields were ;1000 $mmolg^{-1}s^{-1}$ on carbon basis. Catalyst stability was realized at over 100 hours over both catalysts because of suppressed coke formation (less than 20%). Further, the catalytic activity of 3%Mo/HZSM-5 was enhanced through addition of CO_2 to methane feed instead of CO under the same operating conditions (Liu *et al.* 2000).

The CO_2 reforming and reverse Boudouard reaction takes place according to the following globally recognized equations.

$$CO_2 + CH_4 = 2CO + H_2 \quad (68)$$

$$CO_2 + C = 2CO \quad (69)$$

From equation 69, the added CO_2 to methane is transformed into CO, hence the effect of CO_2 appears similar to that realized by addition of CO. The quantity of deposited coke on Mo/HZSM-5 and Fe/Co doped Mo/HZSM-5 was determined using temperature-programmed oxidation (TPO) by (Ohnishi *et al.* 1999). From the TPO experiment, they concluded that unlike CO, co-feeding methane with CO_2 suppressed the formation of inert coke and influenced the conversion of reactive coke to benzene and naphthalene. From the results obtained, the authors concluded that the effect of adding CO to methane feed was based on the formation of small amounts of CO_2 and C by the Boudouard reaction in which C represents the hydrogenated species (CHx), leading to catalyst stability after suppression of coke formation.

2.5.3 Co-feeding methane with small amounts of O_2, H_2 and H_2O

Introducing small amounts of oxygen (Yuan *et al.* 1999), hydrogen (Ma *et al.* 2003), and water (Fouty *et al.* 2017) in methane feed have been found to have a positive influence on the NOCM reaction. Usually, a lot of care is required in introducing oxygen in methane feed such that oxidation of the feed is avoided. At 700℃ and 800℃, the O_2/CH_4 molar ratio should not exceed 0.0065 and 0.024, respectively. The effect of adding small amounts of oxygen in methane feed in methane aromatization was investigated by (Yuan *et al.* 1999). From their studies, they found out that under certain conditions, the aromatization of methane and partial oxidation of methane into syngas can co-exist in the presence of a small amount of oxygen. The added oxygen was believed to maintain the active phase (MoOxCy/HZSM-5) and remove part of the formed coke resulting in partial catalyst regeneration. The type of coke that formed on HZSM-5 was polyolefin and aromatic while that formed on Mo/HZSM-5 was poly-aromatic coke. Studies on methane conversion by co-feeding hydrogen with methane in NOCM reaction was done by (Ma *et al.* 2003). From their findings, they observed that addition of small amounts hydrogen enhanced catalytic activity and stability of Mo/HZSM-5 catalysts by suppressing coke formation, especially the type of coke that was deposited on the Bronsted acid sites at 750℃.

Further, (Baba and Miyaji) reported that, addition of H_2O (1.7-2.2%) to methane feed improved the performance and stability of Mo/HZSM-5 catalyst by inhibiting coke formation.

2.6 Catalyst development for NOCM reaction

2.6.1 The active phase

Non oxidative conversion of methane has received considerable attention because it is a viable route to producing valuable chemicals (Xu *et al.* 2003). Until now, most research work has been focused on Mo/HZSM-5. Activation of methane C-H bond and subsequent formation of C-C bond occur on the reduced molybdenum carbide species. The Mo_2C is formed from the reduction of MoOx species by CH_4 during the initial stages of NOCM reaction whereas the oligomerization of the C_2 hydrocarbon species are catalysed by the Bronsted acid sites in the HZSM-5 zeolite (Wang *et al.* 2000). From literature, active Mo oxide species disperses on the HZSM-5 if % Mo loading is less than 8% wt. and calcination temperature below 550℃ (Liu *et al.* 2006).

The tendency of framework aluminium extraction by Mo oxide species increases with an increase in Mo loading and increase in calcination temperature. As reported elsewhere (Szöke and Solymosi 1996) and (Weckhuysen *et al.* 1998b), the highly dispersed Mo_2C species on the HZSM-5 zeolite are the active sites on which methane activation occurs. It has also been reported that when Mo/HZSM-5 catalyst is calcined at 500℃, all the Mo species replaces the Bronsted acid sites with a stoichiometry ratio of 1:1 in the HZSM-5 zeolite channel (Borry *et al.* 1999). Therefore, the Mo species in the channels were more effective in methane activation and suppressed coke formation (Ding *et al.* 2002) . Reducibility of Mo oxide species is dependent on its location in the HZSM-5 zeolite. The Mo species that is not associated with Bronsted acid sites is reduced to Mo_2C while that Mo species associated with Bronsted sites is partially reduced into MoO_xC_y complexes (Ma *et al.* 2000a).

2.6.2 The promoter

In NOCM reaction, various transition metals such as Mo, W, Re, V, Ga Ir, Cr and Mn supported on different supports have been used. Most promising results have been achieved by Mo/HZSM-5 at 700℃ and gas hourly space velocity of 1500 $ml.g^{-}1cat.h^{-1}$ (Aboul-Gheit and Awadallah 2009). Improvements in catalyst activity and stability has been obtained by addition of Fe, Co, W, Zr, Ru, Cu and Zn (Shu *et al.* 1997). When Mo/HZSM-5 catalyst was used alone in NOCM

reaction, methane conversion and hydrocarbon selectivity were reported in the range of 973-1073K. Under these conditions, methane conversion was 12% and selectivity for aromatics was higher than 90%. Promotion of Mo/HZSM-5 with W at 973K to produce C_2 and C_{12} hydrocarbons only achieved 2-3%conversion. Considering the similarities between MoO_3 and WO_3, parallelism in their catalytic properties were expected. Other researchers reported 18-23% methane conversion and 48-56% hydrocarbon yields on W/HZSM-5 catalyst when NOCM reaction was operated at 1073K. In both NOCM and methanation reactions (Qian *et al.* 2003), metal oxides of alkaline earth metals perform poorly when combined with metal oxides of transition metals.

2.6.3 The support

Supports play a significant role in catalysis (Li *et al.* 1997). Metal oxides like TiO_3, MgO, and SiO_2-MgO perform a bifunctional role as supports and as active components. Perovskite structured oxides have been investigated and applied as catalyst supports (Kuras *et al.* 2008). Good catalytic results by nickel-based catalysts supported on mesoporous carbon nanofibers (CNFs) with large surface area (100-300 m^2/g) have also been achieved. Good quality carbon nanomaterial have been achieved using zeolites as potential supports in the NOCM reaction (Guevara *et al.* 2010).

To obtain highly dispersed surface area for the catalyst that promotes the growth of single walled carbon nanotubes (SWCNTs), various metal oxides such as Al_2O_3, MgO or SiO_2 have been used (Ni *et al.* 2006). Catalysts supported on magnesium oxide demonstrate high formation of carbon nanomaterial because of easy catalyst regeneration from deposited carbon unlike, Al_2O_3 or SiO_2 supported materials. Porous magnesium oxide prepared by thermal decomposition of its salts $Mg(NO_3)_2$ and $MgCO_3$ is desired for growth of SWCNTs. The catalytic activity of Fe/MgO is enhanced when calcined at 113K for 10 hours. This catalyst is desired for generation of small diameter SWCNTs and double walled carbon nanotubes (DWCNTs). Zeolites are crystalline aluminosilicate materials, and their acidic properties depend on the amount of aluminium in the framework. Choosing correct SiO_2/Al_2O_3 molar ratio during crystallization, putting other elements to replace the frame work constituents, and modification of the zeolite are all parameters for adjustment of its acidity (Lu *et al.* 2003).

2.6.4 Metal and support interaction

The type of bonding between a metal catalyst and its support in a catalyst system constitutes a phenomenon called metal-support-interaction (MSI). The extent of MSI affects the reducibility of metal oxides and metal distribution in the overall catalyst system. When the metal-support is strong, it is difficult to reduce the precursor oxide and create room for metal catalyst dispersion which consequently alters the electronic and crystalline state of the metal particle, hence affecting its catalytic activity.

A weak MSI means catalyst crystallites can easily be blown up by the growing carbon nanomaterial thereby promoting the growth of carbon nanomaterial at the tip, while a strong metal support interaction leads to growth at the base of the metal catalyst. In NOCM reaction, a large proportion of SWCNTs do not have metal particles attached to them except a few of them having metal appendages at their ends. There are two movements of metal particles reported in literature; jump movement by charged new layers and smooth movement which forms graphite layers (Chen *et al.* 2001). At low temperatures the particles are usually in crystalline form but possess the characteristics of a quasi-liquid state at high temperatures (Chen *et al.* 2001).

2.6.5 Catalytic activity of different transition metals

Studies on catalytic activity of transition metal catalysts supported on HZSM-5 in non-oxidative conversion of methane have been reported by (Majhi *et al.* 2013b). From literature, Mo, Mn, W, and Re have been found to be more active in NOCM reactions (Weckhuysen *et al.* 1998b) while others like Zn, Pt, Cu, Ni, V, and Cr showed little activity in overall methane conversion (Majhi *et al.* 2013b). Table 2-1 shows catalytic activity of common transition metal catalysts supported on HZSM-5 in terms of methane conversion and hydrocarbon selectivity.

Table 2-1: CH_4 conversions and product selectivity over 0.5%metal/HZSM-5 catalysts.

Catalyst	CH_4 con. (%)	Product selectivity		Reference
		C_2	Aromatics	
HZSM-5	1.0	0.0	100.0	(Wenlong 2000)
Mo/HZSM-5	7.9	12.8	75.7	(Weckhuysen *et al.* 1998b)
Fe/HZSM-5	4.1	22.1	89.5	(Weckhuysen *et al.* 1998b)
W/HZSM-5	2.4	20.1	50.8	(Weckhuysen *et al.* 1998b)
Ni/HZSM-5	0.01	60.0	40	(Wenlong 2000)
Mn/HZSM-5	2.1	5.9	81.8	(Majhi *et al.* 2013b)
Cu/HZSM-5	0.6	34.0	66.0	(Wenlong 2000)
Pt/HZSM-5	0.03	68.6	0.0	(Majhi *et al.* 2013b)
Re/HZSM-5	7.0	4.0	48	(Majhi *et al.* 2013b)
V/HZSM-5	0.6	0.0	63.1	(Majhi *et al.* 2013b)
Cr/HZSM-5	0.3	0.0	19.4	(Majhi *et al.* 2013b)
Zn/HZSM-5	1.0	19.6	69.6	(Majhi *et al.* 2013b)
MoO_3/HZSM-5	4.1	47.7	42.32	(Wenlong 2000)
MoO_3/HZSM-5	5.6	6.6	93.4	(Wenlong 2000)
Mo_2C/HZSM-5	5.71	48.3	51.7	(Wenlong 2000)
Zr/HZSM-5	5.2	5.8	94.2	(Wenlong 2000)
La/HZSM-5	3.3	6.1	93.9	(Wenlong 2000)

2.6.6 Promotion of Mo/HZSM-5 with the second transition metal

Despite Mo/HZSM-5 being the most stable and most promising catalyst in nonoxidative methane conversion, it suffers from limited selectivity towards hydrocarbons and low methane conversion. To this end, several metals have been touted as suitable promoters to enhance its catalytic activity. Stability and selectivity of Mo/HZSM-5 catalyst has been improved by promotion with Ru, Zr, V, Cu, Fe, Zn and W (Shu *et al.* 1997). According to (Chen *et al.* 1995), catalytic activity of 2%Mo/HZSM-5 catalyst improved after being doped with platinum. The role played by Pt was disputed by (Ma *et al.* 2013) and (Sily *et al.* 2006) as it contributed to lower benzene yields and more coke formation. On the other hand, promotion of Mo/HZSM-5 with Co and Re improved methane conversion as reported by (Liu *et al.* 1997) and (Shu and Ichikawa 2001a). However, a repeat of a similar study by (Burns *et al.* 2006) did not find any

significant improvement on its catalytic activity. From Table 2-2, results of 2%Mo/HZSM-5 catalyst promoted with different transition metals are given but, in my opinion, they are not conclusive as different metal loading and transition metal synergism could give totally different results.

Table 2-2: Methane conversion and product selectivity over Mo-doped catalysts loaded on HZSM-5.

Catalyst	CH_4 con. (%)	Product selectivity		Reference
		C_2	Aromatics	
0.5%Pt-2%Mo/HZSM-5	5.9	4.7	79.1	(Majhi *et al.* 2013b)
1.0%La-2%Mo/HZSM-5	3.3	6.1	93.9	(Majhi *et al.* 2013b)
0.5%W-2%Mo/HZSM-5	4.0	5.0	95.0	(Majhi *et al.* 2013b)
1.0%V-2%Mo/HZSM-5	2.7	11.1	88.9	(Majhi *et al.* 2013b)
1.0%Zr-2%Mo/HZSM-5	5.2	5.8	94.2	(Majhi *et al.* 2013b)
0.1%Li-2%Mo/HZSM-5	4.2	23.1	65.7	(Majhi *et al.* 2013b)
0.1%P-2%Mo/HZSM-5	5.4	8.7	79.8	(Majhi *et al.* 2013b)
1.2%Rh-6%Mo/HZSM-5	7.1	6.9	93.1	(Majhi *et al.* 2013b)
1.5%Pt-6%Mo/HZSM-5	7.2	6.7	93.3	(Majhi *et al.* 2013b)
0.3%Pd-2%Mo/HZSM-5	5.2	3.1	91.1	(Majhi *et al.* 2013b)
0.3%Ru-2%Mo/HZSM-5	4.8	4.0	89.7	(Majhi *et al.* 2013b)
0.3%Ir-2%Mo/HZSM-5	4.6	4.4	88.3	(Majhi *et al.* 2013b)

2.6.7 Catalytic activity of molybdenum on different supports in NOCM reaction.

For proper dispersion of the catalyst active component and prevention of excessive coke deposition, several transition metal catalysts have been anchored on different supports. The role played by supports (Aboul-Gheit and Awadallah 2009), the nature of transition metal on the support (Amin 2005), and catalyst doping using the second metal has been extensively studied by various research groups. In the development of catalysts for NOCM process, further efforts have been employed to eliminate undesirable side reactions and delay catalyst deactivation (Wu *et al.* 2005).

Zeolites have stood out as potential candidates for use as catalyst support in NOCM reactions. They are made up of silicon, aluminium, and oxygen in their framework and have cations, water and other molecules in their pores (Weitkamp 2000). They are preferred for application in NOCM reactions due to their high crystallinity, availability of weak and strong acids, thermal stability, and high surface area to ensure shape selective reaction in catalysis (Schwarz *et al.* 1995). Zeolites with pore diameters in the range of 5-6 Å are useful in NOCM reactions. The most used zeolite support for NOCM reaction is ZSM-5 which is also called molecular sieve five (MFI), made from the unit pentasil. Catalytic activity of Mo/HZSM-5 is bifunctional in a sense that, the metal is responsible for hydro/dehydro-condensation of the reactions while the acid sites from the zeolite is responsible for aromatization (Ismagilov *et al.* 2008). The synergetic effect between acid sites of HZSM-5 and Mo was studied by (Chen *et al.* 1995). Catalytic activities of both unsupported Mo and Mo/HZSM-5 catalysts were studied by (Szöke and Solymosi 1996) who found that selectivity towards benzene was only due to Mo. However, other authors (Wang *et al.* 2004) revealed the existence of a strong influence between the nature of the support and Mo on methane conversion.

From literature (Zhang *et al.* 1998), it has been reported that higher selectivities to aromatics can be achieved when Mo is supported on HZSM-5, HZSM-8, HZSM-11, H-MCM-22, H-HMCM-39, H-MCM-41, and ZRP-1. These types of zeolites are best supports for molybdenum in NOCM reactions because their two-dimensional pore structure is equivalent to the kinetic diameter of benzene molecule which plays a role in methane aromatization. From Table 2-3, catalytic activity of Mo on different supports have been reported by different authors. However, a clear picture of each support could have come out well if Mo loading on each support was constant.

Table 2-3: Catalytic activity of Mo catalysts loaded on different supports in non-oxidative methane conversion.

Catalyst	CH_4 con. (%)	Product selectivity		Reference
		C_2	Aromatics	
3%Mo/SiO_2	5.3	2.1	8.7	(Majhi *et al.* 2013b)
3%Mo/Al_2O_3	7.4	2.0	4.0	(Majhi *et al.* 2013b)
3%Mo/HZSM-5	6.9	4.5	91.3	(Shu and Ichikawa 2001a)
3%Mo/USY	6.4	2.2	10.5	(Majhi *et al.* 2013b)
6%Mo/HZSM-8	4.11	3.9	86.7	(Majhi *et al.* 2013b)
3%Mo/HZSM-11	7.61	5.3	91.6	(Majhi *et al.* 2013b)
7%Mo/H-β	3.11	8.8	80.4	(Majhi *et al.* 2013b)
3%Mo/H-MCM-41	0.9	8.7	80.1	(Majhi *et al.* 2013b)
3%Mo/Mordenite	7.3	3.5	4.1	(Majhi *et al.* 2013b)
3%%Mo/FSM-16	6.6	1.6	6.4	(Majhi *et al.* 2013b)
2%Mo/MCM-22	5.7	4.9	67.8	(Majhi *et al.* 2013b)
2%Mo/ZSM-5	9.7	4.1	47.2	(Majhi *et al.* 2013b)
3%Mo/HSAPO-34	0.6	10.1	72.9	(Shu and Ichikawa 2001a)
6%Mo/H-MCM-22	10.0	3.4	84.4	(Shu and Ichikawa 2001a)
6%Mo/nano-HZSM-5	6.8	3.4	60.3	(Shu and Ichikawa 2001a)
6%Mo/micro-HZSM-5	10.5	3.2	73.0	(Shu and Ichikawa 2001a)
6%Mo/HZRP-1	10.5	2.3	79.8	(Shu and Ichikawa 2001a)

2.6.8 Carbonaceous catalysts

During nonoxidative methane conversion, metal oxides are reduced by methane to metal carbides at the induction stage. Formation of metal carbides block catalyst active sites leading to catalyst deactivation. These challenges can be circumvented by use of carbon-based catalysts which are stable with no metal carbide formation, high fuel flexibility, high thermal stability, cheap, resistant to poisoning by sulphur, and they deactivate slowly as compared to solid metal catalysts (Malaika and Kozłowski 2009). Carbon materials can be used both as catalysts and as catalyst support (Dufour *et al.* 2008). Use of carbon-based catalysts in NOCM reaction have received much attention because the generated carbon can further catalyse the reaction and

catalyst regeneration step is not required. Materials for use as carbon catalysts include; activated carbon (AC) (Moliner *et al.* 2005), carbon black (CB) (Lee *et al.* 2004), coal chars (Dufour *et al.* 2008), acetylene black (AB), diamond powder and soot (Muradov 2001a), carbon nanotube (CNTs), graphite (Guil-Lopez *et al.* 2011), and carbon materials with monolithic honeycomb design (Gatica *et al.* 2013). To achieve meaningful methane conversion using carbon based catalysts, high activation energy (143-236kJ/mol) and temperatures in the range of 800℃ to 1000℃ are required for the process (Kim *et al.* 2004).

Methane activation over carbon-based catalysts begins with cleavage of C-H bond, followed by various chain reactions which lead to formation of hydrogen and carbon nanomaterial and hydrocarbons. Initially, a methane molecule interacts with chemically reactive carbon crystallites to break the C-H bond energy forming new C-C bonds in a hexagonal shape. Formation of the new species arises from the fusion of carbon nuclei and growth of carbon nanomaterial. Carbon black is most stable because it is easily accessed by methane molecules despite having low catalytic activity (Suelves *et al.* 2007).

2.6.8.1 Application of activated carbon as catalyst supports in petrochemical industry.

Activated carbon is a highly porous material consisting of graphene layers and hydrophilic surface functional groups. The inherent functional groups are desired for use in adsorption, and catalysis. Activated carbon finds application in oil and natural gas, food, pharmaceuticals, water treatment, hydro metallurgy, gold recovery, and carbon in pulp-process (Soleimani and Kaghazchi 2008). Activated carbon materials are regarded as suitable adsorbents in the treatment of industrial, municipal, and domestic effluents because of simplicity in process design and development. Carbon materials are not affected by corrosion and are not affected by acids and bases (Chen *et al.* 2002).

In addition to purification of gases and liquids with high adsorption potential, activated carbon materials are also used as catalysts and catalyst supports. They play a critical role in most electrochemical devices such as batteries (Endo *et al.* 2000), supper capacitors, and fuel cells. The structure of activated carbon is highly disordered and comprises of aromatic sheets and strips. The voids and gaps of molecular dimensions, between such aromatic sheets are regarded as micro pores. Most commercial activated carbons are either coal based (Kruk *et al.* 2005) or petroleum pitch based (Hayashi *et al.* 2000) which are prone to exhaustion. Industrially,

activated carbon materials are produced either from coal or lignocellulosic materials (Okada *et al.* 2003). In addition to specific advantages like retention of the structural features of the original plant tissue (bio-templating feature), carbon materials produced from botanical sources possess high carbon content. The oxygen to carbon (O/C) and hydrogen to carbon (H/C) atomic ratios are lower in the case of carbon materials produced from plant materials rather than coal. Activated carbon material is produced either by physical or chemical activation. Chemical activation is a one-step process in which an organic precursor is carbonized in the presence of a chemical agent (alkaline earth metal or acid). The role of the activating agent is to act as a dehydrating agent that controls pyrolytic decomposition to prevent formation of tar and thereby improving carbon yields.

The physical activation process comprises of two steps, namely carbonization of the carbonaceous precursor in an inert atmosphere and subsequent activation of the formed char in the presence of carbon gasification reactants (carbon dioxide, steam, or air). In addition to the specific surface area, other parameters such as pore size distribution, surface wettability, and presence of functional groups greatly influence the performance of activated carbon in catalysis. The most important functional groups in activated carbon are represented in scheme 5.

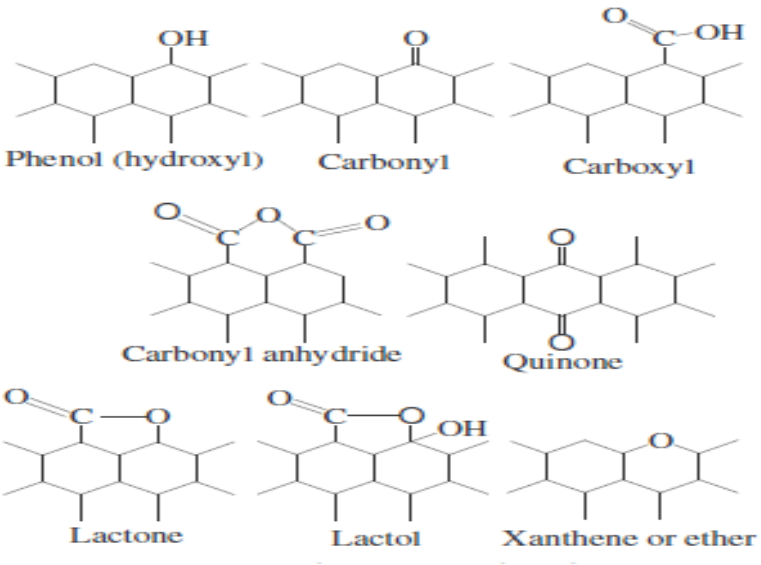

Scheme 5. Schematic representation of oxygen surface functional groups on the surface of carbon surface material. Adapted from (Viswanathan *et al.* 2009).

Carbon materials are interesting candidates for supporting Pt-based electro catalysts. In fact, the nature of carbon material in terms of (oxygen functional groups, electronic conductivity, pore structure, morphology, and electrochemically accessible surface area) determine the electrochemical performance of electrode catalysts. Electronic conductivity, surface area, microstructure, micromorphology, corrosion resistance, and cost are important properties that influence the choice of carbon materials as electrode catalysts. Fourier transform infrared (FT-IR) spectroscopy provides evidence for the presence of specific functional groups on the carbon material. Upon characterization, several characteristic bands were observed in the FT-IR spectrum and shown in Table 2-4.

Table 2-4. Assignment of FT-IR bands to specific oxygen containing surface functional groups on activated carbon material.

No.	Band position cm^{-1}	Assignment	Reference
1	3747	Isolated O-H groups	(Puziy *et al.* 2003) (Budinova *et al.* 2006)
2	3450	O-H stretching vibration of surface hydroxyl groups and adsorbed water. Asymmetry (shoulder-like feature at 3237 cm^{-1} is attributed to hydrogen bonding	(Ji *et al.* 2007) (Biniak *et al.* 1997) (Yu *et al.* 2008)
3	2927	Aliphatic, symmetric C-H stretching vibration of methylene group	(Puziy *et al.* 2003) (Puziy *et al.* 2005)
4	2846	Aliphatic, symmetric C-H stretching vibration of methylene group	(Puziy *et al.* 2005) (Gerçel *et al.* 2007)
5	2315	Ketone group	(Macias-Garcia *et al.* 2006)
6	1637	C=O (carbonyl) stretching vibration in Quinone	(Ji *et al.* 2007) (Biniak *et al.* 1997)
7	1452	In-plane bending vibration of C-H of methylene group	(Puziy *et al.* 2003) (Budinova *et al.* 2006)
8	1372	In-plane bending vibration of C-H of methylene group	(Puziy *et al.* 2003) (Budinova *et al.* 2006)
9	1000-1300	C-O stretching in alcohols, phenols, acids, esthers, and esters	(Guo and Rockstraw 2007)
10	679	Out of plane deformation vibration of C-H groups located at the edges of aromatic planes	(Biniak *et al.* 1997)

Even though a cluster of functional groups is present on the carbon surface, prominent among them are a sharp and intense band centred around 1637 cm^{-1} which is assigned to carbonyl (C=O) stretching vibration of Quinone. The carbon surface is oxidized by treatment with conc. HNO_3 leading to the generation of such Quinone type carbon functional groups which bear significance in the redox chemistry of carbon materials. Such carbonyl functional groups are known to be pronounced in the case of oxidized carbon materials rather than the original parent carbon material. Further, a broad and intense band observed in the range of 3200-3600 cm^{-1}, centred at

3450 cm^{-1} is attributable to O-H stretching vibration of surface hydroxyl groups as well as to adsorbed water. The symmetry of this band (shoulder at lower wave number, 3237 cm^{-1}) indicates the presence of strong hydrogen bond interactions.

Among the various adsorbents like metal-organic frameworks (MOFs), zeolites and other carbon materials offer many advantages such as thermal stability, chemical stability, reversibility, low-cost, availability, and easy regeneration (Lillo-Ródenas and Lozano-Castello 2003). Despite the numerous advantages of carbon materials, the main drawback that limits their application in hydrogenation is their low heat of adsorption (Sethia and Sayari 2016).

2.7 Common catalyst preparation methods.

Catalyst preparation methods are many and as such each individual catalyst may be produced via a specific method. In each catalyst preparation technique, several steps are involved in the catalyst synthesis. Most catalysts (supported metal-oxides) are prepared by successive impregnation, drying, calcination, and final activation while zeolite catalysts are prepared by precipitation of the gel, crystallization, washing, ion exchange, and drying. Important stages in catalyst preparation are mixing catalyst precursors in desired amounts, pre-treatment of the primary solid (1st precursor) by either impregnation, precipitation or crystallization for zeolites. These steps are followed by processing of the primary solid by heat treatment and activation of the catalyst precursor by reduction of metal oxides to metal (hydrogenation), reduction of metal oxides to metal carbides (carburization), formation of sulphides (hydrodesulphurization), and deammoniation (in the case of acidic zeolites).

2.7.1 Impregnation

This method entails contacting a solid with a liquid containing desired amounts of the components to be deposited on the surface. During impregnation, many processes such as selective adsorption of species (charged or not charged) by coulomb's force, van dar Waals forces, ion exchange between the charged surface and the electrolyte, polymerization of the species (ions or molecules) attached to the surface, and partial dissolution of the surface of the solid takes place. Impregnation can be done through different methods such as.

- ✓ Impregnation by soaking or with excess solution in which excess liquid is eliminated by washing or draining. This technique works well where ion-solid interactions are involved.
- ✓ Dry or pore volume impregnation in which the required components are introduced in the volume corresponding to the support pore volume.
- ✓ Incipient wetness impregnation in which appropriate amount of the solution is determined and corresponds to the pore volume of the solute beyond which, the catalyst becomes wet.
- ✓ Another method is deposition by selective reaction with the surface of the support in which the carrier is left to contact with an excess solution for a definite time and the excess liquid is removed by a dipping technique.
- ✓ Impregnation by percolation in which the precursor is sorbed or ion exchanged by percolation of the impregnating solution through a porous bed.
- ✓ Co-impregnation entails introduction of two or more components in a single step.
- ✓ Successive impregnation is where two or several components are introduced one after another in a sequence.

2.7.2 Precipitation and co-precipitation.

In this catalyst preparation method, two distinct steps namely, nucleation and growth are involved. Nucleation requires the system to be far from equilibrium (high super saturation or high solubility for ionic species). The new phase develops as conditions approach the equilibrium state. A phase involving two or more components; where one component is contained in an anion and the second component is in a cation giving rise to a precipitated mixture with a near fixed composition. If both are anions or cations, the nature of the reaction with a common anion or cation of the precipitate, the solubility constants, and the super saturation values will all be different, and the property of the precipitate will change after some time. Low super saturation leads to either; poorly dispersed solids or highly dispersed solids which are thermodynamically unstable. Special maturation (or ageing) step is carried out at the end of precipitation if specific effect is required. There are various precipitation and co-precipitation procedures, the simplest method being drop-wise addition of the solution rich in the desired chemical substance to the precipitating solution and vice versa.

The most widely used catalyst synthesis methods are; impregnation and co-precipitation (Abbas and Wan Daud 2010). A lot of water is required in the above methods during catalyst preparation steps (washing and filtering) which require more energy and time to accomplish. A comparative study of both impregnation and co-precipitation on fusion of metallic nitrates was done by (Suelves *et al.* 2006) and (Echegoyen *et al.* 2007). Based on the results obtained, they concluded that the rate of methane activation without catalyst deactivation remained the same in an 8-hour reaction period. Catalytic activity and stability of $NiO\text{-}Al_2O_3\text{-}SiO_2$ catalysts made by co-precipitation method (Ashok *et al.* 2008) was much better than those obtained by impregnation and mechanical mixing.

Other catalyst synthesis methods include deposition precipitation (Ermakova *et al.* 2000), impregnation (Li *et al.* 2006), reverse impregnation (Suelves *et al.* 2006), mechanochemical activation (Chesnokov and Chichkan 2009), and fusion reverse impregnation (Suelves *et al.* 2006). Catalyst textural properties, phase distribution, and metal support interaction (MSI) influence the performance of the catalyst. Impregnation and deposition-precipitation catalyst preparation methods are suitable for low metal loading of catalysts (e.g., $<$20wt %) which have a weak metal support interaction. Suitable catalysts specially made for achievement of thin diameter MWCNTs and SWCNTs are prepared using Sol-gel method (Piao *et al.* 2002). This method is widely used in catalyst systems that comprise of high metal loading to enhance carbon and hydrogen yields. In most catalyst preparation methods, a Feitknecht compound (FC) is widely used as a precursor to facilitate the formation of a homogeneous precipitate.

To get a good catalyst for methane conversion (Chen *et al.* 2009), an FC precursor of Ni/A_2O_3 is usually calcined at high temperature. High metal loading nickel-based catalysts are usually prepared by reverse impregnation (Abd Hamid *et al.* 2017). This method entails synthesizing nickel oxide via precipitation, drying, and calcining it at high temperature. The synthesis of bulk Raney catalyst from Fe-Co-Ni metal alloy was done by draining out aluminium with NaOH solution at room temperature before using the catalyst for NOCM reaction. Remarkable results were achieved when Cu-Ni Raney-metal was thermally treated *in situ* at 873K during synthesis of Raney catalyst (Cunha *et al.* 2009).

2.7.3 Sol-gel method

The sol-gel process involves the transition of a solution system from a liquid "sol" mostly colloidal into a solid "gel" phase. The starting materials for use are usually inorganic metal salts or organic metal compounds such as metal alkoxides.

In sol-gel process, the precursor undergoes a series of hydrolysis (reaction with water) and polymerization reactions to form a colloidal suspension, or a "sol". Further processing of a sol makes it possible to obtain other forms of materials in different forms such as monoliths, fibres, and monosized powders. Monoliths bulk gels (greater than 1 nm) cast to shape and processed without breaking whereas, composites are a combination of different types of materials to obtain synergistic properties unattainable by one material alone.

The specific features and regularities of this process are considered in Iler's monograph (Pakhomov and Buyanov 2005). Silica gel and other hydrogels can be synthesized by the sol gel method using water hydrolysis of tetrachlorides of various metals (MCl_4) i.e., $SiCl_4$, $TiCl_4$, and $ZrCl_4$. These chlorides are highly volatile and fume in air to form heavy gels laced with chlorine ions. The sol-gel method was widely used when alkoxides of various metals including tetramethoxysilane (TMOS), tetraethoxysilane (TEOS), tetraiso-propoxytitanium, Zirconium isopropoxide, and magnesium methoxide were employed as starting materials

2.7.4 Mechanical mixing

Methods based on mechanical mixing of components are used as an alternative to co-precipitation and deposition. Their advantage is that they produce negligible wastewater or emissions. The most integral part of the method is dispersion and homogenization of the catalyst precursors followed by drying and or calcination. This method is simple and straight forward than co-precipitation or calcination of heteronuclear complexes.

2.8 Market value of non-oxidative conversion of methane products

The market stock of carbon nanomaterial in 2016 was estimated at; 8.1-9.4 million tons of carbon black, 1.9 million tons of activated carbon, and 500 million tons of metallurgical coke (Keipi *et al.* 2016). The same study revealed that, the yearly production of CNTs was 2500 tons in 2010 with a projected increase to 12000 by end of 2016.

Carbon finds numerous application in the building industry as building material, in direct carbon fuel cells, and soil amendment (Muradov 2001b). On the market front presently, the market value for carbon is estimated to be 1500 $/ton of activated carbon, carbon black (555-444) $/ton and the value of metallurgical coke was 169.5 $/ton. The market value of CNTs research grade was 0.6-10 $/g and that of the industrial grade was 380 $/ ton for a diameter of 10 to 30 nm.

Hydrogen gas is another valuable product of methane conversion process. Commercial hydrogen from methane steam reforming was valued at 0.0627-0.1255$/ ton while hydrogen from electrolysis was valued at 0.200 - 0.376$/ ton. As shown in Table 2-5, global hydrogen price is directly proportional to its purity (Y. Li *et al.*2017). The highest purity grade fetches the highest retail price. Despite wide application of hydrogen gas, major challenges are emission of carbonaceous compounds from major hydrogen producing technologies, handling, storage, and flammability of the gas.

Table 2-5: Global market price of hydrogen gas of different purities (2017)

Hydrogen purity	Hydrogen price ($/Kg-$H_2$)
99.9%	4.2
99.99%	5.2
99.999%	6.0
99.9999%	6.9

The current market value of common methane conversion products is given in Table 2-6.

Table 2-6: Global market price of CH_4 conversion products (OPEC 8th Dec. 2020)

Petrochemical	Retail price (USD/MT)
Hydrogen	8990
Methane	34.64
Ethane	560
Ethene (Ethylene)	2350
Acetylene	1600
Propane	3738
Butane	2440
Benzene	5660
Toluene	509.5
Xylene	510
Naphthalene	413
Methanol	342.1
Formaldehyde	122
Acetic acid	268.7
Methyl acetate	1275
Chloromethane	3850
Dichloromethane	505
Chloroform	704
Hydrogen cyanide	2000
Acrylonitrile	2210
Middle distillate/Diesel	450
Distillate fuel oil/Kerosene	517.7
Gasoline/jet fuel	967.4

2.9 Summary

Based on the performance of transition metals and common supports in terms of methane conversion, aliphatic selectivity, reaction rate, and aromatic selectivity, a catalyst system comprising of trimetallic Fe, W, & Mo supported on activated carbon and HZSM-5 can be a suitable candidate for application in non-oxidative conversion of methane into carbon and different petrochemicals. The motivation behind the choice of catalyst, is based on the following premise.

a. **Active component (Fe-W-Mo):** Active components were selected transition metals which facilitate the catalyst dehydrogenation function and improves hydrocarbon selectivity (Shu and Ichikawa 2001b). Much as they are desired, they undergo deactivation due to sintering and coking in the non-oxidative methane conversion reaction (Vogelaar *et al.* 2010). A combination of two or more catalytically active metals will give much improved activity as compared to the results of individual metals. The following metals were chosen as active components based on their catalytic properties.

   i. **Molybdenum:** Based on its surface properties and its reducibility from Mo^{6+} to Mo_2C, it has been found to be the most active metal when supported on zeolite, with 60-75% benzene selectivity and 7-12% methane conversion, (Karakaya and Kee 2016).

   ii. **Tungsten:** Use of tungsten on a suitable support gives good conversion and significant benzene yields. It also promotes selectivity towards aliphatic compounds and inhibits the formation of naphtha (Weckhuysen *et al.* 1998b), (Fila *et al.* 2015).

   iii. **Iron:** Use of iron as a transition metal ion increases selectivity of aromatics and reduces coke selectivity (Aboul-Gheit *et al.* 2008). It is very active and is therefore desired for methane conversion as well.

b. **Catalyst support.**

   i. **Activated carbon:** Activated carbon is stable both in acidic and alkali media and deposited carbon on it can easily be burned off during catalyst regeneration (Shukla *et al.* 2010). It is porous with high surface area (800-1200 m^2/g), very good pore size distribution (Nayak *et al.* 2017), and high mechanical strength (Perrich 2018).

   ii. **HZSM-5 zeolite:** This zeolite has a channel structure, inherent acidity, thermal stability (Ali *et al.* 2002), and with high surface area (Fujikawa *et al.* 2000). The channel structure and acidity of HZSM-5 zeolite enhances the valence location of transition metal. From literature (Khan *et al.* 2018), the activity of acidic supports has been studied and found to occur according to the following pattern; HZSM-5 > γ-Al_2O_3> SiO_2 MgO> ZrO_2 with benzene forming only on HZSM-5 and γ-Al_2O_3.

Direct conversion of methane takes place at high temperature (~1000K) and the products formed are limited to C_2 hydrocarbons (C_2H_6 and C_2H_4). The corresponding mechanism is complex and proceeds both heterogeneously and homogeneously. After CH_3^* radicals are formed by catalyst initiation, the gas self-coupling of CH_3^*, hydrogen, and other alkyl radical's formation proceeds simultaneously. This species can undergo oxidative coupling to form C_2H_6. In all the above three stages of NOCM reaction, C_2H_6 can easily be dehydrogenated in the absence of the catalyst at ~900K.

In non-oxidative methane conversion, a methane molecule is activated on the catalyst surface into CH_3^* radicals and subsequent transformation to benzene and its derivatives. The reaction mechanism comprises of three steps.

i. Catalysis for the formation of C_2H_6 by MoCx. During this stage, MoCx species react with methane to generate a specific carbonaceous intermediate (Intermediate I) on the catalyst surface, which is further converted to C_2H_6 by further reactions of methane with the CH_3^* radicals.
ii. Formation of C_2H_6 via molybdenum-carbene intermediates. At this stage, methane reacts with Mo^{6+} on HZSM-5 zeolite to produce CH_3^+ (a methoxy species on the Bronsted acid sites of the zeolite) and $[Mo\text{-}H]^{5+}$ which are further transformed into a molybdenum-carbene species ($Mo{=}CH_2$). This species further reacts with CH_4 to produce C_2H_6.
iii. Coupling of methyl radicals (CH_3^*) to produce C_2H_6. The reaction of methyl radical (CH_3^*) is another intermediate reaction that forms on the surface of the Mo species to form MoO_3.

Unsupported Mo_2C catalyst is less active and gives rise to C_2 hydrocarbons but not aromatic hydrocarbons. Its catalytic activity is low compared to Mo/H^+ exchanged zeolites. Conversely, Mo/H^+ exchanged zeolites is known to yield both C_2 hydrocarbons as well as the aromatics. This implies that the Bronsted acid sites of the zeolite are responsible for generation of catalyst active sites and the activation of C-C bond to yield benzene and its derivatives.

Since Mo/H^+ exchanged zeolites are bifunctional catalysts, the Mo species on H^+ zeolite must be modified to achieve optimum catalytic activity in terms of conversion and selectivity towards

C_2 hydrocarbons and aromatics. During the induction stage of NOCM reaction, the MoOx species is reduced to molybdenum carbide by methane. Subsequent reactions occur due to interactions between the Mo species and the zeolite Bronsted acid sites. Carbonaceous compounds formed during NOCM reaction are responsible to deactivation of the Mo/H^+ exchanged zeolite catalysts.

Therefore, non-oxidative conversion of methane is envisaged as one of the models for describing complex and multiple reactions that determine and estimate product distribution in NOCM reactions. This study demonstrates the development of a tuneable catalyst system comprising of Fe, W, &Mo supported on HZSM-5 and activated carbon for use in non-oxidative methane conversion. It has been demonstrated that such a tuneable catalyst system at different metal loadings and process conditions could be employed to achieve desired methane conversion and selectivity towards useful petrochemicals in non-oxidative methane conversion.

CHAPTER 3. EXPERIMENTAL

3.1 Introduction

In this study, a series of stable, durable, and tuneable 5.4 %wt. metal binary catalyst systems comprising of Fe, W, &Mo supported on HZSM-5 were synthesized and tested for methane conversion and quantitative determination of product distribution in non-oxidative conversion of methane into carbon and petrochemicals. The catalyst systems were synthesized by various techniques and characterized for surface area, crystallite size, phase identity, and morphology of deposited carbon nano material. Synthesized catalysts were applied for non-oxidative methane conversion in a packed bed reactor at different process conditions. Liquid and gaseous products from the reactor were analysed using an online gas chromatograph (Shimadzu 2014).

3.2 Materials and methods

3.2.1 Materials

The materials were procured and used as obtained. Catalyst precursors were; Ammonium ZSM-5 (NH_4ZSM-5 SiO_2/Al_2O_3 ratio 50) 99.8% pure from Zeolyst International-USA, Activated carbon 99.9% pure from Merck, Ferric nitrate Fe $(NO_3)_3.9H_2O$ 99.8% pure from Sigma Aldrich-USA, Ammonium heptamolybdate $(NH_4)_6Mo_7O_{24}.4H_2O$ 99.8% pure from Merck-USA, Ammonium Para tungstate ATP) $(NH_4)_{10}W_{12}.4H_2O$ 99.9% from Merck-USA, hydrogen gas (99.8% pure from Afrox-South Africa), methane feed mixture (50%CH_4:50%Ar from Afrox-South Africa), nitrogen gas (99.8% pure from Afrox-South Africa) and distilled water.

3.2.2 Equipments used

- ✓ Beakers
- ✓ Burette
- ✓ Motor & pestle
- ✓ Crucibles
- ✓ Packed bed reactor
- ✓ Flow meter
- ✓ Muffle furnace
- ✓ Tube furnace
- ✓ Oven
- ✓ Quartz wool

- ✓ Gas chromatograph
- ✓ Water pump
- ✓ Liebig condenser
- ✓ Conical flask
- ✓ Stopwatch

3.3 Catalyst preparation methods

The Fe, W, & Mo catalyst systems supported on HZSM-5 and AC were synthesized using incipient wetness impregnation, sequential impregnation, and mechanical mixing.

3.3.1 Incipient wetness impregnation

- Dried mixture of NH_4ZSM-5 was calcined at 550℃ for 6 hours to convert it into the hydrogen form (HZSM-5).
- Solutions of each catalyst precursor (Ferrite nitrate, ammonium Para tungstate, and ammonium heptamolybdate) in calculated quantities according to %wt. were prepared and stirred continuously for 2 hours. A resultant solution of three catalyst precursors; Ferrite nitrate (FN), ammonium Para tungstate (APT), and ammonium heptamolybdate (AHM) in calculated quantities according to %wt. was dissolved in distilled water and stirred continuously for 2 hours.
- The resultant solution was then deposited onto calculated amounts of HZM-5 drop-wise up to the point of incipient wetness. The mixture was left to dry overnight (12 hours) at 110℃.
- The dried mixture was then calcined at 500℃ for 6 hours to get a catalyst with corresponding metal oxides loaded on HZSM-5 (Fe_2O_3-WO_4-MoO_3/HZSM-5).

3.3.2 Sequential impregnation

- Dried mixture of NH_4ZSM-5 was calcined at 550℃ for 6 hours to convert it into the hydrogen form (HZSM-5).
- Ammonium heptamolybdate (AHM) in calculated quantities according to required %wt. was dissolved in distilled water and stirred continuously for 2 hours. The resultant solution was then deposited onto calculated amounts of HZM-5 drop-wise up to the point of incipient wetness. The mixture was left to dry overnight (12 hours) at 110℃, dried and calcined at 500℃ to get MoO_3/HZSM-5

- Next, MoO_3/HZSM-5 catalyst was impregnated with a solution of ammonium Para tungstate (APT) in calculated quantities. The mixture was left to dry overnight (12 hours) at 110℃, dried and calcined at 500℃ to get WO_3-MoO_3Mo/HZSM-5.
- Next, WO_3-MoO_3/HZSM-5 catalyst was impregnated with a solution of Ferrite nitrate (FN) in calculated quantities. The mixture was left to dry overnight (12 hours) at 110℃, dried and calcined at 500℃ to get Fe_2O_3-WO_4-MoO_3/HZSM-5

3.3.3 Co-impregnation by mechanical mixing

- Dried mixture of NH_4ZSM-5 was calcined at 550℃ for 6 hours to convert it into the hydrogen form (HZSM-5).
- Metal oxides of iron (Fe_2O_3), tungsten (WO_3) and molybdenum (MoO_3) were prepared from their metal precursors; ferrite nitrate (FN), ammonium Para tungstate (APT), and ammonium heptamolybdate (AHM) in calculated quantities according to required %wt., respectively.
- The three metal oxides were mechanically mixed with HZM-5 and activated carbon in a mortar. The resultant mixture was calcined at 500℃ for 5hrs according to a similar procedure done elsewhere (Borry *et al.* 1998). Catalysts supported on HZSM-5 were calcined in flowing air while those supported on activated carbon were calcined in flowing nitrogen.

3.4 Characterization of synthesized catalysts

The prepared catalysts were characterized for by XRD, BET, SEM, and FT-IR for phase identification, surface area, structural properties, and presence of functional groups, respectively.

3.4.1 XRD-analysis

X-ray diffraction (XRD) analyses of fresh catalysts were carried out sing an XRD instrument (BRUKER AXS-Germany) equipped with a diffractometer (D8 Advance). The measurements were done continuously on a J-J scan in locked coupled mode and the tube was Cu-Ka radiation (lKa_1=1.5406Å). Lynx Eye (Position sensitive detector) at 40kV and 40mA with a V20 variable slit was used. The measurements were recorded from 0.5-130° with an increment of (D2J: 0.034°) most of the time. Data evaluation was done using EVA software from BRUKER **(**PDF database 1999).

3.4.2 SEM analysis

Scanning electron microscopy (SEM) was done using (FEI Nova Nano SEM 230) instrument with a field emission gun to analyse particle size of synthesized catalysts. The samples were imaged using the high-resolution immersion lens. The EDS detector (Oxford X-Max equipped with INCA software Landing E 5.00KeV) and a working distance of HFW 5.97-29.8, Sopt3.5 and WD (5.8-6.7) was used. The samples were prepared by sprinkling a small amount of the sample onto a 12 mm aluminium SEM stub covered with carbon glue. The excess sample was blown off with compressed air and the samples were carbon coated before being loaded into the SEM equipment.

3.4.3 BET analysis

The specific areas, pore volume, and particle size distributions of the catalysts were determined from N_2 adsorption data at -196℃ using a Micromeritics Tristar II 3020 instrument. For each analysis, 0.2 g of each catalyst was degassed at 300℃ for 12 hours to remove residual moisture from the catalyst surface and other adsorbed gases before loading the samples on the BET instrument. Catalyst surface areas were calculated according to B.E.T method and the pore size distributions were obtained according to Barrete Joynere Halenda (BJH) method from the adsorption-desorption isotherm data.

3.4.4 FT-IR Analysis

IR spectra were recorded using a step-scan Fourier transform infrared spectrometer (BIO-RAD FTS-60A/896) with a resolution of 4 cm^{-1}, and a co-accumulation of 64 interferograms to improve the signal/noise ratios of the IR spectra. Sample powders from each catalyst were pressed into a self-supporting wafer (2.0 mm ID, 15-18 mg/cm^2) with a pressure of 50 MPa. The wafer was then mounted in situ IR cell equipped with CaF_2 window. The IR measurements were recorded between (500-400 cm^{-1}) wavenumber and conducted by exposure of the disk containing the catalyst at 723K for 2 hours to pyridine vapour of 1.2 kPa at 300K.

3.5 Catalyst evaluation

Non-oxidative methane conversion experiments were performed in a packed bed reactor of dimensions (ID 8.5 mm, OD 12.7 mm and L-575 mm) at different temperatures, different gas hourly space velocities (GHSVs), different reaction time, and atmospheric pressure. The reactor

was first stuffed with Quartz wool at the middle to hold the catalyst, loaded with 0.5 g of the catalyst, and then pacified with nitrogen gas at a flow rate of (100 ml/min) at 400℃ for 30 minutes to remove residual moisture and volatile matter. Heating was programmed at $5℃/min$ until the desired temperature was attained. Methane gas mixture (50%CH_4:50%Argon) was then introduced into the reactor at different GHSVs. The outlet of the reactor was connected to a condenser and then to a conical volumetric flask to collect the pyrolysis gas. Both liquid and gaseous products from the reaction were analysed using a gas chromatograph (Shimadzu 2014). Mass balance based on total gas flowrate in and out of the reactor was calculated using equation 70 since the mass flow rate of argon as the internal standard gas remains the same in and out of the reactor. Methane% conversion and selectivity of each product containing carbon atom, including CO and CO_2 on carbon basis (S^{carbon}) can be calculated from equation 71 and 73, respectively. Coke selectivity was calculated from (100%-sum of product selectivities (%)).

In equations 70-73, F, X and N^{carbon} represent the total gas flow rate, mole fraction, and carbon number in the hydrocarbon molecule, respectively. Similarly, selectivity for the formation of hydrogen-containing products on a hydrogen base can be calculated and thus the ratio of hydrogen to carbon in the formed coke can be estimated. For each NOMC run, time on stream was set at 4 hours. The performance of each catalyst was evaluated in terms of methane conversion and selectivity towards C_2 hydrocarbons, benzene, toluene, xylene, hydrogen, and coke.

The amount of methane consumed can be calculated from equation 70.

$$\mathrm{F^{inlet}} \times \mathrm{X_{CH4}inlet} - \mathrm{F^{outlet}} \times \mathrm{X_{CH4}outlet} = \text{Methane reacted} \tag{70}$$

Methane conversion and selectivity towards C_2 hydrocarbons, benzene, toluene, xylene, hydrogen, and coke were determined by applying the following equations.

$$\text{Conversion (\%)} = \frac{\mathrm{F^{inlet}}\times\mathrm{X_{CH4inlet}} - \mathrm{F^{outlet}} \times \mathrm{X_{CH4outlet}}}{\mathrm{F^{inlet}} \times \mathrm{X_{CH4inlet}}} \times 100 \tag{71}$$

$$\text{Hydrogen selectivity (\%)} = \frac{\text{moles of } \mathrm{H_2} \text{ out}}{2 \times \text{moles of } \mathrm{CH_4\ (reacted)}} \times 100 \tag{72}$$

Selectivity Hydrocarbon (%) = $\frac{F^{outlet} \times X_{CxHy} \times N_{carbon}}{F^{inlet} \times X_{CH4in} - F^{outlet} \times X_{CH4\ out}} \times 100$ (73)

Where *N* is the carbon number in the hydrocarbon which represents the stoichiometric ratio.

Coke selectivity (%) = 100% - $\sum Pi$ % (74)

Where $\sum Pi$, is the sum of product selectivity (%), other than coke.

Coke selectivity (%) was calculated from equation 74.

Non-oxidative methane conversion process is illustrated in the process flow diagram shown in Figure 3-1.

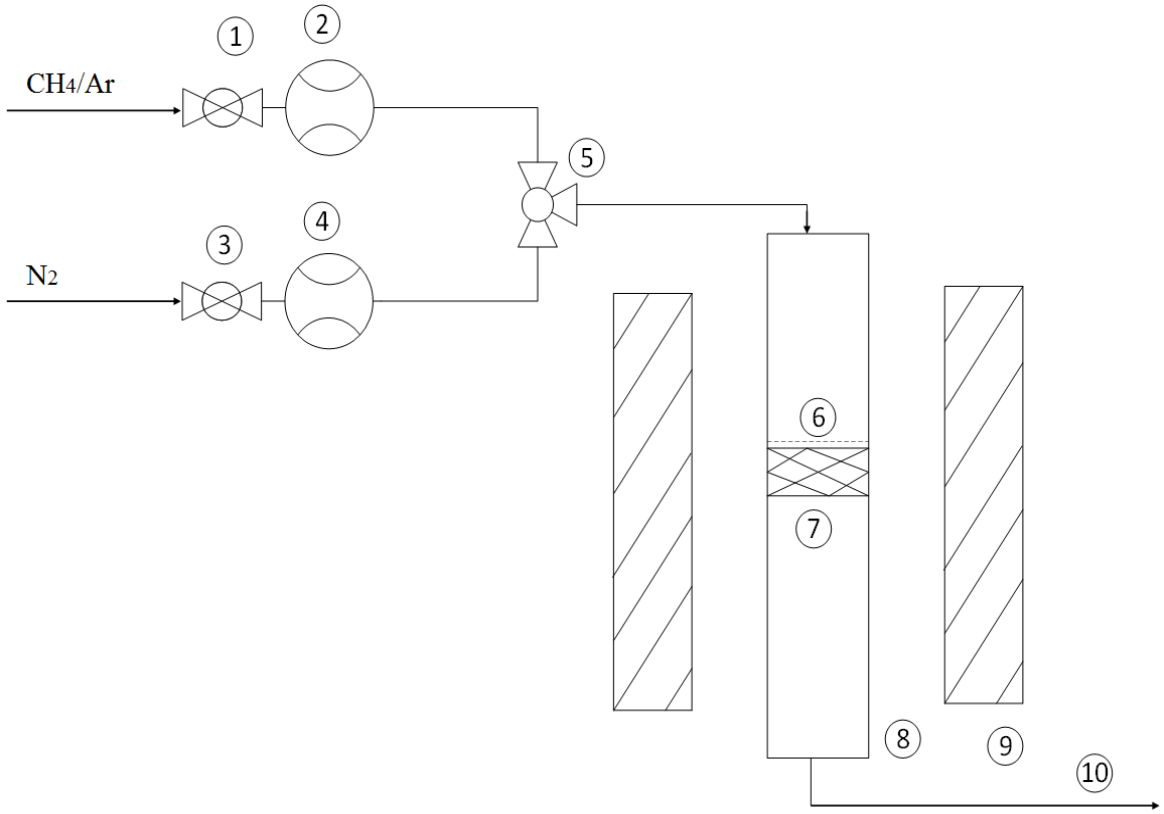

Fig 3-1 Process flow diagram for methane conversion

1-Ball valve, 2-Flow meter, 3-Ball valve, 4-Flow meter, 5-3way plug valve, 6-catalyst, 7-quartz wool, 8-Reactor, 9-Furnace, 10-Products.

3.6 NOCM reaction operating conditions

- Reactor temperature data points were 700℃, 750℃, and 800℃.
- GHSVs; 0.96 $Lg^{-1}_{cat.}h^{-1}$, 1.92 $Lg^{-1}_{cat.}h^{-1}$, and 2.88 $Lg^{-1}_{cat.}h^{-1}$
- Activation time: 1 hour, 2hours, 3hours, and 4hours.
- Reactor pressure: Atmospheric pressure
- Ambient temperature (Durban University room temperature ≈ 25℃))

3.7 Analytical equipment operating conditions

3.7.1 TCD analysis

During TCD analysis, the instrument operating parameters were maintained as follows.

- Nitrogen gas flowrate 15 mL/min
- Detector temperature; 250℃
- Injector temperature; 120℃
- Current; 50 mA
- Hold time;9999.9mins
- Column temperature; 40℃
- Inlet pressure 60K

3.7.2 FID analysis

During FID analysis, the instrument operating parameters were maintained as follows.

- Hydrogen gas flow rate 45 mL/min
- Air flow rate 450 mL/min
- Detector temperature; 275℃
- Injector temperature; 120℃
- Oven temperature 40℃
- Current; 50 mA
- Hold time;9999.9mins
- Split ratio 1:20

3.7.3 Degree of uncertainty

Typical quantification range for all tested components was 0.01mol%

3.8 Characterization of spent catalyst

To analyse the nature and morphology of deposited carbon nanomaterial on the catalyst, Thermogravimetric analysis (TGA) and Transmission Electron Microscopy (TEM) analysis techniques were used.

3.8.1 TGA Analysis

Thermogravimetric analysis of each catalyst was done using a differential thermogravimetric analyzer, TGA-6/DTG of Perkin Elmer (precision of temperature ± 2℃) equipped with a microbalance sensitivity of $< 5\mu g$ to monitor weight loss as functions temperature between 40-900℃. The experiments were carried out in air at atmospheric pressure at a flow rate of 60 ml/min at various linear heating rates of 5,10, 20, and 30 ℃ /min. Small masses (10-25 mg) of each material were used to avoid mass and heat transfer limitations.

3.8.2 TEM analysis

The instrument used in TEM analysis was (JEOL JEM-1010-South Korea, equipped with a high-resolution camera). Before the test, 5 mg of each catalyst was prepared by ultrasonic dispersion in isopropyl alcohol and sonicated for 10 minutes. After sonication, a drop of each catalyst was deposited on a carbon supported film and dried for 15 minutes before putting the sample in the TEM machine. Imaging of test samples were done at high resolution to obtain fine details on the deposited carbon nano material.

CHAPTER 4. RESULTS AND DISCUSSIONS

4.1 Objective I: To investigate the effect of catalyst metal loading on methane conversion and product distribution.

To study the effect of metal loading in the catalyst system on methane conversion and product distribution, various catalyst systems were synthesized and screened based on their activity in methane conversion.

4.1.1 Catalyst screening

To investigate the effect of metal loading on methane conversion and product distribution in NOCM reaction, the following procedure was adopted. Firstly, each single metal catalyst (F/HZSM-5, W/HZSM-5, and Mo/HZSM-5) was prepared at 1.8, 3.6, 5.4, and 7.2 %wt. metal loading and tested for methane conversion at 750℃ in a packed bed reactor. Based on methane conversion, catalysts were screened, and the desired binary catalyst system was built at different metal loading supported on HZSM-5 and AC. The second screening involved coupling of the two metals (Fe-Mo, W-Mo, and Fe-W) on HZSM-5 and AC and evaluated based on methane conversion under the same process conditions. Finally, all the three metals (Fe-W-Mo) at desired metal loading were loaded on the HZSM-5 and AC and tested for methane conversion. Based on the results obtained, three most significant catalysts were discussed further.

The catalyst systems were developed as follows.

- 24 different single metal catalysts were synthesized, (12 metal catalysts supported on AC and 12 metal catalysts supported on HZSM-5)
- 12 Single metal catalysts supported on HZSM-5 were as follows: Fe/HZSM-5 at 1.8%, 3.6%, 5.4%, and 7.2% metal loading, W/HZSM-5 at 1.8%, 3.6%, 5.4%, and 7.2% metal loading, and Mo/HZSM-5 at 1.8%, 3.6%, 5.4%, and 7.2% metal loading.
- 12 Single metal catalysts supported on activated carbon were as follows: Fe/AC at 1.8%, 3.6%, 5.4%, and 7.2% metal loading, W/AC at 1.8%, 3.6%, 5.4%, and 7.2% metal loading, and Mo/AC at 1.8%, 3.6%, 5.4%, and 7.2% metal loading.
- The synthesized catalysts were tested for non-oxidative methane conversion in a packed bed reactor at 750℃, 0.96 GHSV, and 1 atm for 4 hours' time on stream.
- The synthesized catalysts were evaluated based on methane conversion

4.1.2.1 First catalyst screening.

Initial catalyst screening was done by evaluating the performance of single metal catalyst systems at 750℃, 0.96 $Lg^{-1}cat.h^{-1}$, 4hrs time on stream, and 1 atm based on methane conversion. Catalytic activity of the single metal catalyst systems based on methane conversion are given in Table 4-1.

Table 4-1. Methane conversion over single metal catalyst systems loaded on HZSM-5 and AC

No.	Catalyst	CH_4 conv. (%)	No.	Catalyst	CH_4 conv. (%)
1.	HZSM-5	0.3	1.	AC	0.1
2.	7.2%Mo/HZSM-5	3.9	2.	7.2%Mo/AC	6.8
3.	5.4%Mo/HZSM-5	8.3	3.	5.4%Mo/AC	4.1
4.	3.6%Mo/HZSM-5	6.8	4.	3.6%Mo/AC	3.1
5.	1.8%Mo/HZSM-5	3.5	5.	1.8%Mo/AC	1.9
6.	7.2%W/HZSM-5	9.7	6.	7.2%W/AC	7.3
7.	5.4%W/HZSM-5	12.9	7.	5.4%W/AC	4.6
8.	3.6%W/HZSM-5	11.3	8.	3.6%W/AC	3.3
9.	1.8%W/HZSM-5	4.0	9.	1.8%W/AC	2.3
10.	7.2%Fe/HZSM-5	5.8	10.	7.2%Fe/AC	5.5
11.	5.4%Fe/HZSM-5	7.8	11.	5.4%Fe/AC	4.7
12.	3.6%Fe/HZSM-5	3.8	12.	3.6%Fe/AC	3.1
13.	1.8%Fe/HZSM-5	2.0	13.	1.8%Fe/AC	1.5

After the 1st catalyst screening, monometallic, bimetallic, and trimetallic catalysts systems were developed by maintaining overall metal loading at 5.4 %wt. as shown in Table 4-2.

Table 4-2. Composition of monometallic, bimetallic, and trimetallic catalyst systems at 5.4%wt metal loading before loading onto HZSM-5/AC.

Catalyst system	Individual metal loading (%Wt.)	Overall metal loading (%Wt.)
Monometallic catalyst system	5.4	5.4
Bimetallic catalyst system	2.7	5.4
Trimetallic catalyst system	1.8	5.4

4.1.2.2 Selected binary catalyst systems

Equal %wt. metal loading at 1.8 %wt. was taken as the basis for the development of trimetallic catalyst systems. From the 1.8 %wt. basis, every metal catalyst composition was loaded in the overall catalyst system and adjusted to (1.8 ± 0.45) %wt. at a time while maintaining the binary mixture of 5.4 %wt. metal (Fe, W, Mo)/HZSM-5 or AC. From Table 4-2, the difference in metal loading between each catalyst system in the overall 5.4 %wt. metal loading is 0.9 %wt. Therefore, the 0.45 %wt. used to adjust the metal loading upwards and downwards from the 1.8 %wt. basis in the trimetallic catalyst was half of 0.9 %wt. The selected catalyst systems were designated as shown in Table 4-3.

Table 4-3. Nomenclature of the binary catalyst systems loaded on HZSM-5 and AC**.**

No.	Nominal catalyst system	Catalyst composition by Weight
1.	1.8F1.8W1.8M/HZSM-5	1.8%F1.8%W1.8%M/HZSM-5
2.	2.25F2.25W0.9M/HZSM-5	2.2%F2.25%W0.9%M/HZSM-5
3.	2.25F0.9W2.25M/HZSM-5	2.25%F0.9%W2.25%M/HZSM-5
4.	0.9F2.25W2.25M/HZSM-5	0.9%F2.25%W2.25%M/HZSM-5
5.	1.35F1.35W2.7M/HZSM-5	1.35%F1.35%W2.7%M/HZSM-5
6.	1.35F2.7W1.35M/HZSM-5	1.35%F2.7%W1.35%M/HZSM-5
7.	2.7F1.35W1.35M/HZSM-5	2.7%F1.35%W1.35%M/HZSM-5
8.	1.8F1.8W1.8M/AC	1.8%F1.8%W1.8%M/AC
9.	2.25F2.25W0.9M/AC	2.25%F2.25%W0.9%M/AC
10.	2.25F0.9W2.25M/AC	2.25%F0.9%W2.25%M/AC
11.	0.9F2.25W2.25M/AC	0.9%F2.25%W2.25%M/AC
12.	1.35F1.35W2.7M/AC	1.35%F1.35%W2.7%M/AC
13.	1.35F2.7W1.35M/AC	1.35%F2.7%W1.35%M/AC
14**.**	2.7F1.35W1.35M/AC	2.7%F1.35%W1.35%M/AC

4.1.2.3 Second catalyst screening based on methane conversion

From the 2nd screening, catalytic activity of various systems supported on HZSM-5 and AC are given in Table 4-4. From Table 4-4, when all the three noble metals are loaded onto HZSM-5 in equal quantities, least activity in terms of methane conversion was achieved. High methane conversion values were achieved when Mo content was low in the binary catalyst system. From these results, it can be seen that optimum methane conversion cannot be achieved by loading all the three metals in equal quantities onto HZSM-5 or on AC. This could be due to competing reactions. Iron was responsible for rapid catalyst deactivation and low methane conversion after 4hrs time on stream while tungsten improved catalyst stability leading to high catalytic activity.

From catalyst screening results, three catalysts (1.8F1.8W1.8M/HZSM-5, 2.25F2.25W, 0.9Mo/HZSM-5, and 1.35F1.35W2.7M/HZSM-5) were selected and discussed to investigate the effect of metal loading on product distribution. A lot of research on bifunctional catalysis of Mo/HZSM-5 (Wang *et al.* 1993) revealed that MoO_3 crystallites were the active sites for methane activation. An interaction between MoO_3 and the acid sites of the HZSM-5 constitute

the active component of the catalyst (Zhang *et al.* 1998). This was another motivation for investigating catalyst systems where Mo content is both high and low and its effect on methane conversion and product distribution.

Table 4-4. Methane conversion over various catalysts loaded on HZSM-5 and AC at 750℃, 0.96 $Lg^{-1}cat.h^{-1}$ and 1 atm.

No.	Catalyst	Methane conversion (%)
1	1.8F1.8W1.8Mo/HZSM-5	5.9
2	2.25F2.25W0.9Mo/HZSM-5	16.3
3	2.25F0.9W2.25Mo/HZSM-5	13.4
4	0.9F2.25W2.25Mo/HZSM-5	14.5
5	1.35F1.35W2.7Mo/HZSM-5	13.4
6	1.35F2.7W1.35Mo/HZSM-5	13.9
7	2.7F1.35W1.35Mo/HZSM-5	13.6
8	.8F1.8W1.8Mo/AC	8.6
9	2.25F2.25W0.9Mo/AC	10.1
10	2.25F0.9W2.25Mo/AC	8.4
11	0.9F2.25W2.25Mo/AC	7.9
12	1.35F1.35W2.7Mo/AC	6.8
13	1.35F2.7W1.35Mo/AC	7.4
14	2.7F1.35W1.35Mo/AC	6.9

After the second catalyst screening, the final catalyst systems were developed and designated based on %wt. composition as shown in Table 4-5.

Table 4-5. Selected binary catalyst systems for use in non-oxidative methane conversion.

Catalyst	Composition (wt.%)
1.8F1.8W1.8M/HZSM-5	1.8Fe – 1.8%W – 1.8%Mo-94.6%HZSM -5
2.25F2.25W0.9M/HZSM-5	2.25%Fe – 2.25%W – 0.90%Mo-94.6%HZSM -5
1.35F1.35W2.7M/HZSM-5	1.35Fe – 1.35%W – 2.70%Mo-94.6%HZSM -5
1.8F1.8W1.8M/AC	1.8Fe – 1.8%W – 1.8%Mo-94.6%AC
2.25F2.25W0.9M/AC	2.25%Fe – 2.25%W – 0.90%Mo-94.6%AC
1.35F1.35W2.7M/AC	1.35Fe – 1.35%W – 2.70%Mo-94.6%AC

4.1.3 Catalyst characterization

After catalyst screening, selected catalysts in Table 4-6 were characterized using characterization techniques previously given in section 3.4.

4.1.3.1 XRD-analysis

XRD patterns of HZSM-5 and all the three catalyst as shown in Figure 4-1 confirm the presence of distinct HZSM-5 (orthorhombic), $\alpha-Fe_2O_3$ (rhombohedral hematite), $\beta-MoO_3$ (monoclinic), and o-WO_3 (orthorhombic) phases. In all the four catalysts, sharp peaks at 2θ=8.0°, 8.9°, 9.1°, 14.9°, 20.9° and 23.2° are assigned to HZSM-5 according to diffraction peaks classification in JCPDS File no. (00-044-002). Peaks assigned to HZSM-5 are sharp relative to metal oxide peaks due to low metal loading (5.4%metal/HZSM-5). In catalysts 1.8F1.8W1.8M/HZSM-5, 2.25F2.25W0.9M/HZSM-5, and 1.35F1.35W2.7M/HZSM-5, peaks at 2θ=33.2°, 35.7°, 49.5°, and 54.1° are assigned to Fe_2O_3 in conformity with those in JCPDS File no. (87-1166) while peaks at 2θ = 34.3°, and 49.2° are assigned to MoO_3 corresponding to those in JCPDS File no. (05-0508). Low intensity peaks at 2θ=23.2°, 29.0°, 42.1°, and 50.4° are assigned to orthorhombic WO_3 corresponding to diffraction peaks classification in JCPDS File no. (32-1394).

In all catalysts, corresponding metal oxides from their precursors are clearly formed after calcination. Due to low metal loading in each catalyst system, the intensity of metal oxide phases was low because they were masked by HZSM-5. Less sharpness of metal oxide peaks can also be attributed to high dispersion in the support. After impregnating the zeolite with the oxides of Fe_2O_3, WO_3, and MoO_3, the intensity of the peaks decreased but the peak positions remained

unchanged. This implies that, impregnating the zeolite with metal oxides did not change its structure. This finding is similar to what is reported elsewhere (Bajec *et al.* 2019).

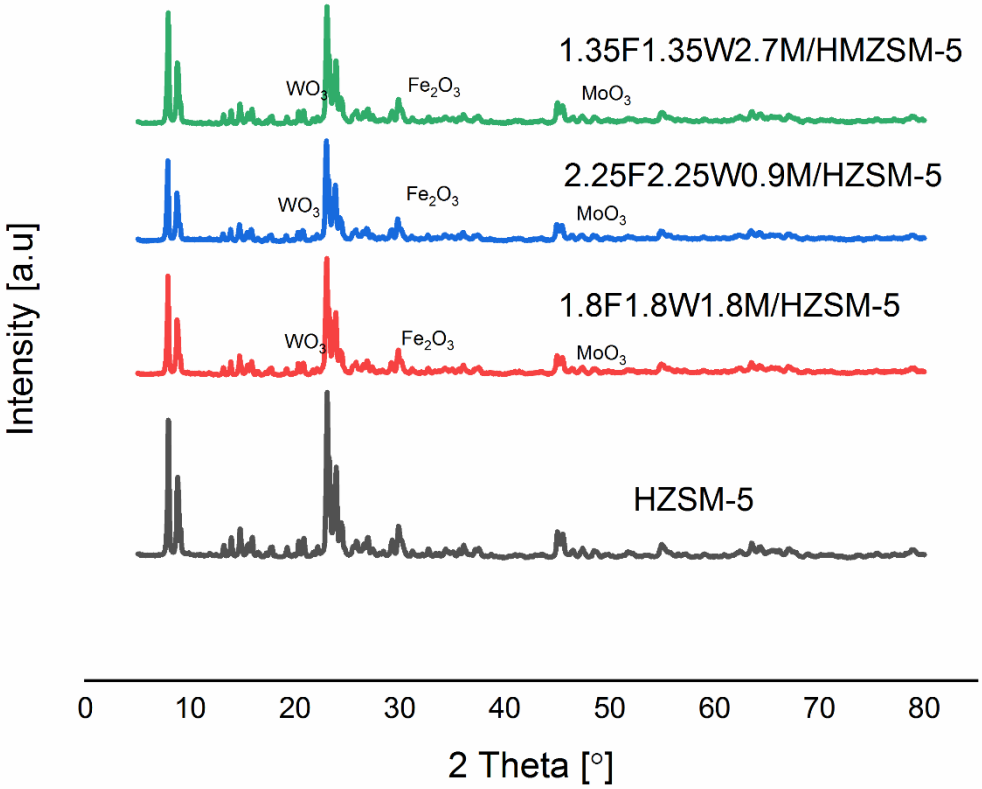

Figure 4-1. XRD patterns for catalyst; HZSM-5, 1.8F1.8W1.8M/HZSM-5, 2.25F2.25W0.9M/HZSM-5, and 1.35F1.35W2.7M/HZSM-5.

Figure 4-2 shows distinct phases of corresponding metal oxides from their precursors after calcination. Due to low metal loading in each catalyst system, the intensity of metal oxide phases was low because they are highly dispersed in the AC support. After impregnating AC with the oxides of Fe_2O_3, WO_3, and MoO_3, the intensity of the peaks decreased but the peak positions remained unchanged. Prominent peaks of activated carbon at 2θ = 23.8°, and 44.0° in each catalyst system implies that the presence of these metal oxides did not alter its structure entirely.

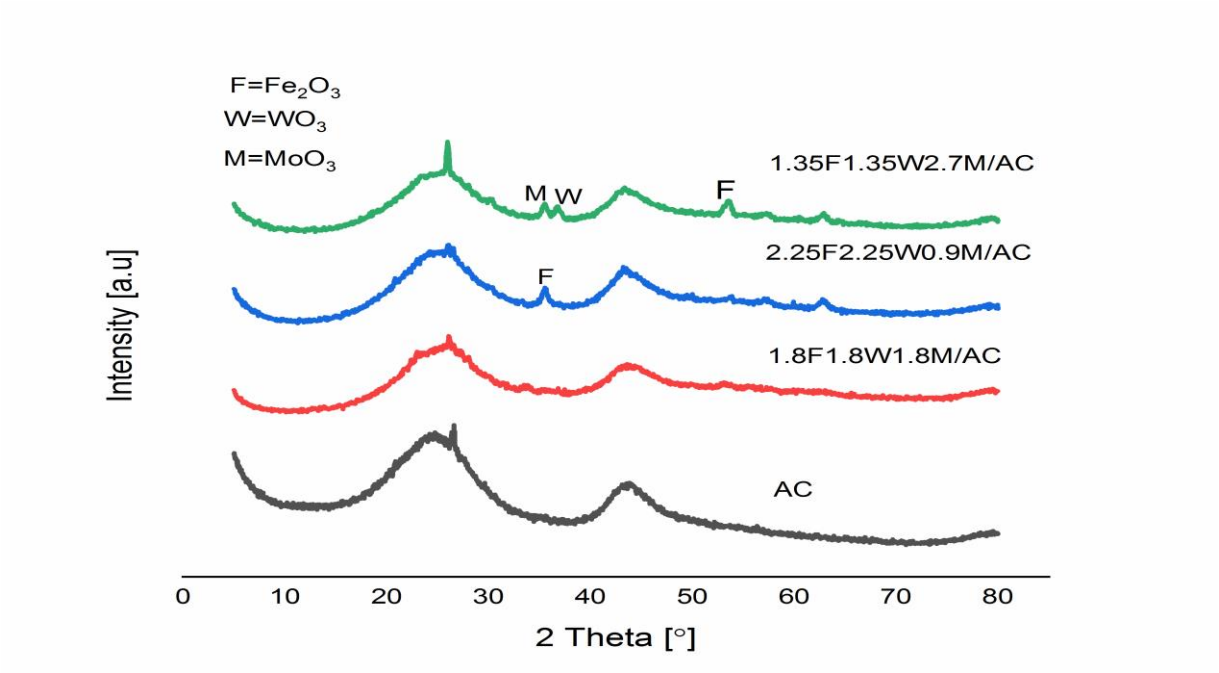

Figure 4-2. XRD patterns for catalyst; AC, 1.8F1.8W1.8M/AC, 2.25F2.25W0.9M/AC, and 1.35F1.35W2.7M/AC.

4.1.3.2 SEM Analysis

Figure 4-3 shows neat structures of nano particles which assume the shape of tri lobes, Quadra lobes, and spheres in catalyst 1.8F1.8W1.8M/HZSM-5. Using Image-J software, the calculated crystallite sizes ranged from 2.57-21.48 nm with an average crystallite size being 6.8 nm. The neatness of stacked structures on top of each other is an indication of little agglomeration after calcination. Similar structures in catalyst 2.25F2.25W0.9M/HZSM-5 with the crystallite size ranging from 2.57-29.04 nm with the average crystallite size being 7.68 nm were seen. An increase in maximum crystallite size in catalyst 2.25F2.25W0.9M/HZSM-5 implies more agglomeration and clumping together of catalyst crystallites than in catalyst 1.8F1.8W1.8M/HZSM-5. In catalyst 1.35F1.35W2.7M/HZSM-5, crystallite sizes ranged from 2.57-31.02 nm. In this catalyst, neat structures of catalyst crystallites with the shape of tri lobes are clearly seen. Based on the above trend, it was inferred that low metal loading in catalyst 1.8F1.8W1.8M/HZSM-5 promotes metal dispersion in the zeolite hence, less agglomeration. High molybdenum inhibits overall metal dispersion in the catalyst, hence more agglomeration. In a nutshell, all the four catalyst crystallite sizes ranged from 2.57 – 31.02 nm, an indication that all the catalyst crystallites were in the nano range.

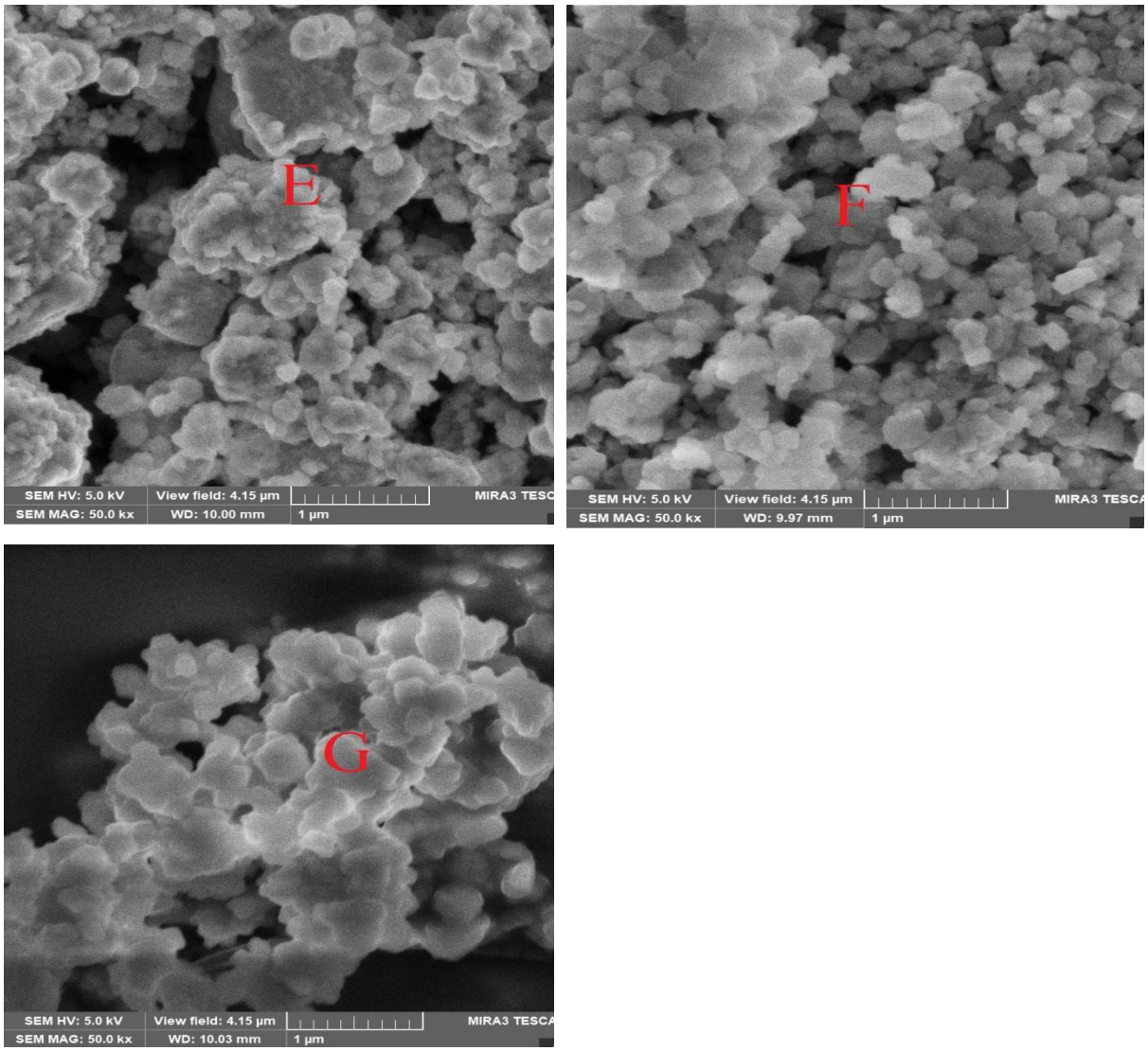

Figure 4-3. SEM Images of various catalyst loaded on HZSM-5; E(1.8F1.8W1.8M/HZSM-5), F(2.25F2.25W0.9M/HZSM-5), G(1.35F1.35W2.7M/HZSM-5).

From Figure 4-4, irregular structures of catalyst crystallites in catalyst 1.8F1.8W1.8M/AC can be seen. This is an evidence of pronounced agglomeration. Reducing the amount of Mo in the catalyst reduces aggregation of catalyst crystallites. This is the reason why there are definite structures neatly packed on top of each other in catalyst 2.25F2.25W0.9M/HZSM-5. Increasing the amount of Mo in the catalyst system led to an improvement in the catalyst structure because of little agglomeration in catalyst 1.35F1.35W2.7Mo/HZSM-5. Using Image J software, the size catalyst crystallites were established as follows: Crystallites of catalyst 1.8F1.8W1.8M/HZSM-5 ranged from 2.57-17.03 nm with the mean particle size being 6.29 nm. Crystallites in catalyst 2.25F2.25W0.9M/HZSM-5 ranged from 2.57-33.76 nm with mean particle size being 16.87 nm.

Crystallite size of catalyst 1.35F1.35W2.7M/HZSM-5 ranged from 2.57-29.83 nm with the mean size being 9.2 nm. The presence of large catalyst crystallites in catalyst 2.25F2.25W0.9M/HZSM-5 is an indication of particle agglomeration. This particle size range implies that catalyst crystallites in each catalyst system were in the nano range.

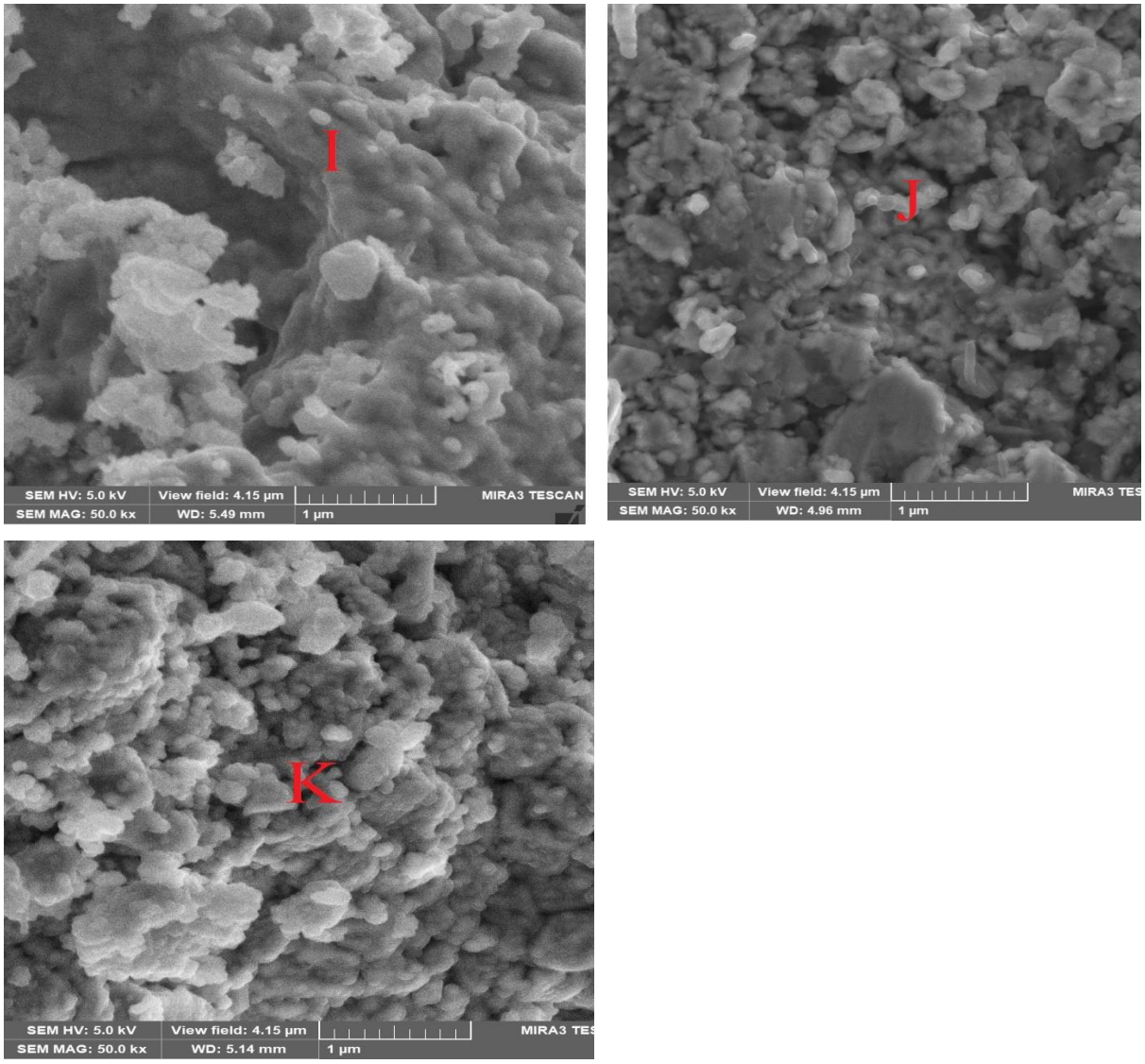

Figure 4-4. SEM Images of various catalysts loaded on AC; I(1.8F1.8W1.8M/AC), J(2.25F2.25W0.9M/HZSM-5), K(1.35F1.35W2.7M/AC).

4.1.3.3 BET analysis

From BET analysis results in Table 4-6, all the catalysts had a surface area above 400 m^2g^{-1}. The reference HZSM-5 zeolite had the following structural properties; surface area 495.877 m^2g^{-1}, pore volume 0.17874 cm^3g^{-1} and pore size of 24.748 Å.

Impregnating the zeolite with iron, tungsten, and molybdenum greatly altered its surface properties. Impregnating the zeolite with 1.8%Fe,1.8%W, and 1.8%Mo as it is typical in catalyst 1.8F1.8W1.8M/HZSM-5 reduced the zeolite surface area by 14.59%, and also reduced the pore volume by 3.97%. Despite a reduction in surface area and pore volume, pore size increased by 22.07%. In catalyst 2.25F2.25W0.9M/HZSM-5, there was a 0.12% and 11.92% increase in surface area and pore volume in reference to HZSM-5 zeolite, respectively. A further reduction in surface area and pore volume was seen in 1.35F1.35W2.7M/HZSM-5 catalyst, even though a notable increase in pore size was recorded in reference to the parent zeolite.

Based on the above trend, the reference HZSM-5 zeolite is a high surface area mesoporous material. Impregnating the zeolite with the oxides of Fe_2O_3, WO_3, and MoO_3 alters its structural properties. Increasing MoO_3 content in the catalyst reduces the surface area and pore volume of the catalyst but slightly increases its pore size. This implies that Mo species easily enters the HZSM-5 channels thereby reducing the zeolite surface area and micro pore volume. This finding is in agreement with what is reported elsewhere (Chen *et al.* 1995). Higher Fe and W loading in the catalyst system enhances the surface area, pore volume, and pore size of the resultant catalyst. Therefore, impregnating HZSM-5 zeolite with of Fe_2O_3, WO_3, and MoO_3 increases the catalyst pore size leading to an increase in tortuosity, which is desired for catalytic activity. In catalyst systems supported on activated carbon, the surface area is above 500 m^2g^{-1}. Impregnating the AC support with equal amounts of Fe_2O_3, WO_3, and MoO_3 increased the catalyst surface area and pore size. Reducing the amount of Mo in the catalyst system reduced its surface area. Based on the results in Table 4-6, it is evident that the presence of Mo on AC support was desired for improvement of the catalyst surface area and pore size.

Table 4-6. Catalyst surface area, pore volume, and pore size

Catalyst Name	BET Surface area (m^2/g)	Pore volume (cm^3/g)	Pore size (Å)
HZSM-5	496	0.1787	24.748
1.8F1.8W1.8M/HZSM-5	424	0.1716	30.210
2.25F2.25W0.9M/HZSM-5	497	0.200	30.339
1.35F1.35W2.7M/HZSM-5	408	0.1656	30.357
AC	571	0.242	34.782
1.8F1.8W1.8M/AC	1001	0.422	35.758
2.25F2.25W0.9M/AC	566	0.235	34.213
1.35F1.35W2.7M/AC	689	0.286	33.265

4.1.3.4 FT-IR analysis

From FT-IR spectra in Figure 4-5, the catalyst lattice vibrations were recorded between 500-4000 cm^{-1}. From Figure 4-5, notable peaks in the fingerprint region, especially at 1071-1080 cm^{-1} and 542-545 cm^{-1} are seen. Bands at 1071-1080 cm^{-1} are assigned to asymmetric stretching, bands at 542-545 cm^{-1} represent double ring while bands at 429-545 cm^{-1} belong to T-O bending vibration of internal tetrahedral (T=Si or Al). FT-IR transmittance peaks at 1226 cm^{-1}, 1100 cm^{-1}, 796 cm^{-1}, 624 cm^{-1},547 cm^{-1}, and 453 cm^{-1} are ascribed to characteristic framework vibration peaks of HZSM-5 zeolite (Cheng *et al.* 2017), i.e. the symmetric stretching vibration, anti-symmetric stretching vibration, vibration of five membered ring and block structure, and of T-O bending vibration peaks, respectively. The anti-symmetric stretching vibration peak at 1226 cm^{-1} is very sensitive to Si/Al ratio of HZSM-5 with the removal of aluminium species in the skeleton shifting the vibration to higher frequencies (Cheng *et al.* 2017). From literature, molybdenum oxide species associated with Bronsted acid sites is responsible for no-oxidative aromatization of methane and the process leads to loss of Bronsted acid sites (Liu *et al.* 2011). An increase in Bronsted acidity is desired for dispersion of metal oxides in the zeolite and improves the interaction between the metal oxides and zeolite thereby improving catalyst activity (Liu *et al.* 2004). In Figure 4-5, functional groups were present in each catalyst. Functional groups may be a source of hydrogen during the catalytic cycle. The formed hydrogen is essential for coupling reactions that lead into the formation of C_2 hydrocarbons.

From literature (Tan *et al.* 2002), these absorption bands at 1080 cm^{-1}, 810 cm^{-1} and 560 cm^{-1} are associated with internal linkages in SiO_4 (or AlO_4) tetrahedral and are very responsive to structural changes. The characteristic bands at 548 cm^{-1} and 1226 cm^{-1} are associated with ZSM-5 (Tan *et al.* 2002). The peak positions in the spectra suggest a little shift in the peak position in the frequency of 548 cm^{-1} or 1226 cm^{-1} adsorption band which can be attributed to dealumination of the of the zeolite lattice. As reported elsewhere (Campbell *et al.* 1996), after calcination surface and structural properties of HZSM-5 play a significant role in the interaction of Mo species and the zeolite support. Pure HZSM-5 zeolite comprises of three hydroxyl groups, Bronsted acidity (≡Al-OH-Si≡), silanol groups (Si-OH), and extra framework aluminium (Al-OH). The densities of these functional groups are different, and this affects their interactions with the zeolite.

Impregnation of the zeolite using Fe_2O_3, WO_3, and MoO_3 reduces the density of acid sites on the external surface of HZSM-5 and the number of molybdenum species deposited on the external surface during the ion exchange process (Wu *et al.* 2005) . This process increases selectivity towards benzene because the active centres of the acid and molybdenum oxide species are located inside the zeolite channels. Since the characteristic vibration peaks of HZSM-5 remained nearly unchanged, it was concluded that impregnation of HZSM-5 with Fe_2O_3, WO_3 and MoO_3 only shifted the peaks from 1071 cm^{-1} to 1080 cm^{-1}.

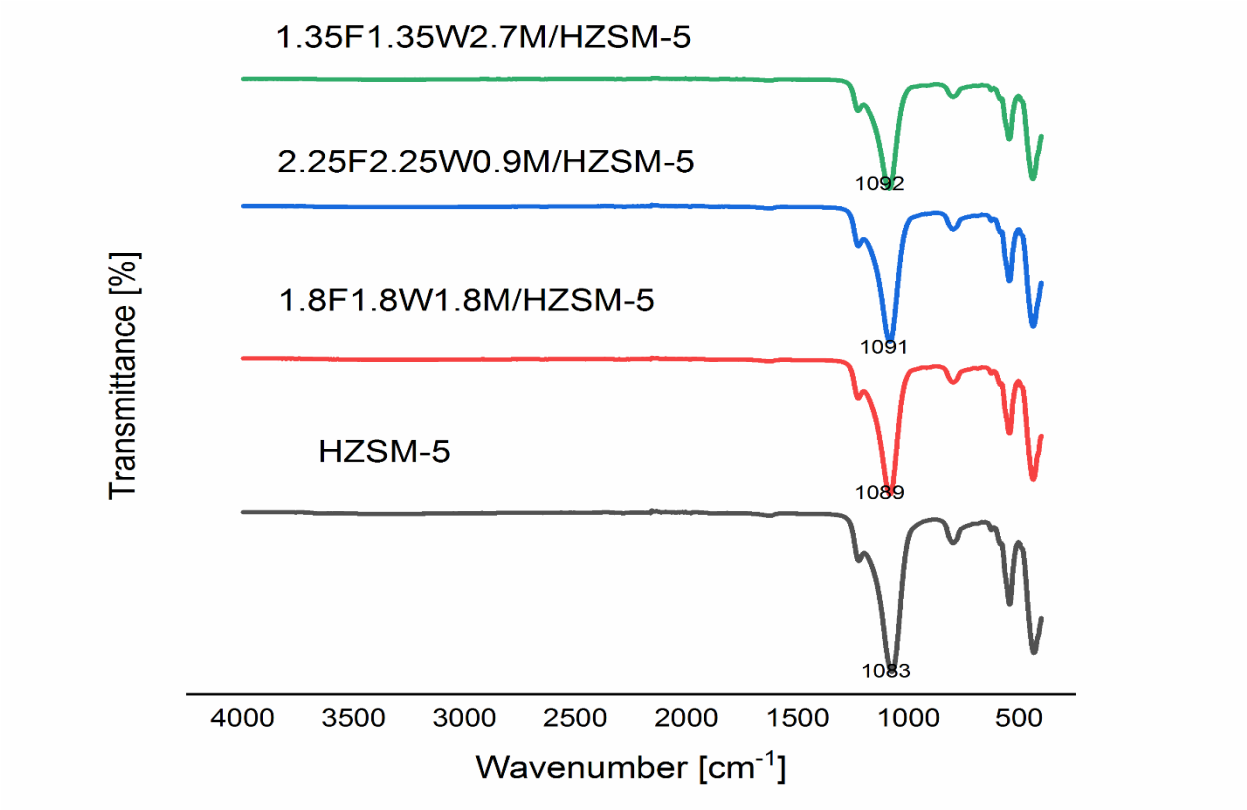

Figure 4-5. FT-IR spectra of HZSM-5 and various catalysts; 1.8F1.8W1.8M/HZSM-5, 2.25F2.25W0.9M/HZSM-5, and 1.35F1.35W2.7M/HZSM-5.

In Figure 4-6, there are no major peaks in the FT-IR spectra of catalysts supported on activated carbon. Since all catalyst were calcined at 500℃, most oxygen containing surface functional groups are thermally decomposed at that temperature. This finding is in agreement with what was reported elsewhere (Mathur *et al.* 2008). Faint peaks at 2100 cm^{-1} are assigned to C=C=O stretching of ketones. The peak at 1092 cm^{-1} represent C-O stretching of secondary alcohol like phenolic acid.

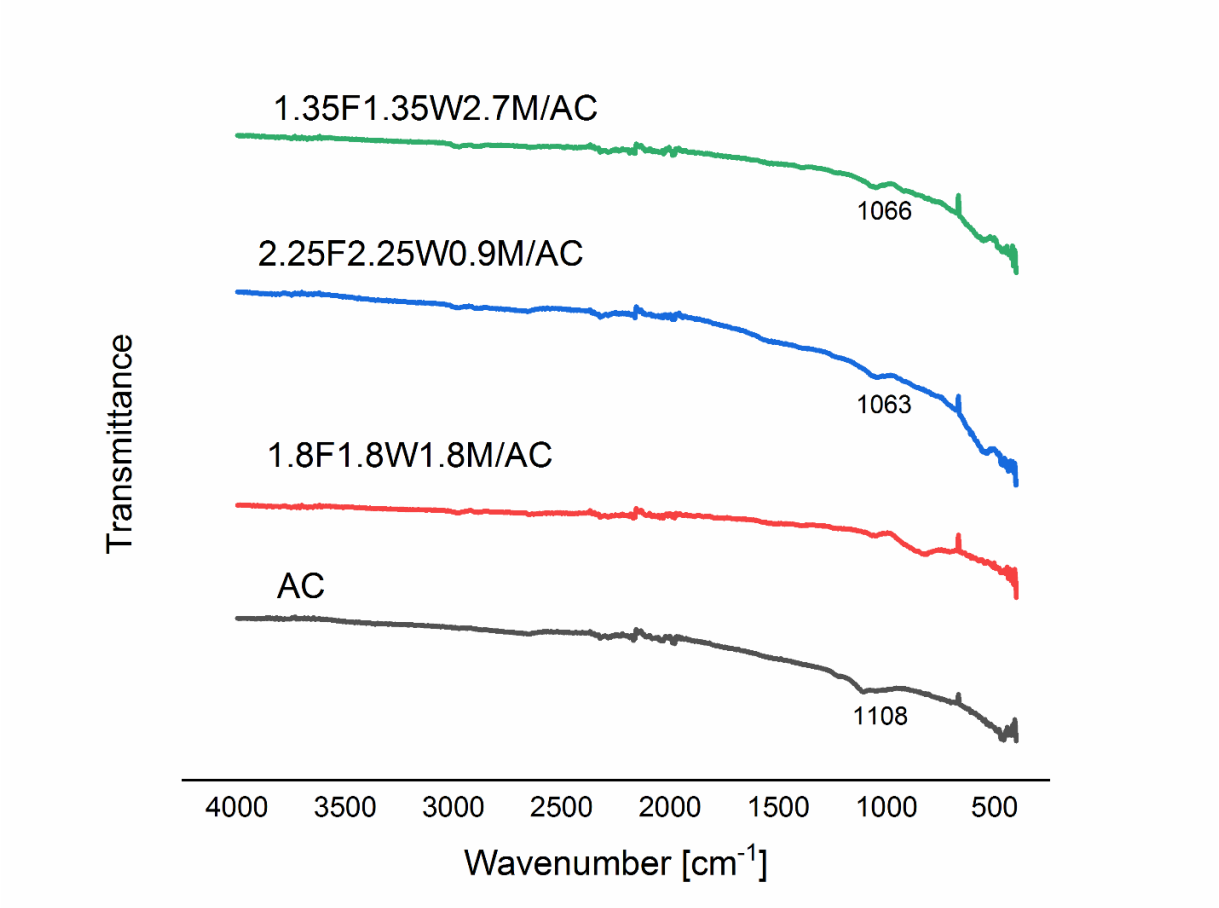

Figure 4-6. FT-IR spectra of AC and various catalyst; 1.8F1.8W1.8M/AC, 2.25F2.25W0.9M/AC, and 1.35F1.35W2.7/AC.

4.1.4 Catalyst evaluation

In Figure 4-7, catalytic activity of all the three catalysts (1.8F1.8W1.8M/HZSM-5, 2.25F2.25W0.9M/HZSM-5, and 1.35F1.35W2.7M/HZSM-5), followed a common trend. In all catalysts, their methane conversion was lowest at 700℃ and highest at 800℃. When the HZSM-5 zeolite was loaded with equal amounts of Fe_2O_3, WO_3, and MoO_3 in an overall 5.4%metal loading, the resultant catalyst (1.8F1.8W1.8M/HZSM-5) was least active in methane conversion and less selective towards benzene, toluene, and xylene but highly selective towards C_2 hydrocarbons and coke. When the quantities of Fe and W were increased to 2.25% each and the quantity of molybdenum reduced to 0.9% in the overall 5.4%metal/ HZSM-5 catalyst, the resultant catalyst (2.25F2.25W0.9M/HZSM-5) became most active in methane conversion (17.4%) at 800℃. Despite being most active in methane conversion and highly selective towards

toluene and coke, this catalyst showed little selectivity towards xylene. Reducing the quantity of Fe and W each to 1.35% and increasing Mo to 2.7% in the overall 5.4% catalyst, the resultant catalyst was less selective towards C_2 and coke, but highly selective towards xylene and benzene.

From the above trend, there exists an opportunity to tune the 5.4% Fe, W, and Mo on HZSM-5 to achieve the desired conversion and product distribution. Non oxidative methane conversion occurs in three distinct phases: (i) Initial C-H activation of methane by dehydrogenation; (ii) C-C coupling to C_2 hydrocarbons and subsequent oligomerization; (iii) Aromatization at the Bronsted acid sites of the zeolite (Sim *et al.* 2020). With respect to iron, carburized (Fe_3C) is the active species formed during the induction period. Activation of methane molecules occurs on the Fe_3C sites (Denardin and Perez-Lopez 2019). A similar report elsewhere (Tan 2016) opines that the stability of carbene, a primary intermediate of activated methane plays an important role in converting methane to carbon or to C_2 hydrocarbons. Carbene is usually unstable on metallic sites and therefore its C-H bond splits further to produce hydrogen. Methane hydrogenates and dimerizes on molybdenum species when Mo/HZSM-5 catalyst is used (Solymosi *et al.* 1999). A lot of research on catalytic activity of Mo/HZSM-5 (Wang *et al.* 1993) revealed that MoO_3 crystallites were the active sites for methane activation. An interaction between MoO_3 and the acid sites of the HZSM-5 constitute the active component of the catalyst (Zhang *et al.* 1998).

In (Fe-W-Mo/HZSM- 5) catalyst system, the effect of metal loading and process conditions have an effect on conversion of methane to carbon and petrochemicals where Fe is desired for stability, C_2 and coke selectivity whereas W is desired for conversion. On the other hand, Mo is desired for the formation of methyl radicals which are oligomerized into C_2H_6. Bronsted acid sites and shape selectivity of HZSM-5 is desired for conversion C_2 intermediates into benzene and its derivatives. Therefore, for high C_2 and coke selectivity, equal metal loading will be a desired recipe. To achieve the highest conversion and most selectivity towards toluene and coke, the amount of molybdenum must be reduced in the overall 5.4%metal catalyst system. Initial methane activation process includes Mo_2C formation through MoO_3 carburization, which subsequently undergoes slow deactivation. Less than 1%Mo loading in the catalyst system is insufficient for methane activation (Han *et al.* 2019). To achieve the most selectivity towards benzene, xylene and suppress coke formation, it is desired to lower the quantities of both Fe and

W and increase the amount of molybdenum in the overall catalyst system. For catalyst systems which were supported on activated carbon, best methane conversion results were achieved by catalyst 2.25F2.25W0.9M/AC while the least activity in terms of methane conversion were achieved by catalyst 1.35F1.35W2.7M/AC. Therefore, reducing the amount of Mo in the catalyst system increases its activity toward methane conversion and increases its selectivity towards C_2 and coke selectivity. Loading metal oxides in equal quantities in the catalyst reduces its activity in terms of methane conversion and reduces its selectivity towards coke. This poor performance is attributed competing reaction between metal oxides.

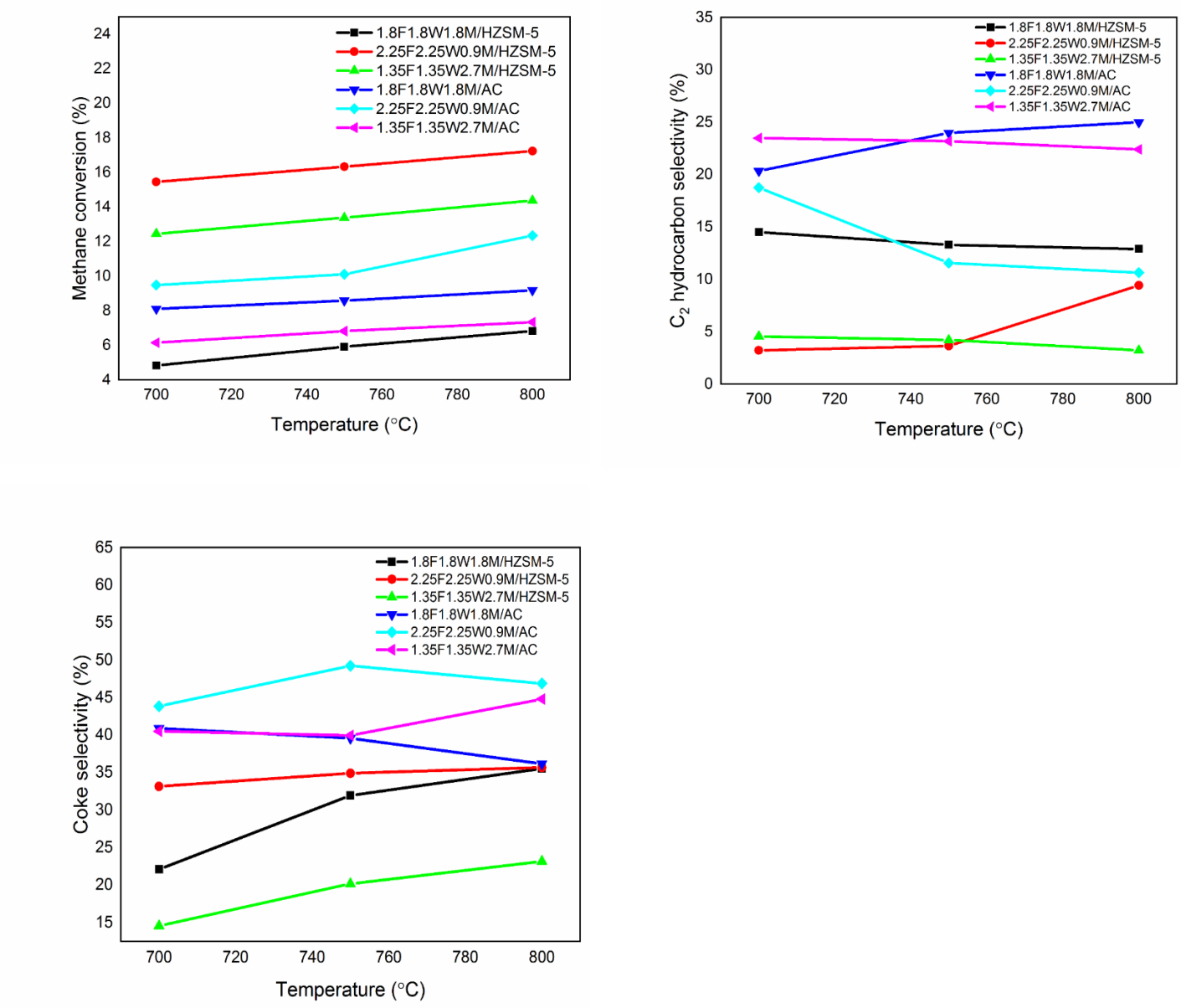

Figure 4-7. Methane conversion, C_2 hydrocarbon and coke selectivity of various catalyst systems at different temperatures, 0.96 $Lg^{-1}cat.h^{-1}$, and 1 atm.

Catalyst systems supported on AC did not show any activity towards the formation of aromatics. Aromatization only occurs inside the HZSM-5 acid sites, a property which is inherently absent in activated carbon. Therefore, catalysts supported on AC were catalytically active in methane conversion and showed selectivity towards C_2 hydrocarbons, hydrogen, and coke. In Figure 4-8, catalyst 2.25F2.25W0.9M/AC was most selective towards hydrogen at 700℃, 750℃ but its

catalytic activity began to drop after 750℃. This was attributed to loss of catalyst stability at higher temperature. On the contrary, catalyst 1.35F1.35W2.7M/AC, despite performing dismally at 700℃ and 750℃, it became most selective towards hydrogen at 800℃. From this trend, it can be inferred that low Mo content in the catalyst system is desired for hydrogen selectivity at low temperatures than at high temperatures. Since the selectivity of hydrogen increases with an increase in temperature in catalyst system with high Mo loading, it was observed that W and Fe metal oxides suppressed the performance of molybdenum in the overall 5.4% metal loaded on HZSM-5/AC.

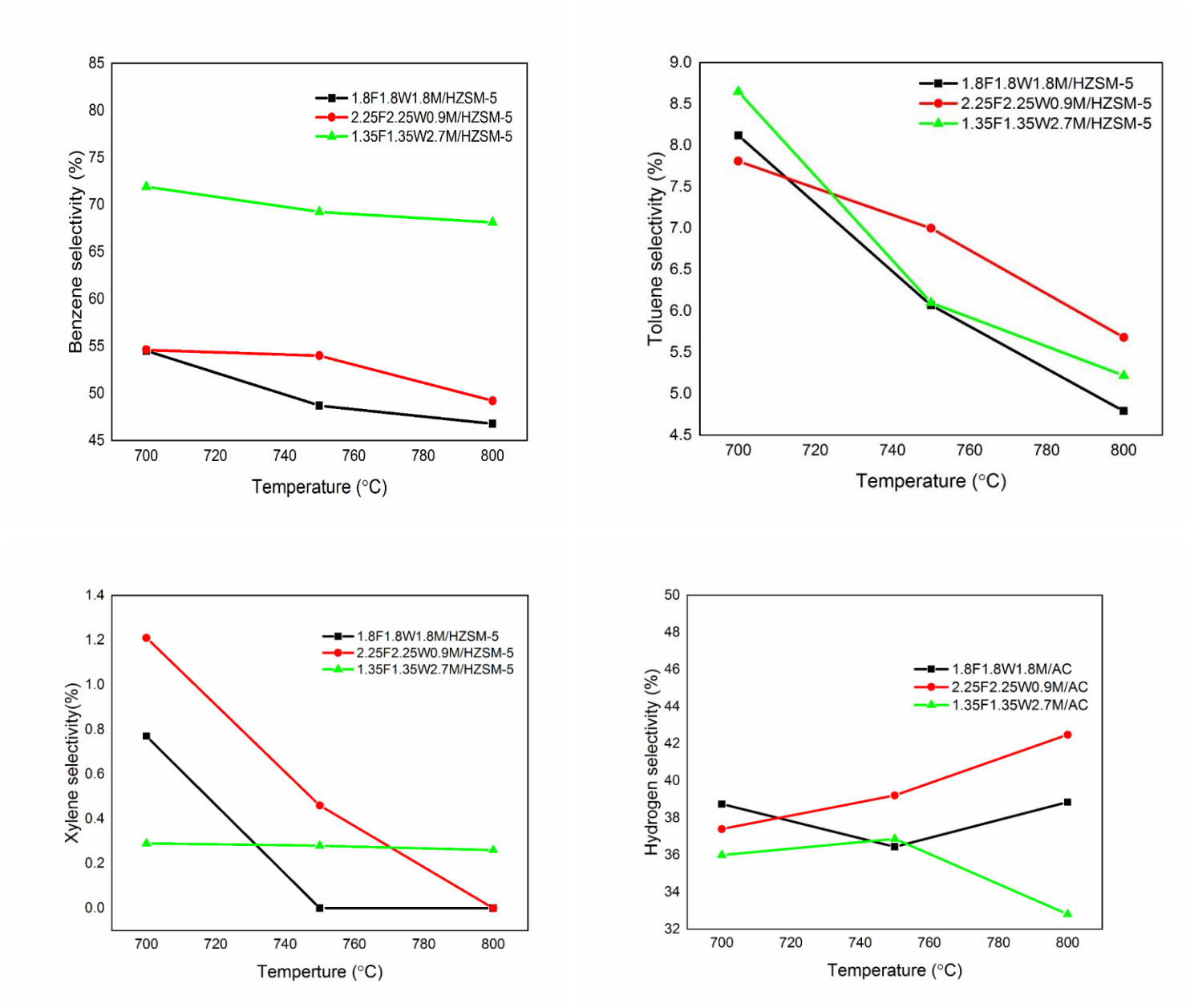

Figure 4-8. Benzene, toluene, xylene, and hydrogen selectivity at different temperatures at 0.96 $Lg^{-1}cat.h^{-1}$ and 1atm.

4.1.5 Characterization of the spent catalyst

4.1.5.1 TGA analysis of catalyst systems supported on HZSM-5

To ascertain the nature and type of deposited carbon nanomaterial, spent catalyst systems were analysed using thermogravimetric analysis. Thermo-gravimetric profiles in Figure 4-9 shows the effect of metal loading on coke deposition at 750℃ after 4 hours' time on stream. Based on the results obtained, the 1st weight loss up to 100℃ was attributed to loss of adsorbed and bound

water (Qi and Yang 2004). After 100℃, there was no change in weight between 300-400℃ . The second weight loss between 500-600℃ was attributed to oxidation of deposited carbon which was complete at 600℃. Coke deposit changes the pore geometry of the catalyst thereby changing the product selectivity. Heavy aromatic compounds formed in the channels become intermediates for the formation of poly-aromatic coke. The size of poly-aromatic coke inhibits the diffusion of smaller intermolecular intermediates from diffusing into the channels of the Zeolite. During the non-oxidative methane conversion, the evolved hydrogen atoms migrate into the coke interface and hydrogenates the poly-aromatic coke into lighter hydrocarbons. Oxidation of carbon at around 583℃ is associated with carbidic carbon of Mo_2C while oxidation of carbon around 600℃ is associated with poly-aromatic carbon found on the Bronsted acid sites. The type of carbon deposited on catalyst systems supported on HZSM-5 was pure low temperature carbon nanomaterial.

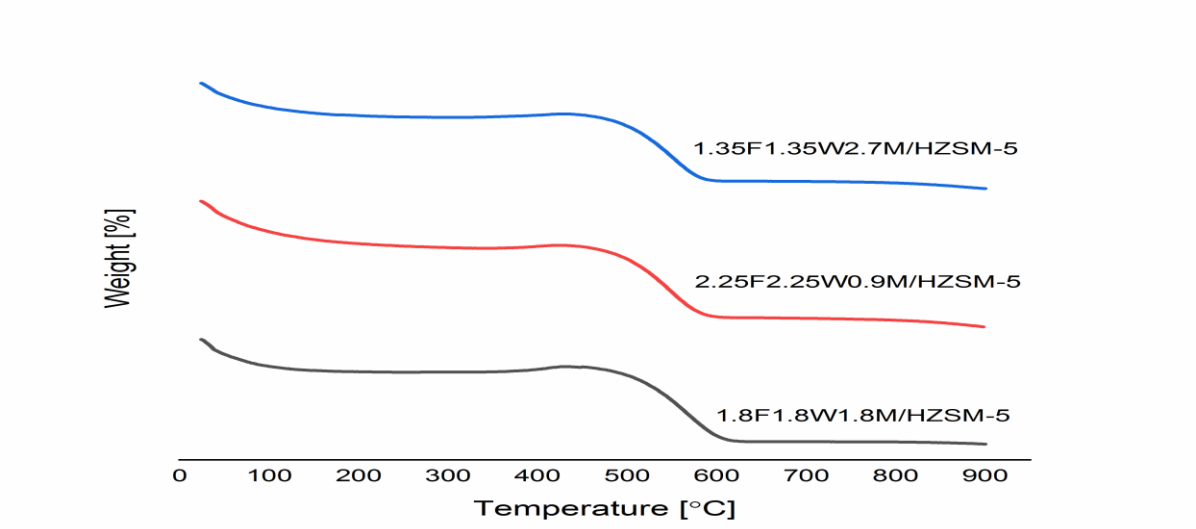

Figure 4-9. TGA pattern of catalyst 1.8F1.8W1.8M/HZSM-5, 2.25F2.25W0.9M/HZSM-5, and 1.35F1.35W2.7M/HZSM-5.

From Figure 4-10, it can be inferred that the type of carbon nanomaterial deposited on catalyst systems supported on activated carbon was non amorphous because there was no weight change between 300-400℃ . This finding is in agreement with what was reported elsewhere (Jiang *et al.* 2014). Since oxidation of all deposited carbon was complete at 500℃, it was attributed to the presence of low temperature carbon.

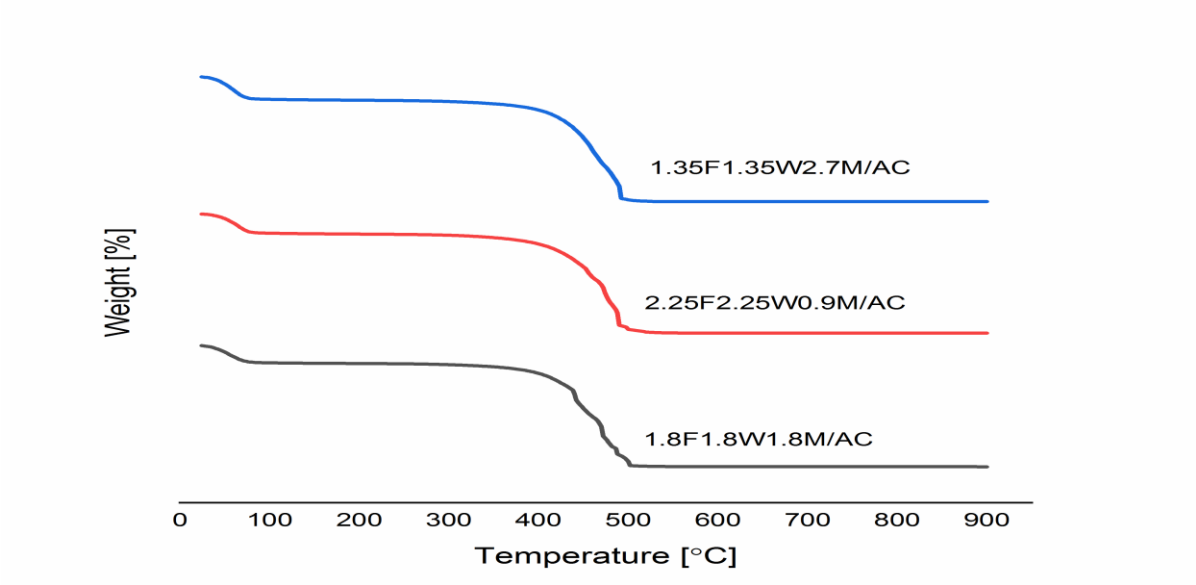

Figure 4-10. TGA pattern of catalyst 1.8F1.8W1.8M/AC, 2.25F2.25W0.9M/AC, and 1.35F1.35W2.7M/AC

4.1.5.2 TEM analysis of deposited carbon

From Figure 4-11, TEM images of deposited carbon nanomaterial are seen on catalyst 1.8F1.8W1.8M/HZSM-5. Carbon nanotubes (CTs) and nanoparticles of metal oxides are seen in the catalyst. From the TEM micrographs of catalyst 2.25F2.25W0.9M/HZSM-5, a dense mass of carbon nanomaterial is seen deposited on the spent catalyst. Clusters of carbon nanomaterial are seen on catalyst 1.35F1.35W2.7M/HZSM-5. The pattern of deposition of these metal oxide nanomaterial growth conformed to "tip-growth and base-growth" mechanism, similar to that reported by (Chen *et al.* 1997). This implies that the carbon nanotubes formed on catalyst 2.25F2.25W0.9M/HZSM-5 were largely due to the presence of Fe_2O_3.

Impregnation of HZSM-5 with Fe improves decomposition of CHx or CH_4 to carbon nanotubes (Xu *et al.* 2012). The formed crystalline CNTs are less reactive than amorphous coke deposits and therefore burns off at high temperatures ($> 800℃$). During catalyst synthesis, Fe is impregnated on the external surface of the zeolite and is effective in the formation of carbon nanotubes (Ma *et al.* 2002). The promotional effect of Fe lies in the formation of CNTs. Coke accumulation in the binary system is the main reason for low catalyst activity in methane conversion. From TEM images in catalyst 2.25F2.25W0.9M/HZSM-5, the growth of CNTs led to disagglomeration of micro-sized zeolite crystallites. Resultant deposits of CNTs limited

molecular diffusion in the catalyst system. This finding is similar to what was reported elsewhere (Cui *et al.* 2011). Apart from formation of nano-sized particles, Fe additives are responsible for the formation of nanoclusters and can also be exchanged at zeolite channel pores. Modifying Fe, W, Mo/HZSM-5 improves catalyst stability. Few uniform CNTs with smooth external surfaces and metal oxide nanomaterial are formed on catalyst 1.35F1.35W2.7M/HZSM-5. This implies that tungsten promotes iron dispersion into the zeolite. Therefore, low yields of carbon nanotubes with low index planes in catalyst 1.35F1.35W2.7M/HZSN-M-5 was due to even dispersion in the zeolite which were unable to effectively activate the C-H bond in methane (Li *et al.* 2016). Molybdenum is known to promote the growth of carbon nanotubes just like iron but since its metal loading in catalyst 1.8F1.8W1.8M/HZSM-5 is too low, its ability to promote the growth of carbon nanotubes is impaired because it is highly dispersed in the zeolite. A similar finding was reported elsewhere (Bajec *et al.* 2019).

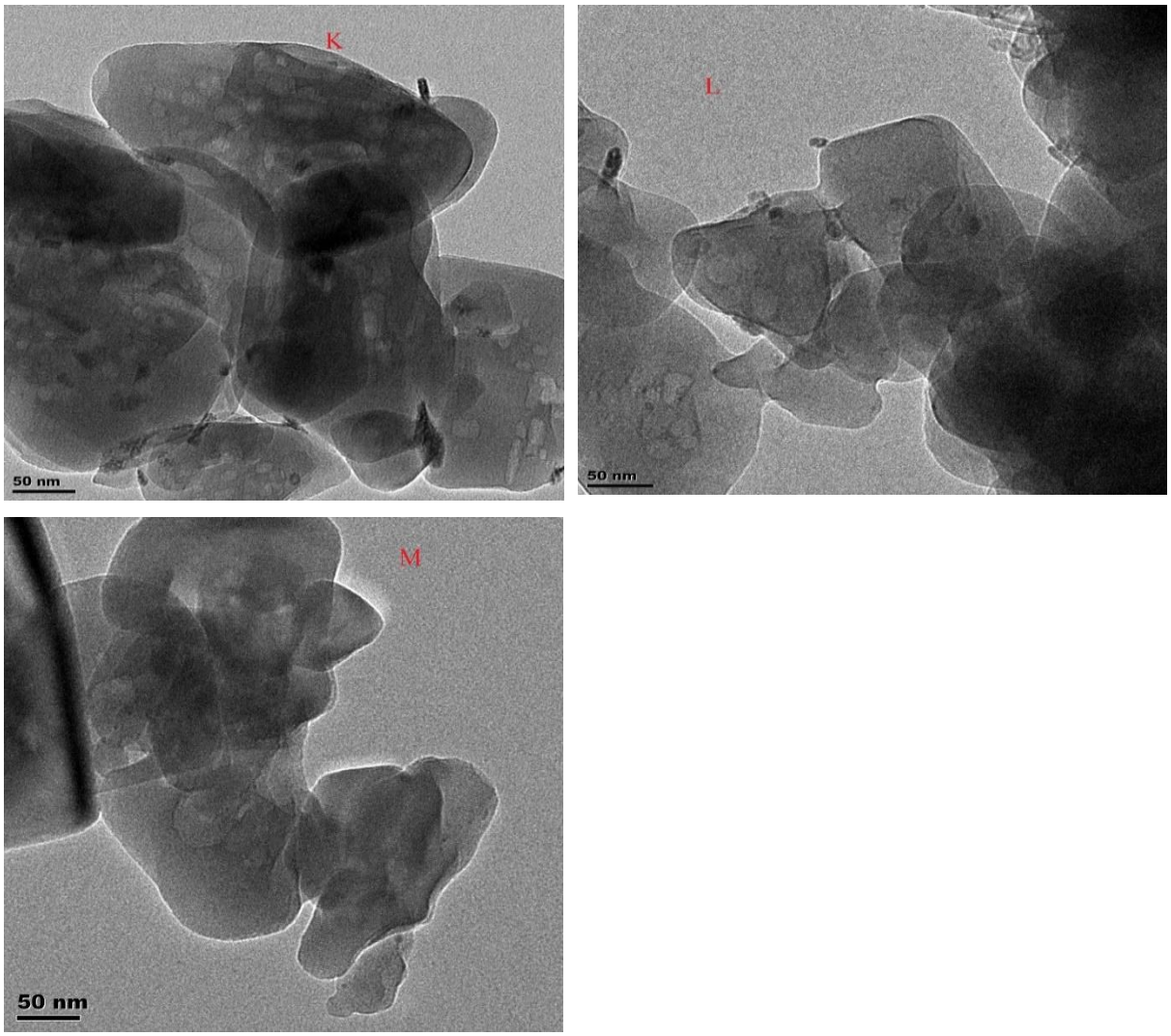

Figure 4-11. TEM Image of various catalysts; K(1.8F1.8W1.8M/HZSM-5), L(2.25F2.25W0.9M/HZSM-5), M(1.35F1.35W2.7M/HZSM-5).

In Figure 4-12, a dense mass of deposited carbon material formed on each catalyst system that was loaded on activated carbon. Absence of definite structures of carbon nanomaterial is an indication that methane conversion reaction took place on the surface of the catalyst and the metal oxides in the catalyst system did not control the formation of particular shapes of carbon nanomaterial.

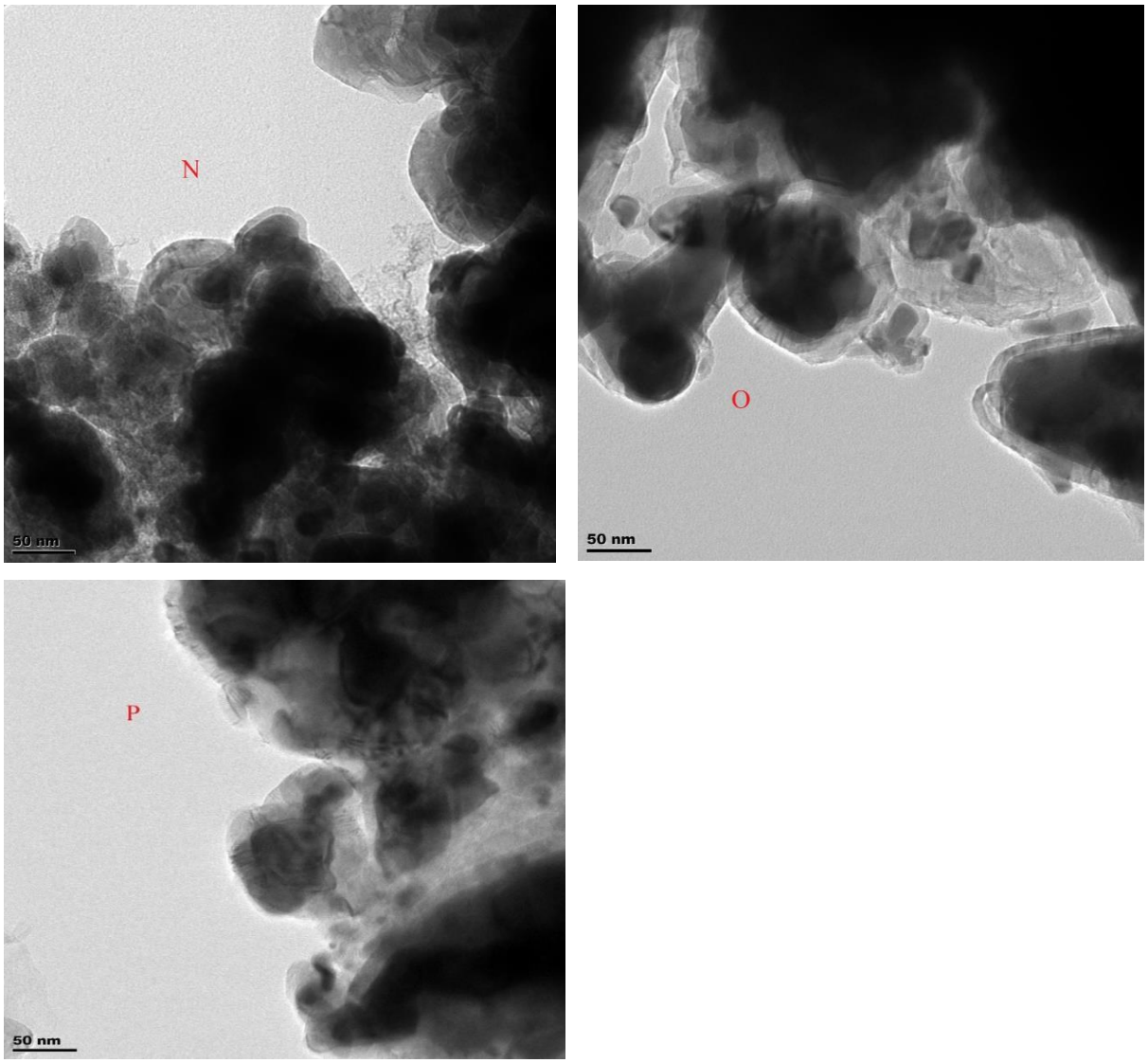

Figure 4-12. TEM Image of various catalysts; N(1.8F1.8W1.8M/AC), O(2.25F2.25W0.9M/AC), P(1.35F1.35W2.7M/AC).

4.1.6 Summary of the findings

Tuning Fe, W, Mo/HZSM-5 catalyst system for qualitative and quantitative control of product distribution in non-oxidative conversion of methane into carbon and petrochemicals has been demonstrated. Based on the results obtained, the effect of metal loading in each catalyst system plays a significant role on methane conversion and product distribution as follows.

- When the HZSM-5 zeolite is loaded with equal amounts of Fe_2O_3, WO_3, and MoO_3 in an overall 5.4%metal loading, the resultant catalyst 1.8F1.8W1.8M/HZSM-5 was least

active in methane conversion and less selective towards benzene, toluene, and xylene but highly selective towards C_2 hydrocarbons and coke.

- In an overall 5.4% (Fe, W, Mo) metal loading on HZSM-5 zeolite, methane conversion was remarkably low when all the three metals are loaded onto the zeolite in equal %wt. loading as it is characteristic in catalyst 1.8F1.8W1.8M/HZSM-5.
- Keeping the amount of Fe and W high and reducing the amount of Mo in the catalyst system improved methane conversion and improved its selectivity towards coke.
- When the quantities of Fe and W were increased to 2.25% each and the quantity of molybdenum reduced to 0.9% in the overall 5.4%metal/ HZSM-5 catalyst, the resultant catalyst 2.25F2.25W0.9M/HZSM-5 became most active in methane conversion (17.4%) at 800℃. Despite being most active in methane conversion and highly selective towards toluene and coke, this catalyst showed little selectivity towards xylene.
- Migration of MoO_3 into the zeolite channel pores is limited, hence higher Mo loading led to a reduction in methane conversion.
- Reducing the quantity of Fe and W each to 1.35% and increasing Mo to 2.7% in the overall 5.4% catalyst, the resultant catalyst was less selective towards C_2 and coke but highly selective towards xylene and benzene. Since the extent of methane conversion is important to yield value added chemicals, selectivity towards desired products (C_2 hydrocarbons, benzene, toluene, xylene, and CNTs) is equally important. Therefore, this study demonstrates that metal loading presents an opportunity to tune the 5.4% Fe, W, and Mo on HZSM-5 to achieve the desired conversion and product distribution.

4.2 Objective II: To investigate the effect of metal synergy on methane conversion and product distribution.

To investigate the synergistic effect of each noble metal in the catalyst system, various catalysts systems were prepared, characterized, and applied for non-oxidative methane conversion. The catalyst systems (Fe-Mo), (W-Mo), (Fe-W), and (Fe-W-Mo) supported on HZSM-5 and AC were synthesized, and their catalytic activity evaluated in terms of methane conversion and product distribution in a packed bed reactor at 750℃, GHSV 0.96 $Lg^{-1}cath^{-1}$, 1 atm, and 4 hours' time on stream.

4.2.1 Materials and methods

Catalyst materials used are given under section 3.2. The prepared catalysts were synthesized using incipient wetness impregnation and designated according to %wt. as shown in Table 4-7.

Table 4-7. Nomenclature of various binary catalyst systems**.**

Catalyst	Composition (wt.%)
2.7F2.7M/HZSM-5	2.7%Fe – 2.7%Mo-94.6%HZSM-5
2.7W2.7M/HZSM-5	2.7%W – 2.7%Mo – 94.6%HZSM -5
2.7F2.7W/HZSM-5	2.7%Fe – 2.7%W - 94.6%HZSM-5
1.8F1.8W1.8M/HZSM-5	1.8Fe – 1.8%W – 1.8%Mo-94.6%HZSM -5
2.7F2.7M/AC	2.7%Fe – 2.7%Mo-94.6%AC
2.7W2.7M/AC	2.7%W – 2.7%Mo – 94.6%AC
2.7F2.7W/AC	2.7%Fe – 2.7%W - 94.6%AC
1.8F1.8W1.8M/AC	1.8Fe – 1.8%W – 1.8%Mo-94.6%AC

4.2.2 Catalyst characterization

Synthesized catalysts in Table 4-8 were characterized using techniques previously described in section 3.4.

4.2.2.1 XRD-analysis

XRD patterns of HZSM-5 and all the four catalysts as shown in Figure 4-13 confirm the presence of distinct HZSM-5 (orthorhombic), $\alpha -Fe_2O_3$ (rhombohedral hematite), $\beta -MoO_3$ (monoclinic), and o-WO_3 (orthorhombic) phases. In all the four catalysts, sharp peaks at 2θ=8.0°, 8.9°, 9.1°, 14.9°, 20.9° , and 23.2° are assigned to HZSM-5 according to diffraction

peaks classification in JCPDS File no. (00-044-002). These magnificent peaks tend to mask the peaks of noble metals in each catalyst due low metal loading (5.4%metal/HZSM-5). In catalyst 2.7F2.7M/HZSM-5, peaks at 2θ=33.2°, 35.7°, 49.5°, and 54.1° are assigned to Fe_2O_3 in conformity with those in JCPDS File no. (87-1166) while peaks at 2θ = 34.3°, and 49.2° are assigned to MoO_3 corresponding to those in JCPDS File no. (05-0508). In catalyst 2.7W2.7M/HZSM-5, faint peaks at 2θ=23.2°, 29.0°, 42.1°, and 50.4° are assigned to orthorhombic WO_3 according to diffraction peaks classification in JCPDS File no. (32-1394).

Fe_2O_3 phase with peaks at 2θ=33.2°, 35.7°, 49.5°, and 54.1° and WO_3 with peaks at 2θ=23.2°, 29.0°, 42.1°, and 50.4° clearly manifest themselves in catalyst 2.7F2.7W/HZSM-5. When metal loading was equal in catalyst 1.8F1.8W1.8M/HZSM-5, peaks corresponding to Fe_2O_3, WO_3, and MoO_3 become very faint due to low metal loading in the catalyst. In all catalysts, corresponding metal oxides from their precursors were clearly formed after calcination. Less sharpness of metal oxide peaks can also be attributed to even dispersion in the support. After impregnating the zeolite with the oxides of Fe_2O_3, WO_2, and MoO_3, the intensity of the peaks decreased but the peak positions remained unchanged. This implies that, impregnating the zeolite with metal oxides did not alter the zeolite structure. A similar finding was reported elsewhere (Bajec *et al.* 2019).

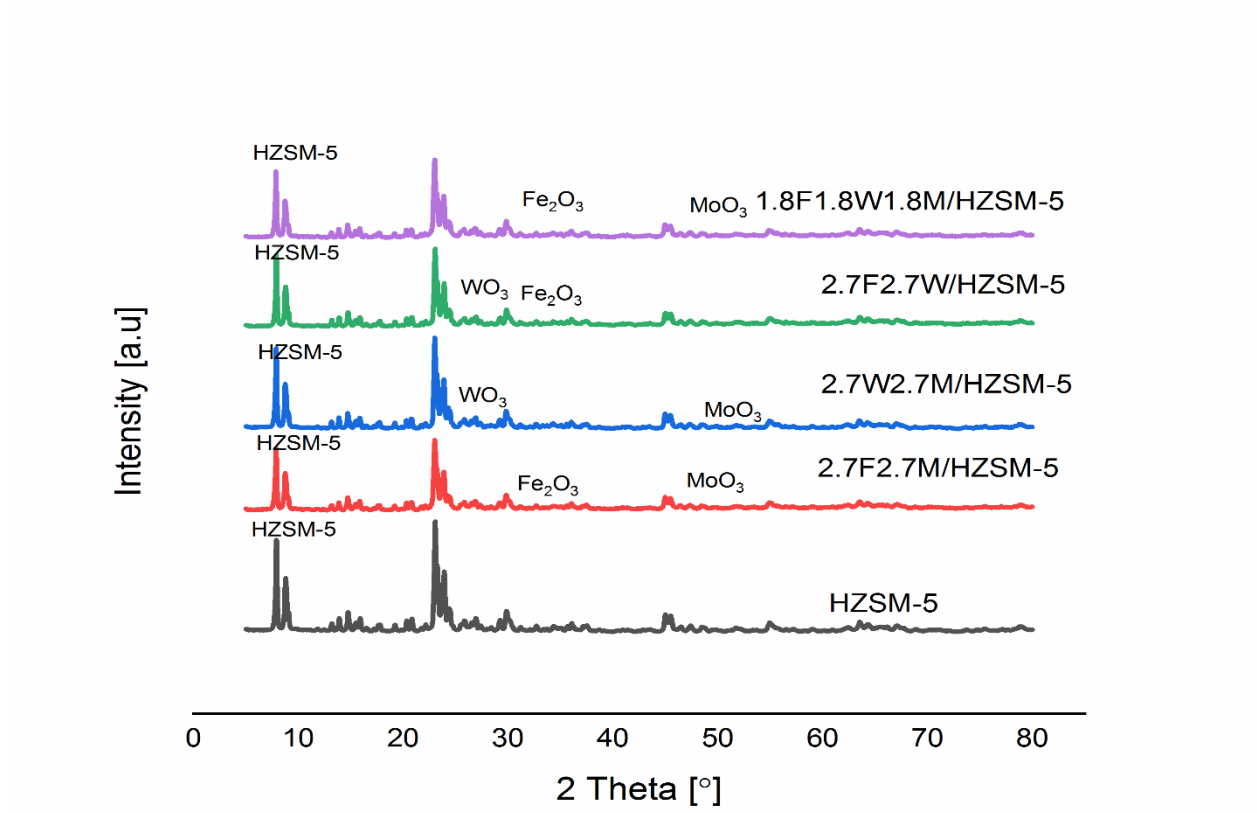

Fig 4-13. XRD patterns for catalysts; HZSM-5, 2.7F2.7M/HZSM-5, 2.7W2.7M/HZSM-5, 2.7F2.7W/HZSM-5, and 1.8F1.8W1.8M/HZSM-5.

Figure 4-14 shows the XRD patterns of all the catalysts supported on activated carbon. Even though faint peaks corresponding to oxides of Fe_2O_3, WO_3, and MoO_3 phases are seen, distinct peaks of activated carbon are replicated in each catalyst system. This is attributed to high dispersion of metal oxides in the support. The structure of the activated carbon support did not change after impregnation with metal oxides because of low %wt. metal loading.

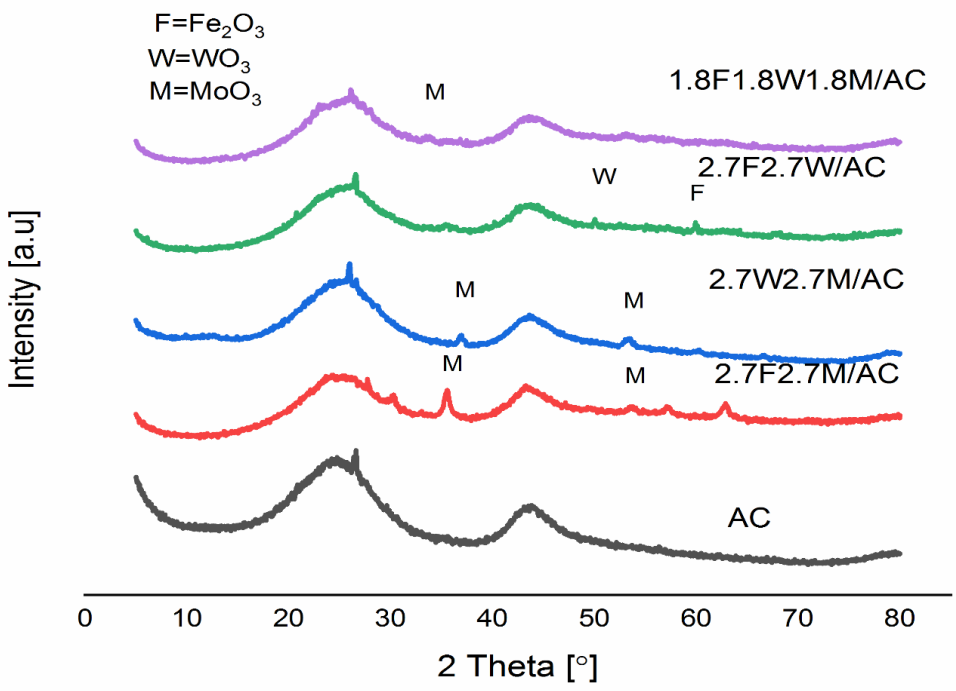

Fig 4-14. XRD patterns for catalyst AC, 2.7F2.7M/AC, 2.7W2.7M/AC, 2.7F2.7W/AC, and 1.8F1.8W1.8M/AC.

4.2.2.2. SEM Analysis

Scanning electron microscopy was used to obtain information on catalyst crystallite size, and shape. Image-J software was used to obtain information on crystallite size. In Figure 4-15, catalyst 2.7F2.7M/HZSM-5 shows neat structures of nano particles which assume the shape of tri lobes, Quadra lobes, and spheres. The crystallite sizes ranged from 2.57-22.96 nm with an average crystallite size being 5.51 nm. The neatness of stacked structures on top of each other is an indication of little agglomeration after calcination. Similar structures also manifested in catalyst 2.7W2.7M/HZSM-5 with the crystallite size ranging from 2.57-16.44 nm. Low maximum crystallite size implies less agglomeration and clumping together of catalyst crystallites. In catalyst 2.7F2.7W/HZSM-5 crystallite sizes ranged from 2.57-14.29 nm. Neat crystallite structures with the shape of tri lobes manifest themselves. When metal loading was equal in catalyst 1.8F1.8W1.8M/HZSM-5, well-defined tetrahedral and cubic structures of nanoparticles were seen on the catalyst. Crystallite sizes ranged from 2.57-21.48 nm. Lumps of catalyst crystallites were seen clumped together due to agglomeration after calcination. In all

the four catalysts, crystallite sizes ranged from 2.57 – 22.96 nm, which is an indication that all the catalyst crystallites were in the nano range.

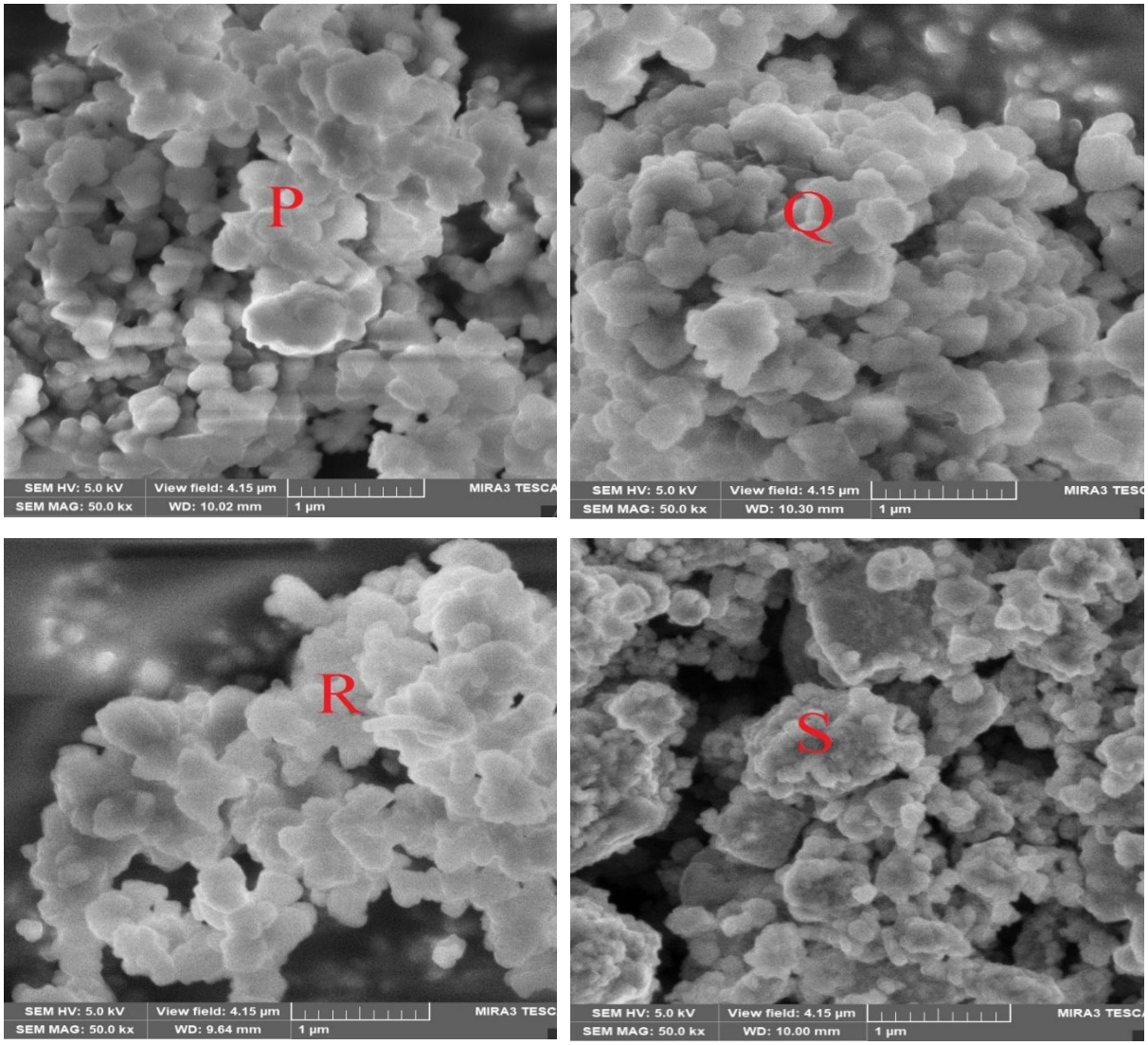

Figure 4-15. SEM Images of various catalysts; P (2.7F2.7M/HZSM-5), Q (2.7W2.7M/HZSM-5), R (2.7F2.7W/HZSM-5), and S (1.8F1.8W1.8M/HZSM-5).

From the SEM images in Figure 4-16, catalyst 2.7F2.7M/AC shows irregular shaped structures of catalyst crystallites stacked on top of each other. Lumping of catalyst crystallite particles in this catalyst is attributed to agglomeration of catalyst crystallites. Using Image-J software, the calculated crystallite sizes ranged from 2.57-33.57.96 nm with a mean crystallite size of 12.43 nm. On the contrary, neat structures of catalyst crystallites in the shape of tri-lobes and Quadra-lopes are clearly seen in catalyst 2.7W2.7M/AC with the crystallite size ranging from 2.57-20.21

nm. Less agglomeration and clumping together of catalyst crystallites could have led to aggregation of neat structure. In catalyst 2.7F2.7W/AC, crystallite sizes ranged from 2.57-32.67 nm with the mean crystallite size being 8.57 nm. Agglomeration of catalyst crystallites was seen in this catalyst system. When metal loading was equal in catalyst 1.8F1.8W1.8M/AC, a dense mass of irregular undefined catalyst crystallites formed due agglomeration. Crystallite sizes ranged from 2.57-17.03 nm with mean crystallite size being 6.29 nm. All the four catalyst systems contained nanoparticles.

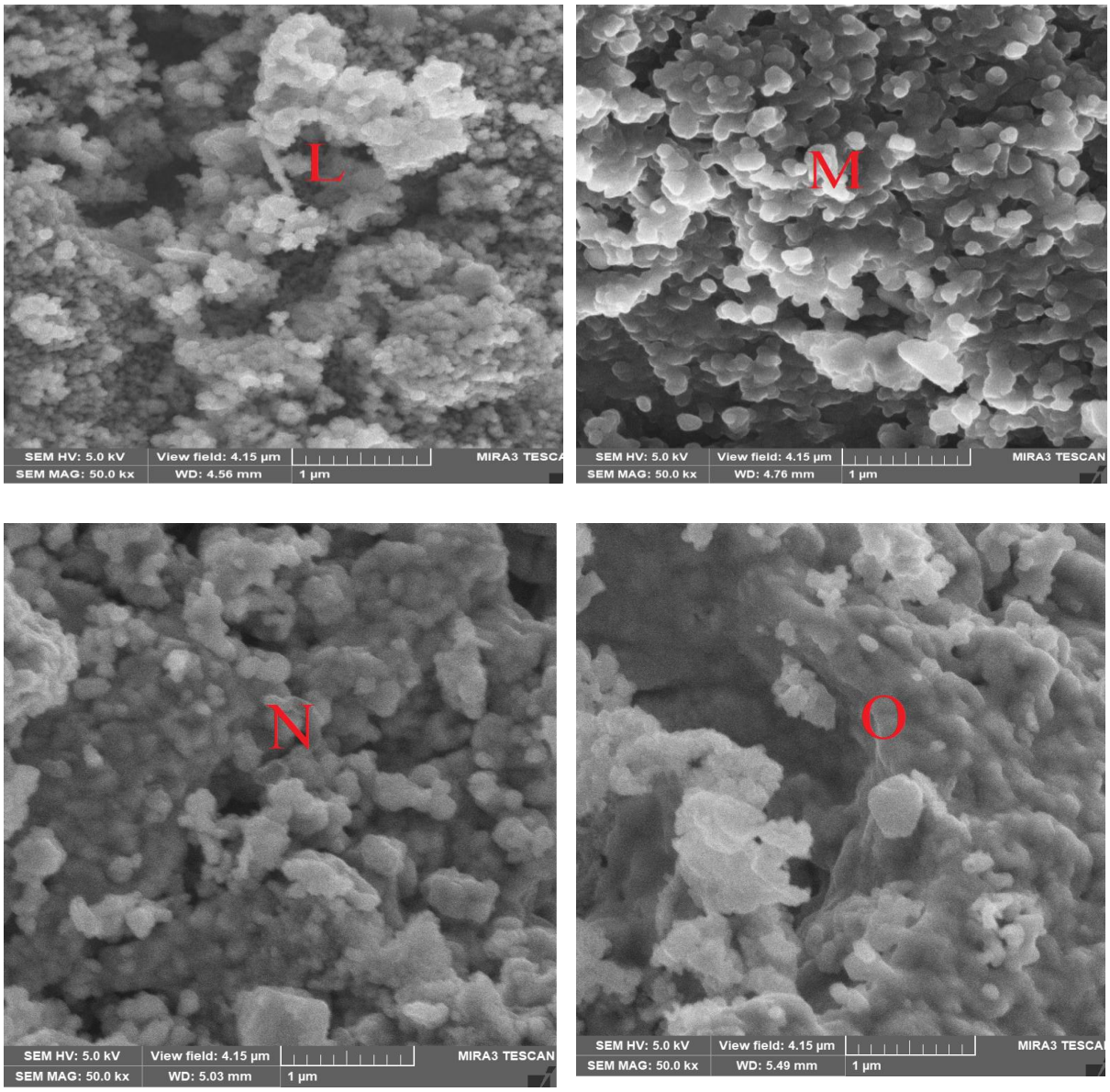

Figure 4-16. SEM Image of various catalysts; L(2.7F2.7M/AC), M(2.7W2.7M/AC), N (2.7F2.7W/AC), and O(1.8F1.8W1.8M/AC).

4.2.2.3 BET analysis

From BET analysis results in Table 4-8, all the four catalysts had a surface area above 200 m^2g^{-1}. The reference HZSM-5 zeolite had the following structural properties; surface area 495.877 m^2g^{-1}, pore volume 0.17874 cm^3g^{-1} and pore size of 24.748 Å.

Impregnating the zeolite with oxides of iron, tungsten, and molybdenum greatly altered its surface properties. Impregnating the zeolite with 2.7%Fe and 2.7%Mo as it is typical in catalyst 2.7F2.7M/HZSM-5 reduced the zeolite surface area and pore volume by 41.49% and 41.24%,

respectively. Despite a reduction in surface area and pore volume, the change in pore size was insignificant. In catalyst 2.7W2.7M/HZSM-5, there was a tremendous decrease in surface area and pore volume in reference to the parent zeolite but with a huge increase in pore size. A further reduction in surface area and pore volume was seen in catalyst 2.7F2.7W/HZSM-5, even though there was a notable increase in pore size in reference to the parent zeolite. When all the noble metals were impregnated into the zeolite in equal quantities as it is in catalyst 1.8F1.8W1.8M/HZSM-5, there was an increase in surface area, pore volume, and pore size.

From the above trend, it can be seen that the reference HZSM-5 zeolite is a high surface area mesoporous material. Impregnating the zeolite with the oxides of Fe_2O_3, WO_3, and MoO_3 reduces its surface area and pore volume. However, this scenario seems true only when metal loading is in excess of 2.0% wt. because in catalyst 1.8F1. 8W1.M/HZSM-5 where metal loading is 1.8% each, there is a reduction in zeolite surface area, insignificant reduction in pore volume and a substantial increase in pore size. Interestingly, when Fe is absent in catalyst 2.7W2.7M/HZSM-5, there was an increase in pore size of 368% in reference to the parent zeolite. Therefore, tungsten could have been responsible for the generation of macrospores in the mesoporous zeolite structure.

In all catalyst systems supported on activated carbon, the surface area was above 400 m^2g^{-1}. Impregnating activated carbon with metal oxides affected its porosity. Impregnating AC support with Fe and Mo resulted in a catalyst system with increased surface area and increased pore size. This characteristic behaviour was replicated when the AC support was impregnated with Fe and W metal oxides. However, when the AC support was loaded with Fe and W, there is a decrease in surface area and an incredible increase in pore size. Most improvement in surface area, pore volume and pore size was realized by a catalyst system with equal metal loading on AC. From the above trend, it was concluded that a combination of W and Mo was desired for enhancement of surface area, pore volume, and pore size in the resultant catalyst but only, when their loading was below 2 %wt. loading in the catalyst system.

Table 4-8. Catalyst surface area, pore volume, and pore size

Catalyst Name	BET Surface area (m^2/g)	Pore volume (cm^3/g)	Pore size (Å)
HZSM-5	496	0.177	24.748
2.7F2.7M /HZSM-5	290	0.105	24.168
2.7W2.7M/HZSM-5	242	0.125	116.011
2.7F2.7W/HZSM-5	217	0.0874	29.836
1.8F1.8W1.8M/HZSM-5	424	0.1716	30.210
AC	571	0.242	34.782
2.7F2.7M /AC	661	0.275	33.529
2.7W2.7M/AC	833	0.353	37.256
2.7F2.7W/AC	429	0.179	34.815
1.8F1.8W1.8M/AC	1001	0.422	35.758

4.2.2.4 FT-IR analysis

From the FT-IR spectra in Figure 4-17, the catalyst lattice vibrations were recorded between 500-4000 cm^{-1}. From Figure 4-17, notable peaks in the fingerprint region, especially at 1071-1080 cm^{-1}, and 542-545 cm^{-1} were seen. Bands at 1071-1080 cm^{-1} are assigned to asymmetric stretching, bands at 542-545 cm^{-1} represent double ring while bands at 429-545 cm^{-1} belongs to T-O bending vibration of internal tetrahedral (T=Si or Al). According to the analysis of attribution by Frixione-Kunszt-Signer (FKS) method (Cheng *et al.* 2017), the absorption peaks at 1226 cm^{-1}, 1100 cm^{-1}, 796 cm^{-1}, 624 cm^{-1},547 cm^{-1}, and 453 cm^{-1} were ascribed to the characteristic framework vibration peaks of HZSM-5 zeolite i.e. the symmetric stretching vibration, anti-symmetric stretching vibration, vibration of five membered ring and block structure, and of T-O bending vibration peaks, respectively. The anti-symmetric stretching vibration peak at 1226 cm^{-1} is very sensitive to Si/Al ratio of HZSM-5, with the removal of aluminium species in the skeleton shifting the vibration to higher frequencies (Cheng *et al.* 2017). From literature (Liu *et al.* 2011) , Mo oxide species associated with Bronsted acid sites are responsible for non-oxidative aromatization of methane and the process leads to loss of Bronsted acid sites. Enhanced Bronsted acidity is responsible for high dispersion of metal oxides in the zeolite and improves the interaction between the metal oxides and zeolite thereby improving catalyst stability (Liu *et al.* 2004).

From literature (Tan *et al.* 2002), these absorption bands at 1080 cm^{-1}, 810 cm^{-1}, and 560 cm^{-1} are associated with internal linkages in SiO_4 (or AlO_4) tetrahedral and are very responsive to structural changes. This is a characteristic of silica (Pudukudy and Yaakob 2015). The characteristic bands at 548 cm^{-1} and 1226 cm^{-1} are associated with ZSM-5 (Tan *et al.* 2002). The peak positions in the spectra suggest a little shift in the peak position in the frequency of 548 cm^{-1} or 1226 cm^{-1} adsorption band which can be attributed to dealumination of the of the zeolite lattice (Campbell *et al.* 1996) after calcination. As reported elsewhere (Cheng *et al.* 2017), pure HZSM-5 zeolite comprises of three hydroxyl groups, Bronsted acidity (≡Al-OH-Si≡), silanol groups (Si-OH), and extra framework aluminium (Al-OH). Since the densities of these functional groups are different, their interactions with the zeolite are different too. Therefore, the composition of SiO_2 and Al_2O_3 of the zeolite would influence the interaction of the surface molybdate and the support. Iron has the least influence on the proportion of Bronsted and Lewis acid in HZSM-5 but has an inhibitory effect on the addition of Mo as reported by (Aboul-Gheit and Awadallah 2009).

Impregnation of the zeolite with Fe_2O_3, WO_3, and MoO_3 reduces the density of acid sites on the external surface of HZSM-5 and the number of molybdenum species deposited on the external surface during the ion exchange process (Wu *et al.* 2005) . This process increases selectivity towards benzene because the active centres of the acid and molybdenum oxide species are located inside the zeolite channels where shape selectivity takes place. Since the characteristic vibration peaks of HZSM-5 remained nearly unchanged, impregnation of HZSM-5 with Fe_2O_3, WO_3, and MoO_3 only shifted the peaks from 1071 cm^{-1} to 1080 cm^{-1} but did not alter the characteristic vibration peaks of HZSM-5 zeolite.

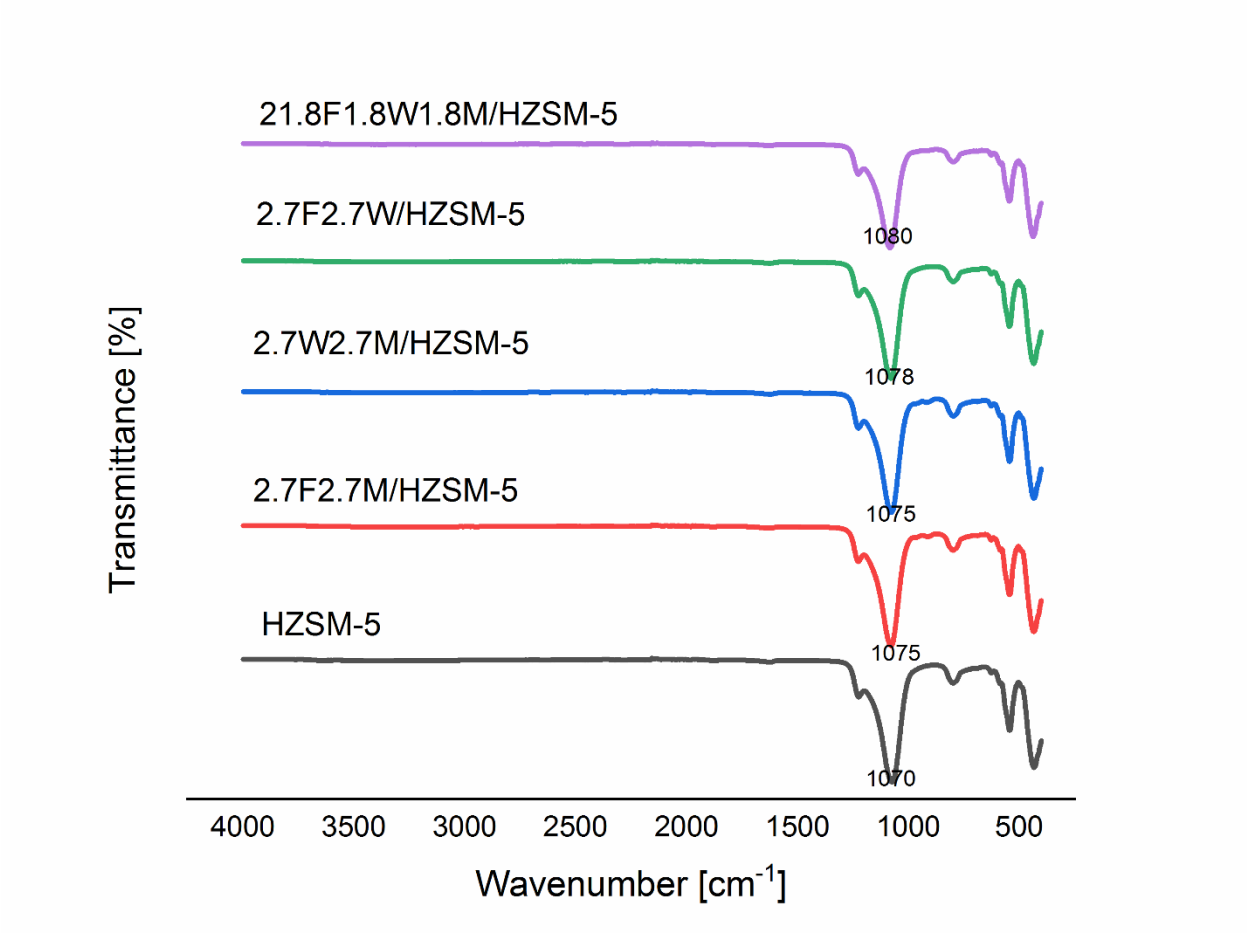

Figure 4-17. FT-IR spectra of catalysts; HZSM-5, 2.7F2.7M/HZSM-5, 2.7W2.7M/HZSM-5, 2.7F2.7W/HZSM-5, and 1.8F1.8W1.8M/HZSM-5.

In Figure 4-18, formation of major peaks in the FT-IR spectra of catalysts supported on activated carbon are ambiguously missing. After catalyst calcination at 500℃, it is believed that expected oxygen containing functional groups are thermally decomposed off at that temperature. This finding is similar to what has been reported elsewhere (Jiang *et al.* 2014). Faint peaks at 2100 cm^{-1} are assigned to C=C=O stretching of ketones.

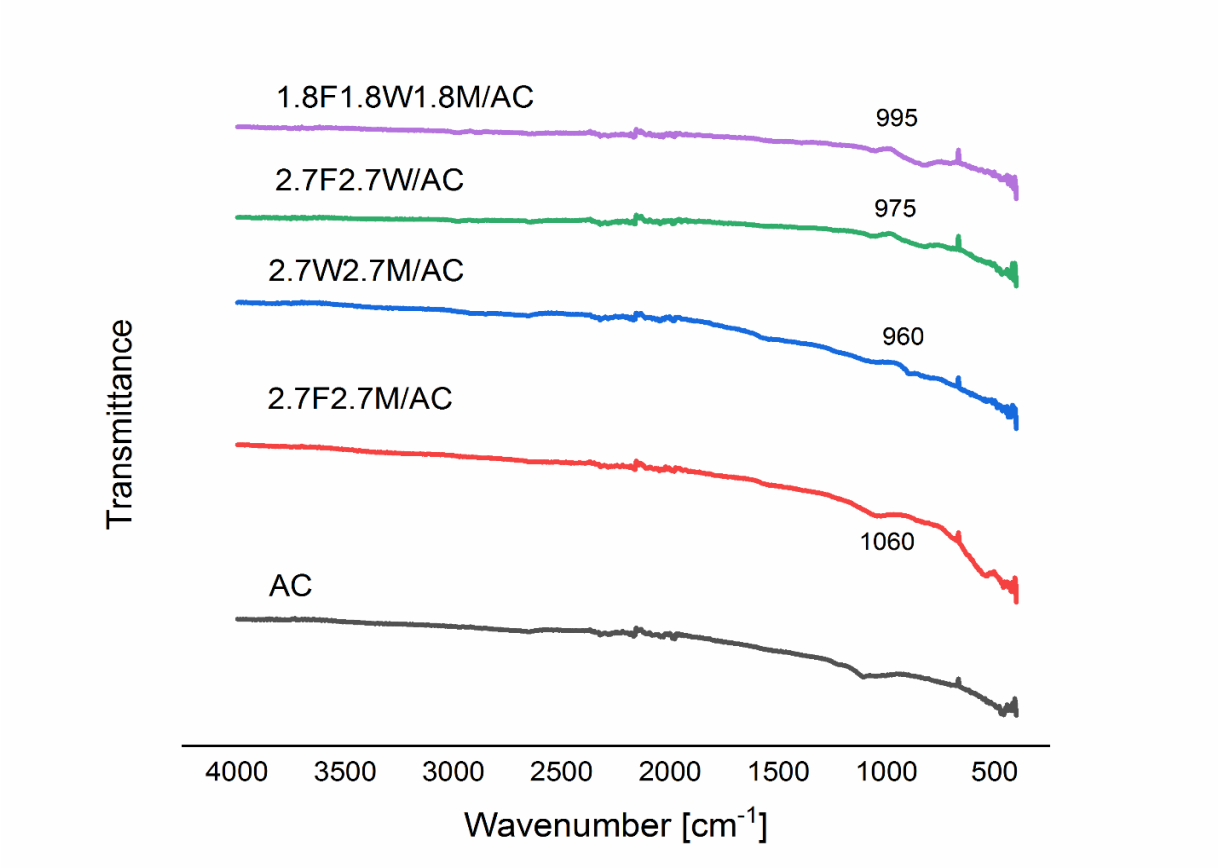

Figure 4-18. FT-IR spectra of catalysts; AC, 2.7F2.7M/AC, 2.7W2.7M/AC, 2.7F2.7W/AC, and 1.8F1.8W1.8M/AC.

4.2.3 Catalyst evaluation

Catalytic activity of each catalyst in terms of methane conversion, selectivity towards hydrogen, coke, and hydrocarbons were calculated using equations (5-9) in section 3.5.

From Table 4-9, catalyst 2.7W2.7M/HZSM-5 was most active in methane conversion and highly selective towards coke while catalyst 2.7F2.7M/HZSM-5 was least active in methane conversion with moderate selectivity towards benzene and coke. Catalyst 2.7F2.7W/HZSM-5 displayed outstanding results with 6.55% methane conversion, 53.43% selectivity towards benzene, and 22.52% selectivity towards coke. However, when the three metals Fe, W, and Mo were loaded on HZSM-5 in equal amounts, a reduction in methane conversion and an increase in both C_2 and coke selectivity was recorded. From the results obtained, Fe and Mo on HZSM-5 were less active in methane conversion but showed some substantial activity towards C_2

hydrocarbon selectivity. Iron and molybdenum on HZSM-5 are desired for methane conversion but they give rise to low benzene and high coke selectivities.

In NOCM reaction, a methane molecule is activated on the catalyst surface to CH_3^* radicals and subsequently transformed into benzene and its derivatives. The reaction mechanism encompasses catalysis for the formation of C_2H_6 by metal oxide species. During this stage, metal oxide species react with methane to yield a specific carbonaceous intermediate on the catalyst surface, which is further transformed into C_2H_6 by continuous reactions of methane with the CH_3^* radicals. Further, methane reacts with metal ions on HZSM-5 to produce CH_3^+ (a methoxy species on the Bronsted acid sites of the zeolite) which are further converted into a metal-carbene species, (Metal=CH_2). The formed methyl radicals (CH_3^*) are coupled to produce C_2H_6 which is further transformed into benzene through oligomerization and cyclization reactions. In a typical Fe-W-M/HZSM- 5 catalyst system, synergetic effect of noble metals comes into play in conversion of methane to carbon and petrochemicals where Fe is desired for stability, C_2 and coke selectivity whereas W is desired for conversion. On the other hand, molybdenum is desired for generation of methyl radicals which are oligomerized into C_2H_6. Bronsted acid sites and shape selectivity of HZSM-5 is desired for conversion C_2 intermediates into benzene and its derivatives.

Table 4-9: Methane conversion and product selectivity over different catalysts loaded on HZSM-5 at 750℃, and GHSV 0.96Lg^{-1}cat.h^{-1}, and 1 atm.

No.	Catalyst	Conversion (%)	C_2 Selectivity (%)	Aromatic selectivity			Coke selectivity (%)
				Benzene (%)	Toluene (%)	Xylene (%)	
1.	2.7F2.7M/HZSM-5	3.94	12.31	45.55	11.59	0.0	30.64
2.	2.7W-2.7M/HZSM-5	15.19	8.48	44.22	10.10	0.0	37.19
3.	2.7F2.7W/HZSM-5	6.55	10.53	53.43	13.46	0.07	22.52
4.	1.8F1.8W1.8M/HZSM-5	5.92	13.29	48.70	6.07	0.0	31.94

From Table 4-10, catalyst 2.7W2.7M/AC (without iron) was least active in methane conversion but highly selective towards coke. Catalyst 2.7F2.7W/AC (without tungsten) was most active towards methane conversion and most selective towards hydrogen. When all the metal oxides were loaded on AC support, the resultant catalyst system became most selective towards C_2 hydrocarbons. From the above characteristic behaviour of catalysts systems, it can be inferred that, tungsten is desired for methane conversion and selectivity towards hydrogen. However, coupling tungsten with molybdenum seem to inhibit the activity of tungsten in the catalyst system. Molybdenum loading at 2.7% in the catalyst system promoted coke selectivity but at 1.8% metal loading in the catalyst system, it promoted methane conversion and selectivity towards C_2 hydrocarbons. Catalyst systems loaded on HZSM-5 were more active on methane conversion than those loaded on AC because the inherent acidity and shape selectivity played a significant role in transformation of generated methyl radicals into various hydrocarbons.

Table 4-10. Methane conversion and product selectivity over various catalysts loaded on activated carbon at 750℃, 0.96 $Lg^{-1}cat.h^{-1}$ and 1 atm.

No.	Catalyst	Methane conversion (%)	C_2 selectivity (%)	Hydrogen selectivity (%)	Coke selectivity (%)
1.	2.7F2.7M/AC	7.8	13.55	33.81	52.64
2.	2.7W2.7M/AC	6.9	20.09	24.97	54.94
3.	2.7F2.7W/AC	10.3	17.42	38.33	44.26
4.	1.8F1.8W1.8M/AC	8.6	23.98	36.44	39.58

4.2.4 Characterization of the spent catalyst

4.2.4.1 TGA analysis of deposited carbon

Figure 4-19 shows TGA patterns of catalysts supported on HZSM-5. From Figure 4-19, there was no change in weight between 300-400℃ . In catalyst 1.8F1.8W1.8M/HZSM-5 and catalyst 2.7F2.7M/HZSM-5, oxidation of deposited carbon nano material was complete at 600℃. After the loss of residual moisture at 100℃, there was negligible change in weight. This is a characteristic of low temperature non-amorphous carbon material

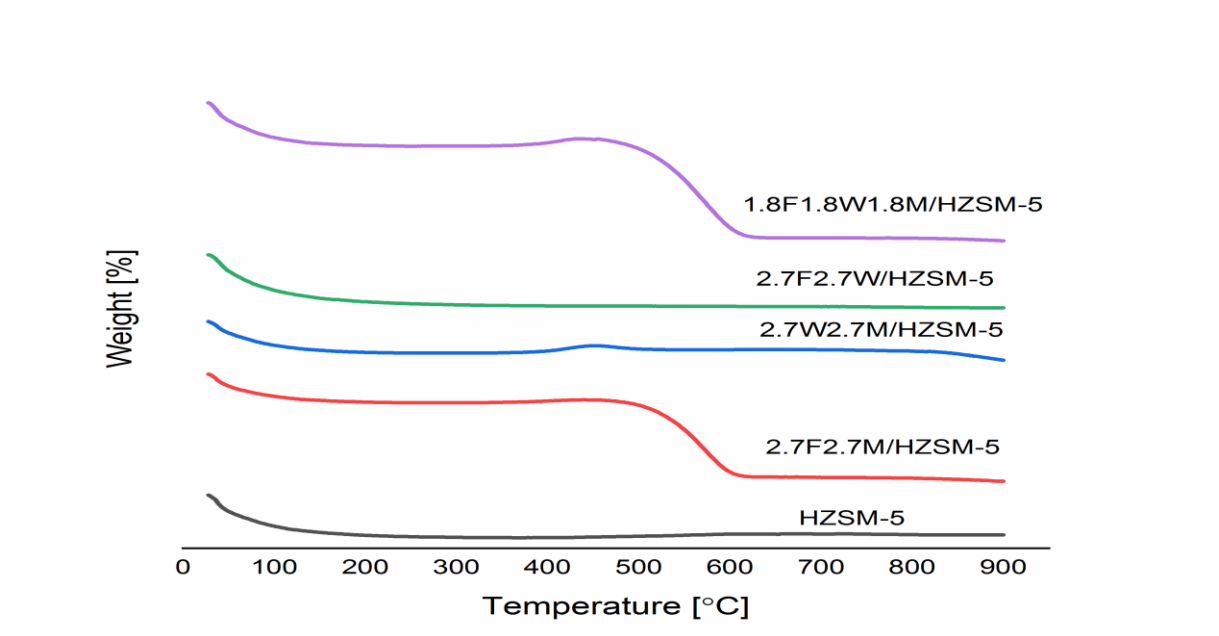

Figure 4-19 TGA pattern of catalysts; HZSM-5, 2.7F2.7M/HZSM-5, 2.7W2.7M/HZSM-5, 2.7F2.7W/HZSM-5, and 1.8F1.8W1.8M/HZSM-5.

Results of thermogravimetric studies of all the four catalysts loaded on AC are given of Figure 4-20. From the Figure 4-20, there was no change in weight between 300-400℃. This is a characteristic of pure carbon nanomaterial. Oxidation of all deposited carbon nanomaterial was virtually complete at 500℃, implying that the nature of formed carbon was "low temperature carbon"

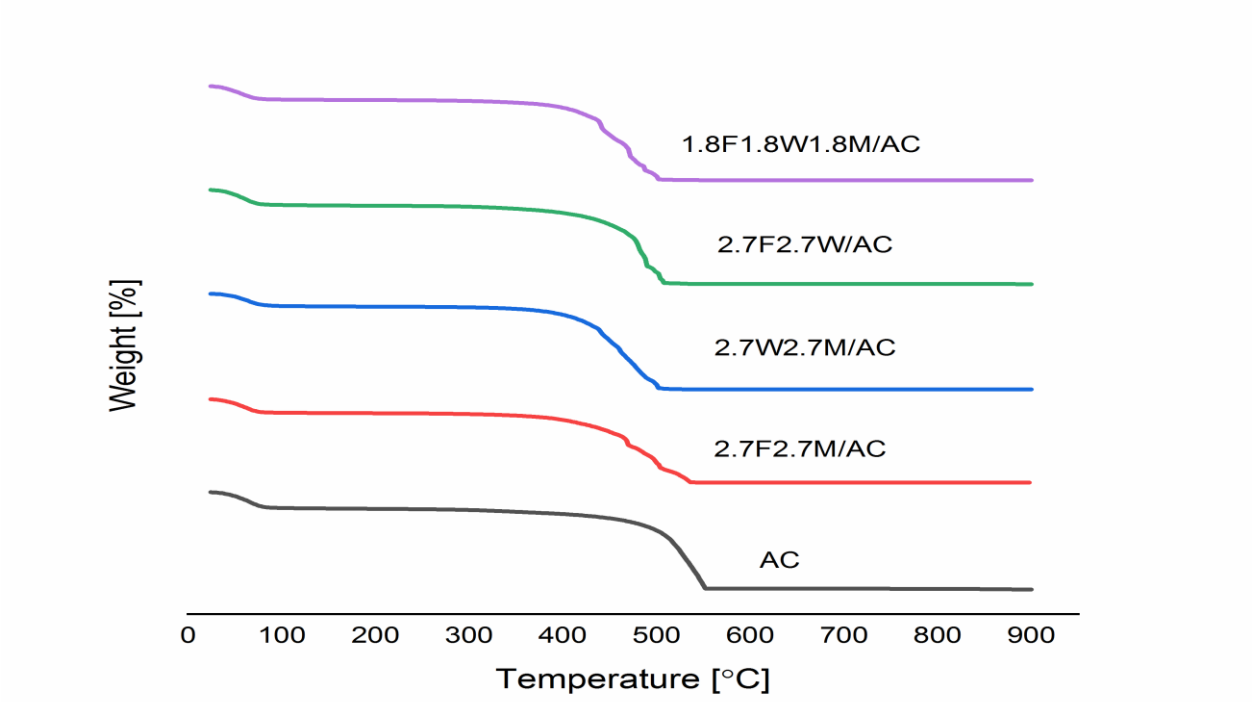

Figure 4-20. TGA pattern of catalysts; AC, 2.7F2.7M/AC, 2.7W2.7M/AC, 2.7F2.7W/AC, and 1.8F1.8W1.8M/AC.

4.2.4.2 TEM analysis of deposited carbon

In Figure 4-21, TEM images of deposited carbon nanomaterial are seen on catalyst 2.7F2.7M/HZSM-5. From the TEM image, clear formation of carbon nanotubes (CTs) and nanoparticles of metal oxides can be identified. From the TEM micrographs of catalyst 2.7W2.7M/HZSM-5, a dense mass of carbon nanomaterial is seen deposited on the spent catalyst. This implies that the carbon nanotubes formed on 2.7F2.7M/HZSM-5 catalyst was largely due to the presence of iron. The pattern of deposition of these metal oxide nanomaterial growth conformed to "tip-growth and base- growth" mechanism, similar to that reported by Chen et al (Chen *et al.* 1997). Few uniform CNTs with smooth external surfaces and metal oxide nanomaterial are formed on catalyst 2.7F2.7W/HZSM-5. Despite the presence of Fe which is

believed to have contributed to the formation of carbon nanotubes on catalyst 2.7F2.7M/HZSM-5, no significant amount of carbon nanotubes was seen on catalyst 2.7F2.7W/HZSM-5. It is therefore believed that tungsten promoted iron dispersion into the zeolite. On the other hand, when all the three metals were equally loaded on the zeolite, there is notable formation of carbon nanotubes on catalyst 1.8F1.8W1.8M/HZSM-5. Similarly, both long and short length micro walled carbon nano tubes (MWCNTs) can also be seen on this catalyst. It can therefore be inferred that low yields of carbon nanotubes in catalyst 2.7F2.7W/HZSN-M-5 was attributed to high dispersion of metal oxides in the zeolite due to the presence of tungsten. This finding is in agreement with another one reported elsewhere (Li *et al.* 2016). The presence of iron in appreciable quantities was responsible for complete decomposition of CH_4 to carbon nanotubes (Xu *et al.* 2012). Molybdenum is known to promote the growth of carbon nanotubes just like iron but since its metal loading in catalyst 1.8F1.8W1.8M/HZSM-5 is too low, its ability to promote the growth of carbon nanotubes was impaired. The inability of low Mo loading in Mo/HZSM-5 catalyst to promote the growth of carbon nanotubes was also reported elsewhere (Bajec *et al.* 2019).

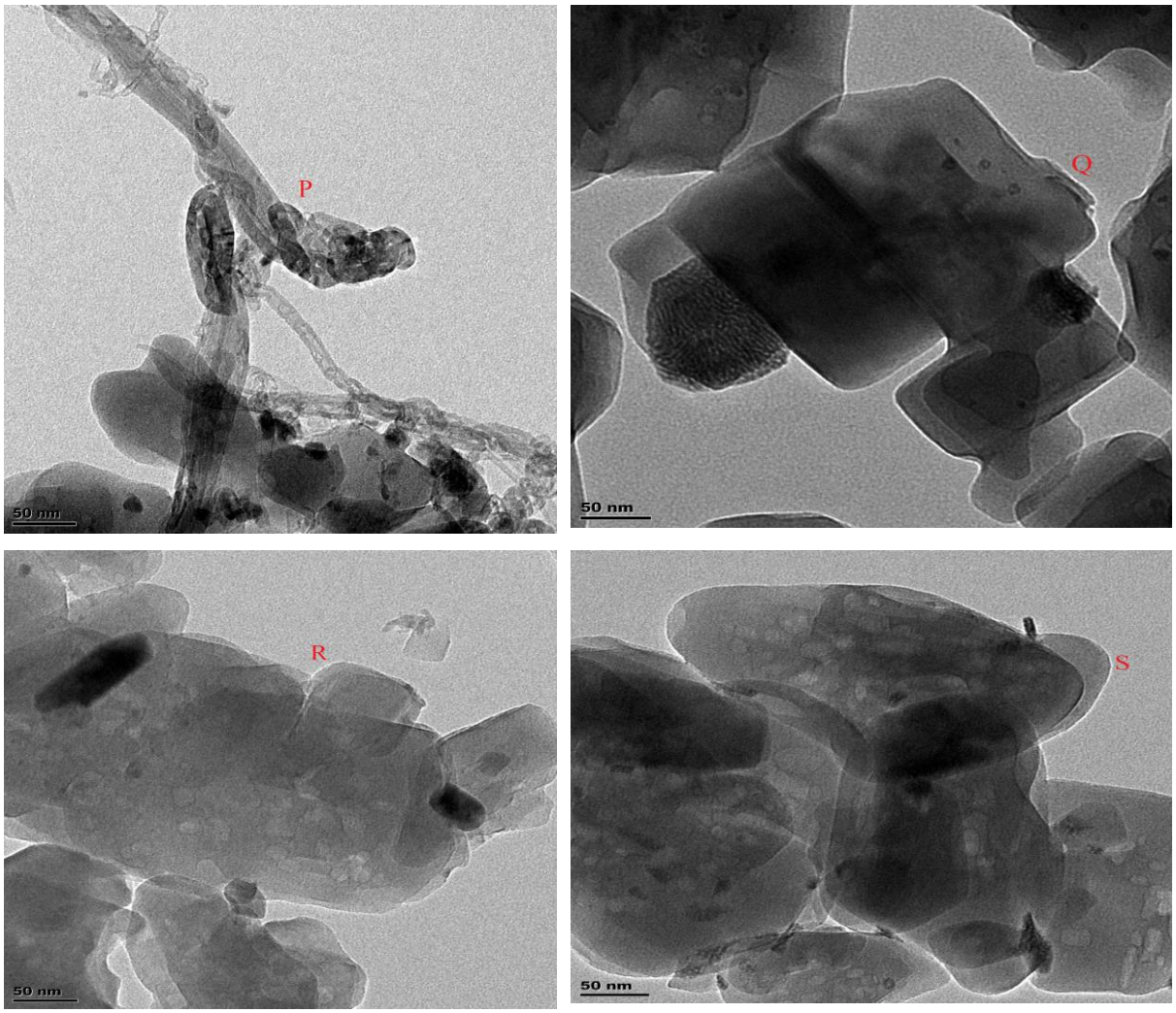

Figure 4-21. TEM Image of various catalysts; P(2.7F2.7M/HZSM-5), Q(2.7W2.7M/HZSM-5), R(2.7F2.7W/HZSM-5), and S(1.8F1.8W1.8M/HZSM-5).

TEM images of catalysts supported on AC shows dense masses of deposited carbon nanomaterial on ach catalyst system. From Figure 4-22, absence of definite structures of carbon nanomaterial is an indication that methane conversion reaction took place on the surface of the catalyst and the metal oxides in the catalyst system did not control the formation of particular shapes of deposited carbon. Shape selectivity of HZSM-5 contributed to the formation of definite structures of carbon nanomaterial.

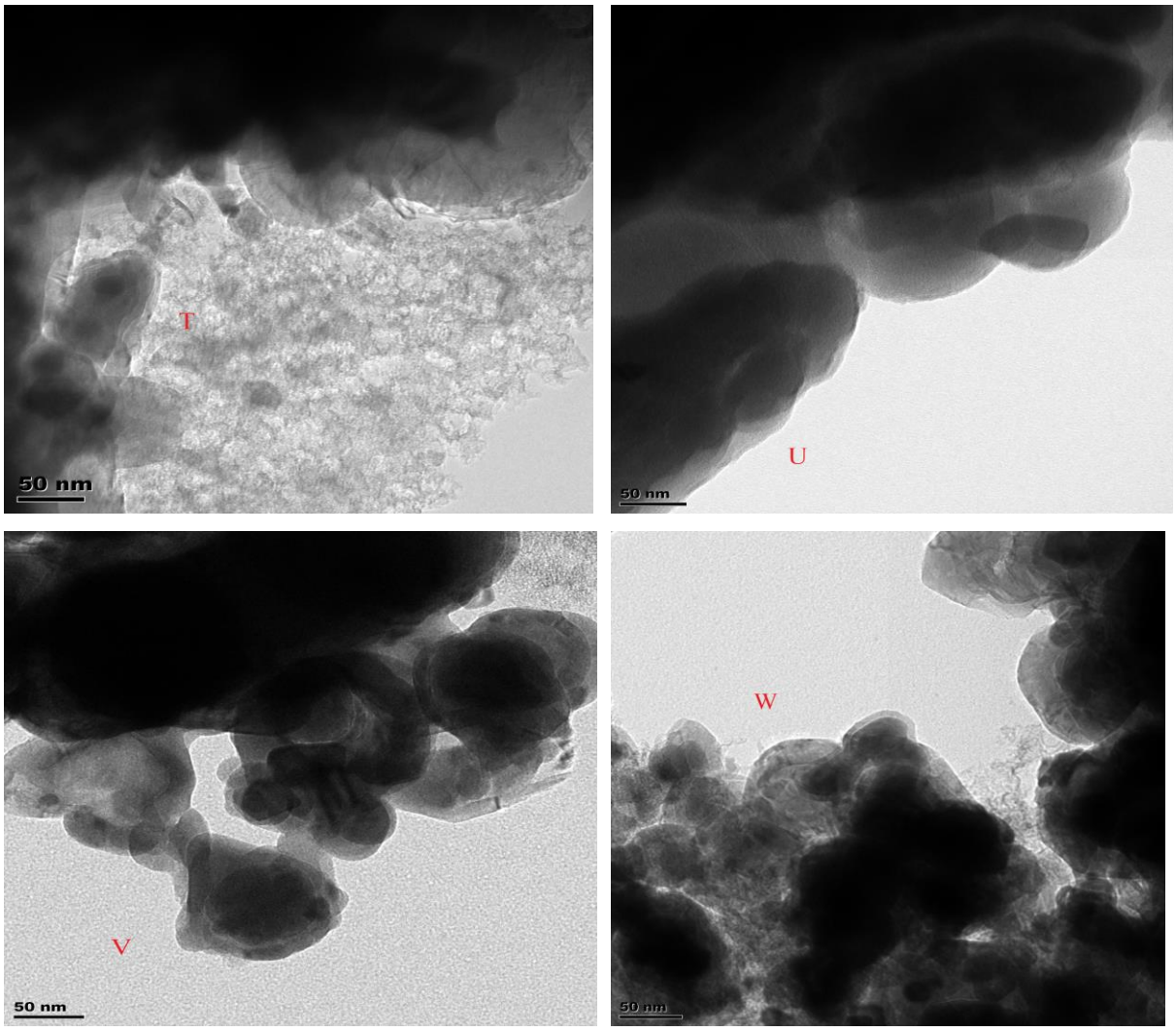

Figure 4-22. TEM Images of various catalysts loaded on AC; T(2.7F2.7M/AC), U(2.7W2.7M/AC), V(2.7F2.7W/AC), and W (1.8F1.8W1.8M/AC).

4.2.5 Summary of the findings

This present work demonstrates the development of a stable and durable Fe-W-Mo/HZSM-5 catalyst system for methane conversion and product distribution in non-oxidative conversion of methane into carbon and petrochemicals. Based on the results obtained, metal synergism in the catalyst system played a significant role on methane conversion and product distribution.

- Catalyst 2.7%Fe-2.7%Mo/HZSM-5 (without W) showed little activity in methane conversion but highly selective towards C_2 hydrocarbons.

- Catalyst 2.7%W-2.7%Mo/HZSM-5 (without Fe) was most active in methane conversion, most selective towards coke but less selective towards benzene.
- Catalyst 2.7%Fe-2.7%W/HZSM-5 (without Mo) was less active in methane conversion, most selective towards toluene but less selective towards coke.
- A combination of W and Mo on HZSM-5 gave the best results in methane conversion but less selective towards benzene and most selective towards coke. Molybdenum has been found to be the most active metal when supported on zeolite because of its reducibility from Mo^{6+} to Mo_2C.
- Tungsten was desired for good conversion and enhanced benzene yields. It was also selective towards aliphatic compounds and inhibited the formation of graphitic coke.
- When all the three metals were loaded on HZSM-5 in equal quantities (1.8%F1.8%W1.8%Mo), the resultant catalyst became more selective towards C_2 hydrocarbons. Based on the above synergistic behaviour of noble metals, it was observed that combining two or more catalytically active metals gives improved activity as compared to the results of individual metals.
- Synergistically, Fe promoted coke and aromatic selectivity, W promoted conversion, and Mo aided the generation of methyl radicals which were oligomerized into C_2 hydrocarbons, hence high selectivity towards C_2 hydrocarbons.

4.3. Objective III: To investigate the effect of process conditions on methane conversion and product distribution.

4.3.1 Catalyst synthesis

To study the effect of process conditions on catalyst activity, the following catalysts in Table 4-11 were synthesized using incipient wetness impregnation, dried, calcined, and used in non-oxidative conversion of methane in a packed bed reactor at different temperature, different gas hourly space velocity, and different reaction time on stream.

Table 4-11. Binary catalyst systems for methane composition**.**

Catalyst	Composition (wt.%)
1.8F1.8W1.8M/HZSM-5	1.8Fe – 1.8%W – 1.8%Mo-94.6%HZSM -5
2.25F2.25W0.9M/HZSM-5	2.25%Fe – 2.25%W – 0.90%Mo-94.6%HZSM -5
1.35F1.35W2.7M/HZSM-5	1.35Fe – 1.35%W – 2.70%Mo
1.8F1.8W1.8M/AC	1.8Fe – 1.8%W – 1.8%Mo-94.6%AC
2.25F2.25W0.9M/AC	2.25%Fe – 2.25%W – 0.90%Mo-94.6%AC
1.35F1.35W2.7M/AC	1.35Fe – 1.35%W – 2.70%Mo-94.6%AC

4.3.2 Catalyst characterization

Synthesized catalysts were characterized by techniques previously described in section 3.4

4.3.3 Catalyst evaluation

Synthesized catalysts were tested for methane conversion at different temperatures, different gas hourly velocities, different activation times, and at 1atm. Methane conversion experiments were carried out according to procedures described in section 3.5.

4.3.3.1 Effect of temperature on methane conversion and product distribution.

To study the effect of temperature on methane conversion and product distribution, the binary catalyst systems were applied for no-oxidative methane conversion at different temperatures (700, 750℃ and 800℃) in a packed bed reactor at 0.96 $Lg^{-1}cath^{-1}$, 1 atm and 4hours' time on stream. In Figure 4-7, all catalysts showed an increase in methane conversion as the temperature increased. An increase in methane conversion with an increase in temperature is attributed to easy C-H activation by both temperature and catalyst effect. From documented literature, a

methane molecule starts losing its stability after 530℃ (Guéret *et al.* 1997). Selectivity towards benzene and toluene decreased with an increase in temperature. As temperature increased, increased coke formation affected the kinematic diameter of benzene molecule, thus inhibiting shape selectivity towards benzene. Aromatic selectivity occurs inside the pores of the zeolite channels. At high temperatures, the zeolite structure starts to lose its structural integrity due to dealumination. As the temperature increases, the rate of methane conversion over AC catalysts increases because methane decomposition is an endothermic reaction. This increase in methane conversion continues up to ~ 900℃ after which deactivation sets in due to blockage of active sites by deposited coke. In Figure 4-8, selectivity towards xylene decreases with an increase in temperature except for the reaction over catalyst 1.35F1.35W2.7M/HZSM-5 whose catalytic activity towards xylene formation remained almost the same at different temperatures. Hydrogen selectivity also increased with an increase in temperature except in the reaction over catalyst 1.35F1.35W2.7M/AC where selectivity towards hydrogen showed a decrease at 800℃. In terms of coke selectivity, all catalyst systems became more selective towards coke as the temperature increased. Since methane conversion increases with an increase in temperature, dealumination of the HZSM-5 starts at ~800℃ . At this temperature, shape selectivity of the zeolite is partly affected. Once the zeolite structure is distracted due to dealumination, methane will be decomposed into carbon and hydrogen at the expense of aromatics, hence high selectivity towards coke.

4.3.3.2 Effect of gas hourly space velocity on methane conversion and product distribution.

To study the effect of gas hourly space velocity on methane conversion and product distribution, the synthesized binary catalyst systems were applied for non-oxidative methane conversion in a packed bed reactor at different gas hourly space velocities (0.96, 1.92, and 2.88) $Lg^{-1}cath^{-1}$ at 750℃ and 1 atm for 4 hours' time on stream. In Figures 4-23 (a & b), catalytic activity of all the catalyst systems in terms of methane conversion and C_2 selectivity decreased with an increase in gas hourly space velocity. As shown in Figure 4-23 (c & d), benzene and toluene selectivity decreased with an increase in in GHSV. This is in agreement with a similar report by (Chen *et al.* 1995) and (Solymosi *et al.* 1996). At higher GHSVs, methane conversion decreases due to reduced contact time between the catalyst and the reactant. Since GHSV is the ratio of raw material flow rate to catalyst mass per unit time, a suitable combination is required to provide

optimal contact time between the catalyst and the reactant as suggested elsewhere (Al-Fatesh *et al.* 2016).

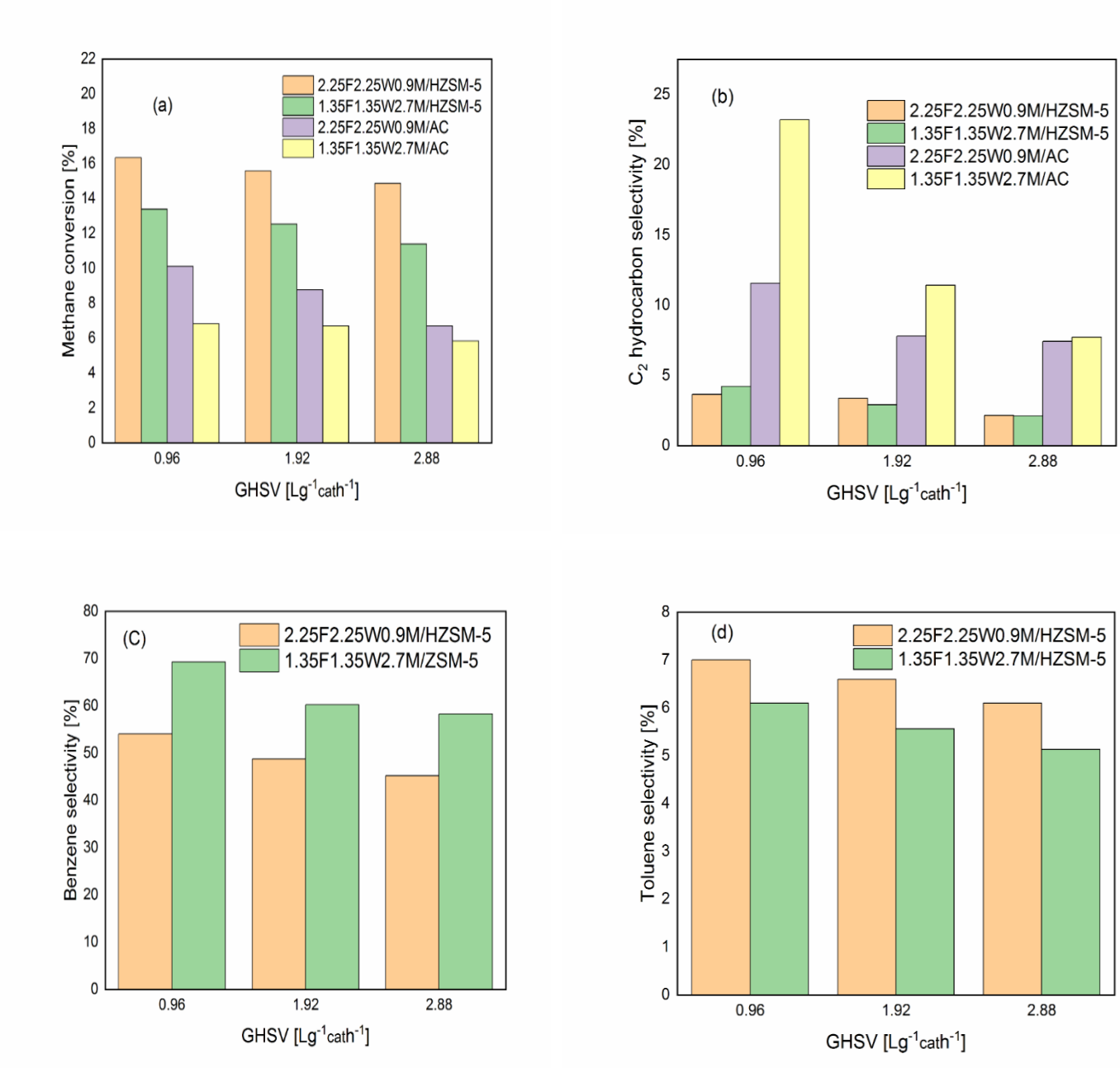

Figure 4-23. Effect of GHV on methane conversion and product selectivity over various catalysts at 750℃ and 1atm.

In Figure 4-24 (e), xylene selectivity was only achieved by catalysts supported on HZSM-5 at 0.96 $Lg^{-1}cat.h^{-1}$. As the GHSV increased, there was no selectivity towards xylene. Hydrogen

formation in Figure 4-24 (f) decreased with an increase in GHSV. Similarly, selectivity towards coke decreased with an increase in GHSV in all catalysts.

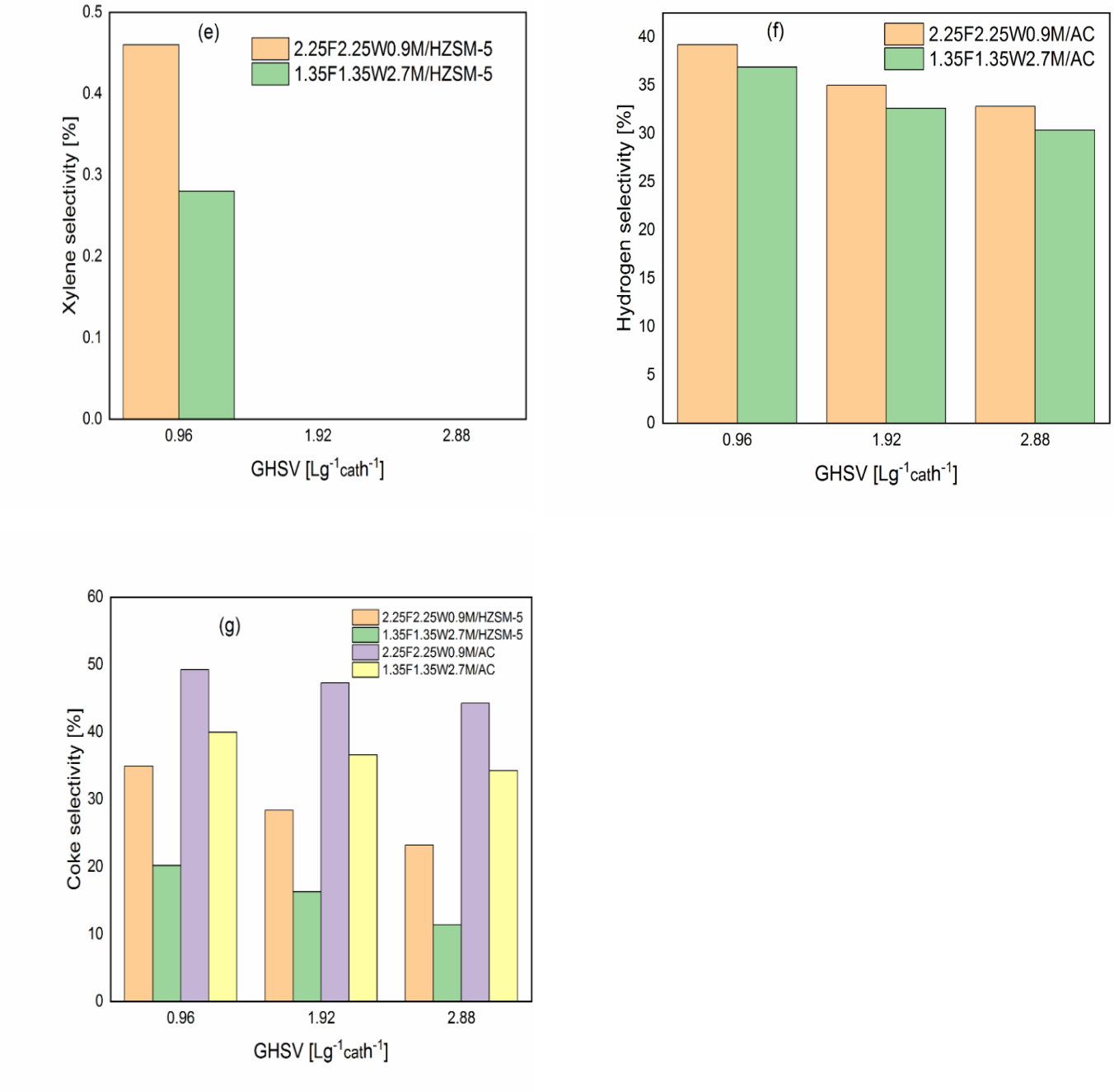

Figure 4-24. Effect of GHSV on xylene, hydrogen, and coke selectivity over different catalysts at 750℃, and 1atm.

4.3.3.3 Effect of reaction time on catalyst activity.

To study the effect of reaction time on methane conversion and product distribution, the binary catalyst systems were applied for non-oxidative methane conversion in a packed bed reactor at different reaction times on stream (1, 2, 3, and 4) hours, 0.96 $Lg^{-1}cath^{-1}$ at 750℃ and 1 atm. From Figure 4-25, catalysts, 2.25F2.25W0.9M/HZSM-5, 1.35F1.35W2.7M/HZSM-5, 2.25F2.250.9M/AC, and 1.35F1.35W2.7M/AC exhibited a declining trend in methane conversion and selectivity towards C_2 hydrocarbons. After 1hour time on stream, catalyst activity values were high but gradually decreased due to catalyst deactivation caused by coking.

Non-oxidative conversion of methane entails initial activation of C-H in a methane molecule by dehydrogenation, coupling of C-C to ethylene, and subsequent oligomerization at the Bronsted acid sites of the zeolite (Sim *et al.* 2020). A similar report elsewhere (Tan 2016) indicates that the stability of carbene, a primary intermediate of activated methane plays a major role in transforming methane to carbon and C_2 hydrocarbons. Carbene is usually unstable on metallic sites and therefore its C-H bond bifurcates further to yield hydrogen. On the other hand, F_3C can stabilize carbene by formation of metal-carbene complex ($C\text{-}Fe{=}CH_2$) so that carbene can dimerize into ethylene, which is further transformed into aromatics in the zeolite acid sites. Therefore, a highly carburized catalyst is desired for high selectivity towards aromatics.

When Mo/HZSM-5 catalyst is used alone, methane hydrogenates and dimerizes on Mo species (Solymosi *et al.* 1999). The active component of the catalyst arises from the interaction between MoO_3 and the acid sites of the HZSM-5 zeolite (Zhang *et al.* 1998). During calcination, the MoO_3 species diffuses into the HZSM-5 where it interacts with the Bronsted acid sites. Once inside the zeolite channel, the MoO_3 reacts with H^+ associated with Bronsted acid sites to form $[MoO_2(OH)]^+$ species, which condenses to form $[MoO_2(H_2O)]$ dimers and H_2O. In Figure 4-27, all catalysts showed an increase in coke selectivity with an increase in time on stream (TOS). This was expected because carbon is one of the products of methane conversion. Accumulation of coke on each catalyst increases with an increase in time on stream.

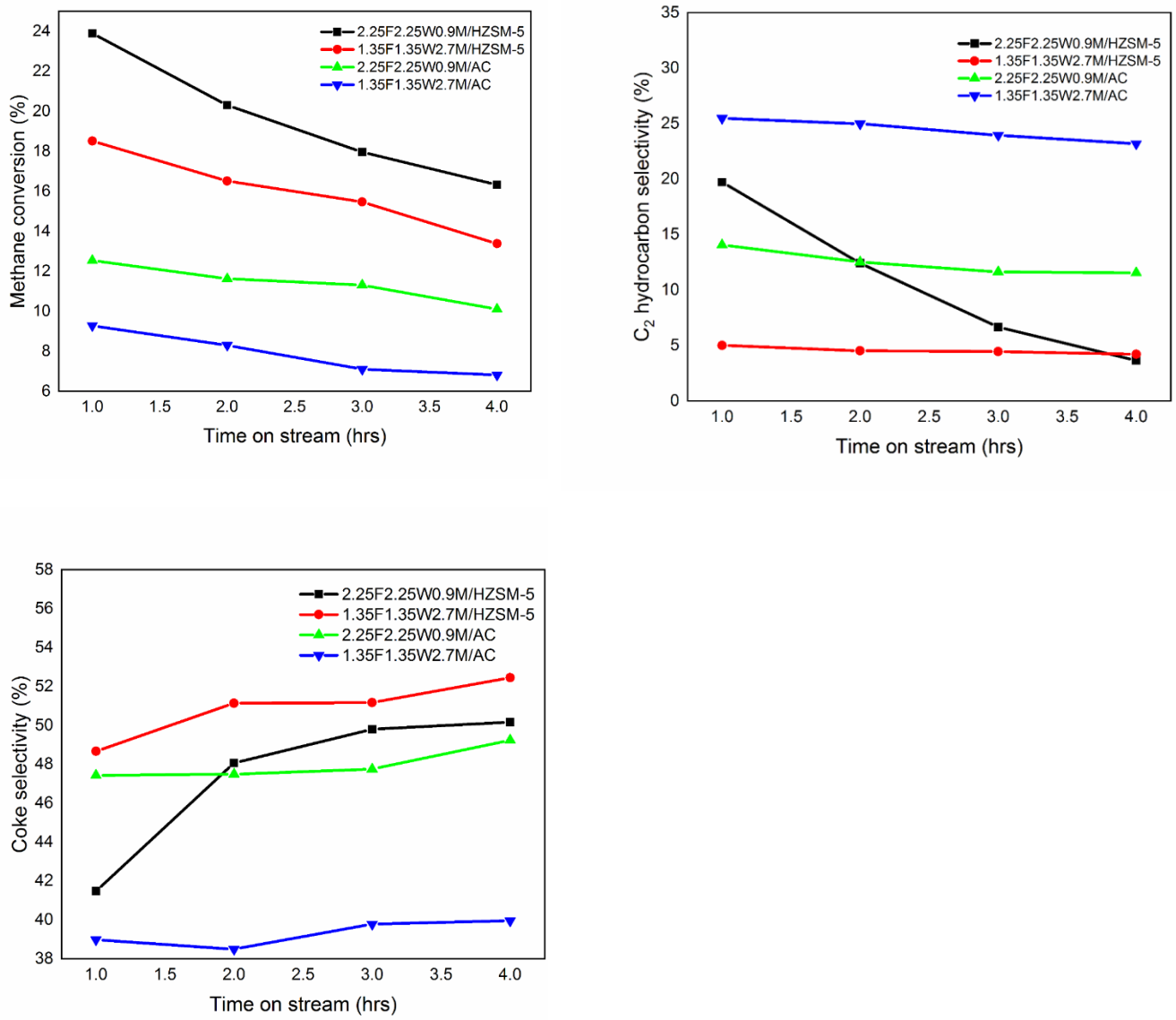

Figure 4-25. Effect of reaction time on methane conversion, C_2 hydrocarbon selectivity, and coke selectivity over various catalysts at 750℃, 0.96 $Lg^{-1}cat.h^{-1}$, and 1 atm.

4.3.2 Summary of the findings

- In all catalyst systems, methane conversion increased with an increase in temperature.
- In all catalysts supported on HZSM-5, selectivity towards benzene, toluene, and xylene decreased with an increase in temperature.
- In all catalyst systems, methane conversion, C_2 hydrocarbon selectivity and coke selectivity decreased with an increase in gas hourly space velocity.

- From 1-4 hours-time on stream, methane conversion, C_2 hydrocarbon selectivity decreased with an increase in TOS while coke formation increased with an increase in in time on stream.

4.4 Objective IV: To investigate the effect support on methane conversion and product distribution.

4.4.1 Catalyst synthesis and designation

To study the effect of support on methane conversion and product distribution, various catalyst systems at different metal loading on HZSM-5 and AC as shown in Table 4-12 were synthesized by incipient wetness impregnation, followed by drying, and calcination.

4.4.2 Catalyst characterization

Synthesized catalysts were characterized by techniques previously described in section 3.4

4.4.3 Catalyst evaluation

From Table 4-12, most catalysts supported on HZSM-5 showed high activity in methane conversion than those catalyst systems supported on activated carbon. On the other hand, catalyst systems supported on AC are more selective towards C_2 hydrocarbon than those supported on HZSM-5. Catalyst systems supported on AC, converted methane into carbon, C_2 hydrocarbons, and hydrogen. As for catalyst systems supported on HZSM-5, the evolved C_2 intermediates were transformed into aromatics through oligomerization and cyclization reactions. Bronsted acid sites and shape selectivity of HZSM-5 aided transformation of C_2 hydrocarbons into benzene and its derivatives.

Table 4-12. Methane conversion and C_2 selectivity over various catalysts at different temperatures, 0.96 $Lg^{-1}cat.h^{-1}$, and 1 atm.

No.	Catalyst	Methane conversion (%)			C_2 hydrocarbon selectivity (%)		
		700℃	750℃	800℃	700℃	750℃	800℃
1.	1.8F1.8W1.8M/HZSM-5	4.8	5.9	6.8	14.5	13.3	12.9
2.	2.25F2.25W0.9M/HZSM-5	15.5	16.3	17.2	3.2	3.6	9.4
3.	1.35F1.35W2.7M/HZSM-5	12.5	13.4	14.4	4.6	4.2	3.2
4.	1.8F1.8W1.8M/AC	8.1	8.6	9.2	20.4	23.9	24.9
5.	2.25F2.25W0.9M/AC	9.5	10.1	12.4	18.8	11.6	10.6
6.	1.35F1.35W2.7M/AC	6.2	6.8	7.3	23.5	23.2	22.4

In Table 4-13, catalyst systems supported on HZSM-5 show selectivity towards benzene and xylene. Between 700-800℃, catalyst 1.35F1.35W2.7M/HZSM-5 was most selective towards benzene while catalyst 1.8F1.8W1.8M/HZSM-5 was least selective towards benzene between the same temperature range. In terms of toluene selectivity, catalyst 1.35F1.35W2.7M/HZSM-5 was most selective towards toluene at 700℃ and 750℃ but showed a slight decline in selectivity towards toluene at 800℃. Zeolite supports are more reactive than AC supports. HZSM-5 zeolite supports have Bronsted acid sites which promote not only methane activation ($CH_4 = CH_X + nH_2$) on the metal carbide sites of metal/HZSM-5 catalysts, but also oligomerizes the dissociative surface species into C_2 hydrocarbons. These C_2 hydrocarbons are further transformed into benzene and naphthalene in the channels of the zeolite.

Table 4-13. Benzene and toluene selectivity at different temperatures over different catalysts at 0.96 $Lg^{-1}cat.h^{-1}$, and 1 atm.

No.	Catalyst	Benzene selectivity (%)			Toluene selectivity (%)		
		700℃	750℃	800℃	700℃	750℃	800℃
1.	1.8F1.8W1.8M/HZSM-5	54.5	48.7	46.8	8.1	6.1	4.8
2.	2.25F2.25W0.9M/HZSM-5	54.6	54.0	49.2	7.8	7.0	5.7
3.	1.35F1.35W2.7M/HZSM-5	71.9	69.3	68.1	8.7	6.1	5.2
4.	1.8F1.8W1.8M/AC						
5.	2.25F2.25W0.9M/AC						
6.	1.35F1.35W2.7M/AC						

In Table 4-14, only catalysts supported on HZSM-5 were selective towards xylene. At 800℃, only catalyst 1.35F1.35W2.7M/HZSM-5 showed some activity towards xylene formation. This implies that MoO_3 played a great role in the formation of xylene. Catalysts supported on AC were highly selective towards coke than those catalyst systems supported on HZSM-5. High surface area of catalyst systems supported on AC is believed to have influenced its selectivity towards coke.

Table 4-14. Xylene and coke selectivity at different temperatures over different catalysts at 0.96 $Lg^{-1}cat.h^{-1}$, and 1 atm.

No.	Catalyst	Xylene selectivity (%)			Coke selectivity (%)		
		700℃	750℃	800℃	700℃	750℃	800℃
1.	1.8F1.8W1.8M/HZSM-5	0.8	0.0	0.0	22.1	31.9	35.5
2.	2.25F2.25W0.9M/HZSM-5	1.2	0.5	0.0	33.2	34.9	35.7
3.	1.35F1.35W2.7M/HZSM-5	0.3	0.3	0.3	14.6	20.2	23.2
4.	1.8F1.8W1.8M/AC				40.9	39.6	36.2
5.	2.25F2.25W0.9M/AC				43.8	49.2	46.9
6.	1.35F1.35W2.7M/AC				40.5	39.9	44.8

Selectivity towards hydrogen was exhibited by catalyst systems supported on AC. From Table 4-15, catalyst 1.8F1.8W1.8M/AC was most selective towards hydrogen than all the catalysts. In all catalyst systems supported on HZSM-5, the evolved hydrogen was coupled with methyl radicals to form C_2 hydrocarbons.

Table 4-15. Hydrogen selectivity over catalyst, at different temperatures, 0.96 $Lg^{-1}cat.h^{-1}$, and 1 atm.

No.	Catalyst	Hydrogen selectivity (%)		
		700℃	750℃	800℃
1.	1.8F1.8W1.8M/HZSM-5	-	-	-
2.	2.25F2.25W0.9M/HZSM-5	-	-	-
3.	1.35F1.35W2.7M/HZSM-5	-	-	-
4.	1.8F1.8W1.8M/AC	38.8	36.4	38.9
5.	2.25F2.25W0.9M/AC	37.4	39.2	42.5
6.	1.35F1.35W2.7M/AC	36.0	36.9	32.8

4.4.4 Summary of the findings

- Most catalysts supported on HZSM-5 were more active on methane conversion than those catalysts supported on AC because HZSM-5 support is more reactive than AC.
- There is wider product range in catalysts supported on HZSM-5 than those supported on activated carbon because HZSM-5 has shape selectivity.
- Catalysts supported on activated carbon were more selective towards hydrogen than those catalysts supported on HZSM-5.
- Bronsted acid sites and shape selectivity of HZSM-5 aided the transformation of C_2 hydrocarbons into benzene and its derivatives.
- Activated carbon does not have acid sites and its pore size is too large (> 5.8 Å) to promote shape selectivity of aromatics.

4.5 Objective V: To investigate the effect of catalyst preparation method in the catalyst system on methane conversion and product distribution.

To investigate the effect of catalyst preparation method on methane conversion and product distribution, selected catalysts were synthesized using various catalyst preparation methods and applied in non-oxidative methane conversion.

4.5.1 Catalyst synthesis

To study the effect of catalyst preparation method on catalyst activity in NOCM reaction, catalysts in Table 4-12 were synthesized using three catalyst preparation methods described under section 3.3 and applied for non-oxidative conversion of methane.

4.5.2 Catalyst characterization

Catalysts synthesized by incipient wetness impregnation were characterized by techniques previously described in section 3.4

4.5.3 Catalyst evaluation

Performance of catalyst systems prepared by each catalyst preparation method was evaluated based on methane conversion and product distribution in a packed bed reactor at 750℃ , 1 atm, and 4hrs time on stream according to procedures described in section 3.5.

Catalytic activity of each catalyst system is given in Figure 4-26 (a-c). In Figure 4-26 (a), catalyst 2.25F2.25W0.9M/HZSM-5 was most active in methane conversion while catalyst 1.35F1.35W2.7M/HZSM-5 was least active in methane conversion. Catalysts prepared by incipient wetness impregnation recorded impressive results compared to those prepared by sequential impregnation and mechanical mixing. Since activation of methane molecules occurs both on the surface and inside the support pores, it is believed that low methane conversion exhibited by catalysts prepared by sequential impregnation and mechanical mixing was due to limited diffusion of Fe_2O_3, WO_3, and MoO_3 into the support. In Figure 4-26 (b), the highest activity in terms of selectivity towards C_2 hydrocarbons was exhibited by catalyst 1.8F1.8W1.8M/AC while catalyst 2.25F2.5W0.9M/AC showed little activity towards selectivity of C_2 hydrocarbons. As shown in Figure 4-26 (c), catalysts supported on AC and prepared by incipient wetness impregnation were more selective towards coke than those prepared by other catalyst preparation methods. Incipient wetness impregnation was the preferred method for preparing catalysts loaded on AC support because they demonstrated high

activity in methane conversion. Significant results towards benzene selectivity were achieved by catalyst systems supported on HZSM-5 and prepared by Incipient wetness impregnation.

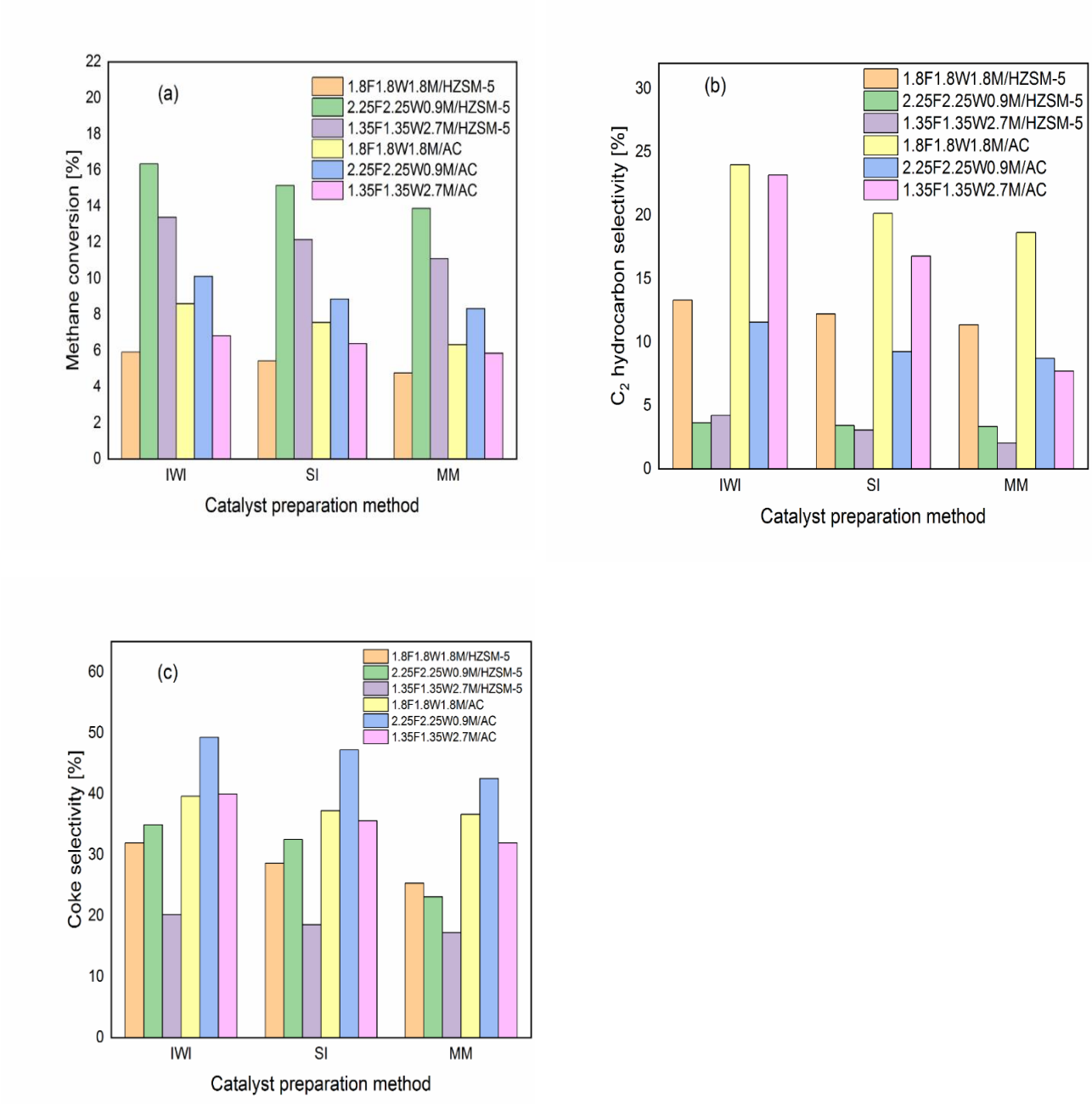

Figure 4-26. Effect of catalyst preparation method on methane conversion, C_2 hydrocarbon selectivity, and coke selectivity over various catalysts at 750℃, 0.96 $Lg^{-1}cat.h^{-1}$, and 1 atm.

In Figure 4-27 (d), catalyst 1.35F1.35W2.7M/HZSM-5 was most selective towards benzene while catalyst 2.25F2.25W0.9/HZSM-5 was least selective towards benzene. This can be explained in terms of the effect of metal loading whereby, high Mo content in the catalyst system is believed to have aided the generation of methyl radicals which were oligomerized into benzene and its derivatives. This finding is in agreement with what was reported by (Wang *et al.* 1996). In Figure 4-27 (e), more promising results in terms toluene selectivity were achieved by catalyst systems supported on HZSM-5 and prepared by mechanical mixing as compared to those prepared by sequential impregnation and incipient wetness impregnation. It is believed that mechanical mixing was the ideal method for diffusion of metal oxides into the zeolite channels. In Figure 4-27 (f), formation of xylene was only achieved by catalyst 2.25F2.25W0.9M/HZSM-5 and catalyst 1.35F1.35W2.7M/HZSM-5 prepared by incipient wetness impregnation. There was no xylene formation by catalysts prepared by sequential impregnation and mechanical mixing. As shown in Figure 4-27 (g), selectivity towards hydrogen was exhibited by catalyst systems supported on AC and prepared by all the three catalyst preparation methods. However, in terms of toluene selectivity, most promising results were achieved by catalyst 2.25F2.25W0.9M/AC compared to those results achieved by catalyst 1.8F1.8W1.8M/HZSM-5. For catalysts supported on AC, methane molecules decomposed into carbon, C_2 and hydrogen whereas the catalysts supported on HZSM-5 converted methane into carbon and C_2 hydrocarbons which were transformed into benzene and its derivatives through oligomerization and cyclization reactions. When modifying carbon materials, chemical modifications such as grafting yields more promising results than physical modifications (Chen *et al.* 2011).

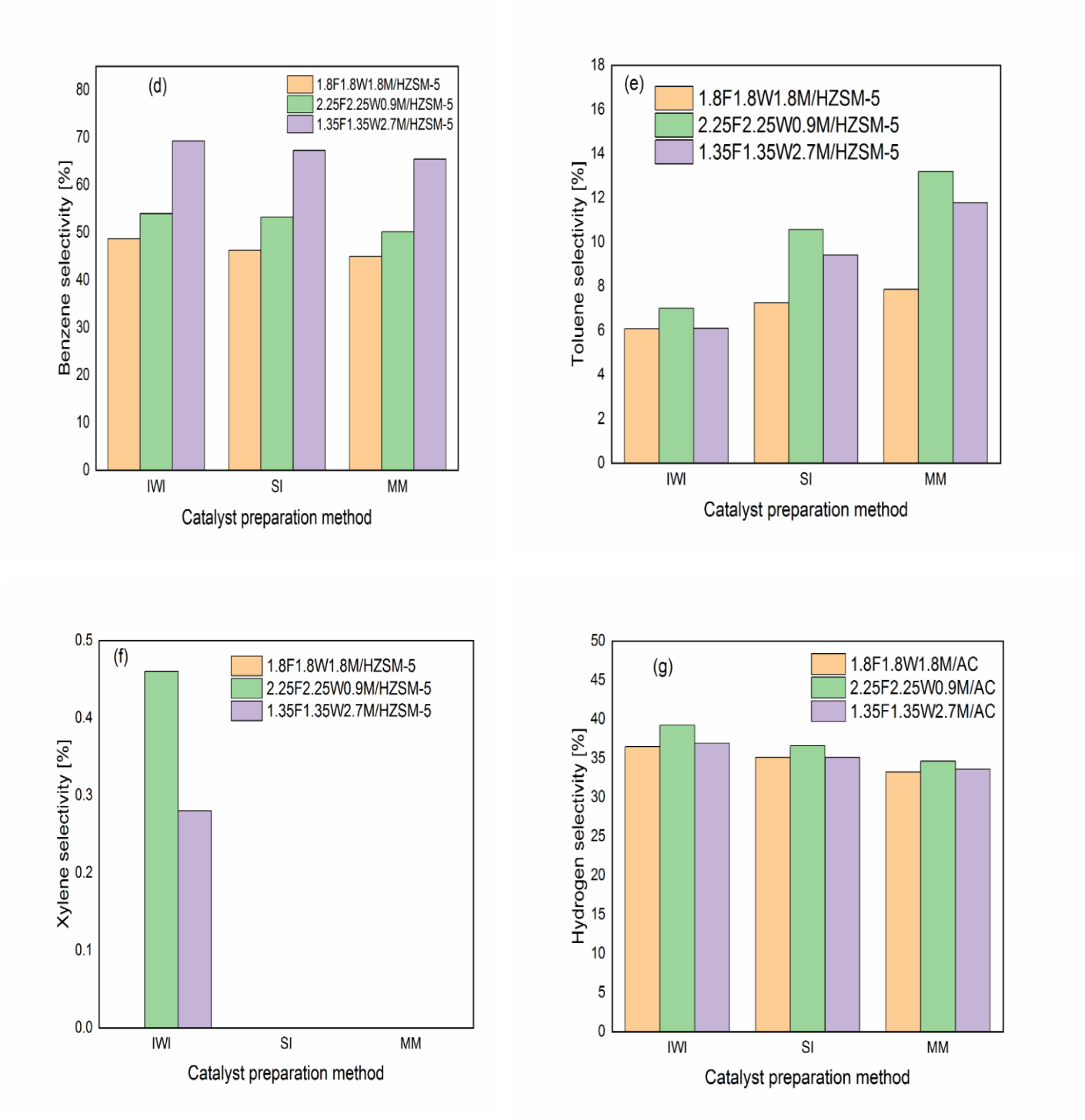

Figure 4-27. Effect of catalyst preparation method on benzene, toluene, xylene, and hydrogen selectivity over various catalysts at 750℃, 0.96 $Lg^{-1}cat.h^{-1}$, and 1 atm.

4.5.4 Summary of the findings

- Catalyst systems prepared by incipient wetness impregnation were most active in methane conversion and highly selective towards C_2 hydrocarbons, benzene, hydrogen, and coke.
- Catalyst systems prepared by sequential impregnation did not show any activity towards xylene formation.
- Catalysts prepared by mechanical mixing were catalytically more active towards toluene formation than those prepared by sequential impregnation and incipient wetness impregnation.
- A wider product distribution was displayed by catalyst systems which were prepared by incipient wetness impregnation.

CHAPTER 5: GENERAL CONCLUSIONS

Non-oxidative conversion of methane is envisaged as one of the models for describing complex and multiple reactions that determine and estimate product distribution in methane conversion. It is regarded as a viable option for producing carbon and valuable petrochemicals from methane. Unlike other methane conversion processes like Fischer-Tropsch and methanol synthesis which have been scaled up to commercial level, NOCM process development remains at laboratory scale due to various challenges such as catalyst deactivation due to coking, process thermodynamics, low conversion, and limited selectivity towards useful products. This study demonstrates the development of a tuneable catalyst system comprising of trimetallic Fe, W, & Mo catalyst systems supported on HZSM-5 and activated carbon for methane conversion and quantitative control of product distribution. It has been demonstrated that such a tuneable catalyst system at different metal loadings and process conditions could be employed to achieve desired methane conversion and selectivity towards useful petrochemicals in non-oxidative methane conversion. Specific findings from the study were as follows.

1. In Fe, W, and Mo catalyst systems supported on HZSM-5, molybdenum aided generation of methyl radicals and subsequent formation of C_2 hydrocarbons through oligomerization reactions.
2. In Fe, W, and Mo catalyst systems supported on HZSM-5, tungsten was desired for methane conversion and enhancement of benzene selectivity.
3. In Fe, W, and Mo catalyst systems supported on HZSM-5, iron enhanced aromatic selectivity and suppressed coke formation.
4. Owing to its inherent acidity and structural properties, HZSM-5 zeolite aided conversion of C_2 intermediates into benzene and its derivatives.
5. In all catalyst systems, methane conversion increased with an increase in temperature between 700-800℃.
6. In all catalyst systems supported on HZSM-5, selectivity towards benzene, toluene, and xylene decreased with an increase in temperature.
7. In all catalyst systems, catalytic activity decreased with an increase in gas hourly space velocity.

8. From 1-4 hours' time on stream, methane conversion, selectivity towards C_2 hydrocarbons decreased with an increase in time on stream while coke formation increased with an increase in time on stream.
9. Catalyst systems supported on HZSM-5 produced a wider range of products as compared to those on AC support.
10. Catalyst systems prepared by incipient wetness impregnation were most active in methane conversion and highly selective towards C_2 hydrocarbons, benzene, hydrogen, and coke.
11. The development of a binary catalyst system which is catalytically active in non-oxidative methane conversion and selective towards useful fuels and petrochemicals with over 10% methane conversion up to 4 hours' time on stream has been demonstrated.
12. It has been demonstrated that Fe, W, &Mo catalyst systems can be tuned to achieve optimum methane conversion and selectivity towards useful petrochemicals by varying the amount of Fe, W, and Mo in the catalyst systems when supported on HZSM-5 and on activated carbon.

CHAPTER 6: RECOMMENDATIONS FOR FURTHER STUDY

Non-oxidative oxidation of methane into fuels and petrochemicals is an interesting area of study. Research into this area can take various dimensions. To current and future interested researchers in this field, further research into this area can focus on some of the following areas which were not part of the research objectives in this present study.

- Use of the developed catalyst systems on different acidic supports and metal oxide composites to improve catalyst activity and address the issue of low methane conversion.
- There is need to develop catalysts aimed at optimizing the process variables.
- Detailed kinetic and thermodynamic studies of non-oxidative methane conversion using catalysts developed in this study.
- The effect of heat and mass transfer on the catalyst systems.
- Testing of the performance of developed catalysts in various types of reactors.

REFERENCES

Abbas, HF and Wan Daud, WMA. 2010. Hydrogen production by methane decomposition: A review. *International Journal of Hydrogen Energy*, 35 (3): 1160-1190.

Abd Hamid, SB, Ambursa, MM, Sudarsanam, P, Voon, LH and Bhargava, SK. 2017. Effect of Ti loading on structure-activity properties of Cu-Ni/Ti-MCM-41 catalysts in hydrodeoxygenation of guaiacol. *Catalysis Communications*, 94: 18-22.

Aboul-Gheit, A and Awadallah, A. 2009. Effect of combining the metals of group VI supported on H-ZSM-5 zeolite as catalysts for non-oxidative conversion of natural gas to petrochemicals. *Journal of natural gas chemistry*, 18 (1): 71-77.

Aboul-Gheit, AK, Awadallah, AE, El-Kossy, SM and Mahmoud, A-LH. 2008. Effect of Pd or Ir on the catalytic performance of Mo/H-ZSM-5 during the non-oxidative conversion of natural gas to petrochemicals. *Journal of Natural Gas Chemistry*, 17 (4): 337-343.

Aiello, R, Fiscus, JE, Zur Loye, H-C and Amiridis, MD. 2000. Hydrogen production via the direct cracking of methane over Ni/SiO2: catalyst deactivation and regeneration. *Applied Catalysis A: General*, 192 (2): 227-234.

Al-Fatesh, AS, Fakeeha, AH, Khan, WU, Ibrahim, AA, He, S and Seshan, K. 2016. Production of hydrogen by catalytic methane decomposition over alumina supported mono-, bi- and tri-metallic catalysts. *International Journal of Hydrogen Energy*, 41 (48): 22932-22940.

Ali, MA, Tatsumi, T and Masuda, T. 2002. Development of heavy oil hydrocracking catalysts using amorphous silica-alumina and zeolites as catalyst supports. *Applied Catalysis A: General*, 233 (1): 77-90.

Alipour-Dehkordi, A and Khademi, MH. 2019. Use of a micro-porous membrane multi-tubular fixed-bed reactor for tri-reforming of methane to syngas: CO2, H2O or O2 side-feeding. *International Journal of Hydrogen Energy*, 44 (60): 32066-32079.

Amariglio, H, Pareja, P and Amariglio, A. 1995. Periodic operation of a catalyst as a means of overcoming a thermodynamic constraint. The case of methane homologation on metals. *Catalysis today*, 25 (2): 113-125.

Amin, N. 2005. Dual effects of supported W catalysts for dehydroaromatization of methane in the absence of oxygen. *Catalysis letters*, 102 (1-2): 69-78.

An, H, Cheng, Y, Li, T, Li, Y and Cheng, Y. 2018. Numerical analysis of methane pyrolysis in thermal plasma for selective synthesis of acetylene. *Fuel Processing Technology*, 172: 195-199.

Arena, F, Italiano, G, Barbera, K, Bonura, G, Spadaro, L and Frusteri, F. 2009. Basic evidences for methanol-synthesis catalyst design. *Catalysis Today*, 143 (1–2): 80-85.

Ashok, J, Raju, G, Reddy, PS, Subrahmanyam, M and Venugopal, A. 2008. Catalytic decomposition of CH4 over Ni-Al2O3-SiO2 catalysts: Influence of pre-treatment conditions for the production of H2. *Journal of Natural Gas Chemistry*, 17 (2): 113-119.

Baba, T and Miyaji, A. Catalysis and the Mechanism of Methane Conversion to Chemicals.

Baba, T and Miyaji, A. 2020. Conversion of Methane to Aromatic Hydrocarbons. In: *Catalysis and the Mechanism of Methane Conversion to Chemicals*. Springer, 127-163.

Bajec, D, Kostyniuk, A, Pohar, A and Likozar, B. 2019. Nonoxidative methane activation, coupling, and conversion to ethane, ethylene, and hydrogen over Fe/HZSM-5, Mo/HZSM-5, and Fe–Mo/HZSM-5 catalysts in packed bed reactor. *International Journal of Energy Research*, 43 (13): 6852-6868.

Baltrusaitis, J, De Graaf, C, Broer, R and Patterson, EV. 2013. H2S-Mediated Thermal and Photochemical Methane Activation. *ChemPhysChem*, 14 (17): 3960-3970.

Balzani, V and Armaroli, N. 2010. *Energy for a sustainable world: from the oil age to a sun-powered future*. John Wiley & Sons.

Biniak, S, Szymański, G, Siedlewski, J and Świątkowski, A. 1997. The characterization of activated carbons with oxygen and nitrogen surface groups. *Carbon*, 35 (12): 1799-1810.

Blasing, T and Smith, K. 2016. *Recent greenhouse gas concentrations*.

Borry, R, Lu, EC, Kim, Y-H and Iglesia, E. 1998. Non-oxidative catalytic conversion of methane with continuous hydrogen removal. *Stud. Surf. Sci. Catal*, 119: 403-410.

Borry, RW, Kim, YH, Huffsmith, A, Reimer, JA and Iglesia, E. 1999. Structure and density of Mo and acid sites in Mo-exchanged H-ZSM5 catalysts for nonoxidative methane conversion. *The Journal of Physical Chemistry B*, 103 (28): 5787-5796.

Brandt, AR, Masnadi, MS, Englander, JG, Koomey, J and Gordon, D. 2018. Climate-wise choices in a world of oil abundance. *Environmental Research Letters*, 13 (4): 044027.

Budde, PK, Singh, AK and Upadhyayula, S. 2018. Non-oxidative methane dehydroaromatization reaction over highly active $${\upalpha} $$-$$\hbox {MoC} _ {1 {-}}\mathrm {x}} $$ MoC1-x ZSM-5 derived from pre-treatment. *Journal of Chemical Sciences*, 130 (3): 27.

Budinova, T, Ekinci, E, Yardim, F, Grimm, A, Björnbom, E, Minkova, V and Goranova, M. 2006. Characterization and application of activated carbon produced by H3PO4 and water vapour activation. *Fuel processing technology*, 87 (10): 899-905.

Burns, S, Hargreaves, JSJ, Pal, P, Parida, KM and Parija, S. 2006. The effect of dopants on the activity of MoO3/ZSM-5 catalysts for the dehydroaromatisation of methane. *Catalysis Today*, 114 (4): 383-387.

Campbell, SM, Bibby, DM, Coddington, JM, Howe, RF and Meinhold, RH. 1996. Dealumination of HZSM-5 zeolites: I. Calcination and hydrothermal treatment. *Journal of Catalysis*, 161 (1): 338-349.

Cargnello, M, Jaén, JD, Garrido, JH, Bakhmutsky, K, Montini, T, Gámez, JC, Gorte, R and Fornasiero, P. 2012. Exceptional activity for methane combustion over modular Pd@ CeO2 subunits on functionalized Al2O3. *Science*, 337 (6095): 713-717.

Chen, J, Li, Y, Ma, Y, Qin, Y and Chang, L. 2001. Formation of bamboo-shaped carbon filaments and dependence of their morphology on catalyst composition and reaction conditions. *Carbon*, 39 (10): 1467-1475.

Chen, J, Ma, Q, Rufford, TE, Li, Y and Zhu, Z. 2009. Influence of calcination temperatures of Feitknecht compound precursor on the structure of Ni–Al2O3 catalyst and the corresponding

catalytic activity in methane decomposition to hydrogen and carbon nanofibers. *Applied Catalysis A: General*, 362 (1–2): 1-7.

Chen, L, Lin, L, Xu, Z, Li, X and Zhang, T. 1995. Dehydro-oligomerization of methane to ethylene and aromatics over molybdenum/HZSM-5 catalyst. *Journal of Catalysis*, 157 (1): 190-200.

Chen, L, Lin, L, Xu, Z, Zhang, T and Li, X. 1996. Promotional effect of Pt on non-oxidative methane transformation over Mo-HZSM-5 catalyst. *Catalysis letters*, 39 (3-4): 169-172.

Chen, P, Zhang, HB, Lin, GD, Hong, Q and Tsai, KR. 1997. Growth of carbon nanotubes by catalytic decomposition of CH4 or CO on a Ni-MgO catalyst. *Carbon*, 35 (10): 1495-1501.

Chen, X, Jeyaseelan, S and Graham, N. 2002. Physical and chemical properties study of the activated carbon made from sewage sludge. *Waste Management*, 22 (7): 755-760.

Chen, Y, Wang, X, Luo, X, Lin, X and Zhang, Y. 2018. Non-oxidative methane conversion using lead-and iron-modified albite catalysts in fixed-bed reactor. *Chinese Journal of Chemistry*, 36 (6): 531-537.

Chen, Z, Ma, L, Li, S, Geng, J, Song, Q, Liu, J, Wang, C, Wang, H, Li, J and Qin, Z. 2011. Simple approach to carboxyl-rich materials through low-temperature heat treatment of hydrothermal carbon in air. *Applied Surface Science*, 257 (20): 8686-8691.

Cheng, X, Yan, P, Zhang, X, Yang, F, Dai, C, Li, D and Ma, X-X. 2017. Enhanced methane dehydroaromatization in the presence of CO2 over Fe-and Mg-modified Mo/ZSM-5. *Molecular Catalysis*, 437: 114-120.

Chesnokov, VV and Chichkan, AS. 2009. Production of hydrogen by methane catalytic decomposition over Ni–Cu–Fe/Al2O3 catalyst. *International Journal of Hydrogen Energy*, 34 (7): 2979-2985.

Chianelli, RR and Torres, B. 2013. *Photochemical Processes and Compositions for Methane Reforming Using Transition Metal Chalcogenide Photocatalysts*: Google Patents.

Choudhary, TV, Aksoylu, E and Wayne Goodman, D. 2003. Nonoxidative activation of methane. *Catalysis reviews*, 45 (1): 151-203.

Choudhary, VR, Banerjee, S and Rajput, AM. 2001. Continuous Production of H2 at Low Temperature from Methane Decomposition over Ni-Containing Catalyst Followed by Gasification by Steam of the Carbon on the Catalyst in Two Parallel Reactors Operated in Cyclic Manner. *Journal of Catalysis*, 198 (1): 136-141.

Cicerone, RJ and Oremland, RS. 1988. Biogeochemical aspects of atmospheric methane. *Global biogeochemical cycles*, 2 (4): 299-327.

Colussi, S, Gayen, A, Farnesi Camellone, M, Boaro, M, Llorca, J, Fabris, S and Trovarelli, A. 2009. Nanofaceted Pd□ O Sites in Pd□ Ce Surface Superstructures: Enhanced Activity in Catalytic Combustion of Methane. *Angewandte Chemie International Edition*, 48 (45): 8481-8484.

Cook, B, Mousko, D, Hoelderich, W and Zennaro, R. 2009. Conversion of methane to aromatics over Mo2C/ZSM-5 catalyst in different reactor types. *Applied Catalysis A: General*, 365 (1): 34-41.

Cui, Y, Xu, Y, Suzuki, Y and Zhang, Z-G. 2011. Experimental evidence for three rate-controlling regions of the non-oxidative methane dehydroaromatization over Mo/HZSM-5 catalyst at 1073 K. *Catalysis Science & Technology*, 1 (5): 823-829.

Cunha, AF, Órfão, JJM and Figueiredo, JL. 2009. Methane decomposition on Ni–Cu alloyed Raney-type catalysts. *International Journal of Hydrogen Energy*, 34 (11): 4763-4772.

De Klerk, A. 2011. Sasol 2 and 3 facilities. *Fischer-Tropsch Refining; Wiley-VCH: Weinheim, Germany*: 181-212.

Degirmenci, V, Uner, D and Yilmaz, A. 2005. Methane to higher hydrocarbons via halogenation. *Catalysis today*, 106 (1-4): 252-255.

Denardin, F and Perez-Lopez, OW. 2019. Tuning the acidity and reducibility of Fe/ZSM-5 catalysts for methane dehydroaromatization. *Fuel*, 236: 1293-1300.

Ding, C, Ai, G, Zhang, K, Yuan, Q, Han, Y, Ma, X, Wang, J and Liu, S. 2015. Coking resistant Ni/ZrO2@SiO2 catalyst for the partial oxidation of methane to synthesis gas. *International Journal of Hydrogen Energy*, 40 (21): 6835-6843.

Ding, K, Derk, AR, Zhang, A, Hu, Z, Stoimenov, P, Stucky, GD, Metiu, H and Mcfarland, EW. 2012. Hydrodebromination and oligomerization of dibromomethane. *ACS Catalysis*, 2 (4): 479-486.

Ding, W, Li, S, D Meitzner, G and Iglesia, E. 2001. Methane conversion to aromatics on Mo/H-ZSM5: structure of molybdenum species in working catalysts. *The Journal of Physical Chemistry B*, 105 (2): 506-513.

Ding, W, Meitzner, GD and Iglesia, E. 2002. The effects of silanation of external acid sites on the structure and catalytic behaviour of Mo/H–ZSM5. *Journal of Catalysis*, 206 (1): 14-22.

Dixon, DA, Feller, D and Peterson, KA. 1997. Accurate calculations of the electron affinity and ionization potential of the methyl radical. *The Journal of Physical Chemistry A*, 101 (49): 9405-9409.

Djinović, P, Batista, J and Pintar, A. 2012. Efficient catalytic abatement of greenhouse gases: methane reforming with CO2 using a novel and thermally stable Rh–CeO2 catalyst. *international journal of hydrogen energy*, 37 (3): 2699-2707.

Du, G, Lim, S, Yang, Y, Wang, C, Pfefferle, L and Haller, GL. 2006. Catalytic performance of vanadium incorporated MCM-41 catalysts for the partial oxidation of methane to formaldehyde. *Applied Catalysis A: General*, 302 (1): 48-61.

Dufour, A, Celzard, A, Fierro, V, Martin, E, Broust, F and Zoulalian, A. 2008. Catalytic decomposition of methane over a wood char concurrently activated by a pyrolysis gas. *Applied Catalysis A: General*, 346 (1–2): 164-173.

Echegoyen, Y, Suelves, I, Lázaro, MJ, Sanjuán, ML and Moliner, R. 2007. Thermo catalytic decomposition of methane over Ni–Mg and Ni–Cu–Mg catalysts: Effect of catalyst preparation method. *Applied Catalysis A: General*, 333 (2): 229-237.

Elbadawi, AH, Ge, L, Zhang, J, Zhuang, L, Liu, S, Tan, X, Wang, S and Zhu, Z. 2020. Partial oxidation of methane to syngas in catalytic membrane reactor: Role of catalyst oxygen vacancies. *Chemical Engineering Journal*, 392: 123739.

Endo, M, Kim, C, Nishimura, K, Fujino, T and Miyashita, K. 2000. Recent development of carbon materials for Li ion batteries. *Carbon*, 38 (2): 183-197.

Enger, BC, Lødeng, R and Holmen, A. 2008. A review of catalytic partial oxidation of methane to synthesis gas with emphasis on reaction mechanisms over transition metal catalysts. *Applied Catalysis A: General*, 346 (1-2): 1-27.

Ermakova, MA and Ermakov, DY. 2002. Ni/SiO2 and Fe/SiO2 catalysts for production of hydrogen and filamentous carbon via methane decomposition. *Catalysis Today*, 77 (3): 225-235.

Ermakova, MA, Ermakov, DY and Kuvshinov, GG. 2000. Effective catalysts for direct cracking of methane to produce hydrogen and filamentous carbon: Part I. Nickel catalysts. *Applied Catalysis A: General*, 201 (1): 61-70.

Faramawy, S, Zaki, T and Sakr, AaE. 2016. Natural gas origin, composition, and processing: A review. *Journal of Natural Gas Science and Engineering*, 34: 34-54.

Farhadian Babadi, M, Mehrabi, B, Tassi, F, Cabassi, J, Pecchioni, E, Shakeri, A and Vaselli, O. 2020. Geochemistry of fluids discharged from mud volcanoes in SE Caspian Sea (Gorgan Plain, Iran). *International Geology Review*: 1-16.

Fila, V, Bernauer, M, Bernauer, B and Sobalik, Z. 2015. Effect of addition of a second metal in Mo/ZSM-5 catalyst for methane aromatization reaction under elevated pressures. *Catalysis Today*, 256: 269-275.

Fouty, NJ, Carrasco, JC and Lima, FV. 2017. Modeling and Design Optimization of Multifunctional Membrane Reactors for Direct Methane Aromatization. *Membranes*, 7 (3): 48.

Fujikawa, T, Idei, K, Ebihara, T, Mizuguchi, H and Usui, K. 2000. Aromatic hydrogenation of distillates over SiO2-Al2O3-supported noble metal catalysts. *Applied Catalysis A: General*, 192 (2): 253-261.

Gao, J, Zheng, Y, Jehng, J-M, Tang, Y, Wachs, IE and Podkolzin, SG. 2015. Identification of molybdenum oxide nanostructures on zeolites for natural gas conversion. *Science*, 348 (6235): 686-690.

García-Sancho, C, Guil-López, R, Sebastián-López, A, Navarro, R and Fierro, J. 2018. Hydrogen production by methane decomposition: A comparative study of supported and bulk ex-hydrotalcite mixed oxide catalysts with Ni, Mg and Al. *International Journal of Hydrogen Energy*, 43 (20): 9607-9621.

Gatica, JM, Gómez, DM, Harti, S and Vidal, H. 2013. Monolithic honeycomb design applied to carbon materials for catalytic methane decomposition. *Applied Catalysis A: General*, 458: 21-27.

Gerçel, Ö, Özcan, A, Özcan, AS and Gercel, HF. 2007. Preparation of activated carbon from a renewable bio-plant of Euphorbia rigida by H2SO4 activation and its adsorption behaviour in aqueous solutions. *Applied surface science*, 253 (11): 4843-4852.

Gimeno, MaP, Soler, J, Herguido, J and Menéndez, M. 2010. Counteracting catalyst deactivation in methane aromatization with a two zone fluidized bed reactor. *Industrial & engineering chemistry research*, 49 (3): 996-1000.

Goodman, B, Hass, K, Schneider, W and Adams, J. 2000. Statistical analysis of Al distributions and metal ion pairing probabilities in zeolites. *Catalysis letters*, 68 (1-2): 85-93.

Gorte, RJ and Vohs, JM. 2003. Novel SOFC anodes for the direct electrochemical oxidation of hydrocarbons. *Journal of catalysis*, 216 (1-2): 477-486.

Guéret, C, Daroux, M and Billaud, F. 1997. Methane pyrolysis: thermodynamics. *Chemical Engineering Science*, 52 (5): 815-827.

Guevara, JC, Wang, JA, Chen, LF, Valenzuela, MA, Salas, P, García-Ruiz, A, Toledo, JA, Cortes-Jácome, MA, Angeles-Chavez, C and Novaro, O. 2010. Ni/Ce-MCM-41 mesostructured catalysts for simultaneous production of hydrogen and nanocarbon via methane decomposition. *International Journal of Hydrogen Energy*, 35 (8): 3509-3521.

Guil-Lopez, R, Botas, JA, Fierro, JLG and Serrano, DP. 2011. Comparison of metal and carbon catalysts for hydrogen production by methane decomposition. *Applied Catalysis A: General*, 396 (1–2): 40-51.

Guisnet, M and Magnoux, P. 2001. Organic chemistry of coke formation. *Applied Catalysis A: General*, 212 (1-2): 83-96.

Guo, Y and Rockstraw, DA. 2007. Physicochemical properties of carbons prepared from pecan shell by phosphoric acid activation. *Bioresource Technology*, 98 (8): 1513-1521.

Han, SJ, Kim, SK, Hwang, A, Kim, S, Hong, D-Y, Kwak, G, Jun, K-W and Kim, YT. 2019. Non-oxidative dehydroaromatization of methane over Mo/H-ZSM-5 catalysts: A detailed analysis of the reaction-regeneration cycle. *Applied Catalysis B: Environmental*, 241: 305-318.

Hayashi, JI, Kazehaya, A, Muroyama, K and Watkinson, AP. 2000. Preparation of activated carbon from lignin by chemical activation. *Carbon*, 38 (13): 1873-1878.

He, J, Xu, T, Wang, Z, Zhang, Q, Deng, W and Wang, Y. 2012. Transformation of Methane to Propylene: A Two-Step Reaction Route Catalyzed by Modified CeO2 Nanocrystals and Zeolites. *Angewandte Chemie International Edition*, 51 (10): 2438-2442.

Herguido, J and Menéndez, M. 2017. Advances and trends in two-zone fluidized-bed reactors. *Current Opinion in Chemical Engineering*, 17: 15-21.

Holmen, A. 2009. Direct conversion of methane to fuels and chemicals. *Catalysis Today*, 142 (1-2): 2-8.

Holmen, A, Olsvik, O and Rokstad, O. 1995. Pyrolysis of natural gas: chemistry and process concepts. *Fuel Processing Technology*, 42 (2-3): 249-267.

Horn, R, Ihmann, K, Ihmann, J, Jentoft, FC, Geske, M, Taha, A, Pelzer, K and Schlögl, R. 2006. Molecular beam mass spectrometer equipped with a catalytic wall reactor for in situ studies in high temperature catalysis research. *Review of scientific instruments*, 77 (5): 054102.

Hornés, A, Bera, P, Fernández-García, M, Guerrero-Ruiz, A and Martínez-Arias, A. 2012. Catalytic and redox properties of bimetallic Cu–Ni systems combined with CeO2 or Gd-doped CeO2 for methane oxidation and decomposition. *Applied Catalysis B: Environmental*, 111–112: 96-105.

Huang, B and Ma, C. 2019. The Modulus-Based Levenberg-Marquardt Method for Solving Linear Complementarity Problem. *Numerical Mathematics: Theory, Methods & Applications*, 12 (1)

Ismagilov, ZR, Matus, EV and Tsikoza, LT. 2008. Direct conversion of methane on Mo/ZSM-5 catalysts to produce benzene and hydrogen: achievements and perspectives. *Energy & Environmental Science*, 1 (5): 526-541.

Ji, Y, Li, T and Zhu, L. 2007. xiaoxian Wang, Qilang Liu. *Applied Surface Science*, 254: 506.

Jiang, R, Zhu, H-Y, Chen, H-H, Yao, J, Fu, Y-Q, Zhang, Z-Y and Xu, Y-M. 2014. Effect of calcination temperature on physical parameters and photocatalytic activity of mesoporous titania spheres using chitosan/poly (vinyl alcohol) hydrogel beads as a template. *Applied surface science*, 319: 189-196.

Karakaya, C and Kee, RJ. 2016. Progress in the direct catalytic conversion of methane to fuels and chemicals. *Progress in Energy and Combustion Science*, 55: 60-97.

Karakaya, C, Zhu, H, Loebick, C, Weissman, JG and Kee, RJ. 2018. A detailed reaction mechanism for oxidative coupling of methane over Mn/Na2WO4/SiO2 catalyst for non-isothermal conditions. *Catalysis Today*,

Keipi, T, Tolvanen, KES, Tolvanen, H and Konttinen, J. 2016. Thermo-catalytic decomposition of methane: The effect of reaction parameters on process design and the utilization possibilities of the produced carbon. *Energy Conversion and Management*, 126: 923-934.

Khan, TS, Balyan, S, Mishra, S, Pant, KK and Haider, MA. 2018. Mechanistic Insights into the Activity of Mo-Carbide Clusters for Methane Dehydrogenation and Carbon-Carbon Coupling Reactions to Form Ethylene in Methane Dehydroaromatization. *The Journal of Physical Chemistry C*,

Kim, MH, Lee, EK, Jun, JH, Kong, SJ, Han, GY, Lee, BK, Lee, T-J and Yoon, KJ. 2004. Hydrogen production by catalytic decomposition of methane over activated carbons: kinetic study. *International Journal of Hydrogen Energy*, 29 (2): 187-193.

Kinage, AK, Ohnishi, R and Ichikawa, M. 2003. Marked enhancement of the methane dehydrocondensation toward benzene using effective Pd catalytic membrane reactor with Mo/ZSM-5. *Catalysis letters*, 88 (3-4): 199-202.

Kirschke, S, Bousquet, P, Ciais, P, Saunois, M, Canadell, JG, Dlugokencky, EJ, Bergamaschi, P, Bergmann, D, Blake, DR and Bruhwiler, L. 2013. Three decades of global methane sources and sinks. *Nature geoscience*, 6 (10): 813-823.

Knittel, K and Boetius, A. 2009. Anaerobic oxidation of methane: progress with an unknown process. *Annual review of microbiology*, 63: 311-334.

Kobayashi, T, Guilhaume, N, Miki, J, Kitamura, N and Haruta, M. 1996. Oxidation of methane to formaldehyde over FeSiO2 and Sn□ W mixed oxides. *Catalysis Today*, 32 (1-4): 171-175.

Kohno, Y, Tanaka, T, Funabiki, T and Yoshida, S. 2000. Reaction mechanism in the photoreduction of CO 2 with CH 4 over ZrO 2. *Physical Chemistry Chemical Physics*, 2 (22): 5302-5307.

Komornicki, A and Dixon, DA. 1992. Accurate proton affinities: ab initio proton binding energies for N2, CO, CO2, and CH4. *The Journal of chemical physics*, 97 (2): 1087-1094.

Kosinov, N, Coumans, FJ, Li, G, Uslamin, E, Mezari, B, Wijpkema, AS, Pidko, EA and Hensen, EJ. 2017. Stable Mo/HZSM-5 methane dehydroaromatization catalysts optimized for high-temperature calcination-regeneration. *Journal of Catalysis*, 346: 125-133.

Kruk, M, Dufour, B, Celer, EB, Kowalewski, T, Jaroniec, M and Matyjaszewski, K. 2005. Synthesis of mesoporous carbons using ordered and disordered mesoporous silica templates and polyacrylonitrile as carbon precursor. *The Journal of Physical Chemistry B*, 109 (19): 9216-9225.

Kuras, M, Zimmermann, Y and Petit, C. 2008. Reactivity of perovskite-type precursor in MWCNTs synthesis. *Catalysis Today*, 138 (1–2): 55-61.

Lee, EK, Lee, SY, Han, GY, Lee, BK, Lee, T-J, Jun, JH and Yoon, KJ. 2004. Catalytic decomposition of methane over carbon blacks for CO2-free hydrogen production. *Carbon*, 42 (12–13): 2641-2648.

Lee, K-Y, Kang, M-Y and Ihm, S-K. 2012. Deactivation by coke deposition on the HZSM-5 catalysts in the methanol-to-hydrocarbon conversion. *Journal of Physics and Chemistry of Solids*, 73 (12): 1542-1545.

Lezcano-González, I, Oord, R, Rovezzi, M, Glatzel, P, Botchway, SW, Weckhuysen, BM and Beale, AM. 2016a. Molybdenum speciation and its impact on catalytic activity during methane dehydroaromatization in zeolite ZSM-5 as revealed by operando X-ray methods. *Angewandte Chemie International Edition*, 55 (17): 5215-5219.

Lezcano-González, I, Oord, R, Rovezzi, M, Glatzel, P, Botchway, SW, Weckhuysen, BM and Beale, AM. 2016b. Molybdenum speciation and its impact on catalytic activity during methane dehydroaromatization in zeolite ZSM-5 as revealed by operando X-ray methods. *Angewandte Chemie*, 128 (17): 5301-5305.

Li, F and Yuan, G. 2006. Hydrated Dibromodioxomolybdenum (VI) Supported on Zn-MCM-48 for Facile Oxidation of Methane. *Angewandte Chemie International Edition*, 45 (39): 6541-6544.

Li, J, Dong, L, Xiong, L, Yang, Y, Du, Y, Zhao, L, Wang, H and Peng, S. 2016. High-loaded NiCuSiO2 catalysts for methane decomposition to prepare hydrogen and carbon filaments. *International Journal of Hydrogen Energy*, 41 (28): 12038-12048.

Li, Q, Zhang, F, Jarvis, J, He, P, Yung, MM, Wang, A, Zhao, K and Song, H. 2018. Investigation on the light alkanes aromatization over Zn and Ga modified HZSM-5 catalysts in the presence of methane. *Fuel*, 219 (NREL/JA-5100-71180)

Li, W, Meitzner, GD, Borry Iii, RW and Iglesia, E. 2000. Raman and X-ray absorption studies of Mo species in Mo/H-ZSM5 catalysts for non-oxidative CH4 reactions. *Journal of Catalysis*, 191 (2): 373-383.

Li, Y, Chen, J and Chang, L. 1997. Catalytic growth of carbon fibres from methane on a nickel-alumina composite catalyst prepared from Feitknecht compound precursor. *Applied Catalysis A: General*, 163 (1): 45-57.

Li, Y, Wu, T, Shen, W, Bao, X and Xu, Y. 2005. Combined single-pass conversion of methane via oxidative coupling and dehydro-aromatization. *Catalysis letters*, 105 (1-2): 77-82.

Li, Y, Zhang, B, Tang, X, Xu, Y and Shen, W. 2006. Hydrogen production from methane decomposition over Ni/CeO2 catalysts. *Catalysis Communications*, 7 (6): 380-386.

Lillo-Ródenas, MA and Lozano-Castello, D. 2003. D. Cazorla-Amoro s, A. Linares-Solano. *Carbon*, 41: 267.

Lin, R, Ding, Y, Gong, L, Dong, W, Wang, J and Zhang, T. 2010. Efficient and stable silica-supported iron phosphate catalysts for oxidative bromination of methane. *Journal of Catalysis*, 272 (1): 65-73.

Lin, R, Ding, Y, Gong, L, Li, J, Chen, W, Yan, L and Lu, Y. 2009. Oxidative bromination of methane on silica-supported non-noble metal oxide catalysts. *Applied Catalysis A: General*, 353 (1): 87-92.

Liu, C-J, Yu, K, Zhang, Y-P, Zhu, X, He, F and Eliasson, B. 2004. Characterization of plasma treated Pd/HZSM-5 catalyst for methane combustion. *Applied Catalysis B: Environmental*, 47 (2): 95-100.

Liu, H, Bao, X and Xu, Y. 2006. Methane dehydroaromatization under nonoxidative conditions over Mo/HZSM-5 catalysts: Identification and preparation of the Mo active species. *Journal of Catalysis*, 239 (2): 441-450.

Liu, H, Shen, W, Bao, X and Xu, Y. 2005. Methane dehydroaromatization over Mo/HZSM-5 catalysts: the reactivity of MoCx species formed from MoOx associated and non-associated with Brönsted acid sites. *Applied Catalysis A: General*, 295 (1): 79-88.

Liu, H, Wu, S, Guo, Y, Shang, F, Yu, X, Ma, Y, Xu, C, Guan, J and Kan, Q. 2011. Synthesis of Mo/IM-5 catalyst and its catalytic behaviour in methane non-oxidative aromatization. *Fuel*, 90 (4): 1515-1521.

Liu, H, Yao, L, Hadj Taief, HB, Benzina, M, Da Costa, P and Gálvez, ME. Natural clay-based Ni-catalysts for dry reforming of methane at moderate temperatures. *Catalysis Today*,

Liu, S, Wang, L, Ohnishi, R and Ichikawa, M. 1999. Bifunctional catalysis of Mo/HZSM-5 in the dehydroaromatization of methane to benzene and naphthalene XAFS/TG/DTA/MASS/FTIR characterization and supporting effects. *Journal of Catalysis*, 181 (2): 175-188.

Liu, S, Wang, L, Ohnishi, R and Lchikawa, M. 2000. Bifunctional catalysis of Mo/HZSM-5 in the dehydroaromatization of methane with CO/CO 2 to benzene and naphthalene. *Kinetics and catalysis*, 41 (1): 132-144.

Liu, W, Xu, Y, Wong, S-T, Wang, L, Qiu, J and Yang, N. 1997. Methane dehydrogenation and aromatization in the absence of oxygen on MoHZSM-5: A study on the interaction between Mo species and HZSM-5 by using 27Al and 29Si MAS NMR. *Journal of Molecular Catalysis A: Chemical*, 120 (1-3): 257-265.

Liu, Z, Li, L and Iglesia, E. 2002. Catalytic pyrolysis of methane on Mo/H-ZSM5 with continuous hydrogen removal by permeation through dense oxide films. *Catalysis letters*, 82 (3-4): 175-180.

Liu, Z, Li, W and Zhou, X. 2010. Product oriented oxidative bromination of methane over Rh/SiO2 catalysts. *Journal of natural gas chemistry*, 19 (5): 522-529.

Lodeng, R, Lindvaag, OA, Soraker, P, Roterud, PT and Onsager, OT. 1995. Experimental and modeling study of the selective homogeneous gas phase oxidation of methane to methanol. *Industrial & engineering chemistry research*, 34 (4): 1044-1059.

Lohrberg, A, Schmale, O, Ostrovsky, I, Niemann, H, Held, P and Von Deimling, JS. 2020. Discovery and quantification of a widespread methane ebullition event in a coastal inlet (Baltic Sea) using a novel sonar strategy. *Scientific reports*, 10 (1): 1-13.

Lü, R and Lin, J. 2014. A interpretation of stepwise bond dissociation energies of CH4. *Computational and Theoretical Chemistry*, 1037: 10-13.

Lu, R, Tangbo, H, Wang, Q and Xiang, S. 2003. Properties and characterization of modified HZSM-5 zeolites. *Journal of Natural Gas Chemistry*, 12 (1): 56-62.

Luo, Y. 2007. Comprehensive Handbook of Chemical Bond Energies. CRC Press, Boca Raton, London.

Ma, D, Lu, Y, Su, L, Xu, Z, Tian, Z, Xu, Y, Lin, L and Bao, X. 2002. Remarkable improvement on the methane aromatization reaction: a highly selective and coking-resistant catalyst. *The Journal of Physical Chemistry B*, 106 (34): 8524-8530.

Ma, D, Shu, Y, Bao, X and Xu, Y. 2000a. Methane dehydro-aromatization under nonoxidative conditions over Mo/HZSM-5 catalysts: EPR study of the Mo species on/in the HZSM-5 zeolite. *Journal of Catalysis*, 189 (2): 314-325.

Ma, D, Zhang, W, Shu, Y, Liu, X, Xu, Y and Bao, X. 2000b. MAS NMR, ESR and TPD studies of Mo/HZSM-5 catalysts: evidence for the migration of molybdenum species into the zeolite channels. *Catalysis letters*, 66 (3): 155-160.

Ma, H, Ohnishi, R and Ichikawa, M. 2003. Highly Stable Performance of Methane Dehydroaromatization on Mo/HZSM-5 Catalyst with a Small Amount of H 2 Addition into Methane Feed. *Catalysis letters*, 89 (1-2): 143-146.

Ma, S, Guo, X, Zhao, L, Scott, S and Bao, X. 2013. Recent progress in methane dehydroaromatization: From laboratory curiosities to promising technology. *Journal of Energy Chemistry*, 22 (1): 1-20.

Macias-Garcia, A, Diaz-Diez, M, Cuerda-Correa, E, Olivares-Marin, M and Gañan-Gómez, J. 2006. Study of the pore size distribution and fractal dimension of HNO3-treated activated carbons. *Applied surface science*, 252 (17): 5972-5975.

Mahmodi, G, Sharifnia, S, Rahimpour, F and Hosseini, S. 2013. Photocatalytic conversion of CO2 and CH4 using ZnO coated mesh: effect of operational parameters and optimization. *Solar energy materials and solar cells*, 111: 31-40.

Majhi, S, Mohanty, P, Wang, H and Pant, K. 2013a. Direct conversion of natural gas to higher hydrocarbons: A review. *Journal of Energy Chemistry*, 22 (4): 543-554.

Majhi, S, Mohanty, P, Wang, H and Pant, KK. 2013b. Direct conversion of natural gas to higher hydrocarbons: A review. *Journal of Energy Chemistry*, 22 (4): 543-554.

Majocchi, L, Groppi, G, Cristiani, C, Forzatti, P, Basini, L and Guarinoni, A. 2000. Partial oxidation of methane to synthesis gas over Rh-hexaaluminate-based catalysts. *Catalysis letters*, 65 (1-3): 49-56.

Malaika, A and Kozłowski, M. 2009. Influence of ethylene on carbon-catalysed decomposition of methane. *International Journal of Hydrogen Energy*, 34 (6): 2600-2605.

Mann, R. 1997. Catalyst deactivation by coke deposition: Approaches based on interactions of coke laydown with pore structure. *Catalysis today*, 37 (3): 331-349.

Mathur, R, Chatterjee, S and Singh, B. 2008. Growth of carbon nanotubes on carbon fibre substrates to produce hybrid/phenolic composites with improved mechanical properties. *Composites Science and Technology*, 68 (7-8): 1608-1615.

Meriaudeau, P and Ha, VTT. 2000. Methane aromatization over Mo/H-ZSM-5: on the reaction pathway. *Catalysis letters*, 64 (1): 49-51.

Mestl, G and Knözinger, H. 2008. Vibrational spectroscopy. *Handbook of Heterogeneous Catalysis: Online*: 932-971.

Michalkiewicz, B. 2004. Partial oxidation of methane to formaldehyde and methanol using molecular oxygen over Fe-ZSM-5. *Applied Catalysis A: General*, 277 (1-2): 147-153.

Mohn, K. 2020. The gravity of status quo: A review of IEA's World Energy Outlook. *Economics of Energy & Environmental Policy*, 9 (1)

Mokrani, T and Scurrell, M. 2009. Gas conversion to liquid fuels and chemicals: the methanol route-catalysis and processes development. *Catalysis Reviews*, 51 (1): 1-145.

Moliner, R, Suelves, I, Lázaro, MJ and Moreno, O. 2005. Thermocatalytic decomposition of methane over activated carbons: influence of textural properties and surface chemistry. *International Journal of Hydrogen Energy*, 30 (3): 293-300.

Muradov, N. 2001a. Catalysis of methane decomposition over elemental carbon. *Catalysis Communications*, 2 (3–4): 89-94.

Muradov, N. 2001b. Hydrogen via methane decomposition: an application for decarbonization of fossil fuels. *International Journal of Hydrogen Energy*, 26 (11): 1165-1175.

Myllykangas, J-P, Hietanen, S and Jilbert, T. 2020. Legacy effects of eutrophication on modern methane dynamics in a boreal estuary. *Estuaries and Coasts*, 43 (2): 189-206.

Nations, U. 2019. World population prospects 2019.

Nayak, A, Bhushan, B, Gupta, V and Sharma, P. 2017. Chemically activated carbon from lignocellulosic wastes for heavy metal wastewater remediation: Effect of activation conditions. *Journal of Colloid and Interface Science*, 493: 228-240.

Ni, L, Kuroda, K, Zhou, L-P, Kizuka, T, Ohta, K, Matsuishi, K and Nakamura, J. 2006. Kinetic study of carbon nanotube synthesis over Mo/Co/MgO catalysts. *Carbon*, 44 (11): 2265-2272.

Nikolla, E, Schwank, J and Linic, S. 2009. Direct electrochemical oxidation of hydrocarbon fuels on SOFCs: improved carbon tolerance of Ni alloy anodes. *Journal of the Electrochemical Society*, 156 (11): B1312-B1316.

Ogihara, H, Tajima, H and Kurokawa, H. 2020. Pyrolysis of mixtures of methane and ethane: activation of methane with the aid of radicals generated from ethane. *Reaction Chemistry & Engineering*, 5 (1): 145-153.

Ogura, K and Kataoka, M. 1988. Photochemical conversion of methane. *Journal of molecular catalysis*, 43 (3): 371-379.

Ohnishi, R, Liu, S, Dong, Q, Wang, L and Ichikawa, M. 1999. Catalytic dehydrocondensation of methane with CO and CO2toward benzene and naphthalene on Mo/HZSM-5 and Fe/Co-modified Mo/HZSM-5. *Journal of Catalysis*, 182 (1): 92-103.

Okada, K, Yamamoto, N, Kameshima, Y and Yasumori, A. 2003. Porous properties of activated carbons from waste newspaper prepared by chemical and physical activation. *Journal of Colloid and Interface Science*, 262 (1): 179-193.

Okolie, C, Lyu, Y, Kovarik, L, Stavitski, E and Sievers, C. 2018. Coupling of Methane to Ethane, Ethylene, and Aromatics over Nickel on Ceria–Zirconia at Low Temperatures. *ChemCatChem*,

Olah, GA. 1987. Electrophilic methane conversion. *Accounts of chemical research*, 20 (11): 422-428.

Olah, GA, Goeppert, A and Prakash, GS. 2018. *Beyond oil and gas: the methanol economy*. John Wiley & Sons.

Paganini, MC, Chiesa, M, Martino, P, Giamello, E and Garrone, E. 2003. EPR study of the surface basicity of calcium oxide. 2: The interaction with alkanes. *The Journal of Physical Chemistry B*, 107 (11): 2575-2580.

Pakhomov, N and Buyanov, R. 2005. Current trends in the improvement and development of catalyst preparation methods. *Kinetics and catalysis*, 46 (5): 669-683.

Peringer, E, Salzinger, M, Hutt, M, Lemonidou, AA and Lercher, JA. 2009. Modified lanthanum catalysts for oxidative chlorination of methane. *Topics in Catalysis*, 52 (9): 1220.

Perrich, JR. 2018. *Activated carbon adsorption for wastewater treatment*. CRC press.

Petroleum, B. 2019. BP Statistical Review of World Energy Report. *BP: London, UK*,

Piao, L, Li, Y, Chen, J, Chang, L and Lin, JYS. 2002. Methane decomposition to carbon nanotubes and hydrogen on an alumina supported nickel aerogel catalyst. *Catalysis Today*, 74 (1–2): 145-155.

Pierella, LB, Wang, L and Anunziata, OA. 1997. Methane direct conversion to aromatic hydrocarbons at low reaction temperature. *Reaction Kinetics and Catalysis Letters*, 60 (1): 101-106.

Pillai, MR, Kim, I, Bierschenk, DM and Barnett, SA. 2008. Fuel-flexible operation of a solid oxide fuel cell with Sr0. 8La0. 2TiO3 support. *Journal of Power Sources*, 185 (2): 1086-1093.

Podkolzin, SG, Stangland, EE, Jones, ME, Peringer, E and Lercher, JA. 2007. Methyl chloride production from methane over lanthanum-based catalysts. *Journal of the American Chemical Society*, 129 (9): 2569-2576.

Pompeo, F, Nichio, NN, Souza, MM, Cesar, DV, Ferretti, OA and Schmal, M. 2007. Study of Ni and Pt catalysts supported on α-Al2O3 and ZrO2 applied in methane reforming with CO2. *Applied Catalysis A: General*, 316 (2): 175-183.

Pudukudy, M and Yaakob, Z. 2015. Methane decomposition over Ni, Co and Fe based monometallic catalysts supported on sol gel derived SiO2 microflakes. *Chemical Engineering Journal*, 262: 1009-1021.

Puziy, A, Poddubnaya, O, Martınez-Alonso, A, Suárez-Garcıa, F and Tascón, J. 2003. Synthetic carbons activated with phosphoric acid III. Carbons prepared in air. *Carbon*, 41 (6): 1181-1191.

Puziy, AM, Poddubnaya, OI, Martínez-Alonso, A, Suárez-García, F and Tascón, JM. 2005. Surface chemistry of phosphorus-containing carbons of lignocellulosic origin. *Carbon*, 43 (14): 2857-2868.

Qi, S and Yang, B. 2004. Methane aromatization using Mo-based catalysts prepared by microwave heating. *Catalysis today*, 98 (4): 639-645.

Qian, W, Liu, T, Wei, F, Wang, Z, Wang, D and Li, Y. 2003. Carbon nanotubes with large cores produced by adding sodium carbonate to the catalyst. *Carbon*, 41 (13): 2683-2686.

Qiu, P, Lunsford, JH and Rosynek, M. 1997. Steady-state conversion of methane to aromatics in high yields using an integrated recycle reaction system. *Catalysis letters*, 48 (1-2): 11-15.

Rice, MJ, Chakraborty, AK and Bell, AT. 1999. Al next nearest neighbor, ring occupation, and proximity statistics in ZSM-5. *Journal of Catalysis*, 186 (1): 222-227.

Rostrup-Nielsen, J and Christiansen, L. 1995. Internal steam reforming in fuel cells and alkali poisoning. *Applied Catalysis A: General*, 126 (2): 381-390.

Rostrup-Nielsen, JR. 1984. Catalytic steam reforming. In: *Catalysis*. Springer, 1-117.

Rostrup-Nielsen, JR, Sehested, J and Nørskov, JK. 2002. Hydrogen and synthesis gas by steam- and C02 reforming.

Sahoo, SK, Rao, P, Rajeshwer, D, Krishnamurthy, KR and Singh, ID. 2003. Structural characterization of coke deposits on industrial spent paraffin dehydrogenation catalysts. *Applied Catalysis A: General*, 244 (2): 311-321.

Saraswat, SK and Pant, KK. 2013. Synthesis of hydrogen and carbon nanotubes over copper promoted Ni/SiO2 catalyst by thermocatalytic decomposition of methane. *Journal of Natural Gas Science and Engineering*, 13: 52-59.

Sastre, F, Fornés, V, Corma, A and García, H. 2011. Selective, room-temperature transformation of methane to C1 oxygenates by deep UV photolysis over zeolites. *Journal of the American Chemical Society*, 133 (43): 17257-17261.

Schreiner, PR. 2000. Does CH5+ Have (a)"Structure?" A Tough Test for Experiment and Theory. *Angewandte Chemie International Edition*, 39 (18): 3239-3241.

Schwach, P, Pan, X and Bao, X. 2017. Direct conversion of methane to value-added chemicals over heterogeneous catalysts: challenges and prospects. *Chemical reviews*, 117 (13): 8497-8520.

Schwarz, JA, Contescu, C and Contescu, A. 1995. Methods for preparation of catalytic materials. *Chemical Reviews*, 95 (3): 477-510.

Sethia, G and Sayari, A. 2016. Activated carbon with optimum pore size distribution for hydrogen storage. *Carbon*, 99: 289-294.

Shi, D, Feng, Y and Zhong, S. 2004. Photocatalytic conversion of CH4 and CO2 to oxygenated compounds over Cu/CdS–TiO2/SiO2 catalyst. *Catalysis Today*, 98 (4): 505-509.

Shu, Y and Ichikawa, M. 2001a. Catalytic dehydrocondensation of methane towards benzene and naphthalene on transition metal supported zeolite catalysts: templating role of zeolite micro pores and characterization of active metallic sites. *Catalysis today*, 71 (1-2): 55-67.

Shu, Y and Ichikawa, M. 2001b. Catalytic dehydrocondensation of methane towards benzene and naphthalene on transition metal supported zeolite catalysts: templating role of zeolite micro pores and characterization of active metallic sites. *Catalysis Today*, 71 (1): 55-67.

Shu, Y, Ma, D, Bao, X and Xu, Y. 2000a. Methane dehydro-aromatization over a Mo/phosphoric rare earth-containing penta-sil type zeolite in the absence of oxygen. *Catalysis letters*, 66 (3): 161-167.

Shu, Y, Ma, D, Xu, L, Xu, Y and Bao, X. 2000b. Methane dehydro-aromatization over Mo/MCM-22 catalysts: a highly selective catalyst for the formation of benzene. *Catalysis Letters*, 70 (1-2): 67-73.

Shu, Y, Ohnishi, R and Ichikawa, M. 2002. Pressurized dehydrocondensation of methane toward benzene and naphthalene on Mo/HZSM-5 catalyst: optimization of reaction parameters and promotion by CO2 addition. *Journal of Catalysis*, 206 (1): 134-142.

Shu, Y, Xu, Y, Wong, S-T, Wang, L and Guo, X. 1997. Promotional effect of Ru on the dehydrogenation and aromatization of methane in the absence of oxygen over Mo/HZSM-5 catalysts. *Journal of Catalysis*, 170 (1): 11-19.

Shukla, PR, Wang, S, Sun, H, Ang, HM and Tadé, M. 2010. Activated carbon supported cobalt catalysts for advanced oxidation of organic contaminants in aqueous solution. *Applied Catalysis B: Environmental*, 100 (3): 529-534.

Sily, PD, Noronha, FB and Passos, FB. 2006. Methane direct conversion on Mo/ZSM-5 catalysts modified by Pd and Ru. *Journal of Natural Gas Chemistry*, 15 (2): 82-86.

Sim, JP, Lee, BJ, Han, G-H, Kim, DH and Lee, K-Y. 2020. Promotional effect of Au on Fe/HZSM-5 catalyst for methane dehydroaromatization. *Fuel*, 274: 117852.

Skutil, K and Taniewski, M. 2006. Some technological aspects of methane aromatization (direct and via oxidative coupling). *Fuel processing technology*, 87 (6): 511-521.

Soleimani, M and Kaghazchi, T. 2008. Adsorption of gold ions from industrial wastewater using activated carbon derived from hard shell of apricot stones–An agricultural waste. *Bioresource Technology*, 99 (13): 5374-5383.

Solymosi, F, Bugyi, L, Oszko, A and Horvath, I. 1999. Generation and reactions of CH2 and C2H5 species on Mo2C/Mo (111) surface. *Journal of Catalysis*, 185 (1): 160-169.

Solymosi, F, Cserényi, J, Szőke, A, Bánsági, T and Oszkó, AZ. 1997. Aromatization of methane over supported and unsupported Mo-based catalysts. *Journal of Catalysis*, 165 (2): 150-161.

Solymosi, F, Szöke, A and Cserenyi, J. 1996. Conversion of methane to benzene over Mo 2 C and Mo 2 C/ZSM-5 catalysts. *Catalysis letters*, 39 (3-4): 157-161.

Souza, MM, Aranda, DA and Schmal, M. 2001. Reforming of methane with carbon dioxide over Pt/ZrO2/Al2O3 catalysts. *Journal of Catalysis*, 204 (2): 498-511.

Souza, MM and Schmal, M. 2003. Combination of carbon dioxide reforming and partial oxidation of methane over supported platinum catalysts. *Applied Catalysis A: General*, 255 (1): 83-92.

Souza, MM and Schmal, M. 2004. Production of synthesis gas from natural gas using ZrO2-supported platinum. In: *Studies in surface science and catalysis*. Elsevier, 133-138.

Suelves, I, Lázaro, MJ, Moliner, R, Echegoyen, Y and Palacios, JM. 2006. Characterization of NiAl and NiCuAl catalysts prepared by different methods for hydrogen production by thermo catalytic decomposition of methane. *Catalysis Today*, 116 (3): 271-280.

Suelves, I, Lázaro, MJ, Moliner, R, Pinilla, JL and Cubero, H. 2007. Hydrogen production by methane decarbonization: Carbonaceous catalysts. *International Journal of Hydrogen Energy*, 32 (15): 3320-3326.

Sun, C, Yao, S, Shen, W and Lin, L. 2009. Hydrothermal post-synthesis of HMCM-49 to enhance the catalytic performance of the Mo/HMCM-49 catalyst for methane dehydroaromatization. *Microporous and mesoporous materials*, 122 (1-3): 48-54.

Sun, Z-F, Jia, S, Yuan, Q, Sun, C-Y and Chen, G-J. 2020. One-dimensional study on gas production characteristics of methane hydrate in clayey sediments using depressurization method. *Fuel*, 262: 116561.

Szöke, A and Solymosi, F. 1996. Selective oxidation of methane to benzene over K2MoO4/ZSM-5 catalysts. *Applied Catalysis A: General*, 142 (2): 361-374.

Takeguchi, T, Kani, Y, Yano, T, Kikuchi, R, Eguchi, K, Tsujimoto, K, Uchida, Y, Ueno, A, Omoshiki, K and Aizawa, M. 2002. Study on steam reforming of CH4 and C2 hydrocarbons and carbon deposition on Ni-YSZ cermets. *Journal of Power Sources*, 112 (2): 588-595.

Talebizadeh, A, Mortazavi, Y and Khodadadi, A. 2009. Comparative study of the two-zone fluidized-bed reactor and the fluidized-bed reactor for oxidative coupling of methane over Mn/Na2WO4/SiO2 catalyst. *Fuel Processing Technology*, 90 (10): 1319-1325.

Tan, P. 2016. Active phase, catalytic activity, and induction period of Fe/zeolite material in nonoxidative aromatization of methane. *Journal of catalysis*, 338: 21-29.

Tan, P, Leung, Y, Lai, S and Au, C. 2002. The effect of calcination temperature on the catalytic performance of 2 wt.% Mo/HZSM-5 in methane aromatization. *Applied Catalysis A: General*, 228 (1-2): 115-125.

Teramura, K, Tanaka, T, Ishikawa, H, Kohno, Y and Funabiki, T. 2004. Photocatalytic reduction of CO2 to CO in the presence of H2 or CH4 as a reductant over MgO. *The Journal of Physical Chemistry B*, 108 (1): 346-354.

Tessonnier, J-P, Louis, B, Rigolet, S, Ledoux, MJ and Pham-Huu, C. 2008. Methane dehydro-aromatization on Mo/ZSM-5: About the hidden role of Brønsted acid sites. *Applied Catalysis A: General*, 336 (1-2): 79-88.

Trimm, DL. 1999. Catalysts for the control of coking during steam reforming. *Catalysis today*, 49 (1-3): 3-10.

Van Amstel, A. 2012. Methane. A review. *Journal of Integrative Environmental Sciences*, 9 (sup1): 5-30.

Van Donk, S, Bitter, JH and De Jong, KP. 2001. Deactivation of solid acid catalysts for butene skeletal isomerisation: on the beneficial and harmful effects of carbonaceous deposits. *Applied Catalysis A: General*, 212 (1-2): 97-116.

Varghese, JJ, Saravanan, B, Vach, H, Peslherbe, GH and Mushrif, SH. 2018. First-Principles Investigation of the Coupling-Induced Dissociation of Methane and its Transformation to Ethane and Ethylene. *Chemical Physics Letters*,

Vella, G, Imoberdorf, GE, Sclafani, A, Cassano, AE, Alfano, OM and Rizzuti, L. 2010. Modeling of a TiO2-coated quartz wool packed bed photocatalytic reactor. *Applied Catalysis B: Environmental*, 96 (3–4): 399-407.

Villacampa, JI, Royo, C, Romeo, E, Montoya, JA, Del Angel, P and Monzón, A. 2003. Catalytic decomposition of methane over Ni-Al2O3 coprecipitated catalysts: Reaction and regeneration studies. *Applied Catalysis A: General*, 252 (2): 363-383.

Viswanathan, B, Neel, PI and Varadarajan, T. 2009. Methods of activation and specific applications of carbon materials. *India, Chennai*,

Vogelaar, BM, Eijsbouts, S, Bergwerff, JA and Heiszwolf, JJ. 2010. Hydroprocessing catalyst deactivation in commercial practice. *Catalysis Today*, 154 (3–4): 256-263.

Wang, D, Kan, Q, Xu, N, Wu, P and Wu, T. 2004. Study on methane aromatization over MoO3/HMCM-49 catalyst. *Catalysis today*, 93: 75-80.

Wang, D, Lunsford, JH and Rosynek, MP. 1996. Catalytic conversion of methane to benzene over Mo/ZSM-5. *Topics in Catalysis*, 3 (3-4): 289-297.

Wang, D, Lunsford, JH and Rosynek, MP. 1997. Characterization of a Mo/ZSM-5 catalyst for the conversion of methane to benzene. *Journal of Catalysis*, 169 (1): 347-358.

Wang, H, Liu, Z, Shen, J, Liu, H and Zhang, J. 2005. High-throughput screening of HZSM-5 supported metal-oxides catalysts for the coupling of methane with CO to benzene and naphthalene. *Catalysis Communications*, 6 (5): 343-346.

Wang, L, Murata, K, Sayari, A, Grandjean, B and Inaba, M. 2001. Production of ultra highly pure H2 and higher hydrocarbons from methane in one step at mild temperatures and development of the catalyst under non-equilibrium reaction conditions. *Chemical Communications*, (19): 1952-1953.

Wang, L, Ohnishi, R and Ichikawa, M. 2000. Selective dehydroaromatization of methane toward benzene on Re/HZSM-5 catalysts and effects of CO/CO2 addition. *Journal of Catalysis*, 190 (2): 276-283.

Wang, L, Tao, L, Xie, M, Xu, G, Huang, J and Xu, Y. 1993. Dehydrogenation and aromatization of methane under non-oxidizing conditions. *Catalysis Letters*, 21 (1-2): 35-41.

Wang, S-G, Liao, X-Y, Hu, J, Cao, D-B, Li, Y-W, Wang, J and Jiao, H. 2007. Kinetic aspect of CO2 reforming of CH4 on Ni (1 1 1): a density functional theory calculation. *Surface Science*, 601 (5): 1271-1284.

Wassie, SA, Cloete, S, Spallina, V, Gallucci, F, Amini, S and Van Sint Annaland, M. 2018. Techno-economic assessment of membrane-assisted gas switching reforming for pure H 2 production with CO 2 capture. *International Journal of Greenhouse Gas Control*, 72: 163-174.

Weckhuysen, BM, Rosynek, MP and Lunsford, JH. 1998a. Characterization of surface carbon formed during the conversion of methane to benzene over Mo/H-ZSM-5 catalysts. *Catalysis letters*, 52 (1-2): 31-36.

Weckhuysen, BM, Wang, D, Rosynek, MP and Lunsford, JH. 1998b. Conversion of methane to benzene over transition metal ion ZSM-5 zeolites: I. Catalytic characterization. *Journal of catalysis*, 175 (2): 338-346.

Weitkamp, J. 2000. Zeolites and catalysis. *Solid state ionics*, 131 (1-2): 175-188.

Wenlong, W. 2000. Direct dehydroaromatization of methane. *Journal of Natural Gas Chemistry*, 9 (1)

Wilhelm, D, Simbeck, D, Karp, A and Dickenson, R. 2001. Syngas production for gas-to-liquids applications: technologies, issues and outlook. *Fuel processing technology*, 71 (1-3): 139-148.

Wu, P, Kan, Q, Wang, X, Wang, D, Xing, H, Yang, P and Wu, T. 2005. Acidity and catalytic properties for methane conversion of Mo/HZSM-5 catalyst modified by reacting with organometallic complex. *Applied Catalysis A: General*, 282 (1-2): 39-44.

Xu, M and Lunsford, JH. 1991. Effect of temperature on methyl radical generation over Sr/La 2 O 3 catalysts. *Catalysis letters*, 11 (3-6): 295-300.

Xu, Y, Bao, X and Lin, L. 2003. Direct conversion of methane under nonoxidative conditions. *Journal of Catalysis*, 216 (1-2): 386-395.

Xu, Y and Lin, L. 1999. Recent advances in methane dehydro-aromatization over transition metal ion-modified zeolite catalysts under non-oxidative conditions. *Applied Catalysis A: General*, 188 (1-2): 53-67.

Xu, Y, Liu, S, Guo, X, Wang, L and Xie, M. 1994. Methane activation without using oxidants over Mo/HZSM-5 zeolite catalysts. *Catalysis letters*, 30 (1-4): 135-149.

Xu, Y, Liu, W, Wong, S-T, Wang, L and Guo, X. 1996. Dehydrogenation and aromatization of methane in the absence of oxygen on Mo/HZSM-5 catalysts before and after NH 4 OH extraction. *Catalysis letters*, 40 (3-4): 207-214.

Xu, Y, Lu, J, Wang, J, Suzuki, Y and Zhang, Z-G. 2011. The catalytic stability of Mo/HZSM-5 in methane dehydroaromatization at severe and periodic CH4–H2 switch operating conditions. *Chemical engineering journal*, 168 (1): 390-402.

Xu, Y, Wang, J, Suzuki, Y and Zhang, Z-G. 2012. Improving effect of Fe additive on the catalytic stability of Mo/HZSM-5 in the methane dehydroaromatization. *Catalysis today*, 185 (1): 41-46.

Yao, B, Chen, J, Liu, D and Fang, D. 2008. Intrinsic kinetics of methane aromatization under non-oxidative conditions over modified Mo/HZSM-5 catalysts. *Journal of Natural Gas Chemistry*, 17 (1): 64-68.

Yazdanpour, N and Sharifnia, S. 2013. Photocatalytic conversion of greenhouse gases (CO2 and CH4) using copper phthalocyanine modified TiO2. *Solar energy materials and solar cells*, 118: 1-8.

Yu, C, Qiu, JS, Sun, YF, Li, XH, Chen, G and Zhao, ZB. 2008. Adsorption removal of thiophene and dibenzothiophene from oils with activated carbon as adsorbent: effect of surface chemistry. *Journal of Porous Materials*, 15 (2): 151-157.

Yuan, S, Li, J, Hao, Z, Feng, Z, Xin, Q, Ying, P and Li, C. 1999. The effect of oxygen on the aromatization of methane over the Mo/HZSM-5 catalyst. *Catalysis letters*, 63 (1-2): 73-77.

Zaikovskii, V, Vosmerikov, A, Anufrienko, V, Korobitsyna, L, Kodenev, E, Echevskii, G, Vasenin, N, Zhuravkov, SP, Matus, E and Ismagilov, Z. 2006. Properties and deactivation of the active sites of an MoZSM-5 catalyst for methane dehydroaromatization: Electron microscopic and EPR studies. *Kinetics and catalysis*, 47 (3): 389-394.

Zhang, C-L, Li, S, Yuan, Y, Zhang, W-X, Wu, T-H and Lin, L-W. 1998. Aromatization of methane in the absence of oxygen over Mo-based catalysts supported on different types of zeolites. *Catalysis letters*, 56 (4): 207-213.

Zhang, Q, Li, Y, An, D and Wang, Y. 2009. Catalytic behaviour and kinetic features of FeOx/SBA-15 catalyst for selective oxidation of methane by oxygen. *Applied Catalysis A: General*, 356 (1): 103-111.

Zhang, T and Amiridis, MD. 1998. Hydrogen production via the direct cracking of methane over silica-supported nickel catalysts. *Applied Catalysis A: General*, 167 (2): 161-172.

Zhang, W and Smirniotis, PG. 1999. On the exceptional time-on-stream stability of HZSM-12 zeolite: relation between zeolite pore structure and activity. *Catalysis letters*, 60 (4): 223-228.

Zhang, Z-G. 2019. Process, reactor and catalyst design: Towards application of direct conversion of methane to aromatics under nonoxidative conditions. *Carbon Resources Conversion*, 2 (3): 157-174.

Zhou, D, Ma, D, Liu, X and Bao, X. 2001. Study with density functional theory method on methane dehydro-aromatization over Mo/HZSM-5 catalysts I: Optimization of active Mo species bonded to ZSM-5 zeolite. *The Journal of Chemical Physics*, 114 (20): 9125-9129.

APPENDICES

APPENDIX A: CATALYST PRECURSORS

Table A-1 Elemental composition of catalyst precursors

- **Ferric nitrate nonahydrate**

  Formula ……...$Fe(NO_3)_3.(H_2O)_9$

  Molecular weight…….403.98822

  Elemental composition by mass: Iron……...13.82%

  : Nitrogen….....10.40%

  : Oxygen…….71.28%

  : Hydrogen …….4.49%

- **Ammonium Para tungstate**

  Formula……...$(NH_4)_{10}(H_2W_{12}O_{42}).4H_2O$

  Molar mass……3132.493g

  Elemental composition by mass: Tungsten……70.43%

  : Nitrogen…….….4.47%

  : Hydrogen…….1.61%

  : Oxygen…….23.49%

- **Ammonium heptamolybdate**

  Formula……$(NH_4)_6Mo_7O_{24}$

  Molar mass…….…….1163.85436g

  Elemental composition by mass: Molybdenum…….57.71%

  : Nitrogen…….…….7.22%

  : Oxygen……32.99%

  : Hydrogen……..…2.08%

APPENDIX B: PARTICLE SIZE DISTRIBUTION USING IMAGE-J SOFTWARE

Table B-1: Particle size distribution in HZSM-5 obtained using Image-J software.

No.	Area	Mean	Min	Max	r^2	r	d	Normal	Upper Bin	Bin	Frequ.	%Frequ.
1	23	255	255	255	7.32	2.71	5.41	0.1272				
2	10	255	255	255	3.18	1.78	3.57	0.1323	2	0-1.9	0	0.00
3	5	255	255	255	1.59	1.26	2.52	0.1133	4	2-3.9	33	70.21
4	10	255	255	255	3.18	1.78	3.57	0.1323	6	4-5.9	8	17.02
5	6	255	255	255	1.91	1.38	2.76	0.1188	8	6-7.9	3	6.38
6	41	255	255	255	13.05	3.61	7.23	0.0830	10	8-9.9	0	0.00
7	175	255	255	255	55.70	7.46	14.93	0.0002	12	10-11.9	0	0.00
8	19	255	255	255	6.05	2.46	4.92	0.1337	14	12-13.9	1	2.13
9	41	255	255	255	13.05	3.61	7.23	0.0830	16	14-15.9	2	4.26
10	5	255	255	255	1.59	1.26	2.52	0.1133			0	0.00
11	7	255	255	255	2.23	1.49	2.99	0.1233			47	100.0
12	16	255	255	255	5.09	2.26	4.51	0.1363				
13	14	255	255	255	4.46	2.11	4.22	0.1366				
14	6	255	255	255	1.91	1.38	2.76	0.1188				
15	29	255	255	255	9.23	3.04	6.08	0.1138				
16	8	255	255	255	2.55	1.60	3.19	0.1270	Std Dev.	Min	Max	Mean
17	9	255	255	255	2.86	1.69	3.39	0.1299	2.92	2.52	15.84	4.31
18	9	255	255	255	2.86	1.69	3.39	0.1299				
19	5	255	255	255	1.59	1.26	2.52	0.1133				
20	11	255	255	255	3.50	1.87	3.74	0.1341				
21	8	255	255	255	2.55	1.60	3.19	0.1270				
22	10	255	255	255	3.18	1.78	3.57	0.1323				
23	9	255	255	255	2.86	1.69	3.39	0.1299				
24	123	255	255	255	39.15	6.26	12.51	0.0026				
25	18	255	255	255	5.73	2.39	4.79	0.1348				
26	5	255	255	255	1.59	1.26	2.52	0.1133				
27	13	255	255	255	4.14	2.03	4.07	0.1362				
28	5	255	255	255	1.59	1.26	2.52	0.1133				
29	5	255	255	255	1.59	1.26	2.52	0.1133				
30	7	255	255	255	2.23	1.49	2.99	0.1233				

31	10	255	255	255	3.18	1.78	3.57	0.1323
32	5	255	255	255	1.59	1.26	2.52	0.1133
33	8	255	255	255	2.55	1.60	3.19	0.1270
34	197	255	255	255	62.71	7.92	15.84	0.0001
35	11	255	255	255	3.50	1.87	3.74	0.1341
36	14	255	255	255	4.46	2.11	4.22	0.1366
37	8	255	255	255	2.55	1.60	3.19	0.1270
38	7	255	255	255	2.23	1.49	2.99	0.1233

Table B-2: Particle size distribution in catalyst 2.7F2.7M/HZS-5 obtained using Image-J software.

No.	Area	Mean	Min	Max	r^2	r	d	Normal	Upper Bin	Bin	Frequ.	%Frequ.
1	15.53	255	255	255	4.94	2.22	4.45	0.1032				
2	10.35	255	255	255	3.29	1.82	3.63	0.0946	2	0-1.9	0	0.0
3	25.88	255	255	255	8.24	2.87	5.74	0.1073	4	2-3.9	16	33.3
4	5.18	255	255	255	1.65	1.28	2.57	0.0785	6	4-5.9	21	43.8
5	5.18	255	255	255	1.65	1.28	2.57	0.0785	8	6-7.9	5	10.4
6	20.70	255	255	255	6.59	2.57	5.13	0.1070	10	8-9.9	3	6.3
7	36.23	255	255	255	11.53	3.40	6.79	0.1013	12	10-11.9	0	0.0
8	56.93	255	255	255	18.12	4.26	8.51	0.0775	14	12-13.9	1	2.1
9	51.76	255	255	255	16.47	4.06	8.12	0.0840	16	14-15.9	0	0.0
10	41.41	255	255	255	13.18	3.63	7.26	0.0962	18	16-17.9	1	2.1
11	31.05	255	255	255	9.88	3.14	6.29	0.1052	20	18-19.9	0	0.0
12	15.53	255	255	255	4.94	2.22	4.45	0.1032	22	22-23.9	1	2.1
13	119.04	255	255	255	37.89	6.16	12.31	0.0200			48	100.0
14	25.88	255	255	255	8.24	2.87	5.74	0.1073				
15	15.53	255	255	255	4.94	2.22	4.45	0.1032				
16	20.70	255	255	255	6.59	2.57	5.13	0.1070	Std Dev.	Min	Max	Mean
17	5.18	255	255	255	1.65	1.28	2.57	0.0785	3.71	2.57	22.96	5.51
18	25.88	255	255	255	8.24	2.87	5.74	0.1073				
19	31.05	255	255	255	9.88	3.14	6.29	0.1052				
20	20.70	255	255	255	6.59	2.57	5.13	0.1070				
21	10.35	255	255	255	3.29	1.82	3.63	0.0946				
22	10.35	255	255	255	3.29	1.82	3.63	0.0946				
23	5.18	255	255	255	1.65	1.28	2.57	0.0785				
24	5.18	255	255	255	1.65	1.28	2.57	0.0785				
25	414.06	255	255	255	131.80	11.48	22.96	0.0000				
26	20.70	255	255	255	6.59	2.57	5.13	0.1070				
27	248.43	255	255	255	79.08	8.89	17.79	0.0005				
28	5.18	255	255	255	1.65	1.28	2.57	0.0785				
29	15.53	255	255	255	4.94	2.22	4.45	0.1032				
30	10.35	255	255	255	3.29	1.82	3.63	0.0946				
31	15.53	255	255	255	4.94	2.22	4.45	0.1032				

32	15.53	255	255	255	4.94	2.22	4.45	0.1032
33	31.05	255	255	255	9.88	3.14	6.29	0.1052
34	25.88	255	255	255	8.24	2.87	5.74	0.1073
35	15.53	255	255	255	4.94	2.22	4.45	0.1032
36	10.35	255	255	255	3.29	1.82	3.63	0.0946
37	5.18	255	255	255	1.65	1.28	2.57	0.0785
38	56.93	255	255	255	18.12	4.26	8.51	0.0775

Table B-3: Particle size distribution in catalyst 2.7W2.7M/HZSM-5 obtained using Image-J software.

No.	Area	Mean	Min	Max	r^2	r	d	Normal	Upper Bin	Bin	Frequ.	%Frequ.
1	165.62	255	255	255	52.72	7.26	14.52	0.0484				
2	77.64	255	255	255	24.71	4.97	9.94	0.0973	2.5	0-2.4	0	0.00
3	20.70	255	255	255	6.59	2.57	5.13	0.0526	5	2.5-4.9	26	44.07
4	5.18	255	255	255	1.65	1.28	2.57	0.0215	7.5	5-7.4	16	27.12
5	20.70	255	255	255	6.59	2.57	5.13	0.0526	10	7.5-9.9	8	13.56
6	119.04	255	255	255	37.89	6.16	12.31	0.0793	12.5	10-12.4	5	8.47
7	10.35	255	255	255	3.29	1.82	3.63	0.0327	15	12.5-14.9	2	3.39
8	5.18	255	255	255	1.65	1.28	2.57	0.0215	17.5	15-17.4	2	3.39
9	31.05	255	255	255	9.88	3.14	6.29	0.0692			0	0.00
10	20.70	255	255	255	6.59	2.57	5.13	0.0526			59	100.0
11	15.53	255	255	255	4.94	2.22	4.45	0.0430				
12	20.70	255	255	255	6.59	2.57	5.13	0.0526				
13	212.20	255	255	255	67.55	8.22	16.44	0.0249				
14	134.57	255	255	255	42.83	6.54	13.09	0.0689				
15	5.18	255	255	255	1.65	1.28	2.57	0.0215				
16	10.35	255	255	255	3.29	1.82	3.63	0.0327				
18	36.23	255	255	255	11.53	3.40	6.79	0.0760				
19	67.28	255	255	255	21.42	4.63	9.26	0.0970	Std. Dev.	Min	Max	Mean
20	10.35	255	255	255	3.29	1.82	3.63	0.0327	3.55	2.57	16.44	7.52
21	15.53	255	255	255	4.94	2.22	4.45	0.0430				
23	5.18	255	255	255	1.65	1.28	2.57	0.0215				
24	41.41	255	255	255	13.18	3.63	7.26	0.0819				
25	15.53	255	255	255	4.94	2.22	4.45	0.0430				
27	5.18	255	255	255	1.65	1.28	2.57	0.0215				
28	5.18	255	255	255	1.65	1.28	2.57	0.0215				
29	51.76	255	255	255	16.47	4.06	8.12	0.0907				
30	82.81	255	255	255	26.36	5.13	10.27	0.0965				
31	82.81	255	255	255	26.36	5.13	10.27	0.0965				
32	31.05	255	255	255	9.88	3.14	6.29	0.0692				
33	113.87	255	255	255	36.24	6.02	12.04	0.0826				

34	10.35	255	255	255	3.29	1.82	3.63	0.0327
35	191.50	255	255	255	60.96	7.81	15.61	0.0340
36	82.81	255	255	255	26.36	5.13	10.27	0.0965
37	20.70	255	255	255	6.59	2.57	5.13	0.0526
38	5.18	255	255	255	1.65	1.28	2.57	0.0215

Table B-4: Particle size distribution in catalyst 2.7F2.7W/HZSM-5 obtained using Image-J software.

No.	Area	Mean	Min	Max	r^2	r	d	Normal	Upper Bin	Bin	Frequ.	%Frequ.
1	15.53	255	255	255	4.94	2.22	4.45	0.0685				
2	10.35	255	255	255	3.29	1.82	3.63	0.0630	1.5	0-1.4	0	0.0
3	20.70	255	255	255	6.59	2.57	5.13	0.0721	3	1.5-2.9	11	16.7
4	51.76	255	255	255	16.47	4.06	8.12	0.0740	4.5	3-4.4	19	28.8
5	10.35	255	255	255	3.29	1.82	3.63	0.0630	6	4.5-5.9	10	15.2
6	5.18	255	255	255	1.65	1.28	2.57	0.0544	7.5	6-7.4	7	10.6
7	15.53	255	255	255	4.94	2.22	4.45	0.0685	9	7.5-8.9	7	10.6
8	10.35	255	255	255	3.29	1.82	3.63	0.0630	10.5	9-10.4	5	7.6
9	20.70	255	255	255	6.59	2.57	5.13	0.0721	12	10.5-11.9	3	4.5
10	129.39	255	255	255	41.19	6.42	12.84	0.0397	13.5	12-13.4	1	1.5
11	31.05	255	255	255	9.88	3.14	6.29	0.0757	15	13.5-14.9	3	4.5
12	10.35	255	255	255	3.29	1.82	3.63	0.0630			0	0.0
13	51.76	255	255	255	16.47	4.06	8.12	0.0740			66	100.0
14	15.53	255	255	255	4.94	2.22	4.45	0.0685				
15	15.53	255	255	255	4.94	2.22	4.45	0.0685				
16	10.35	255	255	255	3.29	1.82	3.63	0.0630				
17	10.35	255	255	255	3.29	1.82	3.63	0.0630				
18	5.18	255	255	255	1.65	1.28	2.57	0.0544				
19	15.53	255	255	255	4.94	2.22	4.45	0.0685	Std Dev.	Min	Max	Mean
20	25.88	255	255	255	8.24	2.87	5.74	0.0744	3.15	2.57	14.29	5.98
21	51.76	255	255	255	16.47	4.06	8.12	0.0740				
22	5.18	255	255	255	1.65	1.28	2.57	0.0544				
23	36.23	255	255	255	11.53	3.40	6.79	0.0761				
24	10.35	255	255	255	3.29	1.82	3.63	0.0630				
25	160.45	255	255	255	51.07	7.15	14.29	0.0278				
26	31.05	255	255	255	9.88	3.14	6.29	0.0757				
27	15.53	255	255	255	4.94	2.22	4.45	0.0685				
28	108.69	255	255	255	34.60	5.88	11.76	0.0491				
29	77.64	255	255	255	24.71	4.97	9.94	0.0640				
30	67.28	255	255	255	21.42	4.63	9.26	0.0686				
31	10.35	255	255	255	3.29	1.82	3.63	0.0630				

32	93.16	255	255	255	29.65	5.45	10.89	0.0566
33	20.70	255	255	255	6.59	2.57	5.13	0.0721
34	25.88	255	255	255	8.24	2.87	5.74	0.0744
35	77.64	255	255	255	24.71	4.97	9.94	0.0640
36	46.58	255	255	255	14.83	3.85	7.70	0.0752
37	36.23	255	255	255	11.53	3.40	6.79	0.0761
38	93.16	255	255	255	29.65	5.45	10.89	0.0566

Table B-5: Particle size distribution in catalyst 1.8F1.8W1.8M/HZSM-5 obtained using Image-J software.

No.	Area	Mean	Min	Max	r^2	r	d	Normal	Upper Bin	Bin	Frequ.	%Frequ.
1	25.88	255	255	255	8.24	2.87	5.74	0.0321				
4	5.18	255	255	255	1.65	1.28	2.57	0.0276	3	0-2.9	9	16.4
5	186.33	255	255	255	59.31	7.70	15.40	0.0317	6	3-5.9	21	38.2
6	31.05	255	255	255	9.88	3.14	6.29	0.0327	9	6-8.9	15	27.3
7	15.53	255	255	255	4.94	2.22	4.45	0.0305	12	9-11.9	3	5.5
8	15.53	255	255	255	4.94	2.22	4.45	0.0305	15	12-14.9	2	3.6
9	25.88	255	255	255	8.24	2.87	5.74	0.0321	18	15-17.9	2	3.6
11	5.18	255	255	255	1.65	1.28	2.57	0.0276	21	18-20.9	2	3.6
13	10.35	255	255	255	3.29	1.82	3.63	0.0293	24	21-23.9	1	1.8
14	5.18	255	255	255	1.65	1.28	2.57	0.0276			0	0.0
15	5.18	255	255	255	1.65	1.28	2.57	0.0276			55	100.0
16	181.15	255	255	255	57.66	7.59	15.19	0.0320				
17	10.35	255	255	255	3.29	1.82	3.63	0.0293	Std Dev.	Min	Max	Mean
18	31.05	255	255	255	9.88	3.14	6.29	0.0327	4.46	2.57	21.48	6.78
19	20.70	255	255	255	6.59	2.57	5.13	0.0314				
21	25.88	255	255	255	8.24	2.87	5.74	0.0321				
22	25.88	255	255	255	8.24	2.87	5.74	0.0321				
23	36.23	255	255	255	11.53	3.40	6.79	0.0332				
24	129.39	255	255	255	41.19	6.42	12.84	0.0341				
25	41.41	255	255	255	13.18	3.63	7.26	0.0336				
26	20.70	255	255	255	6.59	2.57	5.13	0.0314				
27	295.02	255	255	255	93.91	9.69	19.38	0.0257				
28	20.70	255	255	255	6.59	2.57	5.13	0.0314				
29	46.58	255	255	255	14.83	3.85	7.70	0.0339				
30	82.81	255	255	255	26.36	5.13	10.27	0.0349				
31	41.41	255	255	255	13.18	3.63	7.26	0.0336				
32	15.53	255	255	255	4.94	2.22	4.45	0.0305				
33	41.41	255	255	255	13.18	3.63	7.26	0.0336				
34	10.35	255	255	255	3.29	1.82	3.63	0.0293				
35	5.18	255	255	255	1.65	1.28	2.57	0.0276				
36	15.53	255	255	255	4.94	2.22	4.45	0.0305				

37	5.18	255	255	255	1.65	1.28	2.57	0.0276
38	362.30	255	255	255	115.32	10.74	21.48	0.0218

Table B-6: Particle size distribution in catalyst 2.25F2.25W0.9M/HZSM-5 obtained using Image-J software.

No.	Area	Mean	Min	Max	r^2	r	d	Normal	Upper Bin	Bin	Frequ.	%Frequ.
1	284.66	255	255	255	90.61	9.52	19.04	0.0137				
2	662.49	255	255	255	210.88	14.52	29.04	0.0003	2.2	0-2.1	0	0.0
3	20.70	255	255	255	6.59	2.57	5.13	0.0562	4.4	2.2-4.3	13	30.2
4	31.05	255	255	255	9.88	3.14	6.29	0.0592	6.6	4.4-6.5	15	34.9
5	5.18	255	255	255	1.65	1.28	2.57	0.0448	8.8	6.6-8.7	5	11.6
6	5.18	255	255	255	1.65	1.28	2.57	0.0448	11	8.8-10.9	1	2.3
7	15.53	255	255	255	4.94	2.22	4.45	0.0537	13.2	11-13.1	4	9.3
8	119.04	255	255	255	37.89	6.16	12.31	0.0473	15.4	13.2-15.3	0	0.0
9	41.41	255	255	255	13.18	3.63	7.26	0.0604	17.6	15.4-17.5	0	0.0
10	31.05	255	255	255	9.88	3.14	6.29	0.0592	19.8	17.6-19.7	2	4.7
11	20.70	255	255	255	6.59	2.57	5.13	0.0562	22	19.8-21.9	0	0.0
12	5.18	255	255	255	1.65	1.28	2.57	0.0448	24.2	22-24.1	0	0.0
13	51.76	255	255	255	16.47	4.06	8.12	0.0604	26.4	24.2-26.3	2	4.7
14	10.35	255	255	255	3.29	1.82	3.63	0.0501	28.6	26.4-28.5	0	0.0
15	15.53	255	255	255	4.94	2.22	4.45	0.0537	30.8	28.6-30.7	1	2.3
16	108.69	255	255	255	34.60	5.88	11.76	0.0500			0	0.0
17	5.18	255	255	255	1.65	1.28	2.57	0.0448			43	100.0
18	31.05	255	255	255	9.88	3.14	6.29	0.0592				
19	51.76	255	255	255	16.47	4.06	8.12	0.0604				
20	98.34	255	255	255	31.30	5.59	11.19	0.0525	Std Dev.	Min	Max	Mean
21	496.87	255	255	255	158.16	12.58	25.15	0.0018	6.59	2.57	29.04	7.68
22	15.53	255	255	255	4.94	2.22	4.45	0.0537				
23	20.70	255	255	255	6.59	2.57	5.13	0.0562				
24	5.18	255	255	255	1.65	1.28	2.57	0.0448				
25	20.70	255	255	255	6.59	2.57	5.13	0.0562				
26	20.70	255	255	255	6.59	2.57	5.13	0.0562				
27	20.70	255	255	255	6.59	2.57	5.13	0.0562				
28	98.34	255	255	255	31.30	5.59	11.19	0.0525				
29	15.53	255	255	255	4.94	2.22	4.45	0.0537				
30	10.35	255	255	255	3.29	1.82	3.63	0.0501				
31	284.66	255	255	255	90.61	9.52	19.04	0.0137				

32	46.58	255	255	255	14.83	3.85	7.70	0.0605
33	5.18	255	255	255	1.65	1.28	2.57	0.0448
34	5.18	255	255	255	1.65	1.28	2.57	0.0448
35	10.35	255	255	255	3.29	1.82	3.63	0.0501
36	77.64	255	255	255	24.71	4.97	9.94	0.0571
37	20.70	255	255	255	6.59	2.57	5.13	0.0562
38	543.45	255	255	255	172.99	13.15	26.30	0.0011

Table B-7: Particle size distribution in catalyst 1.35F1.35W2.7M/HZSM-5 obtained using Image-J software.

No.	Area	Mean	Min	Max	r^2	r	d	Normal	Upper Bin	Bin	Frequ.	%Frequ.
1	5.176	255	255	255	1.65	1.28	2.57	0.0603				
2	25.879	255	255	255	8.24	2.87	5.74	0.0793	2.2	0-2.1	0	0.0
3	5.176	255	255	255	1.65	1.28	2.57	0.0603	4.4	2.2-4.3	22	34.4
4	67.284	255	255	255	21.42	4.63	9.26	0.0671	6.6	4.3-6.5	24	37.5
5	51.757	255	255	255	16.47	4.06	8.12	0.0747	8.8	6.6-8.7	8	12.5
6	439.94	255	255	255	140.04	11.83	23.67	0.0002	11	8.8-10.9	6	9.4
7	10.351	255	255	255	3.29	1.82	3.63	0.0691	13.2	11-13.1	0	0.0
8	31.054	255	255	255	9.88	3.14	6.29	0.0798	15.4	13.2-15.3	0	0.0
9	20.703	255	255	255	6.59	2.57	5.13	0.0776	17.6	15.4-17.5	0	0.0
10	46.581	255	255	255	14.83	3.85	7.70	0.0768	19.8	17.6-19.7	2	3.1
11	5.176	255	255	255	1.65	1.28	2.57	0.0603	22	19.8-21.9	0	0.0
12	5.176	255	255	255	1.65	1.28	2.57	0.0603	24.2	22-24.1	1	1.6
13	10.351	255	255	255	3.29	1.82	3.63	0.0691	26.4	24.2-26.3	0	0.0
14	10.351	255	255	255	3.29	1.82	3.63	0.0691	28.6	26.4-28.5	0	0.0
15	15.527	255	255	255	4.94	2.22	4.45	0.0744	30.8	28.6-30.7	0	0.0
16	5.176	255	255	255	1.65	1.28	2.57	0.0603	33	30.8-32.9	1	1.6
17	15.527	255	255	255	4.94	2.22	4.45	0.0744			0	0.0
18	31.054	255	255	255	9.88	3.14	6.29	0.0798			64	100.0
19	15.527	255	255	255	4.94	2.22	4.45	0.0744				
20	15.527	255	255	255	4.94	2.22	4.45	0.0744	Std Dev.	Min	Max	Mean
21	56.933	255	255	255	18.12	4.26	8.51	0.0724	5.00	2.57	31.02	6.31
22	5.176	255	255	255	1.65	1.28	2.57	0.0603				
23	269.14	255	255	255	85.67	9.26	18.51	0.0041				
24	25.879	255	255	255	8.24	2.87	5.74	0.0793				
25	67.284	255	255	255	21.42	4.63	9.26	0.0671				
26	31.054	255	255	255	9.88	3.14	6.29	0.0798				
27	62.109	255	255	255	19.77	4.45	8.89	0.0698				
28	36.23	255	255	255	11.53	3.40	6.79	0.0794				
29	20.703	255	255	255	6.59	2.57	5.13	0.0776				
30	51.757	255	255	255	16.47	4.06	8.12	0.0747				
31	62.109	255	255	255	19.77	4.45	8.89	0.0698				

32	5.176	255	255	255	1.65	1.28	2.57	0.0603
33	5.176	255	255	255	1.65	1.28	2.57	0.0603
34	20.703	255	255	255	6.59	2.57	5.13	0.0776
35	20.703	255	255	255	6.59	2.57	5.13	0.0776
36	5.176	255	255	255	1.65	1.28	2.57	0.0603
37	20.703	255	255	255	6.59	2.57	5.13	0.0776
38	5.176	255	255	255	1.65	1.28	2.57	0.0603

Table B-8: Particle size distribution in AC obtained using Image-J software.

No.	Area	Mean	Min	Max	r^2	r	d	Normal	Upper Bin	Bin	Frequ	%Frequ
1	10.35	117	117	117	3.29	1.82	3.63	0.0514				
2	31.05	117	117	117	9.88	3.14	6.29	0.0636	1.8	0.0-1.7	0	0.0
3	67.28	117	117	118	21.42	4.63	9.26	0.0643	3.6	1.8-3.5	11	22.0
4	5.18	117	117	117	1.65	1.28	2.57	0.0447	5.4	3.6-5.3	13	26.0
5	424.41	123	117	134	135.09	11.62	23.25	0.0026	7.2	5.4-7.1	5	10.0
6	5.18	117	117	117	1.65	1.28	2.57	0.0447	9	7.2-8.9	6	12.0
7	5.18	117	117	117	1.65	1.28	2.57	0.0447	10.8	9.0-10.7	4	8.0
8	36.23	117	117	117	11.53	3.40	6.79	0.0648	12.6	10.8-12.5	3	6.0
9	455.46	117	117	118	144.98	12.04	24.08	0.0018	14.4	12.6-14.3	0	0.0
10	5.18	117	117	117	1.65	1.28	2.57	0.0447	16.2	14.4-16.1	0	0.0
11	336.42	117	117	118	107.09	10.35	20.70	0.0070	18	16.2-17.9	4	8.0
12	20.70	117	117	117	6.59	2.57	5.13	0.0594	19.8	18.0-19.7	0	0.0
13	108.69	118	117	119	34.60	5.88	11.76	0.0538	21.6	19.8-21.5	1	2.0
14	5.18	117	117	117	1.65	1.28	2.57	0.0447	23.4	21.6-23.3	2	4.0
15	56.93	117	117	118	18.12	4.26	8.51	0.0656	25.2	23.4-25.1	1	2.0
16	46.58	118	117	118	14.83	3.85	7.70	0.0659			0	0.0
17	15.53	117	117	117	4.94	2.22	4.45	0.0560			50	100.0
18	238.08	118	117	121	75.78	8.71	17.41	0.0192				
19	46.58	117	117	118	14.83	3.85	7.70	0.0659				
20	20.70	117	117	117	6.59	2.57	5.13	0.0594	Std Dev.	Min	Max	Mean
21	51.76	117	117	117	16.47	4.06	8.12	0.0659	6.05	2.57	24.08	7.90
22	25.88	117	117	117	8.24	2.87	5.74	0.0619				
23	5.18	117	117	117	1.65	1.28	2.57	0.0447				
24	232.91	120	117	123	74.14	8.61	17.22	0.0201				
25	15.53	117	117	117	4.94	2.22	4.45	0.0560				
26	10.35	117	117	117	3.29	1.82	3.63	0.0514				
27	103.51	117	117	117	32.95	5.74	11.48	0.0553				
28	10.35	117	117	117	3.29	1.82	3.63	0.0514				
29	25.88	117	117	117	8.24	2.87	5.74	0.0619				
30	5.18	117	117	117	1.65	1.28	2.57	0.0447				
31	10.35	117	117	117	3.29	1.82	3.63	0.0514				
32	238.08	118	117	119	75.78	8.71	17.41	0.0192				

33	10.35	117	117	117	3.29	1.82	3.63	0.0514
34	5.18	117	117	117	1.65	1.28	2.57	0.0447
35	424.41	117	117	119	135.09	11.62	23.25	0.0026
36	20.70	117	117	117	6.59	2.57	5.13	0.0594
37	5.18	117	117	117	1.65	1.28	2.57	0.0447
38	20.70	117	117	117	6.59	2.57	5.13	0.0594

Table B-9: Particle size distribution in catalyst 2.7F2.7M/AC obtained using Image-J software.

No.	Area	Mean	Min	Max	r^2	r	d	Normal	Upper Bin	Bin	Frequ.	%Freq
1	31.05	119	116	122	9.88	3.14	6.29	0.0382				
2	82.81	117	116	117	26.36	5.13	10.27	0.0515			0	0.0
3	46.58	117	116	119	14.83	3.85	7.70	0.0439	3.5	0.0-3.4	3	5.6
4	129.39	119	116	124	41.19	6.42	12.84	0.0537	7	3.5-6.9	11	20.4
5	5.18	116	116	116	1.65	1.28	2.57	0.0222	10.5	7.0-10.4	11	20.4
6	403.71	132	116	149	128.50	11.34	22.67	0.0207	14	10.5-13.9	11	20.4
7	139.74	120	116	125	44.48	6.67	13.34	0.0534	17.5	14-17.4	5	9.3
8	56.93	116	116	116	18.12	4.26	8.51	0.0468	21	17.5-20.9	4	7.4
9	15.53	116	116	117	4.94	2.22	4.45	0.0301	24.5	21.0-24.4	6	11.1
10	377.83	118	116	123	120.27	10.97	21.93	0.0237	28	24.5-27.9	1	1.9
11	87.99	117	116	118	28.01	5.29	10.58	0.0521	31.5	28.0-31.4	1	1.9
12	62.11	119	116	122	19.77	4.45	8.89	0.0480	35	31.5-34.9	1	1.9
13	160.45	117	116	119	51.07	7.15	14.29	0.0521			0	0.0
14	20.70	116	116	116	6.59	2.57	5.13	0.0332			54	100.0
15	129.39	118	116	121	41.19	6.42	12.84	0.0537				
16	72.46	118	116	119	23.06	4.80	9.61	0.0500	Std Dev.	Min	Max	Mean
17	15.53	116	116	116	4.94	2.22	4.45	0.0301	7.42	2.57	33.57	12.43
18	403.71	116	116	117	128.50	11.34	22.67	0.0207				
19	25.88	118	116	119	8.24	2.87	5.74	0.0358				
20	248.43	120	116	125	79.08	8.89	17.79	0.0414				
21	93.16	119	116	122	29.65	5.45	10.89	0.0526				
22	56.93	117	116	118	18.12	4.26	8.51	0.0468				
23	103.51	117	116	119	32.95	5.74	11.48	0.0533				
24	10.35	116	116	116	3.29	1.82	3.63	0.0266				
25	10.35	116	116	116	3.29	1.82	3.63	0.0266				
26	760.83	124	116	134	242.18	15.56	31.12	0.0022				
27	362.30	119	116	123	115.32	10.74	21.48	0.0256				
28	113.87	118	116	121	36.24	6.02	12.04	0.0537				
29	36.23	116	116	116	11.53	3.40	6.79	0.0403				
30	25.88	116	116	117	8.24	2.87	5.74	0.0358				
31	10.35	116	116	116	3.29	1.82	3.63	0.0266				

32	331.25	118	116	121	105.44	10.27	20.54	0.0296
33	377.83	118	116	122	120.27	10.97	21.93	0.0237
34	150.10	116	116	117	47.78	6.91	13.82	0.0528
35	150.10	118	116	121	47.78	6.91	13.82	0.0528
36	170.80	117	116	119	54.37	7.37	14.75	0.0512
37	470.99	118	116	121	149.92	12.24	24.49	0.0144
38	5.18	116	116	116	1.65	1.28	2.57	0.0222

Table B-10: Particle size distribution in catalyst 2.7W2.7M/AC obtained using Image-J software.

No.	Area	Mean	Min	Max	r^2	r	d	Normal	Upper Bin	Bin	Frequ.	%Frequ.
1	56.93	255	255	255	18.12	4.26	8.51	0.0797				
2	36.23	255	255	255	11.53	3.40	6.79	0.0762				
3	320.89	255	255	255	102.14	10.11	20.21	0.0047	2.2	0.0-2.1	0	0.0
4	36.23	255	255	255	11.53	3.40	6.79	0.0762	4.4	2.2-4.3	9	16.4
5	5.18	255	255	255	1.65	1.28	2.57	0.0413	6.6	4.4-6.5	15	27.3
6	25.88	255	255	255	8.24	2.87	5.74	0.0700	8.8	6.6-8.7	14	25.5
7	36.23	255	255	255	11.53	3.40	6.79	0.0762	11	8.8-10.9	3	5.5
8	46.58	255	255	255	14.83	3.85	7.70	0.0792	13.2	11-13.1	5	9.1
9	56.93	255	255	255	18.12	4.26	8.51	0.0797	15.4	13.2-15.3	2	3.6
10	20.70	255	255	255	6.59	2.57	5.13	0.0653	17.6	15.4-17.5	2	3.6
11	31.05	255	255	255	9.88	3.14	6.29	0.0736	19.8	17.6-19.7	3	5.5
12	46.58	255	255	255	14.83	3.85	7.70	0.0792	22	19.8-21.9	2	3.6
13	113.87	255	255	255	36.24	6.02	12.04	0.0603			0	0.0
14	5.18	255	255	255	1.65	1.28	2.57	0.0413			55	100.0
15	36.23	255	255	255	11.53	3.40	6.79	0.0762				
16	46.58	255	255	255	14.83	3.85	7.70	0.0792				
17	134.57	255	255	255	42.83	6.54	13.09	0.0504	Std Dev.	Min	Max	Mean
18	20.70	255	255	255	6.59	2.57	5.13	0.0653	5.00	2.57	20.21	8.30
19	10.35	255	255	255	3.29	1.82	3.63	0.0516				
20	5.18	255	255	255	1.65	1.28	2.57	0.0413				
21	25.88	255	255	255	8.24	2.87	5.74	0.0700				
22	15.53	255	255	255	4.94	2.22	4.45	0.0593				
23	113.87	255	255	255	36.24	6.02	12.04	0.0603				
24	15.53	255	255	255	4.94	2.22	4.45	0.0593				
25	25.88	255	255	255	8.24	2.87	5.74	0.0700				
26	20.70	255	255	255	6.59	2.57	5.13	0.0653				
27	5.18	255	255	255	1.65	1.28	2.57	0.0413				
28	15.53	255	255	255	4.94	2.22	4.45	0.0593				
29	98.34	255	255	255	31.30	5.59	11.19	0.0675				
30	46.58	255	255	255	14.83	3.85	7.70	0.0792				
31	82.81	255	255	255	26.36	5.13	10.27	0.0738				

32	5.18	255	255	255	1.65	1.28	2.57	0.0413
33	181.15	255	255	255	57.66	7.59	15.19	0.0309
34	77.64	255	255	255	24.71	4.97	9.94	0.0756
35	41.41	255	255	255	13.18	3.63	7.26	0.0781
36	320.89	255	255	255	102.14	10.11	20.21	0.0047
37	41.41	255	255	255	13.18	3.63	7.26	0.0781
38	196.68	255	255	255	62.60	7.91	15.82	0.0257

Table B-11: Particle size distribution in catalyst 2.7F2.7W/AC obtained using Image-J software.

No.	Area	Mean	Min	Max	r^2	r	d	Normal	Upper Bin	Bin	Frequ.	%Frequ.
1	93.16	255	255	255	29.65	5.45	10.89	0.0587				
2	351.95	255	255	255	112.03	10.58	21.17	0.0088			0	0.00
3	41.41	255	255	255	13.18	3.63	7.26	0.0614	3	0.0-2.9	8	15.69
4	5.18	255	255	255	1.65	1.28	2.57	0.0402	6	3-5.9	15	29.41
5	5.18	255	255	255	1.65	1.28	2.57	0.0402	9	6-8.9	10	19.61
6	144.92	255	255	255	46.13	6.79	13.58	0.0460	12	9-11.9	9	17.65
7	25.88	255	255	255	8.24	2.87	5.74	0.0568	15	12-14.9	4	7.84
8	46.58	255	255	255	14.83	3.85	7.70	0.0621	18	15-17.9	1	1.96
9	139.74	255	255	255	44.48	6.67	13.34	0.0474	21	18-20.9	0	0.00
10	25.88	255	255	255	8.24	2.87	5.74	0.0568	24	21-23.9	2	3.92
11	77.64	255	255	255	24.71	4.97	9.94	0.0613	27	24-26.9	0	0.00
12	20.70	255	255	255	6.59	2.57	5.13	0.0542	30	27-29.9	1	1.96
13	15.53	255	255	255	4.94	2.22	4.45	0.0508	33	30-32.9	1	1.96
14	51.76	255	255	255	16.47	4.06	8.12	0.0626			0	0.00
15	51.76	255	255	255	16.47	4.06	8.12	0.0626			51	100.0
16	20.70	255	255	255	6.59	2.57	5.13	0.0542				
17	103.51	255	255	255	32.95	5.74	11.48	0.0565	Std Dev.	Min	Max	Mean
18	98.34	255	255	255	31.30	5.59	11.19	0.0576	6.36	2.57	32.67	8.57
19	82.81	255	255	255	26.36	5.13	10.27	0.0605				
20	10.35	255	255	255	3.29	1.82	3.63	0.0464				
21	10.35	255	255	255	3.29	1.82	3.63	0.0464				
22	67.28	255	255	255	21.42	4.63	9.26	0.0624				
23	103.51	255	255	255	32.95	5.74	11.48	0.0565				
24	20.70	255	255	255	6.59	2.57	5.13	0.0542				
25	46.58	255	255	255	14.83	3.85	7.70	0.0621				
26	25.88	255	255	255	8.24	2.87	5.74	0.0568				
27	31.05	255	255	255	9.88	3.14	6.29	0.0588				
28	5.18	255	255	255	1.65	1.28	2.57	0.0402				
29	113.87	255	255	255	36.24	6.02	12.04	0.0540				
30	46.58	255	255	255	14.83	3.85	7.70	0.0621				

31	15.53	255	255	255	4.94	2.22	4.45	0.0508
32	838.47	255	255	255	266.89	16.34	32.67	0.0000
33	46.58	255	255	255	14.83	3.85	7.70	0.0621
34	20.70	255	255	255	6.59	2.57	5.13	0.0542
35	5.18	255	255	255	1.65	1.28	2.57	0.0402
36	41.41	255	255	255	13.18	3.63	7.26	0.0614
37	5.18	255	255	255	1.65	1.28	2.57	0.0402
38	25.88	255	255	255	8.24	2.87	5.74	0.0568

Table B-12: Particle size distribution in catalyst 1.8F1.8W1.8M/AC obtained using Image-J software.

No.	Area	Mean	Min	Max	r^2	r	d	Normal	Upper Bin	Bin	Frequ.	%Frequ.
1	227.73	255	255	255	72.49	8.51	17.03	0.0014				
2	124.22	255	255	255	39.54	6.29	12.58	0.0247	1.8	0.0-1.7	0	0.0
3	46.58	255	255	255	14.83	3.85	7.70	0.1017	3.6	1.8-3.5	10	17.9
4	82.81	255	255	255	26.36	5.13	10.27	0.0603	5.4	3.6-5.3	18	32.1
5	51.76	255	255	255	16.47	4.06	8.12	0.0966	7.2	5.4-7.1	16	28.6
6	5.18	255	255	255	1.65	1.28	2.57	0.0650	9	7.2-8.9	8	14.3
7	15.53	255	255	255	4.94	2.22	4.45	0.0964	10.8	9.0-10.7	2	3.6
8	10.35	255	255	255	3.29	1.82	3.63	0.0839	12.6	10.8-12.5	1	1.8
9	51.76	255	255	255	16.47	4.06	8.12	0.0966	14.4	12.6-14.3	0	0.0
10	15.53	255	255	255	4.94	2.22	4.45	0.0964	16.2	14.4-16.1	0	0.0
11	82.81	255	255	255	26.36	5.13	10.27	0.0603	18	16.2-17.9	1	1.8
12	62.11	255	255	255	19.77	4.45	8.89	0.0849			0	0.0
13	31.05	255	255	255	9.88	3.14	6.29	0.1096			56	100.0
14	36.23	255	255	255	11.53	3.40	6.79	0.1086				
15	10.35	255	255	255	3.29	1.82	3.63	0.0839				
16	10.35	255	255	255	3.29	1.82	3.63	0.0839				
17	10.35	255	255	255	3.29	1.82	3.63	0.0839				
18	5.18	255	255	255	1.65	1.28	2.57	0.0650				
19	10.35	255	255	255	3.29	1.82	3.63	0.0839	Std Dev.	Min	Max	Mean
20	31.05	255	255	255	9.88	3.14	6.29	0.1096	2.77	2.57	17.03	6.29
21	5.18	255	255	255	1.65	1.28	2.57	0.0650				
22	5.18	255	255	255	1.65	1.28	2.57	0.0650				
23	31.05	255	255	255	9.88	3.14	6.29	0.1096				
24	5.18	255	255	255	1.65	1.28	2.57	0.0650				
25	36.23	255	255	255	11.53	3.40	6.79	0.1086				
26	10.35	255	255	255	3.29	1.82	3.63	0.0839				
27	25.88	255	255	255	8.24	2.87	5.74	0.1084				
28	15.53	255	255	255	4.94	2.22	4.45	0.0964				
29	20.70	255	255	255	6.59	2.57	5.13	0.1042				
30	36.23	255	255	255	11.53	3.40	6.79	0.1086				
31	5.18	255	255	255	1.65	1.28	2.57	0.0650				

32	62.11	255	255	255	19.77	4.45	8.89	0.0849
33	10.35	255	255	255	3.29	1.82	3.63	0.0839
34	31.05	255	255	255	9.88	3.14	6.29	0.1096
35	20.70	255	255	255	6.59	2.57	5.13	0.1042
36	5.18	255	255	255	1.65	1.28	2.57	0.0650
37	41.41	255	255	255	13.18	3.63	7.26	0.1058
38	10.35	255	255	255	3.29	1.82	3.63	0.0839

Table B-13: Particle size distribution in catalyst 2.25F2.25W0.9M/AC obtained using Image-J software.

No.	Area	Mean	Min	Max	r^2	r	d	Normal	Upper Bin	Bin	Frequ.	%Frequ.
1	56.93	255	255	255	18.12	4.26	8.51	0.0281				
2	729.78	255	255	255	232.29	15.24	30.48	0.0158			0	0.0
3	714.25	255	255	255	227.35	15.08	30.16	0.0165	8	0.0-7.99	8	21.1
4	517.57	255	255	255	164.75	12.84	25.67	0.0271	16	8.0-15.99	10	26.3
5	56.93	255	255	255	18.12	4.26	8.51	0.0281	24	16.0-23.99	11	28.9
6	310.54	255	255	255	98.85	9.94	19.88	0.0381	32	24.0-31.99	5	13.2
7	15.53	255	255	255	4.94	2.22	4.45	0.0184	40	32.0-39.99	4	10.5
8	25.88	255	255	255	8.24	2.87	5.74	0.0215	48	40.0-47.99	0	0.0
9	843.64	255	255	255	268.54	16.39	32.77	0.0113			38	100.0
10	403.71	255	255	255	128.50	11.34	22.67	0.0337				
11	895.40	255	255	255	285.01	16.88	33.76	0.0096				
12	750.48	255	255	255	238.88	15.46	30.91	0.0149				
13	295.02	255	255	255	93.91	9.69	19.38	0.0387				
14	305.37	255	255	255	97.20	9.86	19.72	0.0383				
15	445.11	255	255	255	141.68	11.90	23.81	0.0314	Std Dev.	Min	Max	Mean
16	67.28	255	255	255	21.42	4.63	9.26	0.0299	10.00	2.57	33.76	16.87
17	15.53	255	255	255	4.94	2.22	4.45	0.0184				
18	843.64	255	255	255	268.54	16.39	32.77	0.0113				
19	703.90	255	255	255	224.06	14.97	29.94	0.0170				
20	129.39	255	255	255	41.19	6.42	12.84	0.0368				
21	879.87	255	255	255	280.07	16.74	33.47	0.0101				
22	82.81	255	255	255	26.36	5.13	10.27	0.0321				
23	72.46	255	255	255	23.06	4.80	9.61	0.0306				
24	5.18	255	255	255	1.65	1.28	2.57	0.0143				
25	10.35	255	255	255	3.29	1.82	3.63	0.0166				
26	98.34	255	255	255	31.30	5.59	11.19	0.0340				
27	5.18	255	255	255	1.65	1.28	2.57	0.0143				
28	77.64	255	255	255	24.71	4.97	9.94	0.0314				
29	25.88	255	255	255	8.24	2.87	5.74	0.0215				
30	25.88	255	255	255	8.24	2.87	5.74	0.0215				
31	258.79	255	255	255	82.37	9.08	18.15	0.0396				

32	424.41	255	255	255	135.09	11.62	23.25	0.0326
33	139.74	255	255	255	44.48	6.67	13.34	0.0375
34	222.56	255	255	255	70.84	8.42	16.83	0.0399
35	253.61	255	255	255	80.73	8.98	17.97	0.0397
36	284.66	255	255	255	90.61	9.52	19.04	0.0390
37	181.15	255	255	255	57.66	7.59	15.19	0.0393
38	227.73	255	255	255	72.49	8.51	17.03	0.0399

Table B-14: Particle size distribution in catalyst 1.35F1.35W2.7M/AC obtained using Image-J software

No.	Area	Mean	Min	Max	r^2	r	d	Normal	Upper Bin	Bin	Frequ.	%Frequ.
1	10.35	255	255	255	3.29	1.82	3.63	0.0420				
2	119.04	255	255	255	37.89	6.16	12.31	0.0531				
3	212.20	255	255	255	67.55	8.22	16.44	0.0333			0	0.0
4	5.18	255	255	255	1.65	1.28	2.57	0.0365	5	0.0-4.9	19	30.2
5	201.85	255	255	255	64.25	8.02	16.03	0.0354	10	5.0-9.9	22	34.9
6	20.70	255	255	255	6.59	2.57	5.13	0.0493	15	10.0-14.9	10	15.9
7	165.62	255	255	255	52.72	7.26	14.52	0.0433	20	15.0-19.9	7	11.1
8	191.50	255	255	255	60.96	7.81	15.61	0.0376	25	20.0-24.9	3	4.8
9	31.05	255	255	255	9.88	3.14	6.29	0.0539	30	25.0-29.9	2	3.2
10	20.70	255	255	255	6.59	2.57	5.13	0.0493	35	30.0-34.9	0	0.0
11	641.79	255	255	255	204.29	14.29	28.59	0.0010			0	0.0
12	25.88	255	255	255	8.24	2.87	5.74	0.0518			63	100.0
13	170.80	255	255	255	54.37	7.37	14.75	0.0422				
14	119.04	255	255	255	37.89	6.16	12.31	0.0531				
15	5.18	255	255	255	1.65	1.28	2.57	0.0365				
16	698.72	255	255	255	222.41	14.91	29.83	0.0006				
17	20.70	255	255	255	6.59	2.57	5.13	0.0493				
18	310.54	255	255	255	98.85	9.94	19.88	0.0169	Std Dev.	Min	Max	Mean
19	403.71	255	255	255	128.50	11.34	22.67	0.0081	6.75	2.57	29.83	9.20
20	15.53	255	255	255	4.94	2.22	4.45	0.0461				
21	41.41	255	255	255	13.18	3.63	7.26	0.0567				
22	5.18	255	255	255	1.65	1.28	2.57	0.0365				
23	25.88	255	255	255	8.24	2.87	5.74	0.0518				
24	10.35	255	255	255	3.29	1.82	3.63	0.0420				
25	170.80	255	255	255	54.37	7.37	14.75	0.0422				
26	5.18	255	255	255	1.65	1.28	2.57	0.0365				
27	5.18	255	255	255	1.65	1.28	2.57	0.0365				
28	227.73	255	255	255	72.49	8.51	17.03	0.0302				
29	15.53	255	255	255	4.94	2.22	4.45	0.0461				
30	279.49	255	255	255	88.96	9.43	18.86	0.0212				
31	31.05	255	255	255	9.88	3.14	6.29	0.0539				

32	160.45	255	255	255	51.07	7.15	14.29	0.0445
33	93.16	255	255	255	29.65	5.45	10.89	0.0573
34	5.18	255	255	255	1.65	1.28	2.57	0.0365
35	5.18	255	255	255	1.65	1.28	2.57	0.0365
36	5.18	255	255	255	1.65	1.28	2.57	0.0365
37	36.23	255	255	255	11.53	3.40	6.79	0.0555
38	36.23	255	255	255	11.53	3.40	6.79	0.0555